MODELING OF THE FISHERIES ACOUSTICS PROBLEM

A

DISSERTATION

Presented to the Faculty

of the University of Alaska Fairbanks

in Partial Fulfillment of the Requirements

for the Degree of

DOCTOR OF PHILOSOPHY

By

Barbara L. Adams, M.S., B.A.

Fairbanks, Alaska

August 2002

MODELING OF THE FISHERIES ACOUSTICS PROBLEM

by

Barbara L. Adams

RECOMMENDED:

Vikas S. Sonwalkar (Advisory Committee Chair)

John J. Kelley

Ronald P. Barry

Joseph G. Hawkins

Department Head

APPROVED:

Dean, College of Science, Engineering and Mathematics

Dean of Graduate School

Date

Abstract

This dissertation presents a mathematical model of the overall fisheries acoustics problem posed by enumeration of fish populations using sonar. Emphasis is placed on three key components: a new geometric model for the target strength (TS) of Pacific salmon, a fish distribution for sockeye salmon, and generation of artificial sonar data. Results of the TS and fish distribution models show TS varies on height and breadth of fish as much as on fish length and TS from the air-filled swimbladder is the major contributor as reported by Foote [1985]. A fish roll factor within 45° leads to TS variations within 7 dB for normal incidence, side aspect and 2 dB for dorsal aspect. Also second order effects of ray propagation through fish flesh on TS from the swimbladder provide TS results up to 20 dB lower at high aspect angles. The geometric model predicts TS values that match extremely well with TS data collected on Pacific salmon and other species in river and ocean environments. By varying fish size and swimbladder parameters and considering the effect of fish flesh, the model covers the range of TS values that occur in the field, thus identifying and quantifying the uncertainty in the experimental data. The overall approach in this work is to construct a direct model providing artificial sonar data, then use an inverse model (echo integration algorithm) with that data or with experimental data to compare results. The echo integration results are not reliable at any fish rate for a fixed river cross-section. Estimated fish counts of 0-7 are obtained from 100 simulations for a known fish distribution of 3 fish (0.1 fish/sec). Similarly, at 0.5 fish/sec with 15 known fish, estimates of 0-30 were obtained; at 1 fish/sec with 30 known fish, estimates of 0-50; and at 5 fish/sec with 150 known fish, estimates of 0-100 fish. Fish counts ranged from 0-19 for 3 known fish when ping rate changed from 1-10 pings/sec and when pulse width varied from 0.1-1.0 ms.

Contents

List of Figures

List of Tables

Acknowledgments

I would like to give thanks to my advisor, Dr. Vikas Sonwalkar, for his many hours and his thoughtful insight into this research. Thanks also for the constant support, encouragement, and guidance. I would like to express my appreciation to Dr. John Kelley for initiating the acoustics research at the University of Alaska Fairbanks (UAF). In particular, thanks to Dr. Kelley for introducing me to the fisheries acoustics problem and providing a variety of seminars and conferences allowing all of us to stay connected with colleagues elsewhere. I would also like to thank my other committee members: Dr. Joseph Hawkins and Dr. Ronald Barry for their support and aid in this work.

I would like to acknowledge work accomplished by others at UAF that contributed directly to my work. Thanks to John Pham and Mark Ayers for development of the sonar model and Biao Chen and Zhiguo Lai for development of the fish movement and direct models.

I would like to acknowledge the various people contributing experimental data: David Daum of U.S. Fish and Wildlife Service (USFWS), Deborah Burwen of the Sports Fishing Division of Alaska Department of Fish and Game (ADFG), and Deborah Hart formerly of the Regional Division of Alaska Department of Fish and Game. Thanks also to Mike Holliman for taking x-rays of the sockeye salmon and providing x-ray data for the rainbow trout. Special thanks to Gary Martinek of the Gulkana Hatchery for providing sockeye salmon for research purposes.

So many people from various aspects of the field have contributed time and knowledge in conversation and have been encouraging to me throughout this project:

Dan Huttunen (ADFG), Dave Daum (USFWS), Dr. Pham Quang (UAF), Carl Pfisterer (ADFG), Deborah Burwen (ADFG), Steve Fleischman (ADFG), James Dawson (BioSonics Inc.), Dan Wiggins (BioSonics Inc.), Dr. Steve Parry (ADFG), Samuel Johnston (HTI Inc.), Suzie Maxwell (ADFG), Daniel Bosch (ADFG), Bruce Ransom (HTI Inc.), Dr. Timothy Mulligan (Department of Fisheries and Oceans Pacific Biological Station, Canada), Dr. Robert Kieser (Department of Fisheries and Oceans Pacific Biological Station, Canada), Dr. Peter Dahl (University of Washington), Dr. John Horne (University of Washington), Dr. Jan Kubecka (Royal Holloway College, Czech Republic), Dr. Sathy Naidu (UAF), Chris Stark (UAF), Dr. James Reynold (UAF), and Hal Geiger (ADFG).

I also feel indebted to my colleagues and friends for their support and encouragement and for making this trip more enjoyable: Hu Yua, Anirban Chowdhury, Xiangdong Chen, Biao Chen, Zhiguo Lai, and Dr. Jon Bolles. I want to give a special thanks to Dr. Jayashree Harikumar without whose friendship this could never have been bearable.

Finally I would like to thank my family for always allowing me to be who I am and especially my husband, Todd, for all his support, patience, and for his many sacrifices during my studies. I give thanks and praise to my Lord and Savior Jesus Christ for imparting His wisdom, patience, and perseverance (I Peter 4:11).

This work was sponsored by grants from Alaska Science and Technology Foundation, "Modeling Riverine Fisheries Acoustics: New Methods to Estimate Fish Abundance, Composition, and Uncertainties in Data Analysis" (Grant 97-4-147) and Alaska Department of Fish and Game (RSA log #1185167). This work was also supported in part by a grant of HPC time from the Arctic Region Supercomputing Center.

Chapter 1

INTRODUCTION

The overall objective of this dissertation is to provide physically and scientifically sound modeling efforts on the fisheries acoustics problem that provide insight into the identification and quantification of uncertainties in sonar data. In this chapter a background of sonar is first provided in section 1.1, followed by the use and importance of sonar to Alaska in 1.2. The sonar equation and necessary sonar terminology is discussed in section 1.3 and typical sonar systems and processing methods in use today are given in 1.4. The new approach to the fisheries acoustics problem as well as the problem itself are introduced in section 1.5. The organization of the dissertation is listed in 1.6. Lastly, section 1.7 details the contributions of the present work.

1.1 Background of Sonar

Sonar involves transmitting acoustic waves into water, which then hits a target and returns an echo to the receiver. The echo includes properties representing the transmitting and receiving instrument, the sound waves, the medium through which it travels, the distance traveled (range), and the target encountered. Figure 1.1.1

(taken from MacLennan and Simmonds [1992] page 31) illustrates the reflection of sound from a large target. The transmitted sound (incident wave) and the echoes (reflected waves) after hitting a large target are shown as plane waves. The angle of incidence and angle of reflection are the same and are measured from an imaginary line perpendicular to the surface of the target at the point of incidence. Usually, when the sound is first transmitted, the waves are spherical, but after traveling a sufficient distance, spread out and become nearly plane waves. The reflected wave from a large target usually takes the form of a plane wave; however, when the target is small compared to the wavelength of the sound, the reflected waves tend to be more spherical. The quantification of this process is presented in the sonar equation further explained in section 1.3 below [MacLennan and Simmonds, 1992].

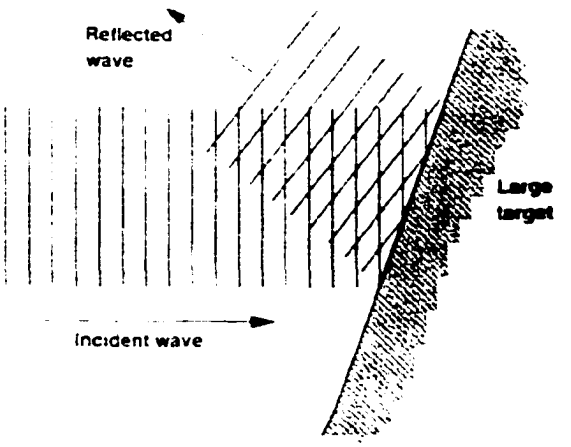

Figure 1.1.1 Reflection of sound from a large target. The transmitted sound, called the incident wave, and the echoes, called the reflected waves, are shown after hitting a large target. Both the incident and reflected waves are shown as plane waves. The angle of incidence and angle of reflection are the same and are measured from an imaginary line perpendicular to the surface of the target at the point of incidence [MacLennan and Simmonds, 1992, p. 31].

The basic idea of sonar is well understood with contributions from the research

performed primarily during the efforts of submarine warfare in World War II. The historical research focused on submarines as targets. They were large, smooth surfaces acting in a somewhat predictable manner. The sonar was able to locate the submarine's position and estimate the submarine's speed relative to its own location. Although much of the knowledge gained from this work is still used today, applications to fisheries involve biological creatures with few of the same properties of the submarines [Urick, 1983].

Implementation of sonar to enumerate fish began as early as the 1960s. The first types of sonar systems included echo counters and echo integrators [MacLennan and Holliday, 1996]. These systems resembled a little black box that would provide an output in the form of a number every so often referring to a fish count. The process used little software as we know it now and was performed mainly inside the physical device. Although instruments similar to these are still used today, much improvement has been made in hardware, software and storage as discussed later in section 1.4 [Medwin and Clay, 1998].

1.2 Use of Sonar in Alaska Fisheries

The management decisions of fisheries agencies, such as the Alaska Department of Fish and Game (ADFG), are based on fisheries information gathered from several sources such as aerial surveys of spawning salmon, gill net sampling, and hydroacoustic sounding (sonar) data. The information may include fish counts, fish species composition within a river or area, migratory paths and behavior, and size, age, and sex of fish. The information on stock specific estimates or indices of escapement are used to design fish harvesting strategies, both short-term and long-term. As fisheries is the second largest industry in Alaska and is relied on by many Alaskans for

subsistence and livelihoods, high importance is placed on achieving accurate scientific results for fish counts and species estimates [Dawson and Johnston, 1997]. For example, most field surveys in Alaska are performed for the purpose of fisheries management of several salmon species and are published in the form of reports [Burwen and Bosch, 1996; Daum and Osborne, 1996; Fleischman, *et al.*, 1995; Huttunen and Skvorc, 1994, 1996; Konte *et al.*, 1996; LaFlamme, 1995; Maxwell *et al.*, 1997; Osborne and Daum, 1997; Vania and Huttunen, 1996; Vaught and Molyneaux, 1995]. These reports often contain for example, target strength (TS) distributions (obtained from sonar data as discussed in Chapter 3), length distributions, swimming behavior, and diurnal patterns. It is now becoming more common for feasibility studies to be conducted before attempting to begin new projects, and evaluation studies to be provided after a new approach is used. These assessments are usually considered technical reports rather than field survey reports and focus more on a scientific perspective than the fisheries management reports [BioSonics, 1998; Burwen *et al.*, 1995; Dahl *et al.*, 2000; Ehrenberg, 1989, 1995; Ehrenberg and Johnston, 1996; Iverson, 1995; Steig and Johnston, 1996; Xie *et al.*, 1997].

Figure 1.2.1 shows the 24 locations across the state of Alaska where sonar projects are currently employed. (Map was provided by Debbie Hart of Alaska Department of Fish and Game.) The sites are marked on the map by their corresponding number. The chart in the upper right corner lists the number next to the name of the river or drainage. The sonar systems used at the various sites range in their level of sophistication from most basic to advanced as listed in the chart by 'x's in the two right columns (or written at the bottom left side of the page). An 'x' in the first column shows the sites with the most basic equipment. An 'x' in the furthest right column shows sites with the most advanced systems. These sonar systems

will be discussed further in section 1.4. Most of the locations for sonar sites have been identified as key rivers and drainages in the migratory paths of various Pacific salmon species used for subsistence, sport, and commercial fishing [Dawson and Johnston, 1997].

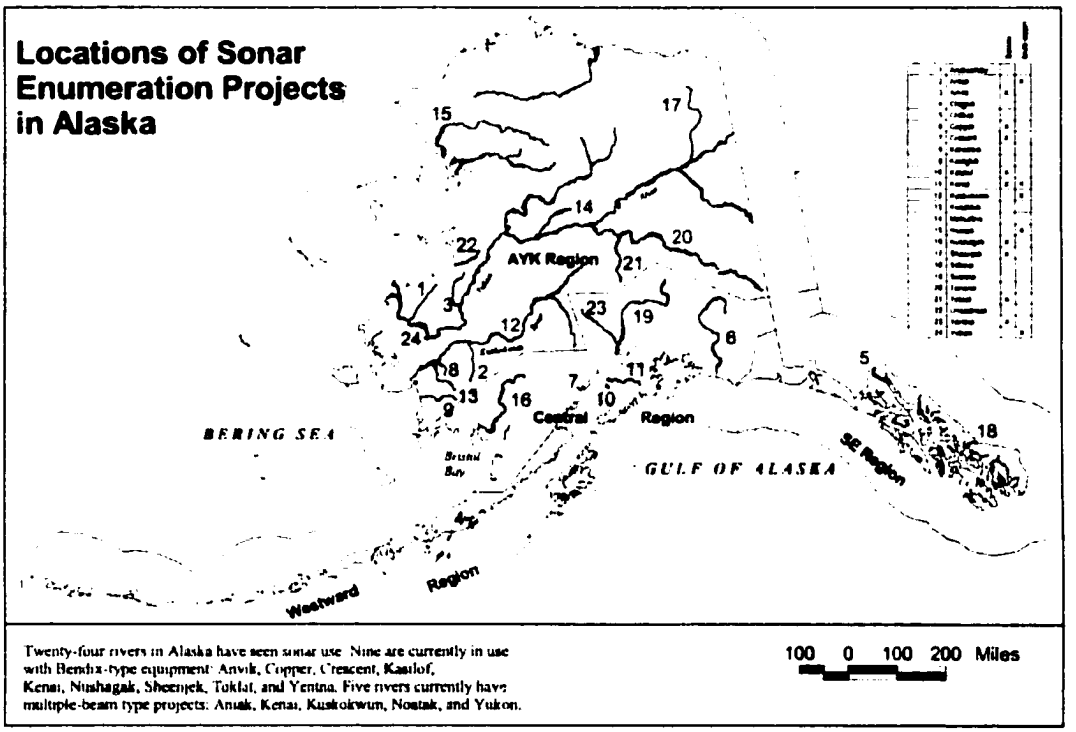

Figure 1.2.1 Map with Alaska sonar sites pinpointed. Shown are the 24 locations across the state of Alaska where sonar projects are currently employed. The sites are marked on the map by their corresponding number. The chart in the upper right corner lists the number next to the name of the river or drainage. The sonar systems used at the various sites range in their level of sophistication from most basic to advanced as listed in the chart by 'x's in the two right columns and written underneath the map. An 'x' in the first column shows the sites with the most basic equipment. An 'x' in the furthest right column shows sites with the most advanced systems. Most of the locations for sonar sites have been identified as key rivers and drainages in the migratory paths of various Pacific salmon species used for subsistence, sport, and commercial fishing.

Other methods of sampling are still active on rivers whether or not sonar systems are used there: however, interest in using sonar methods over others stems from the ability to assess fish populations by passive means and in cloudy or turbid (heavy

sediment) water. On the contrary, gill net sampling for instance involves actual fishing with nets and removing the salmon from the river. Tower counts are another passive method used but are limited to situations when the water is very clear. Despite these advantages to sonar use, the method is not employed exclusively as it is expensive and not conducive to all river situations. For example, if a river has a high level of debris in the water, the scattering from particles along with the scattering from the fish may produce sonar data that is difficult to interpret and use [Dawson and Johnston, 1997].

The sonar situation in the ocean varies from the setup in the river in several ways. In the ocean, sonar systems are usually downward looking and attached to moving vessels. In this situation, the ocean bottom is easily identified and removed from the analysis. Often a global positioning system (GPS) is used to aid in data collection along the transverse to keep records accurate. The GPS data corresponds with the sonar data in time and provides an accurate position of the sonar system at the time the data was collected [MacLennan and Simmonds, 1992]. In the riverine setting, the sonar is employed horizontally with a tilt angle downward along the river bottom cross-section. The sonar is stationary on the riverbank, aimed at a certain location, and only moved when water levels or other environmental conditions change in a manner as to create problems. These less than frequent problems may include when high water pushes the sonar system out of place or when water levels drop so low the sonar is no longer in the water and is unable to be used. The placement of the sonar system on the bank is determined by physical attributes of the river location and expected swimming behavior of the fish in that section of water [Daum and Osborne, 1998]. The physical attributes of the river include for example a river bottom that is less reflective, such as sand over pebbles, or a water velocity that forces the fish

to continue moving, such as a bend in the river with higher water velocity rather than a calm pool area with low water velocity where fish may tend to rest and swim in circles (often referred to as milling behavior) [Dawson and Johnston, 1997].

1.3 Sonar Equation and Terminology

The use of sonar in fisheries poses the challenge of combining properties of instruments (the sonar system itself), the physical environment, and biota. As the sonar system forces sound to travel through the water and reflect off the fish, the properties of each factor affecting sound transmission are taken into account. For example, some properties of the sonar system include the amount of power or pressure used to force the sound into the water and the rate at which the sound travels through the water. Examples of properties of the physical environment include how fast the sound travels through the water based on its temperature and salinity. Lastly, the shape and size of the fish are examples of the properties of the biota. In this section, these various properties will be discussed within the framework of the sonar equation based on the analytical formulas of wave propagation theory.

In general, the incident sound pressure can be described as a function of time by [Medwin and Clay, 1998]

$$p_{inc}(t) = D \ \frac{p_0(t - R/c)R_0}{R} \ 10^{-\alpha R/20}. \tag{1.3.1}$$

where D is the directivity, p_0 is the initial pressure output of the transducer, R is the range in m, c is the speed of sound through water in m/s, R_0 is a reference range usually of 1 m, and α is the attenuation coefficient in dB/m.

The scattered sound pressure of a fish located at range R is then proportional

to the incident sound pressure and is given by

$$p_{scat}(t) = D \frac{p_{inc}(t - R/c)L_{bs}}{R} 10^{-\alpha R/20}. \quad (1.3.2)$$

where L_{bs} is the acoustical backscattering length of the fish.

Combining Equations 1.3.1 and 1.3.2 provides the scattering sound pressure in terms of the initial sound pressure.

$$p_{inc}(t) = D^2 \frac{p_0(t - 2R/c)L_{bs}R_0}{R^2} 10^{-\alpha R/10}. \quad (1.3.3)$$

Since the units of measure for pressure tend to be small, these equations are translated into a decibel form, called the sonar equation. The sonar equation is given by

$$\mathrm{RL} = \mathrm{SL} + \mathrm{RS} + \mathrm{TS} - \mathrm{TVG} - \mathrm{ABS} + 2\mathrm{B}(\theta, \phi) \quad (1.3.4)$$

where RL is the amplitude of the received signal in dB referenced to 1 micro-Pascal (commonly written as dB//1 μPa) and relates to the p_{scat} from Equation 1.3.3. SL is the source level of the transducer in dB//1 μPa and relates to the term p_0 given above. RS is the receive sensitivity of the transducer in dB//1 μPa. TS is the target strength of the ensonified object in dB and is related to L_{bs} of the fish. TVG is the time-varied-gain in dB//1 m and accounts for the $1/R^2$ term in Equation 1.3.3. ABS is absorption in dB and relates to the last term of $10^{-\alpha R/10}$. $\mathrm{B}(\theta, \phi)$ is the beam pattern function in dB//1 m depending on the angles off axis and accounts for the two-way directivity D^2. Each term is further discussed below [Urick, 1983].

SL, RS and $\mathrm{B}(\theta, \phi)$ are constants depending on the transducer. The source level is the amount of pressure exerted in or transmitted to the water by the transducer and is based on a high voltage electronic pulse from the transmitter. When a signal is returned, the opposite process must take place. Sound pressure is converted back

into electrical energy. During both processes, some signal loss occurs between the transmitter and the transducer. A fixed receive sensitivity value compensates for the loss in signal between the transducer and the transmitter. The manufacturer provides these values with each sonar system. An example of typical values for these parameters include a sonar system with SL = 215 dB//1 μPa with a RS = -64 dB//1 μPa both measured at a range of 1 m [BioSonics, 1998].

The sonar transducer generates sound in a certain pattern within a fixed beam width based on its physical design, such as size, shape (circular or elliptical), and frequency of the beam. For example, a circular beam with physical diameter of ~6.75 mm and carrier frequency of 100 kHz provides a 3 dB beam width of 9.6° [Dawson and Johnston, 1997]. The directional pattern of the intensity of the sound is called the beam pattern factor, $B(\theta, \phi)$. The angles θ and ϕ describe the position of an object within the beam in two dimensions (horizontally or θ and vertically or ϕ with respect to the acoustic axis described below). The beam pattern is determined specifically for each transducer under ideal situations (in a tank with no environmental noise, etc) by transmitting sound and plotting the relative received intensity values compared to the transmitted intensity value. Figure 1.3.1 shows an example of a transducer's beam pattern factor (also called the directivity) as intensity (RL) versus angle of rotation of the transducer. This example, consistent with SL and RS given above, shows the directivity for a BioSonics' 4° circular transducer operating at a carrier frequency of 420 kHz [BioSonics, 1998].

The main lobe, also called the acoustic axis, is the center section where most of the sound intensity is focused (angle of 0° in Figure 1.3.1). Based on the design, the side lobes will vary in size, intensity, and number. Since the side lobes have a lower intensity, when reflection occurs from an object located off the acoustic axis, a

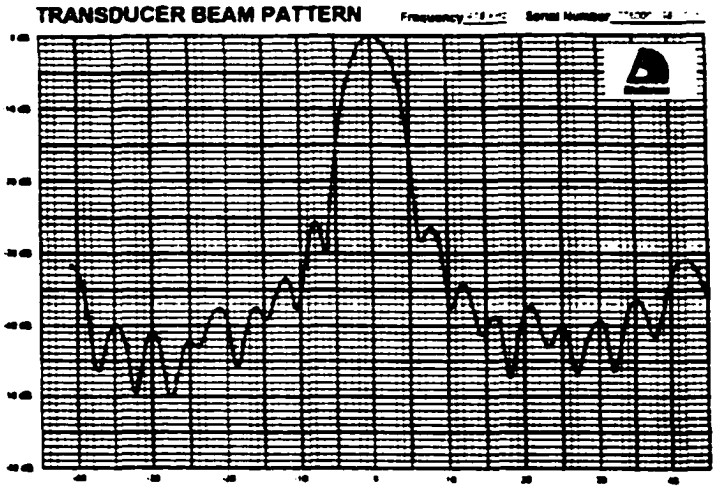

Figure 1.3.1 Example of a beam pattern for a 420 kHz transducer. Drawing of a typical beam pattern showing that the main lobe is the center section where most of the sound intensity is focused. Based on the design, the side lobes will vary in size and number [Dawson and Johnston, 1997, p. 20].

reduction in intensity is inherent and compensation is required. The manufacturer provides a drawing of the beam pattern factor for each system as well as methods of calculation to allow for compensation [MacLennan and Simmonds, 1992].

Environmental parameters are introduced when mathematically describing the travel of the sound wave by its intensity in space and time. As the sound wave travels through water, its intensity decreases depending on properties of the water and the distance traveled. This decrease, often characterized as the transmission loss (TL), includes both the time-varied gain (TVG) and the absorption (ABS). The spreading of the beam forces the intensity of the sound to decline as $1/R^2$, where R is the range from the transducer to the target [MacLennan and Simmonds, 1992]. The time-varied gain is a term used to compensate for this spreading and is found by

$$\mathrm{TVG} = 40 \log \mathrm{R}. \tag{1.3.5}$$

where R is the range to the target in meters. The term, time-varied gain is used since the distance traveled and the time elapsed are proportionally related through the speed of sound in water. The absorption parameter, ABS, given by Urick [1983] depends on range and additionally on the attenuation coefficient (α), which is calculated using the transducer frequency and measurable water parameters. First, the temperature-dependent relaxation frequency, f_T, in kHz must be calculated where T is the temperature of the water in degrees Celsius.

$$f_T = 21.9 \times 10^{6-\frac{1520}{T+273}}. \tag{1.3.6}$$

Then to find α in dB/m the frequency of the transducer, f, in kHz and the salinity, S, of the water in parts per thousand are combined with the above f_T as follows

$$\alpha = \frac{1}{914.4}\left[\frac{0.0186 S f_T f^2}{{f_T}^2 + f^2} + \frac{0.0268 f^2}{f_T}\right]. \tag{1.3.7}$$

The absorption term is then given in dB by

$$\text{ABS} = 2\alpha \text{R}. \tag{1.3.8}$$

For fresh water ($S = 0$ ppt), this formula reduces to a simplified formula (using the second term only) showing absorption as a function of frequency and temperature only. So, for an object at a range of 10 m from a 420 kHz transducer located on the acoustical axis in 5° C fresh water would have a TVG value of 40 dB//1 m and ABS of 1.37 dB.

Lastly, the environmental and biological parameters are introduced in the TS measurement. When the sound encounters a target of interest, such as a fish, the intensity of the reflection from that target compared to the transmitted intensity is called the target strength, TS, usually measured at a range of 1 m. Figure 1.3.2

from Crick [1983] shows a plane wave (represented by the parallel lines) incident on a general target at the point C. The reflected wave, shown as the dotted curves, is compared to the incident wave to determine target strength. The comparison is made at a unit distance from the target as shown by the points P and P'.

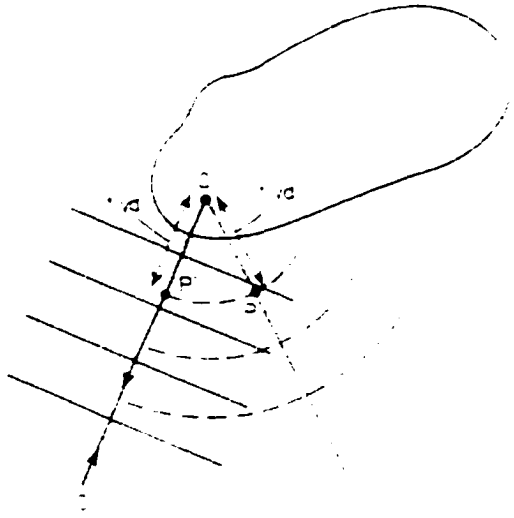

Figure 1.3.2 Geometry of target strength. A plane wave represented by the parallel lines is shown incident on a general target at the point C. The reflected wave, shown as the dotted curves, is compared to the incident wave to determine target strength. The comparison is made at a unit distance from the target as shown by the points P and P' [Crick, 1983, p. 292].

More correctly, the comparison of the transmitted and received intensities is better described with the backscattering cross-section, σ_{bs}. Assuming the intensity of the incident wave is I_i, then

$$\sigma_{bs} = 4\pi R^2 I_b / I_i \tag{1.3.9}$$

describes the relationship between energy per unit area received from the target at range R with intensity I_b and the transmitted intensity. Thus, $\sigma_{bs} I_i$ can be considered as the power of the incident wave passing through the area of size σ_{bs}.

The TS is then the decibel form of the backscattering cross-section given by

$$\mathrm{TS} = 10 \log \sigma_{\mathrm{bs}}/4\pi. \tag{1.3.10}$$

The 4π refers to the cross-sectional area of a target with 1 m radius at a range of 1 m and thus has units of m^2. This forces the TS term to be a ratio and thus the appropriate units are just dB. For nearly all fish the TS ranges within -60 and -20 dB, providing backscattering coefficient values of 0.000013 and 0.13 m^2 [MacLennan and Simmonds, 1992].

The backscattered intensity, I_b also depends on the reflection properties of the target. The reflection of the wave at the target surface depends on the acoustic impedance of both the water and the fish. The acoustic impedance, η, of a medium is defined as $\eta = c\rho$, where ρ is the density of the medium and c is the speed of sound through the medium. The reflection coefficient, R, between 2 media is then defined as

$$R = \frac{\eta_2 - \eta_1}{\eta_2 + \eta_1}. \tag{1.3.11a}$$

or equivalently

$$R = \frac{\rho_2 c_2 - \rho_1 c_1}{\rho_2 c_2 + \rho_1 c_1}. \tag{1.3.11b}$$

where the subscripts of 1 or 2 represent the first and second medium. If the acoustical impedance through both medium 1 and 2 are very similar, such as in the case of water as medium 1 (ρ_1 = 1000 kg/m^3, c_1 = 1500 m/s) and fish flesh as medium 2 (ρ_2 = 1070 kg/m^3, c_2 = 1530 m/s), then the reflection is very small [Denny, 1993; Furusawa, 1988; Shibata, 1970]. When large differences exist such as in the case of water as medium 1 and air as medium 2 (ρ_2 = 1.29 kg/m^3, c_2 = 330 m/s) [Denny, 1993], then the reflection is closer to 1 [Elmore and Heald, 1969]. Reflection of sound and target strength are further discussed in detail in Chapter 3.

All parameters listed in the sonar equation have been discussed, but a final topic involving both environmental and mechanical properties needs to be addressed here. This is the topic of noise. In general noise can be defined as any unwanted echoes (received signals) and can be labeled as either system noise, reverberation, or background noise.

System noise is generated by any sonar system and is present in the receiver output even when the transmitter is switched off. Specifically, it may contain thermal noise in the receiving amplifier due to the random movement of electronics or electrical interference from other surrounding equipment. This mechanical noise can usually be measured before collecting data and accounted for numerically by the RS term in the sonar equation [MacLennan and Simmonds, 1992; Dawson and Johnston, 1997].

Reverberation includes echoes from any unwanted targets and thus depends on the objective of data collection. If the goal is to collect data on large fish, then echoes from smaller fish or other biota are considered reverberation, known as volume reverberation. Debris (for example, floating sticks) in the water may also provide unwanted echoes thus adding to the volume reverberation. Reverberation from inhomogeneities and roughness at the top and bottom surfaces of the water give rise to surface reverberation. This may include river-state noise due to wind blowing, waves breaking, rain and other disturbances in the river [MacLennan and Simmonds, 1992].

Lastly, background noise is any unwanted signal other than the reverberation. Background noise encompasses any other unwanted signals usually generated by environmental conditions not categorized as possible targets [MacLennan and Simmond, 1992]. The typical sources generating background noise are thermal noise in

the water due to the random movement of molecules causing pressure fluctuations at the transducer face or external noise due to machinery, such as a ship's propeller cavitation and water flow over the hull or interference generated by passing motor boats on the river [Mitson, 1983].

1.4 Sonar Systems and Processing Methods in Use

As seen in Figure 1.2.1 the sonar systems currently used in Alaska range in their level of sophistication from most basic to advanced. This section will briefly discuss the various levels of sonar hardware and software most widely used today.

Several different sonar devises exist to count fish. The oldest type used in Alaska was a single beam system developed in 1962 by Al Menin based on the Doppler principle [Menin, 1997]. After the system went through several stages of modification, by 1975, a single transducer side looking system, designed as an echo sounder, was developed and remains the most widely used sonar system in Alaska. This system is also referred to as the Adult Pacific Salmon counter or more often as the Bendix system [Menin, 1997]. The Bendix processor assumes a certain number of echoes per fish and builds this conversion factor into the electronics of the system. The operator observes the average number of echoes per fish, then adjusts the pulse rate of the Bendix echo counter to make the observed average as close as possible to the built-in conversion factor.

Systems following the Bendix system consisted of a transmitter that usually also acts as a receiver, a pulse generator, and a chart recorder. Figure 1.4.1 shows the basic configuration in the field of a relatively modern generic sonar system. The transmitter is usually mounted on a stable platform in the river and connected to the computers receiving and storing the data. The computers are then connected

to machines providing visual printouts of the sonar data. In this configuration, a pulse is transmitted and the receiver waits for returned echoes. The echoes are recorded on a chart recorder, with darker marks corresponding to higher target strengths. The returned echoes are arranged on the chart as a function of target range. Figure 1.4.2 provides an example of an echogram from Mitson [1983]. The dark shading at the bottom of the figure represents the return from the river bottom. The shading in the middle of the figure represents echoes received from fish in the water column. Early systems provided only a qualitative measure of fish or biomass density. Only a very few parameters could be modified to try to fit the system to the environment or fish species. They worked at fixed frequencies and were not able to store any data. As electronics technology progressed, the single beam systems became more sophisticated and eventually the introduction of the dual beam and split beam systems came in the 1980s [MacLennan and Holliday, 1996].

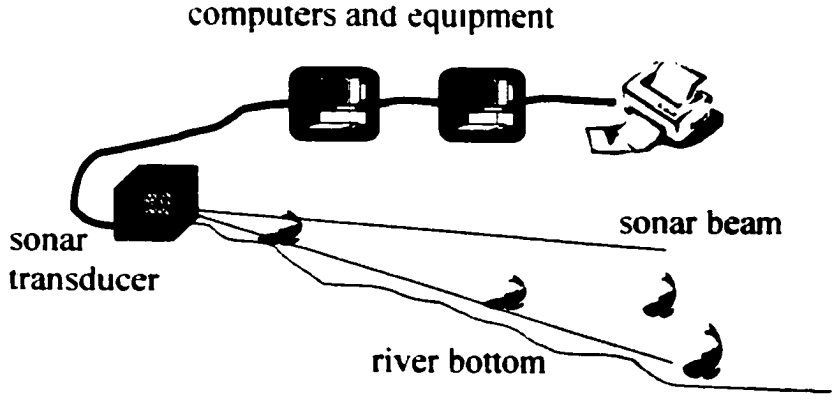

Figure 1.4.1 Experimental configuration. This schematic shows the basic configuration in the field of a generic sonar system. The transmitter is usually mounted on a stable platform in the river and connected to the computers receiving and storing the data. The computers are then connected to machines providing visual printouts of the sonar data.

Sonar beams are now available in single beam, dual beam, split-beam, multi-

Figure 1.4.2 Example of an echogram. This example of an echogram shows the returned echoes arranged on a chart as a function of target range for a downward looking sonar. The dark shading at the bottom of the figure represents the return from the seabed. The shading in the middle of the figure represents echoes received from fish in the water column [Mitson, 1983, p. 78].

frequency, and wide-band. Figure 1.4.3 provides a sketch of the three most common transducer types, single, dual, and split-beam [Dawson and Johnston, 1997]. Dual beam sonar is constructed of two concentric circular elements: the outside circular element is called the narrow beam and the inner circular element is the wide beam. The sound is transmitted using all the elements, but received on the narrow and wide elements separately as well as combined. The advantage of this design allowed for determination of how far off axis the target was by comparing amplitudes received on each element. This allowed for angle off axis compensation and target strength calculation. An example of the beam pattern from a dual beam sonar system is shown in Figure 1.4.4 [MacLennan and Simmonds, 1992]. The narrow and wide beam patterns are represented by the solid and dashed lines respectively. Split-beam sonar is constructed with four quadrants instead, labeled in the sketch (Figure 1.4.3) as up/down and left/right elements. Again, the transducer sends on all elements together, but receives data on the four quadrants separately and all together. This design allows for 3D location of any echo. The arrival times of echoes

are compared between pairs of elements, either up/down or left/right, to find the angle off axis in that plane. The amplitude is measured by the echoes received with all elements combined. Multi-frequency sonar is constructed in such a manner as to allow transmission of sound at up to 3 various frequencies. The objective is that comparison of the echoes among the 3 frequencies may provide further detailed information to more accurately estimate both fish size and species [Ehrenberg, Traynor, and Kaczynski, 1984; Demer, et. al, 1999]. Wide-band systems use a much wider bandwidth than the aforementioned systems in hope that more information will be gathered. The assumptions that species discrimination may be possible with the use of wide-band sonar leans heavily on the idea that sonar data collected from different species will respond to changes in frequencies differently. Thus the patterns among the frequencies provide the new information. Wide-band systems are not commonly used yet, but interest is developing [MacLennan and Simmonds, 1992]. In each case, as the hardware technology progressed more information became available, leading to the need for better storage and new methods of processing as provided in software.

Counting fish populations using single beam sonar can be done with processing techniques called echo integration and echo counting. These two commonly used (indirect) methods for obtaining stock size estimates depend on the acoustic size of the individual fish. Echo integration is a simple technique where all of the energy in the returned echoes is summed. This integrated energy is then divided by an average energy expected for one fish, providing a more quantitative measure of the number of fish present [MacLennan and Simmonds, 1992]. A schematic from MacLennan and Simmonds [1992] is shown in Figure 1.4.5 to further explain the principles of echo integration. The received signals are summed for a specific range (between R_1 and R_2) taking into account the difference in echo strength (this is the purpose of the

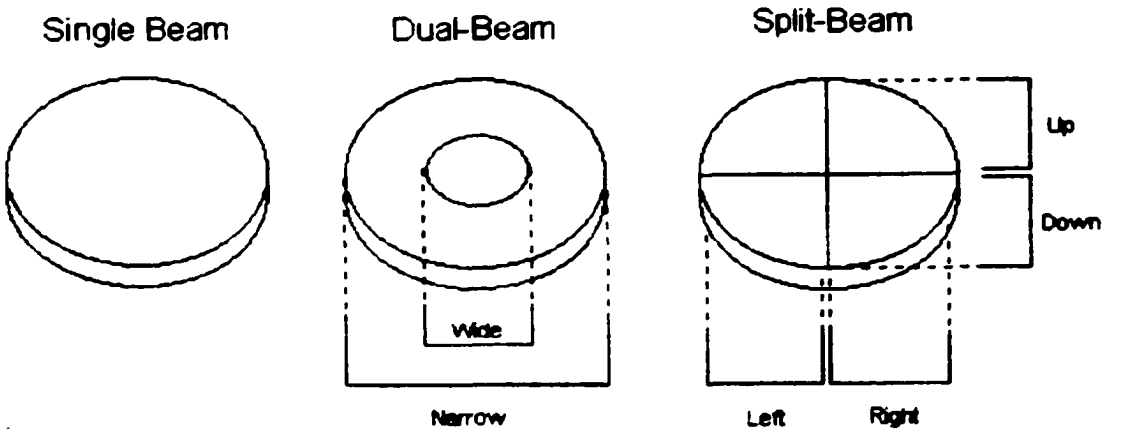

Figure 1.4.3 Single beam, dual-beam, and split-beam arrangements. Transducer element arrangements are shown for single beam, dual-beam, and split-beam sonar. The dual-beam allows data to be received on the wide and the narrow axis. The split-beam allows data to be received on all four quadrants separately as well as the total sum [Dawson and Johnston, 1997, p. 24].

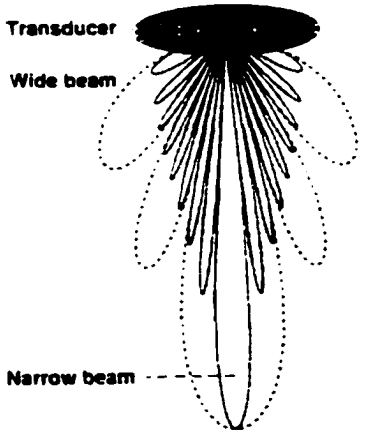

Figure 1.4.4 Beam pattern for dual beam transducer. This schematic shows the beam pattern for a dual beam transducer. The narrow and wide beam patterns are represented by the solid and dashed lines respectively [MacLennan and Simmonds, 1992, p. 55].

TVG function discussed in section 1.3). From the transmitted signal with amplitude $V(t)$ returning reflections from all the targets in the beam, a total return signal of $e(t)$ is found. This is the signal, $e(t)$, that is then used to calculate the integration. Several problems exist with echo integration. The echoes from the river bottom must be removed from the echoes to be integrated, possibly leading to errors if the fish being counted are near the bottom. Also the average fish echo energy can lead to large errors in the fish count because fish target strength can vary by as much as 30 dB depending on the orientation of the fish in the transducer beam [MacLennan and Simmonds, 1992]. A few attempts have been made to better the echo integration algorithm, such as applying scaling methods to echo integration results by Ransom iet al. [1995], using an alternative to thresholding through noise cancellation by Nunnallee [1990], and comparing results collected from both the narrow and wide beams with a dual-beam system presented by Takao and Furusawa [1996].

When fish are sparsely distributed in the water, as opposed to clumped in schools or layers, it may be possible to detect the echoes from individuals [MacLennan and Simmonds, 1992]. This process is called echo counting. When applying echo counting, accurate estimates of both the length of time the fish is in the beam and the individual fish target strength are needed. Problems arise with this method when fish are on the edge of the beam, fish sizes varying drastically or when changes in fish orientation with respect to the sonar provide wide varying target strength values. [Ehrenberg and Torkelson, 1981; Nunnallee, 1982]. Statistical procedures have been developed to increase accuracy through echo counting methods by reducing the bias against fish located on the edge of the beam [Mulligan and Chen, 1998; Mulligan and Kieser, 1996]. Other attempts have been made to avoid the assumption that all targets are of the same acoustical size by implementing a statistical model within

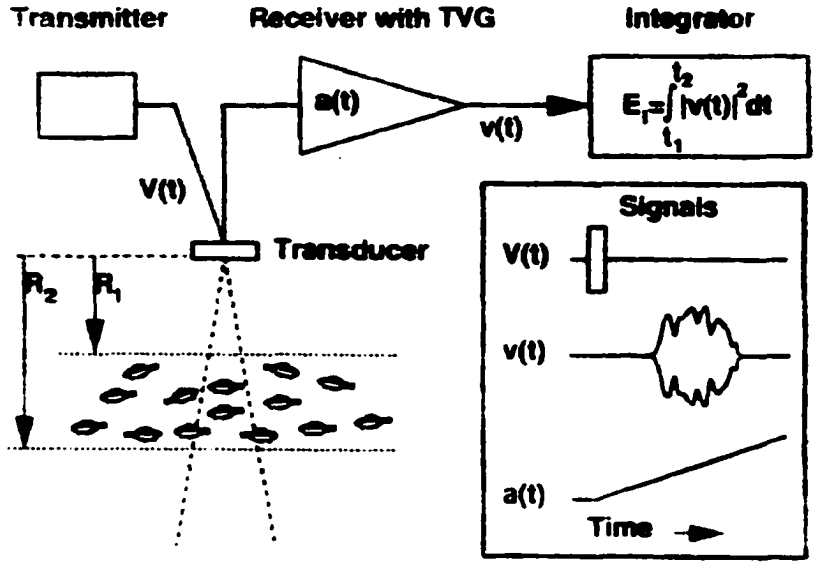

Figure 1.4.5 Principles of echo integration. The received signals summed together for a specific range (here in between R_1 and R_2) are shown taking into account the difference in echo strength (this is the purpose of the TVG function). From the transmitted signal with amplitude $V(t)$ returning reflections from all the targets in the beam, a total return signal of $v(t)$ is found. This is the signal, $v(t)$, that is then used to calculate the integration [MacLennan and Simmonds, 1992, p. 148].

the echo counting algorithm [Kieser and Ehrenberg, 1990].

With the advancement of technology, today's sonar sites include more computers and hardware to accomplish more sophisticated methods of processing and immense storage capacities. Processing methods include not only echo integration and echo counting, which can be used with any of the systems, but also target tracking based on the data received by the split-beam sonar [Burwen and Fleischman, 1998; Daum and Osborne, 1996; Osborne and Daum, 1997; Mulligan *et al.*, 1997; Ransom *et al.*, 1996]. Target tracking attempts to link simultaneous echoes together through grouping by location and target strength values. The linked echoes are called a track. Based on various parameters and filters, the track may be deemed as a fish and thus the enumeration of fish is obtained. Figure 1.4.6 provides two examples of fish tracks obtained from different split-beam systems. Although the data contains

three dimensional locations. here the tracks are plotted in 2D for better viewing with the range parameter suppressed. The plots show angle off axis in degrees or meters for the horizontal plane on the x-axis and the vertical plane on the y-axis. The $*$ denotes the starting point of each track while the $\times$ marks the ending point. A straight line connects two echoes based on consecutive time values referring to when the echo was received. Difficulties in target tracking arise when the fish density in the beam becomes too large, angles of orientation provide widely varying target strength values, or a low SNR hides too many of the echoes [MacLennan and Simmonds, 1992; BioSonics, 1998].

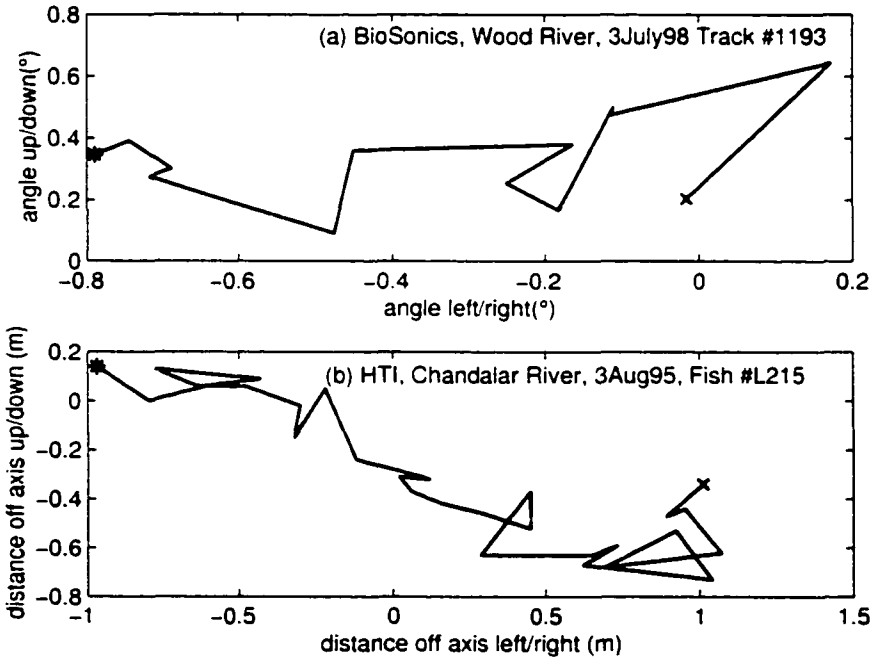

Figure 1.4.6 Examples of fish tracks. Two examples of fish tracks obtained from different sonar split-beam systems are shown. The company name, experiment label, and fish number are listed at the top. Although the data contains three dimensional locations, here the tracks are plotted in 2D for better viewing with the range parameter suppressed. The plots show angle off axis in degrees or meters for the horizontal plane on the x-axis and the vertical plane on the y-axis. The $*$ denotes the starting point of each track while the $\times$ marks the ending point. A straight line connects two echoes based on consecutive time values referring to when the echo was received.

1.5 New Approach

Current research on sonar data tends to fall into the extreme categories of either mathematically too simple or too complicated or too species specific. For example, often sonar data is interpreted using limited relationships, such as TS as a function of fish length and frequency in linear equations given by Love [1971] as empirical fits using specific fish species. Here the TS estimates are inaccurate due to important missing characteristics of the fish. Complications arise when fish specific digitized swimbladder models are used within Kirchhoff-ray mode models to calculate TS [Clay and Horne, 1994]. Also, detailed analytical solutions based on specific geometric solids lead to difficulties in TS calculations [Stanton, 1988a, b, c]. In both examples, the TS estimates are not useful in the field as the process is time consuming and too specific. Many models are built specific to the fish species, not allowing for generalization [Cooper and Temple, 1983; Fleischer *et al.*, 1997; Foote, [1978]; Huang and Clay, 1980; Kubecka, 1994]. Some work has been done using a general approach that is applicable to various species, such as Furusawa [1988] who used a prolate spheroid model. Lastly, an extensive amount of work exists that simply provides sonar measurements for specific species [Chu, *et al.*, 1993; Cushing, *et al.*, 1963; Dawson and Karp, 1990; Ehrenberg, 1980; Enzenhofer, *et al.*, 1998; Foote and Ona, 1985; McCartney and Stubbs, 1971; McClatchie, *et al.*, 1999; Shibata, 1970; Thiel, 1984; Traynor and Ehrenberg, 1990; Wiebe, *et al.*, 1997].

The new approach presented in this work uses an even more general shape that most fish can be modeled by and leads to a simple numerical model that is easily applicable in the field. Figure 1.5.1 schematically shows various building blocks of the theoretical and numerical model used as the approach presented here to the fisheries

sonar problem involving four steps [Sonwalkar, 1999]. First, determine the output of the sonar instrument given a distribution of fish by formulating the direct problem analytically. A correct physical formulation of the direct problem is essential for estimating various uncertainties inherent in the sonar technique. Here, a separate model is developed for the transmitter, propagation, fish distribution, scattering, noise, and the receiver. Once combined together, the output is sonar data similar to that obtained in the field. Second, based on this formulation build a numerical model. A numerical model allows testing of the direct model under realistic conditions. Third, apply the numerical model to various experimental scenarios that closely mimic various ADFG sonar data collection projects. This provides validation of the model. Fourth, investigate the inverse problem, i.e., given the sonar data and the experimental method, determine the fish distribution and a corresponding margin of error. This formulation is carried out in the inverse problem. Using the sonar data obtained from the direct model, applying assumptions and a model for the sonar equipment, the analysis model leads to abundance and possibly species identification results. The inverse problem is ill posed and requires additional assumptions to obtain a unique answer - a much more difficult task than anticipated. Thus the majority of effort was placed in the first three steps focusing on the uncertainties obtained at each level. To obtain an improved model, the results are compared and uncertainties and errors are assessed. In practice, many of these uncertainties were not well understood and thus ignored, for example, the uncertainties that arise due to the use of 1 or 2 fish size parameters (instead of 3) as used in the work performed by Haslett [1962a, b; 1964], Love [1978], and Furusawa [1988] for example. It is hoped that the findings of this research will begin to be used and that the research will be continued to begin solving the problems already discovered

through the inverse model approach.

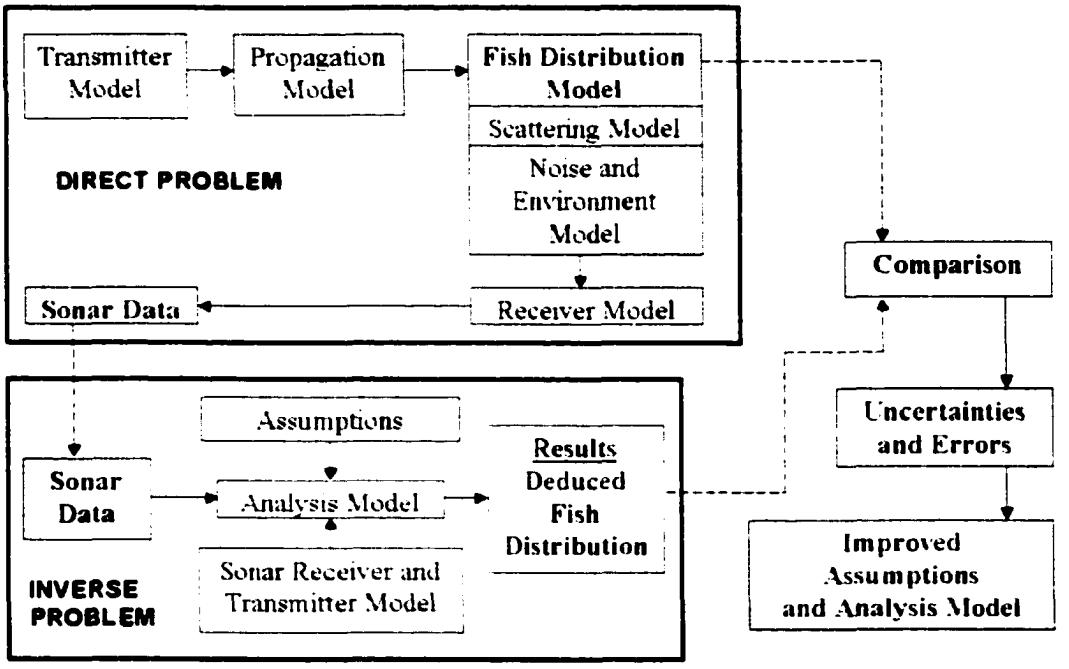

Figure 1.5.1 Direct and inverse flow-chart. This schematic shows the various building blocks of the theoretical and numerical model used as the approach presented here to the fisheries acoustics problem. In the direct problem, a separate model is developed for the transmitter, propagation, fish distribution, scattering, noise, and the receiver. Once combined together, the output is sonar data similar to that obtained in the field. In the inverse problem, using the sonar data obtained from the direct model, applying assumptions and a model for the sonar equipment, the analysis model leads to abundance and possibly species identification results. To obtain an improved model, the results are compared and uncertainties and errors are assessed [Sonwalkar, 1999].

From data collected for the fish size, a probability density function (pdf) representing a fish size distribution was developed. Using x-ray data on the swimbladder, the size and shape of the fish are statistically related to that of the swimbladder. This connection along with the pdf for the fish size has allowed calculations of possible TS variation of a fish of a given length as well as that of an ensemble of fish at arbitrary aspect.

The numerical model, combining both the theoretical model and the fish size distribution, provides estimates of uncertainties in determination of fish size and aspect

based on TS measurements. These uncertainties will be important in both sonar methods to estimate biomass and to discriminate species [Burwen and Fleischman, 1998]. Not only does this model incorporate a vast array of important attributes, it also calculates the TS results in a quick and efficient manner, allowing for use in the field. Lastly, the numerical model calculates the target strength of an individual fish or of ensembles of fish and provides an excellent agreement with experimental data.

The statistical formulation of the TS problem provides a model that can potentially be used in practice to interpret large amount of data obtained in the field. Although the analysis is specific to sockeye salmon in this paper, the results may be applicable to other varieties of salmon, and perhaps also to other fish species with roughly convex fish body and swimbladder. The model is also directly applicable when the swimbladder is modeled as convex surfaces that are combinations of ellipsoids, spheroids, and cylinders. The main limitations of the TS model include that it does not take into account reflections from small-scale irregularities present on the surfaces of the swimbladder and fish and is not valid at low frequencies (< 100 kHz) since the theory requires a smooth convex surface.

1.6 Organization of Dissertation

In the following chapters, two of the main blocks (fish distribution and scattering model) of the direct model are discussed in detail before combining all blocks of the direct model in Chapter 4 and then applying the inverse model to both generated and experimental sonar data in Chapter 5.

The fish distribution model is presented in Chapter 2. Here the size distribution for sockeye salmon is developed using a statistical approach based on experimental

data. The size includes three parameters, length, height and breadth of the fish. These sizes also depend on the sex of the fish and results for both the differentiated (male/female) and undifferentiated data are presented and analyzed. The swimbladder model for sockeye salmon including size, shape and orientation is discussed next. The parameters for the swimbladder depend on the fish size parameters and were developed from digitized x-ray data. Lastly the distribution of salmon in the river is presented based on information collected during field studies. A model of fish behavior created in parallel with this work is included to complete the fish distribution model [Chen, 2001; Lai, 2002]. The entire fish distribution model is presented prior to the target strength model discussed in Chapter 3 since the fish size, shape, and location results are needed for use in calculating target strength. The distribution results can easily be generalized to other Pacific salmon species and even to other fish species given the collection of the necessary data.

The target strength model is presented in Chapter 3. The derivation of the geometric model is independent of the species of fish with the exceptions that the fish body and swimbladder surfaces must be a smooth, convex surfaces and the radii of curvature must be large compared to the wavelength. The limitations and restrictions are discussed in detail prior to explanations of the various special case formulae capable of being calculated and useful for quick checks. A comparison of the Kirchhoff Integral results to the geometric results for an ellipsoid is considered next. Finally various model results are shown to express the power of the model and the uncertainties ascertainable through this approach. A comparison of the target strength model results with experimental data is used to show how the uncertainties in the data can be accounted for by properties other than those usually discussed in the field of fisheries acoustics.

In Chapter 4, models developed outside of this work for the individual blocks of the direct model are then put together with the fish distribution and target strength models to generate sonar data. Target strength results based on fish motion calculated from the model are compared to the experimental data of one fish track. The uncertainty in the experimental data is explained by the various parameters used in the models. This shows that the model provides an accurate representation of what is collected in the field.

Chapter 5 explains the approach used in the inverse model, that is, given the sonar data, how to recreate the fish distribution in size, time, and space. Results from generated sonar data using the direct model are interpreted by applying an echo integration algorithm for various cases of fish density and noise level. A similar analysis is applied to experimental sonar data under similar conditions.

Lastly Chapter 6 provides conclusions and discussion on the comparison of this approach to others used in the past and currently, any weaknesses of this overall approach or specific portions of the model, and suggested improvements and future work.

1.7 Contributions of the Present Work

In this work, a new approach is presented to the fisheries acoustics problem. In modeling of the various components of the direct problem, a new geometric model of TS and a fish size distribution of sockeye salmon were developed. Through both the direct and inverse problems, uncertainties within various components were identified and quantified.

This work presents a model for the target strength (TS) of Pacific salmon, in particular, sockeye salmon (*Oncorhynchus nerka*), built using a geometric approach

that incorporates an extensive amount of influencing factors. The theoretical TS model incorporates the variation in all three fish size parameters (length, height, and breadth), and in the size, shape, location and orientation of the swimbladder. The fish size distribution is specific to sockeye salmon found in Alaskan waters but can be easily modified with size data on other species. The model can be applied at any angle of incidence in three dimensions at high frequencies (> 100 kHz), and thus is applicable in both ocean and river settings. The theory allows for simulation of fish with air-filled swimbladders, oil-filled swimbladders, or no swimbladders. It calculates target strength of the fish as modeled by a swimbladder alone, fish flesh only, or as a swimbladder inside fish flesh. When modeled as in the latter case, it can calculate target strength ignoring the second-order effect of the fish flesh on the swimbladder echoes or by incorporating them. The TS model provides TS dependence on several parameters not recognized in earlier work on sound scattering by fish.

1. Effects of each parameter on TS can be analyzed independently (unlike the ka terms typical in other models where k is the wave number and a is the radius of the sphere or cylinder). Specifically, the TS model allows for quantification of the variations in TS dependent on the fish parameters and the swimbladder size and shape. Also, the TS model allows for placement and orientation of the swimbladder at arbitrary location within the fish body.

2. The TS model takes into account both the scatters from swimbladder (major contribution to TS) and fish body (minor contribution). This allowed for the discovery that the fish flesh plays an important role in the TS of swimbladder at large aspects and can reduce the same by as much as 10 dB or more.

3. The ellipsoid model provides a more realistic shape for a fusiform fish such as salmon as well as their swimbladders, requiring three parameters of length, height and breadth (L, H, B). The height and breadth variation of the fish plays as important a role as the length in determining TS. Previous studies have in general modeled fish by one (length) or two (length and average diameter) parameters [Love, 1975; Furusawa, 1988].

4. Although the fish body and swimbladder are modeled as ellipsoids, they need only be convex surfaces with fish length to wavelength ratio greater than 25 for the TS model to be valid. This model can be used as long as the radii of curvature can be obtained for any point on the surface of the target.

5. The TS model can easily be adapted to other species given appropriate morphological parameters as long as both fish body and swimbladder are convex surfaces. It can also be applied to fish with no swimbladder.

6. This model along with the measurements on fish provides not only accurate predictions of TS but also the variations in TS resulting from the variations in other parameters (such as fish height and breadth as a function of length), consistent with observations. These calculations provide uncertainties in using TS to estimate biomass or to perform species discrimination.

With the TS model and the fish size distribution, the direct model approach is used to generate artificial sonar data. The sonar data is consistent with experimental sonar data. With the ability to change parameters in any of the blocks of the direct model, the artificial sonar data can be analyzed with respect to any contributing parameters. This result provides a method of studying the interaction of sonar parameters to conclude which will work best for each situation of sonar use. The

inverse model allows for fish counting from either artificial or experimental sonar data, thus allowing for more reliable measures of error in fish counts, and for methods of improvement to the fisheries acoustics problem.

MATLAB (v. 5.3, R11.1) is used to generate all numerical, statistical and graphical results throughout this work [Hanselman and Littlefield, 1998]. A description of the programs designed to perform the numerical simulations in the fisheries acoustics problem are provided in a separate report [Sonwalkar, *et al.*, 2002].

Chapter 2

FISH DISTRIBUTION MODEL

To begin the direct model of the fisheries acoustics problem, the fish distribution model is needed. This overall distribution has several parts. First, the model uses a distribution of the size of the fish taking into account the shape and size of the fish body. Next, the model uses a distribution of the shape and size of the swimbladder. The swimbladder is important as it is an essential organ in many fish species providing the majority of sound reflection [Foote, 1980]. Lastly, the model determines the distribution of the fish in the water ensonified by the beam. The location of the fish in the beam is essential to correctly calculate the beam factor and adjust the target strength appropriately. When several fish are in the beam, the locations are needed to correctly calculate the interference, if any, of the returning echoes.

2.1 Size Distribution for Sockeye Salmon

The size distribution of sockeye salmon is discussed in this section. Often, the only size parameter measured or discussed is the length of the fish. Sometimes, under the assumption that the fish has a circular cross-section, a radius is also mentioned. Sockeye salmon do not have a circular cross-section, but rather an ellipsoidal cross-

section in all three planes. thus a length. height. and breadth are considered. These parameters have been measured by a few researchers for other fish species [Furusawa. 1988: Haslett. 1960: Foote and Ona. 1985: Jech *et al.*. 1995] providing similar measurements as discussed later in this section. Little work has been done in this area for Pacific salmon. Dahl [1982] provided TS estimates for Pacific salmon: however. only using a length estimate. Most of the fisheries management and technical reports listed in section 1.2 have length distributions for various Pacific salmon. but this is the extent of morphological information [Daum and Osborne. 1996: Fleischman. *et al.*. 1995: Huttunen and Skvorc. 1994. 1996: Konte *et al.*. 1996: LaFlamme. 1995: Maxwell *et al.*. 1997: Osborne and Daum. 1997: Vania and Huttunen. 1996: Vaught and Molyneaux. 1995: BioSonics. 1998: Burwen *et al.*. 1995: Dahl *et al.*. 2000: Ehrenberg. 1989. 1995: Ehrenberg and Johnston. 1996: Iverson. 1995: Steig and Johnston. 1996: Xie *et al.*. 1997] A distribution model for the size of the sockeye salmon fish body is determined analytically and then specifically using data.

Figure 2.1.1 shows a schematic of a typical sockeye salmon found in Alaska waters. the coordinate system used. and the ellipsoid model. Panel (a) shows a schematic diagram of a fish with its orientation in the assumed coordinate system. The fish is assumed to be oriented with its length. L_f. along the z-axis. height. H_f. along the y-axis. and breadth. B_f. along the x-axis. Biologists call the salmon a fusiform fish. which means the fish body naturally takes on an ellipsoid shape - not a prolate spheroid or spheroid shape [Bond. 1996]. Panel (b) shows the fish and the swimbladder modeled as separate ellipsoids each with three parameters. length L. height H. and breadth B and shown as ellipses in the $y - z$ plane (projection of ellipsoids). Subscripts of 'f' and 's' are used to distinguish between fish parameters and swimbladder parameters. The incident wave and reflected waves from both the

fish body and the swimbladder are shown as well. This model is a good approximation to the general shape of the fish, except near the tail end, where the fish is about 10% longer than the corresponding ellipsoid.

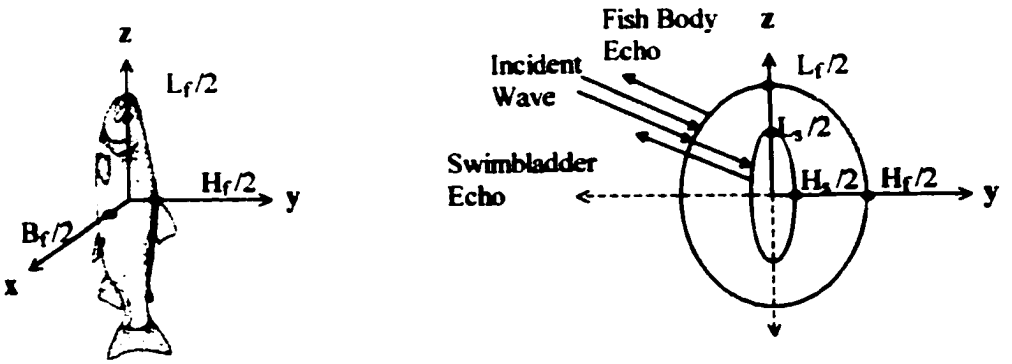

Figure 2.1.1 Schematic of sockeye salmon and ellipsoid model. (a) Schematic diagram of a fish shows its orientation in the assumed coordinate system. The fish is assumed to be oriented with its length, L_f, along the z-axis, height, H_f, along the y-axis, and breadth, B_f, along the x-axis. (b) The fish and the swimbladder are modeled as separate ellipsoids and shown as ellipses in the $y-z$ plane (projection of ellipsoids). The incident wave is shown falling on the fish body surface with some reflection and some transmission of the sound wave. The reflected waves are shown from both the fish body and the swimbladder.

Measurements of length, height and breadth of 610 sockeye salmon (270 male and 340 female) from the Wood River near Dillingham, Alaska and in Cook Inlet near Anchorage, Alaska were collected during the summer of 1998. The fish were caught using seine nets, measurements were taken using millimeter calipers, the sex was determined visually by an ADFG fisheries technician, and the fish were released. Although data was collected from two different regions, the sockeye salmon tend to be relatively at the same growth stage in both locations and thus the data are consistent. Also, the seine nets do not introduce a size selection bias as would gill

nets. Figure 2.1.2 shows the raw data for all fish combined into one set by plotting the height and breadth separately as functions of length. Figure 2.1.3 shows the raw data in the same format as the previous figure after separating the data into two sets, data obtained from the female salmon and from the male salmon. All measurements are in mm.

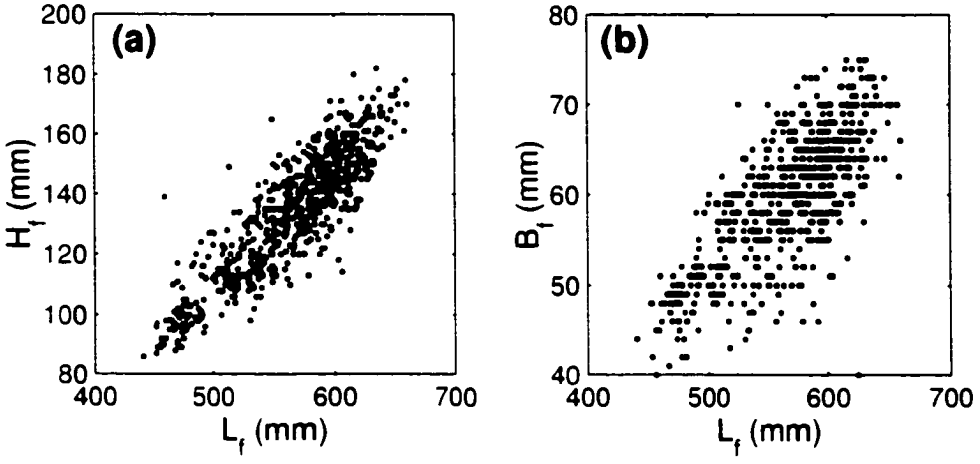

Figure 2.1.2 Raw size data for all fish. The raw size data is shown for all fish combined into one set by plotting the fish height and fish breadth separately as functions of fish length. The data for the 610 fish were collected from the Wood River near Dillingham, Alaska and from Cook Inlet, Alaska. All measurements are in mm.

In most cases of morphological data collection, some form of the fish length is generally the only size data collected. For salmon species, total fish length is measured from the tip of the snout to the fork of the tail. Fork length is measured from mid-eye to the fork of the tail. In order to calculate the other size measurements from a given fish length, a statistical distribution is calculated from the data as a function of fish length. The procedure and results are given in more detail below.

The fish size distribution can be represented by a probability density function (pdf), defined as $f_{size}(B_f, H_f, L_f, S_f)$, where the variable S_f represents the sex ($S_f = 1$, male; $S_f = 2$, female) of the fish. The pdf for f_{size} is assumed to have the following

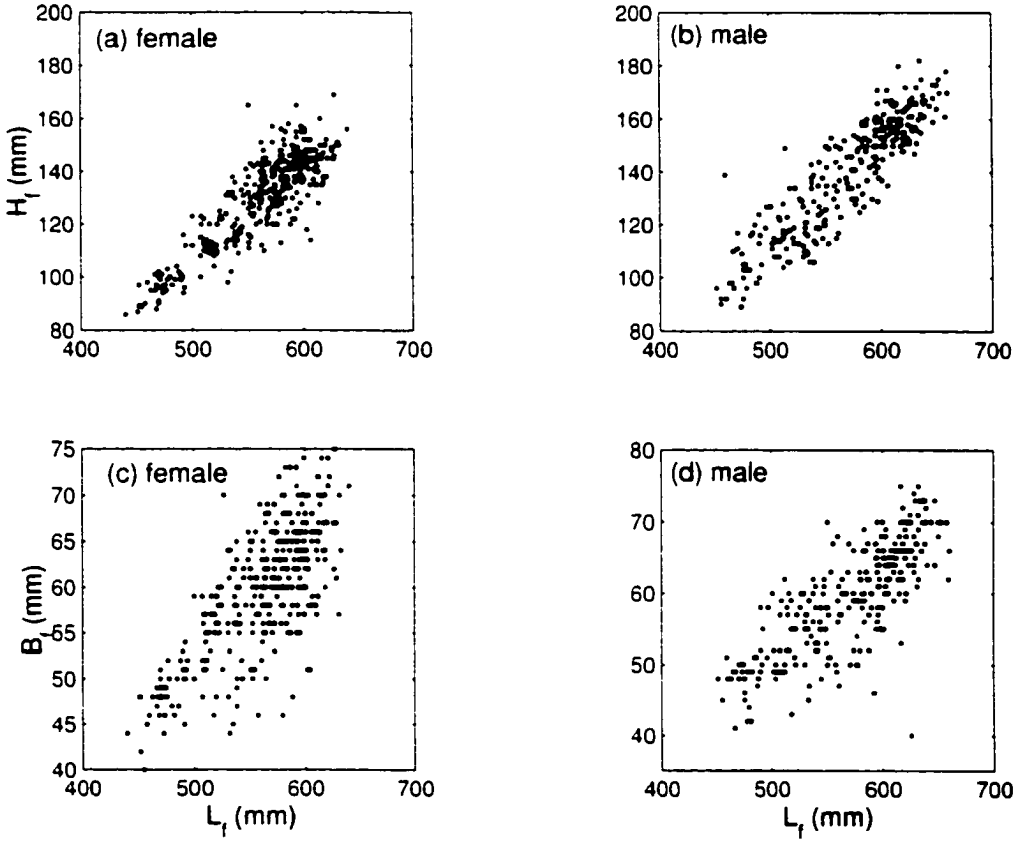

Figure 2.1.3 Raw size data for female and male fish. The raw size data shown in Figure 2.1.2 is now plotted separately for data obtained from female salmon (left two panels) and data obtained from male salmon (right two panels). Again, the fish height and fish breadth measurements are shown as functions of fish length and all measurements are in mm.

form.

$$f_{size}(B_f, H_f, L_f, S_f) = f_S(S_f) \cdot f_L(L_f|S_f) \cdot f_H(H_f|L_f, S_f) \cdot f_B(B_f|L_f, H_f, S_f), \tag{2.1.1a}$$

where $f_S(S_f)$ is the pdf for the sex of the fish, $f_L(L_f|S_f)$, is the conditional pdf for the length given the sex, $f_H(H_f|L_f, S_f)$ is the conditional pdf for height given length for each sex, and $f_B(B_f|L_f, H_f, S_f)$ is the pdf for breadth given height and length for each sex. It is assumed $f_S(S_f)$ is a binomial distribution with α_m the probability of the fish being male. All these distributions must be determined empirically from data, and so may vary depending on species, location, time of year, or other attributes. The distributions for only sockeye salmon are given here with comparisons of the measurement data to the few other references available.

Often, the sex of the fish may be unknown, so a second pdf can be obtained from Equation (2.1.1a) by using the distributions independent of S_f. The pdf without regard to sex becomes

$$f_{size}(B_f, H_f, L_f) = f_L(L_f) \cdot f_H(H_f|L_f) \cdot f_B(B_f|L_f, H_f). \tag{2.1.1b}$$

The analysis performed on the total data is similar to that performed on the data after separating measurements of male fish and female fish. The discussion will pertain to the data set without regard to sex but results will also be given for male and female separately when possible.

The data suggests that $f_L(L_f|S_f)$ or $f_L(L_f)$ may be modeled as a Gaussian or a gamma distribution. Figure 2.1.4 (top panel) shows the histogram of the length of all fish (without regard to sex) and the maximum likelihood estimate (MLE) fits assuming Gaussian (solid line) and gamma (dotted line) fits. The MLE estimates give about the same results for these two distributions. The dashed line shows

a skewed gamma distribution fitted to the data by inspection. In this thesis, it is assumed that the length pdf is given by an MLE Gaussian distribution. Thus two parameters, the mean length m_L and the standard deviation σ_L completely represent the distribution. The results are not very sensitive to the details of these distributions.

The data further suggest that $f_H(H_f|L_f, S_f)$ or $f_H(H_f|L_f)$ may be modeled as Gaussian distributions. To determine $f_H(H_f|L_f, S_f)$ or $f_H(H_f|L_f)$, the data (without regard to sex) were divided into ten length bins. The bottom panel of figure 2.1.4 shows the histograms of height within each bin and the clearly good MLE Gaussian fit. From this figure a regression line is extracted that determines the mean height, m_H for a given length. The standard deviation of height, σ_H, is roughly independent of the length.

Length distributions for the data from the female salmon and male salmon are shown in the top panel of figures 2.1.5 and 2.1.6, respectively. Distributions for the separated (female,male) data are shown in the bottom panel of figures 2.1.5 and 2.1.6, respectively.

To determine the distribution, $f_B(B_f|L_f, H_f)$, the original length data were divided into 4 bins organized by increasing length. The size of the data set was too small to perform this process for $f_B(B_f|L_f, H_f, S_f)$. Within each bin the data were further divided into 4 height sub-bins by increasing height. Within each of these 16 bins an average length and an average height are known, and a mean breadth, m_B, and standard deviation, σ_B can be calculated. Figure 2.1.7 shows the breadth distribution within each of the 16 bins with Gaussian fits. From these results, multiple linear regression is used to determine the best fit to the breadth data based on the length and height data. The standard deviation of breadth, σ_B, is roughly

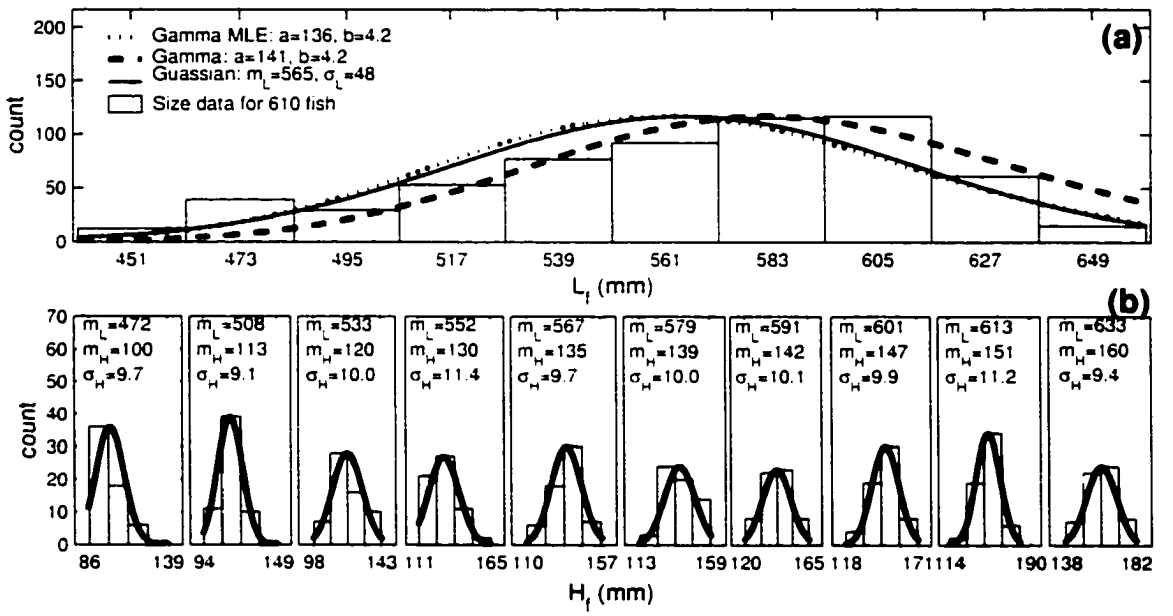

Figure 2.1.4 Histograms for length and height using data from all fish. (a) The histogram is shown of the length of all fish (without regard to sex) and the maximum likelihood estimate (MLE) fits assuming Gaussian (solid line) and gamma (dotted line) fits. The MLE parameters for each fit are listed in the legend. The MLE estimates give about the same results for these two distributions. The dashed line shows a skewed gamma distribution fitted to the data by inspection. Ten fish length bins were used based on the size of the data. (b) The height distribution within each length bin is shown as a histogram with a Gaussian distribution fit. The average length, m_L, average height, m_H, and the standard deviation of the heights, σ_H are shown for each bin.

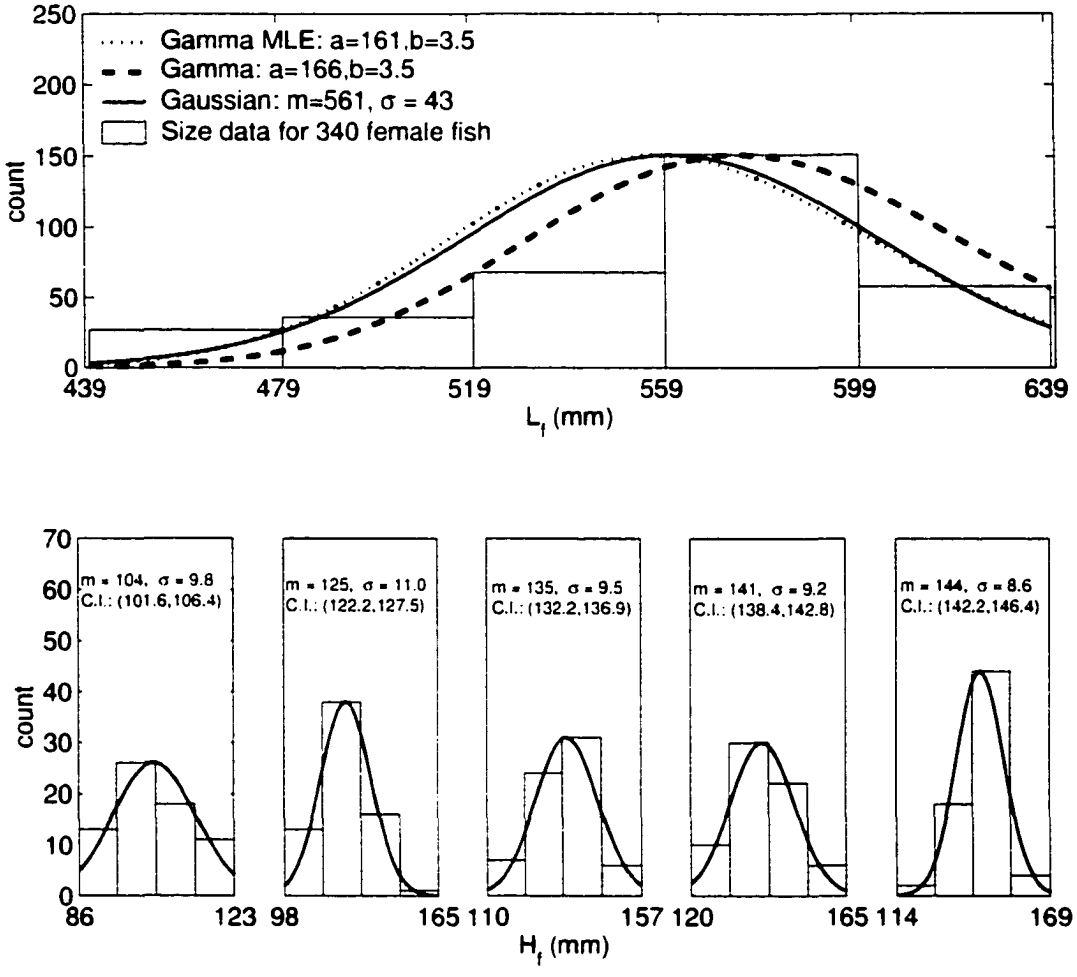

Figure 2.1.5 Histograms for length and height using data from female salmon. (a) The histogram is shown of the length of fish from female salmon only and the maximum likelihood estimate (MLE) fits assuming Gaussian (solid line) and gamma (dotted line) fits. The MLE parameters for each fit are listed in the legend. The MLE estimates give about the same results for these two distributions. The dashed line shows a skewed gamma distribution fitted to the data by inspection. Five length bins were used based on the size of the data. (b) The height distribution within each length bin is shown as a histogram with a Gaussian distribution fit. The average height, m, the standard deviation of the heights, σ, and a 95% confidence interval are shown for each bin.

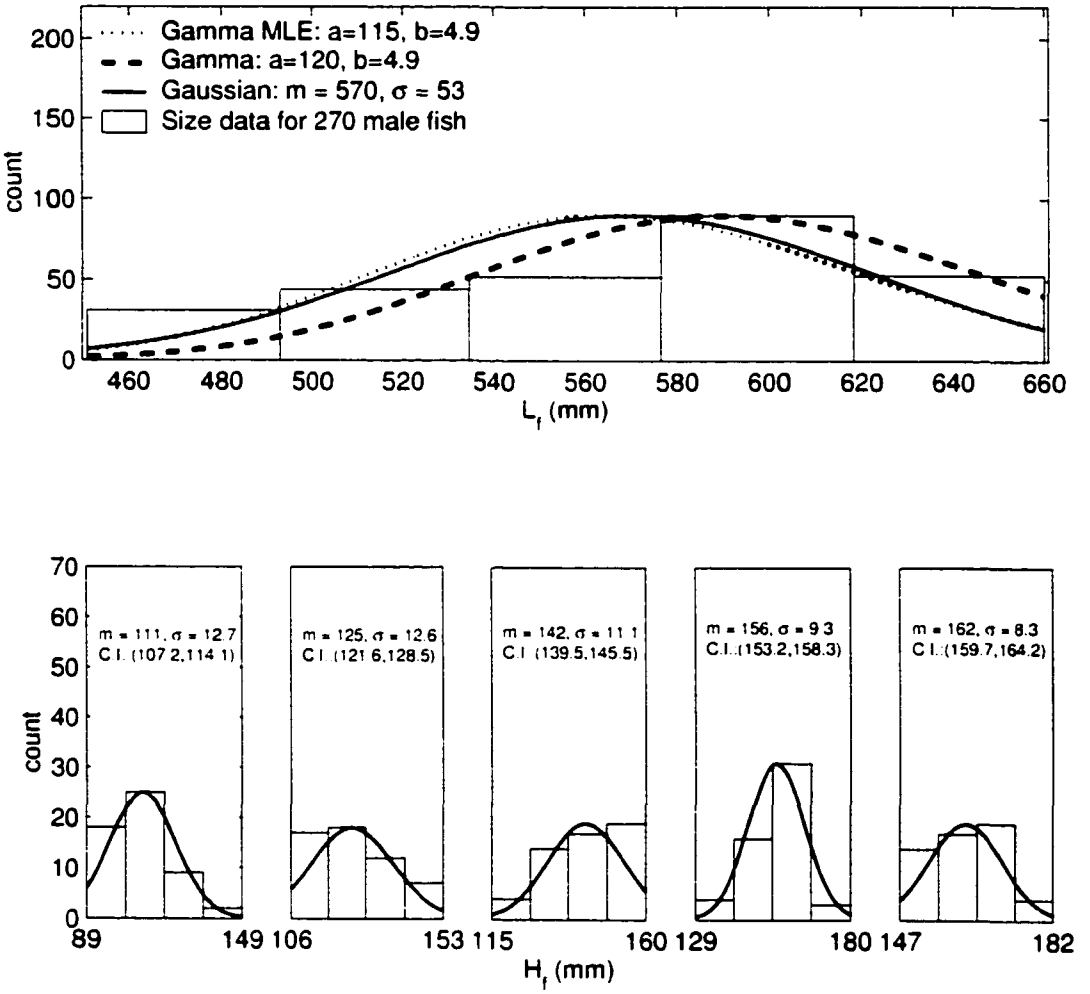

Figure 2.1.6 Histograms for length and height using data from male salmon. The same distributions are shown as in Figure 2.1.5 but for the size data collected on male salmon only..

independent of the length and height. This fit will allow for reasonable fish sizes to be chosen at random.

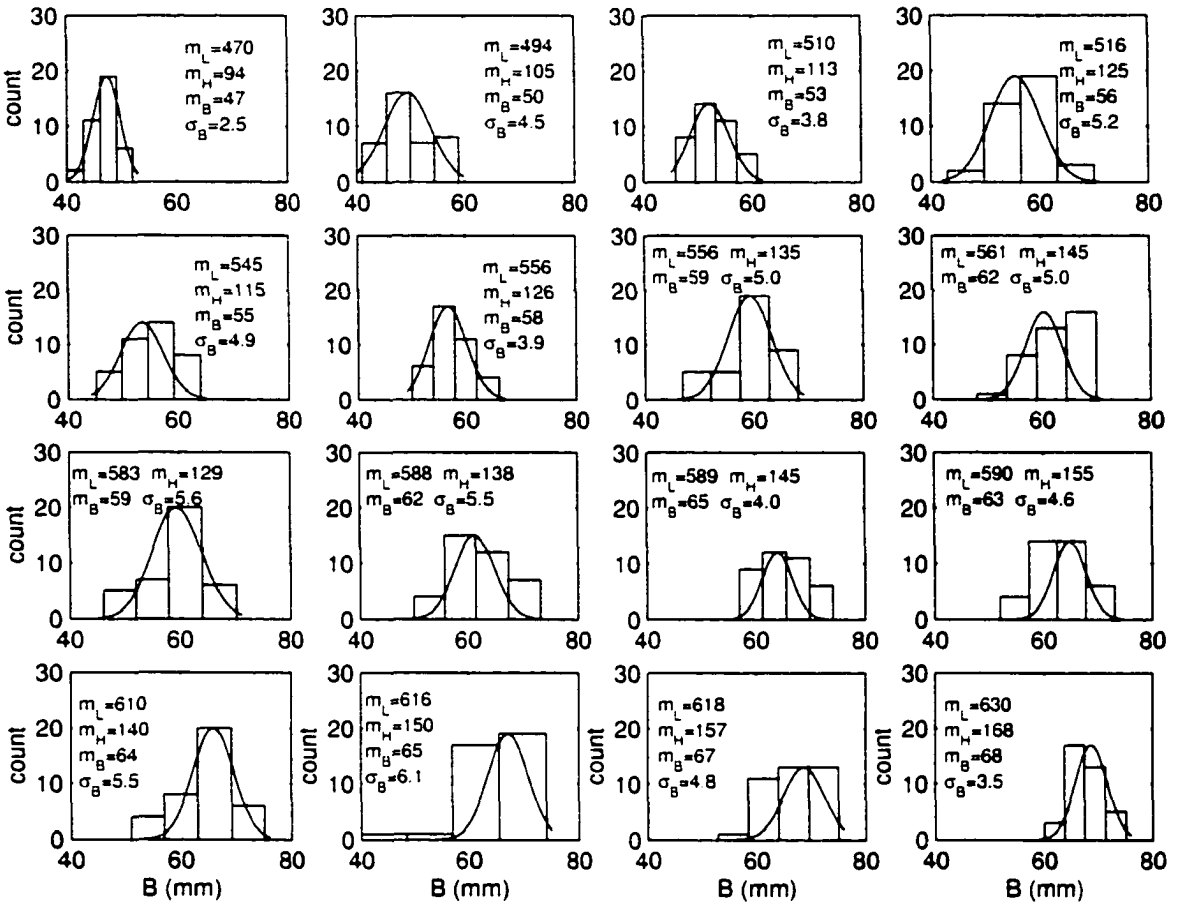

Figure 2.1.7 Histograms for breadth using data from all fish. The length data shown in Figure 2.1.4 were divided into 4 bins organized by increasing length and then each were further divided into 4 height sub-bins by increasing height. The breadth distributions for each of these 16 bins are shown with Gaussian fits. The average length, m_L, average height, m_H, average breadth, m_B, and the standard deviation of the breadths, σ_B are shown for each bin.

The results of the statistical analysis are summarized in Table 2.1. Note that although the regression line may be slightly more accurate when the data are separated by sex, this approach is not as realistic for real time data collection since the sex is unknown as the salmon moves through the sonar beam.

The table provides the mean (m_L) and standard deviation (σ_L) of the length

Table 2.1 Statistical Parameters for Sockeye Salmon Size in mm.

	all	male	female
m_L	565	570	561
σ_L	48	53	43
m_H	$0.369 * L - 74.4$	$0.374 * L - 74.1$	$0.346 * L - 64.7$
(R^2)	(99.7%)	(99.0%)	(99.7%)
σ_H	10.0497	10.8144	9.6267
m_B	$0.0728 * L + 0.1379 * H$	NA	NA
(R^2)	(99.9%)		
σ_B	4.9	NA	NA

data collected from each of the three sets of data (data from all fish, data from males only, data from females only) in mm. The regression lines are calculated for each set of data for the average height dependent on the fish length as shown under the column (m_H). The standard deviation of height data for each set are listed under (σ_H). The regression line for the average breadth conditional on height and length for the data set of all fish combined is shown under the column (m_B) with the standard deviation of breadth last under (σ_B). Again, the data sets for male and female only were too small to perform the analysis of breadth depending on height and length and thus those places in the table are left empty.

Using various parameter values given in Table 2.1, it is possible to construct an ensemble of salmon of various sizes consistent with the data. In obtaining such distributions, random number generators are used that are appropriate for each distribution. The high R^2 values for each regression line indicate a good fit of the model with the data in each case. To avoid generating physically meaningless size data, only those values of each parameter lying within 2.5 standard deviations of the

respective means are kept. This process has been accounted for in the probability models.

2.2 Swimbladder Model for Sockeye Salmon

The swimbladder shape and size are more complicated than the fish body itself. As the salmon swims, the swimbladder changes shape and position filling with air and losing air. However, the swimbladder is confined within the body due to the location of the kidney above, the ribs surrounding it, and the intestines and reproductive organs below it. With this in mind, the shape can still be thought of as various types of ellipsoid models as discussed below. Also, the swimbladder size will depend on the fish size. Extra parameters are used to keep this relationship within reason.

An analysis using x-ray pictures of fifteen sockeye salmon was performed to determine the size and shape of the swimbladder. Three sockeye salmon x-rays were provided by Dr. John Horne with fish obtained from Kenai, Alaska by Debby Burwen of Alaska Department of Fish and Game (ADFG). The other twelve were x-rayed at Fairbanks: three sockeye were obtained from the Copper River, near Chitna, Alaska and the remaining nine were obtained from the Gulkana Hatchery at the Gulkana River, Paxson, Alaska. Each swimbladder was characterized by three parameters, length L_s, height H_s, and breadth B_s. The features found are in general true for all the fifteen sockeye salmon inspected.

Figure 2.2.1 shows an example of one set of digitized swimbladder x-rays from Kenai, Alaska with various model fits. The set includes a cross-section in the $y-z$ plane (lateral or side view) showing length, L_s, and height, H_s, in both (a) and (b) and one in the $x-z$ plane (dorsal view) showing length, L_s, and breadth, B_s in both (c) and (d). The figure shows that in general the shape of the swimbladder is convex

and relatively ellipsoidal: however, several modifications to a full ellipsoid model can be implemented to better fit the x-ray outline. An ellipse in the dorsal cross-section, except for the tail end, can represent the swimbladder to the first approximation. Since the tail end is so small compared to the rest of the swimbladder, it is likely that an effective length ($L_{s,\,eff}$) of about 80% of the length of the swimbladder will produce a better model. The figure also shows that in general the shape of the swimbladder in the lateral view can be approximated using either a full or half ellipse with an effective length of 80% of the swimbladder length. Lastly, an improved model for the dorsal view can be obtained by considering two different ellipses that fit the data. The model used in (a) is a full ellipse, (b) is a half ellipse, (c) is a full ellipse using $L_{s,eff} = 0.8L_s$, and (d) two ellipses to cover head and tail sections separately.

Figure 2.2.2 shows the remaining cross section data and model. Panel (a) shows a photo of the third possible cross section (in the $x - y$ plane) of a swimbladder from one sockeye salmon. The fish was flash frozen using liquid nitrogen and then cut into 1 inch thick cross-sections with a table saw. Digital pictures were taken immediately. Panels (b) and (c) show a digitized version of the outline of the swimbladder with model fits. They show that as a first approximation the cross-section may be represented by a half ellipse (b), and more accurately by two ellipses (c). Note that to calculate the TS (as introduced in Chapter 1 and more fully discussed in Chapter 3) at dorsal and side incidence, the half ellipsoid is a good model. However, to calculate TS at ventral incidence the cross-section made of two ellipses must be considered since the half ellipse cross-section will give non-zero return only for normal incidence at ventral aspect. Based on this data set, the model will represent the swimbladder as a single half ellipsoid as a first approximation and

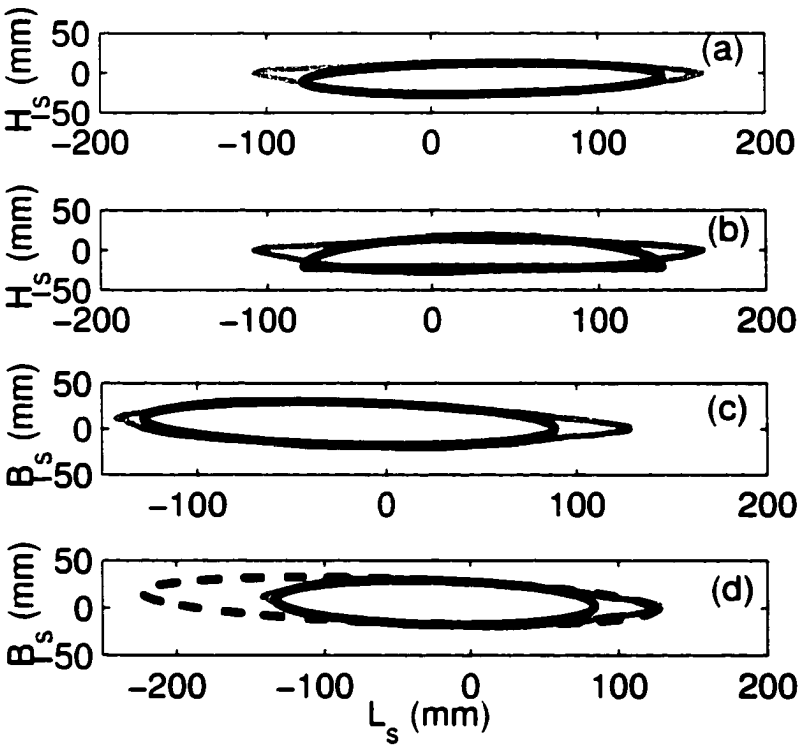

Figure 2.2.1 Model and digitized cross-sections of sockeye swimbladders. An example of one set of digitized swimbladder x-rays from Kenai, Alaska with various model fits is shown. The set includes a cross-section in the $y-z$ plane (lateral or side view) showing length, L_s, and height, H_s, in both (a) and (b) and one in the $x-z$ plane (dorsal view) showing length, L_s, and breadth, B_s in both (c) and (d). In each panel the model fit is shown with a black solid line and the digitized swimbladder is shown with a gray solid line. The model used in (a) is a full ellipse, (b) is a half ellipse, (c) is a full ellipse, and (d) two ellipses to cover head and tail sections separately. The ellipse model used to fit the head section is shown with a black solid line and the ellipse model used to fit the tail section is the dotted black line.

then as composed of four semi- ellipsoids as an improved approximation as described below.

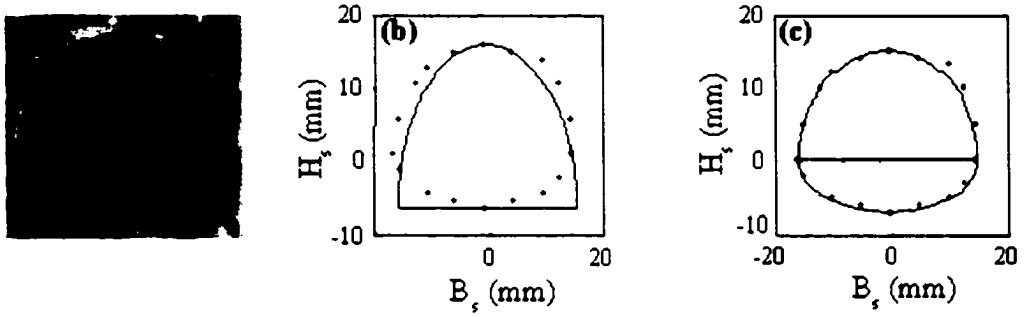

Figure 2.2.2 Digitized cross-section of a sockeye swimbladder. In panel (a) a photo of the third possible cross section (in the $x-y$ plane) of a swimbladder from one sockeye salmon is shown. The dark middle section is the inside of the swimbladder whereas the white outline shows the shape of the swimbladder wall. Panels (b) and (c) show a digitized version of the outline of the swimbladder with model fits to the height (H_s) and breadth (B_s). The digitized swimbladder is plotted using small circles and the model fits are shown as solid lines. These figures illustrate that as a first approximation the cross-section may be represented by a half ellipse as displayed in (b), and more accurately by two ellipses as shown in (c).

The discussion has focused on the swimbladder independently thus far: however, the fish body and swimbladder parameters are not independent. For example, to maintain hydrostatic equilibrium, the volume of the swimbladder is related to that of the fish through the ratio of average density of the fish flesh and air-filled swimbladder and that of water. The examination of the x-rays also shows that the length of the swimbladder is related to that of the total length of the fish. The following three parameters along with the fish size parameters are used to obtain the swimbladder parameters (L_s, H_s, B_s). The parameters provide a ratio of swimbladder length to fish length, p, a ratio of swimbladder height to swimbladder breadth, r, and a ratio of the swimbladder volume to fish volume, q. The range of values of these parameters based on the x-ray data is also given.

$$p = L_s/L_f, \quad 0.24 < p < 0.50 \qquad (2.2.1a)$$

Table 2.2 Morphological Parameters for Sockeye Salmon.

TL (mm)	L_f (mm)	H_f (mm)	B_f (mm)	L_s (mm)	p	H_s (mm)	B_s (mm)	r	$2r$
Kenai									
634	592	131	75	271	0.46	39	47	0.83	1.7
660	611	141	82	296	0.48	47	47	1.00	2.0
591	552	128	72	254	0.46	28	46	0.61	1.2
Copper									
540	480	100	50	243	0.51	23	36	0.64	1.3
570	530	135	69	255	0.48	32	36	0.89	1.8
435	405	83	45	157	0.39	10	23	0.43	0.87
Gulkana									
680	568	160	49	240	0.42	30	32	0.94	1.9
655	551	147	48	250	0.45	35	40	0.88	1.8
565	508	97	46	180	0.35	22	25	0.88	1.8
660	570	158	54	225	0.39	23	28	0.82	1.6
620	541	114	54	235	0.43	26	30	0.87	1.7
690	604	181	52	215	0.36	16	23	0.70	1.4
600	528	138	45	276	0.52	37	33	1.12	2.2
720	596	179	55	257	0.43	20	25	0.80	1.6
660	555	154	43	235	0.42	28	23	1.22	2.4

$$r = H_s/B_s, \quad 0.6 < r < 1.2 \tag{2.2.1b}$$

$$q = V_s/V_f, \quad 0.02 < q < 0.11 \tag{2.2.1c}$$

Table 2.2 shows the measurements taken for each fish taken from the Kenai, Copper, and Gulkana Rivers respectively, where TL is the total length discussed above, and the calculated swimbladder parameters p and r. Usually, q is a fixed value depending on the water salinity. Also, if a half ellipsoid model is used then the value of $2r$ is needed and is also shown in the table.

Note that assuming the net fish density is roughly the same as that of water, it can be shown that for typical fish flesh and water densities the volume of the

swimbladder will be about 2-11% of the volume of the fish. For sea water, the swimbladder volume is typically 2-6% and for fresh water 5-11% of the volume of the fish.

Given the fish body parameters (L_f, H_f, B_f) and the model parameters (p, q, r), the swimbladder size parameters (L_s, H_s, B_s) can be determined completely from Equations (2.2.1). Also, by using these same equations the swimbladder height and breadth can be written in terms of fish size parameters for the half ellipsoid model.

$$L_s = pL_f \tag{2.2.2a}$$

$$B_s = \sqrt{\frac{2q}{pr} H_f B_f} \tag{2.2.2b}$$

$$H_s = \sqrt{\frac{2qr}{p} H_f B_f}. \tag{2.2.2c}$$

For more sophisticated (hybrid) models of the swimbladder represented by multiple half ellipsoids, each half-ellipsoid must have its own set of parameters as described above.

This data set on swimbladder parameters is rather limited and provides only a range of values that are possible. Future work should involve a more detailed characterization of swimbladder parameters along the lines of the fish size model developed above. This will require analysis of a large number of x-ray data on swimbladders, which is beyond the scope of this work.

External verification of these parameter values was obtained through other x-ray pictures and through literature. X-ray pictures of 18 rainbow trout (*Oncorhynchus mykiss*) were provided by Mike Holliman, Ph.D. candidate, Alaska Cooperative Fish and Wildlife Research Unit, University of Alaska Fairbanks. The fish were obtained

Table 2.3 Morphological Parameters for Rainbow Trout.

TL (mm)	L_f (mm)	H_f (mm)	B_f (mm)	L_s (mm)	p	H_s (mm)	B_s (mm)	r	$2r$
280	230	60	38	105	0.46	15	19	0.79	1.58
300	240	62	35	110	0.46	11	20	0.55	1.10
305	247	67	38	114	0.46	18	22	0.82	1.64
311	250	60	34	117	0.47	16	16	1.00	2.00
316	255	73	40	128	0.50	15	20	0.75	1.50
326	265	70	61	130	0.49	19	21	0.90	1.81
331	269	55	40	136	0.51	20	20	1.00	2.00
340	270	66	50	136	0.50	19	30	0.63	1.27
345	280	78	55	142	0.51	21	23	0.91	1.83
350	285	80	45	140	0.49	23	23	1.00	2.00
356	280	78	42	132	0.47	18	18	1.00	2.00
358	287	65	44	153	0.53	21	21	1.00	2.00
361	295	77	40	150	0.51	18	22	0.82	1.64
387	320	85	50	170	0.53	12	20	0.60	1.20
390	325	80	53	165	0.51	23	24	0.96	1.92
396	327	82	45	165	0.50	15	19	0.79	1.58
406	332	92	60	180	0.54	26	22	1.18	2.36
408	342	95	57	184	0.54	20	25	0.80	1.60

from the Fort Richardson Hatchery in Anchorage, Alaska. These fish were part of a pilot study on electrofishing injury conducted in June, 1998. The fish were electroshocked and killed immediately afterward by immersion in a solution of the chemical tricaine methanesulfonate (MS-222). The fish were placed on ice and x-rayed from both a dorsal and side aspect about 24 hours later. From the available 18 x-ray pictures of rainbow trout, a fish belonging to the same biological genus as the sockeye salmon, similar features of fish body shape and size and swimbladder shape and size were found within the same range of values. See Table 2.3 below for values those equivalent categories as in Table 2.2 including total length (TL), size parameters (L_f, H_f, B_f) and swimbladder parameters (p, q, r).

The ranges for the swimbladder parameters p, r are consistent with those found in literature for other species of swimbladder fish. Furusawa [1988] listed the morphological and physical parameters for fish such as sardine (*Sardinops melanostictus*), Japanese mackerel (*Scomber japonicus*), spotted mackerel (*Scomber tapeinocephalus*), Alaska pollack (*Theragra chalcogramma*), sea bream (*Chrysophrys major*), and yellowtail (*Seriola quinqueradiata*) found in another study (published in Japanese) showing similar results to those given in this thesis. Haslett [1960] performed a detailed analysis on the measurement of 6 dissected freshly-caught whiting (*Gadus merlangus*) with 3 dissected transversely and 3 longitudinally, finding comparable results. Foote and Ona [1985] conducted a swimbladder cross section study on 13 pollack (*Pollachius pollachius*) and 2 saithe (*Pollachius virens*) and found consistent values for p only. Also, Jech *et al.* [1995] measured these parameters for threadfin shad (*Dorosoma petenense*) and found similar results for p only.

The results of the sockeye salmon size distributions have been submitted for publication in the Journal of the Acoustical Society of America [Sonwalkar *et al.*, 1999b].

2.3 Spatial Distribution of Sockeye Salmon in River

The distribution of the salmon in the river is important in understanding the sonar data obtained. This distribution includes not only the location of a fish at a certain time, but the idea of the fish movement from location to location and in general its movement while in the sonar beam. The location of a fish at a given time may not always be discernible. When split beam sonar is used, the location can be determined from the received data by using the time difference on the top and bottom receivers and the left and right receivers. Often, in fish studies conducted

in clear water situations, the fish behavior is monitored visually. There have even been some studies performed using video cameras in clear water situation to better understand the movement of fish in a river. From the understanding of fish behavior given in the fisheries management and technical reports a model of fish movement was developed. Both are discussed below [BioSonics, 1998; Burwen *et al.*, 1995; Dahl *et al.*, 2000; Ehrenberg, 1989, 1995; Ehrenberg and Johnston, 1996; Iverson, 1995; Steig and Johnston, 1996; Xie *et al.*, 1997].

2.3.1 Spatial distribution given in reports

Although each sonar configuration is different depending on river conditions and equipment used, some general procedures are certain. Figure 2.3.1.1 shows a typical configuration for a sonar project on an Alaskan river [Osborne and Daum, 1997]. This figure comes from the field study performed on the Chandalar River, August 8 - September 22, 1996. The river bottom is shown as the dark line, the sonar beams are shown as shaded regions. In this example, two sonar systems are employed, one on each bank of the river to more fully cover a cross-section of the river. The sonar beams are aimed to point downward along the bottom of the beam. Often there may be additional apparatus, such as a weir, used to push fish further away from the bank, in front of the sonar, for better counting. Figure 2.3.1.2 provides data on the number of fish and their distribution in the beam collected throughout the field study by the sonar stationed on the right bank. The top panel provides the vertical distribution of the fish within the sonar beam. The peak is centered around $\sim -1^\circ$ with a mean of -0.66° showing that the fish are swimming close to the river bottom. The bottom panel shows the range of the fish counted for over 130,000 fish. Notice that the peak of the distribution for upstream migrating chum salmon

Oncorhynchus keta) centers around 11 m. with a mean of 15.5 m, rather close to the bank for a river $\sim$ 130 m wide [Osborne and Daum. 1997].

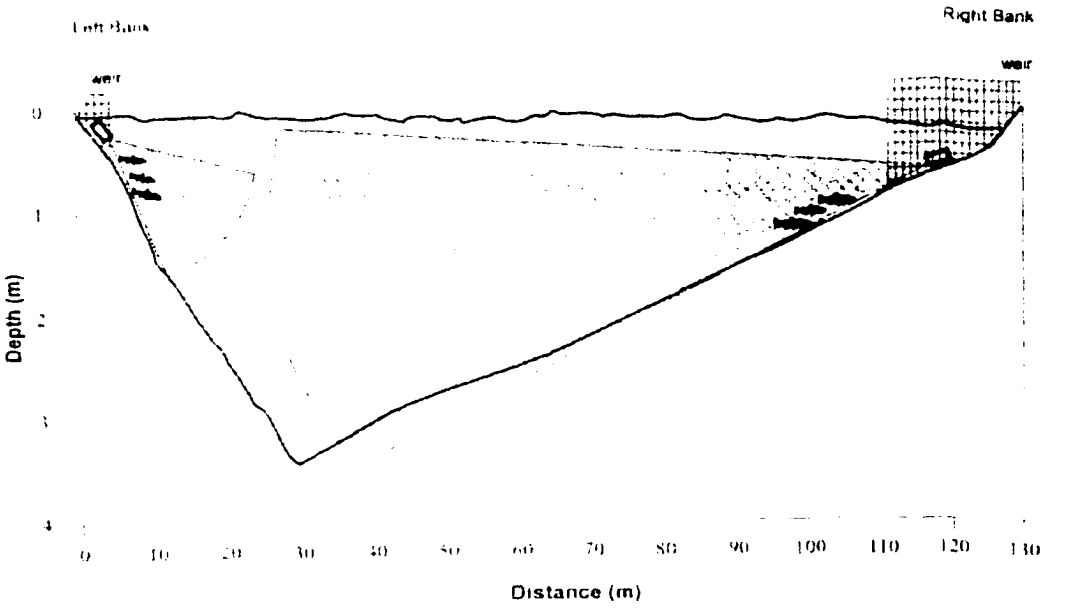

Figure 2.3.1.1 Typical riverine sonar configuration. A typical configuration for a sonar project on an Alaskan river is shown. The $x-$ axis shows the width in meters of the river, the $y-$ axis shows the depth in meters. The outline of the river profile is shown with the dark solid lines including the river bottom and the water surface. The sonar beams are illustrated by the shaded region [Osborne and Daum. 1997. p. 28].

These findings of fish distribution in the river are similar to those published by other agencies working with Pacific salmon. Burwen. *et al.* [1995] discovered the distribution of chinook salmon. *Oncorhynchus tshawytscha.* to also follow close to the river bottom and to the banks of the 90 m Kenai river. Maxwell. *et al.* [1997] reported on several species of *Oncorhynchus* with range distributions averaging between 30 and 50 m from the banks of the 300 m wide Yukon river.

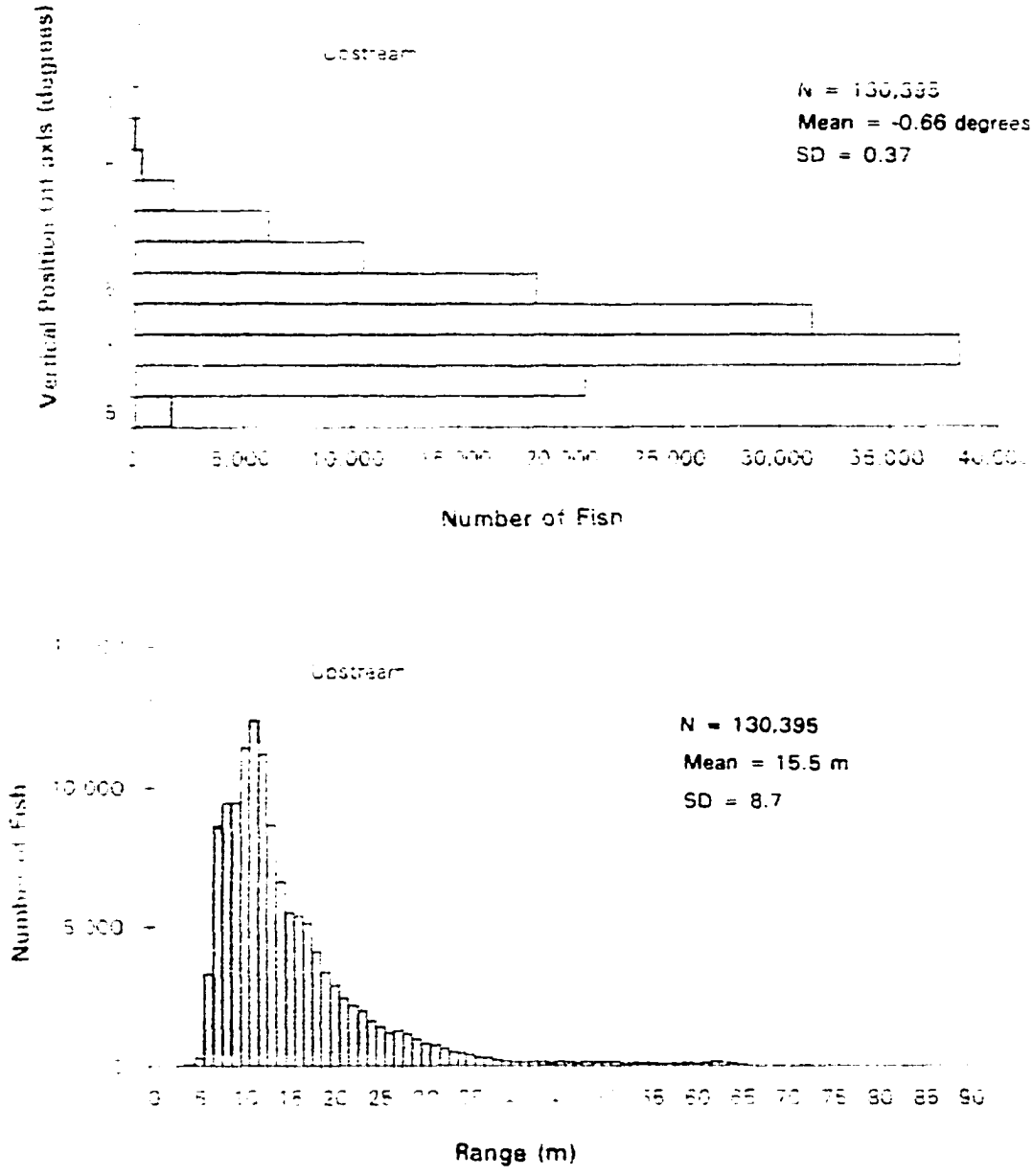

Figure 2.3.1.2 Fish distribution in river. This histogram provides data on the number of fish and their distribution in the beam collected throughout the field study using the sonar system stationed on the right bank. The top panel provides the vertical distribution of the fish within the sonar beam. The peak is centered around ~ −1° with a mean of −0.66° showing that the fish are swimming close to the river bottom. The bottom panel shows the range of the fish counted for over 130.000 fish. Notice that the peak of the distribution centers around 11 m, with a mean of 15.5 m. rather close to the bank for a river ~ 130 m wide [Osborne and Daum. 1997].

2.3.2 Spatial distribution model results

Another aspect of the fish distribution model is the fish movement or swimming behavior. On the average, salmon move either downstream or upstream, but their detailed motion through the sonar beam is complicated. Although some patterns in movement have been observed in migrating salmon, in general they move through the river changing direction and velocity at random. Furthermore the inaccuracies in the measurement of aspect using split-beam sonar creates more difficulties in understanding their true patterns of movement. A model developed by Biao Chen [2001] includes a model of fish movement. The swimming behavior includes the fish location in the river, modeled as close to the banks and the river bottom, and the velocity distribution calculated from each recognized location of the fish in the beam.

Chen [2001] built a fish movement model based on the data collected during the experiment conducted by Osborne and Daum [1997] mentioned above. From the experimental split-beam sonar location data, a velocity distribution was created. A velocity distribution, along with fish locations, accounts for (1) the location of the fish at a given time, (2) the direction in which the fish moves at that time, and (3) the time it takes for the fish to arrive at its next location in modeling fish movement. It is important to analyze the velocity distribution from existing sonar data to be consistent and accurate.

Using the fish velocity model, a fish location model was developed by defining a cross-section of the river and a corridor in which the fish swim. The river cross-section is defined as a segmented linear function and the corridor by an exponential probability density function. Through this pdf, a random perpendicular distance from the fish to the bottom of the river is chosen and thus confines the random fish

distribution to that corridor. For this purpose a parameter, D, is defined, which is the average distance of the salmon from the banks or the bottom. By choosing the correct value of D, the distribution of the fish or essentially how close they are to the banks or the bottom can be decided. Physically, when the fish is swimming, it does not literally leave the water through the surface of the river or become embedded in the river bottom. Thus fish movement constraints and stop conditions are considered to allow the fish track to remain in the river cross section and follow a realistic path. Figure 2.3.2.1 shows four examples of the modeling results based on values of D. The river cross-section is shown with the lines representing the bottom. The randomly generated fish positions are shown as stars. Note that as the value of D becomes smaller, the distribution becomes tighter to the bank and bottom [Chen, 2001].

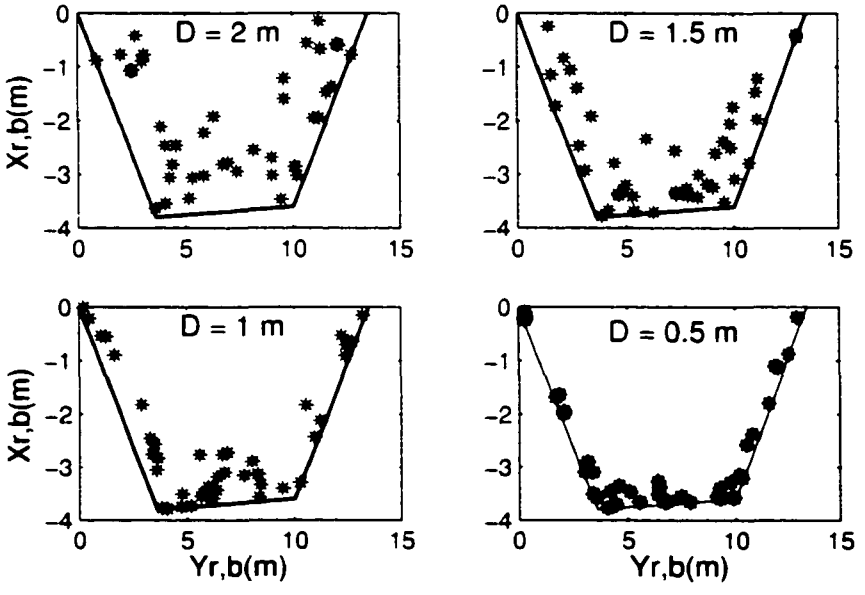

Figure 2.3.2.1 Model results of fish distribution. Model results of the fish distribution are shown based on values of D. A generic river cross-section is shown using solid lines in each panel. The randomly generated fish positions are shown as stars in the two-dimensional view of the river cross-section. As the value of D becomes smaller, the fish positions are closer to the river banks and bottom [Chen, 2001].

Figure 2.3.2.2 shows modeling of 3D fish motion using the approach from that work. The top panel shows projections of three fish tracks generated by a computer model of the fish motion. The fish is assumed to begin its motion at (0, -5, 5) and move in the x direction with an average speed of 1 m/s. The changes in the fish velocity are assumed to take place at random (Poisson distribution) with roughly 2 per second. Speeds in the x, y, z directions vary at random (Gaussian distribution) with mean velocity in the y and z direction zero and standard deviations 1 m/s. The middle left panel shows the geometry and the right panel shows the 3D plot of the tracks shown in the top panel.

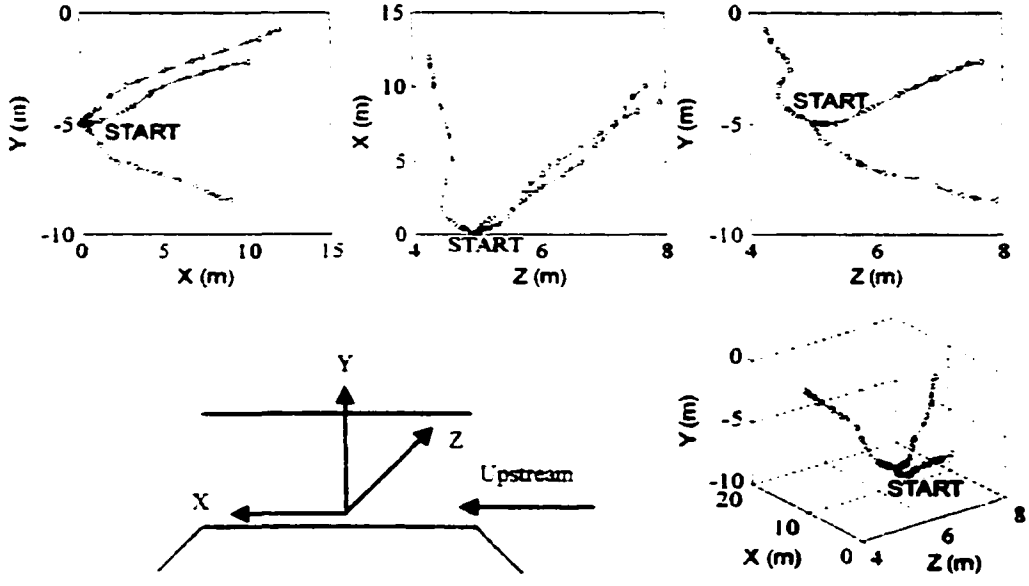

Figure 2.3.2.2 Fish motion generated randomly. Modeling of the three-dimensional fish motion is shown using various views. The knowledge gained from the analysis of fish tracks was used to create a model representing the motion of the fish through the water. With the same starting position, the model provides random paths as shown here with three examples. The path in three-dimensions is shown in the bottom right panel. The two-dimensional views are shown in the three top panels. The river coordinate system is shown in the bottom left panel. See text for further details [Chen, 2001].

The results of this chapter will be used to generate a fish track moving through a sonar beam to generate sonar data. The data, based on the sonar equation described

in section 1.3. will include a measure of the size and shape of the fish and its swimbladder through the target strength parameter (TS) and a reference to its location in the beam through the angular position given by (θ, ϕ).

Chapter 3

TARGET STRENGTH MODEL

The target strength of an object is a key parameter in determining the amplitude of the sonar echo. Much research has been accomplished to understand this parameter through theory, experiments, and empirical studies [MacLennan and Simmonds, 1992; MacLennan and Holliday, 1996]. The earlier work on TS involved experimental work using physical spheroidal models to determine scattering [Haslett, 1962a, b, 1964b] and empirical fits to observed scattering from marine fish [Love, 1975; Foote, 1985]. Most of the theoretical work is done for marine animals, e.g., zooplankton, at low frequencies (< 100 kHz) such that typical length (L) to wavelength (λ) ratio is smaller than ~ 25 [Stanton, 1988a, b, c, 1989, 1993, Stanton *et al.*, 1998a, b, c; Chu and Stanton, 1999], sometimes even less than one. As a result increasingly complicated anatomical models such as those constructed from x-rays of swimbladders are used with Kirchhoff's integral scattering approach to calculate TS of marine fish [Clay and Horne, 1994; Horne and Clay, 1998]. These numerical models involve complex calculations taking into account detailed physical shape of the swimbladder at either dorsal or side aspect.

Riverine fisheries acoustics, on the other hand, involve relatively large frequencies ($\sim 200 - 400$ kHz) and, in Alaska, large fish ($L > 50$ cm) giving a rather large

$L/\lambda \geq 150$. The Pacific salmon and its swimbladder have roughly convex shape that can be approximated by shapes such as ellipsoids. Recognition of these two factors allowed development of a geometrical approach to TS calculation for salmon as a function of size, shape, and aspect.

This chapter presents the derivation of the geometric model of TS using an ellipsoid model for the target, the limitations and restrictions of this model and various special cases providing analytic results for TS. A comparison of the geometric model with the Kirchhoff's Integral for the ellipsoid model is given next providing further justification for the use of the geometric model. Next, to show the model's versatility, various model results are shared for TS as a function of size, shape, and aspect of the target. Lastly, a comparison of model results with experimental results is given to show the accuracy of the model and to discuss how the model can quantify uncertainties in sonar data and attribute the uncertainties to other factors, such as unknown size data.

The results presented in this chapter have been submitted to the Journal of the Acoustical Society of America for publication [Sonwalkar *et al.*, 1999a].

3.1 Derivation of the Geometric Model

The target strength model presented here is a geometrical scattering model developed using arbitrarily oriented ellipsoids for both the fish body and the swimbladder. As discussed in Chapter 2, these models work well for the sockeye salmon and other Pacific salmon. Figure 2.1.1 indicates the size parameters used for an ellipsoid model for both the fish (L_f, H_f, B_f) and its swimbladder (L_s, H_s, B_s). These parameters will be used in developing the geometric model of TS.

In general, the model calculates TS using the backscattering coefficient, σ,

through the equation

$$\mathrm{TS} = 10\log(\frac{\sigma}{4\pi}) \tag{3.1.1a}$$

where

$$\sigma = \pi R_P R_1 R_2 \tag{3.1.1b}$$

and where R_1 and R_2 are the radii of curvature of the ellipsoid at the point where the acoustic wave is normal to the surface. R_P is the power reflection coefficient determined using the acoustical impedance of the media at the boundary of reflection. The acoustical impedance for a medium is defined as $\eta = c\rho$ where c is the speed of sound through the medium and ρ is the density of the medium. Figure 3.1.1 shows the radii of curvature R_1, R_2 for a general convex surface when the incident wave **k** hits the surface at the point P. This general definition of target strength focuses on only one boundary; however, more complex definitions are shown later in the chapter. Based on this basic geometric model, more complicated models including contribution from the fish flesh and tilt of the swimbladder with respect to the fish body are also developed and will be discussed later.

Equation (3.1.1) is valid when

$$kR_1, kR_2 >> 1 \tag{3.1.2a}$$

where k is the wave number and R_1 and R_2 are the radii of curvature. Equivalently,

$$2\pi R_1/\lambda >> 1 \quad \text{and} \quad 2\pi R_2/\lambda >> 1. \tag{3.1.2b}$$

where λ is the wavelength.

This inequality is easily satisfied at all aspect angles when the sonar operates at 100 - 400 kHz ($\lambda \sim$ a few mm) and with sockeye salmon as the target (length $\sim$ 500 mm, height $\sim$ 100 mm, breadth $\sim$ 50 mm). It is this recognition that makes it

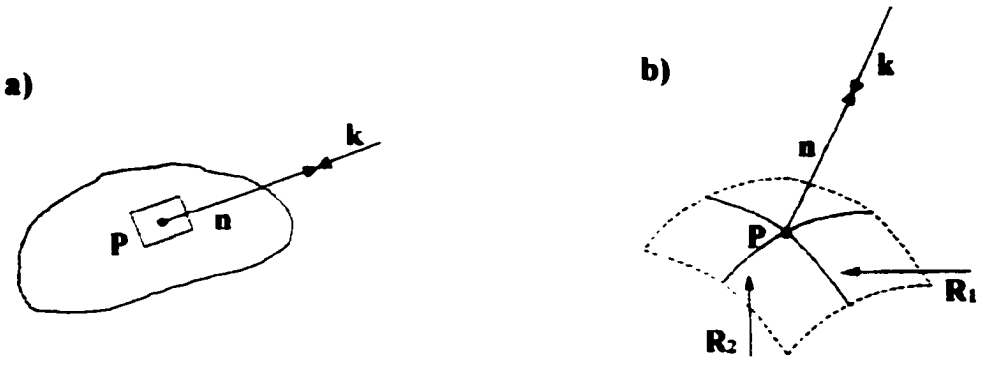

Figure 3.1.1 Radii of curvature for a convex surface. (a) When an incident wave **k** falls on a general, convex surface at a point P, the radii of curvature can be found by considering a small local section of the surface. (b) The radii of curvature R_1, R_2 are shown for a general convex surface at the point P.

possible to calculate TS as a function of aspect using the simple geometric model. At higher frequencies (> 200 kHz) the model is reasonably accurate at all aspect angles. At low frequencies (< 100 kHz), the model will not be accurate at very high aspect (wave incident on the head of the fish). These limitations are further discussed in section 3.3 below.

The model begins by assuming that the fish can be approximated as two concentric ellipsoids - one representing the fish body and the other for the swimbladder. These are given by the following equations using ellipsoid parameters (b_f, h_f, l_f) to define the fish body and (b_s, h_s, l_s) to define the swimbladder.

$$\frac{x^2}{b_f^2} + \frac{y^2}{h_f^2} + \frac{z^2}{l_f^2} = 1. \qquad (3.1.3a)$$

$$\frac{x^2}{b_s^2} + \frac{y^2}{h_s^2} + \frac{z^2}{l_s^2} = 1. \qquad (3.1.3b)$$

Note that l_f, h_f, b_f are semi-axes lengths and thus the total length, height, and breadth are $L_f = 2l_f, H_f = 2h_f, and B_f = 2b_f$, respectively and similarly for the swimbladder parameters. The swimbladder model (3.1.3b) can be modified to use

various shapes other than a full ellipsoid, such as a semi-ellipsoid with flat bottom or combinations of ellipsoids and/or semi-ellipsoids as discussed in chapter 2 above.

The aspect of the fish is defined by two angles (θ_i, ϕ_i) that the incident wave makes in the fish-coordinate system defined in Figure 3.1.1. Figure 3.1.2 provides the definitions of the angles of incidence and the special aspect cases. When the wave normal vector **k** is contained in the $z - x$ plane, it is called side aspect with corresponding range of incidence angles $0° < \theta_i < 180°$ and $\phi_i = 0°$ or 180°. The term normal incidence, side aspect will be used for $\theta_i = 90°$. When the wave normal vector **k** is contained in $y - z$ plane, it is called dorsal or ventral aspect with corresponding range of incidence angles $0° < \theta_i < 180°$ and $\phi_i = 90°$ (ventral) or 270° (dorsal). The term normal incidence, dorsal or ventral aspect will be used for $\theta_i = 90°$.

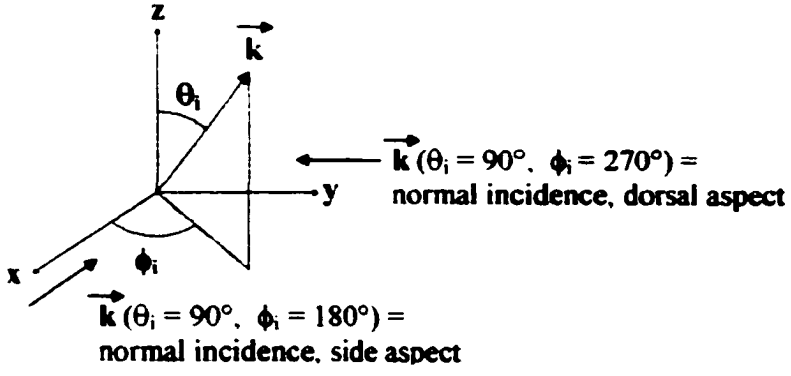

Figure 3.1.2 Notation and incident angle definitions. This schematic provides the definitions of angles of incidence and special aspect cases used in this work. When the incident wave **k** falls on the surface with incident angles of $\theta_i = 90°$, $\phi_i = 180°$ then the terminology normal incidence, side aspect is used. When the incident angles are $\theta_i = 90°$, $\phi_i = 270°$ then the terminology normal incidence, dorsal aspect is used. See text for remaining terminology.

The point (x_0, y_0, z_0) at which the incident wave is normal to the ellipsoid is

given by

$$\mathbf{n_0} = \frac{2x_0}{b^2}\mathbf{x} + \frac{2y_0}{h^2}\mathbf{y} + \frac{2z_0}{l^2}\mathbf{z} = -\mathbf{k}(\theta_i, \phi_i), \tag{3.1.4}$$

where $\mathbf{k}(\theta_i, \phi_i)$ is the unit vector in the direction of the incident wave and $\mathbf{n_0}$ is the normal to the ellipsoid at (x_0, y_0, z_0). Equations (3.1.3) and (3.1.4) can be solved simultaneously to find (x_0, y_0, z_0). Then the two principal radii of curvature can be obtained as follows.

To calculate R_1, consider the ellipse of intersection of the plane $(\mathbf{n_0}, \mathbf{z})$, where $\vec{z}$ is the unit normal in the z direction, with ellipsoid (3.1.3a) (See Figure 3.1.3, wave is incident at the point P). In a certain coordinate system $(x_{\parallel}, y_{\parallel}, z_{\parallel})$ frame this ellipse can be describe by

$$\frac{x_{\parallel}^2}{a_{\parallel}^2} + \frac{y_{\parallel}^2}{b_{\parallel}^2} = 1, \tag{3.1.5}$$

where $a_{\parallel}$ and $b_{\parallel}$ are the semi-major (or semi-minor) and semi-minor (or semi-major) axes lengths of the ellipse. The point (x_0, y_0, z_0) is given by $(x_{0\parallel}, y_{0\parallel})$ on this ellipse. The expressions for $a_{\parallel}$ and $b_{\parallel}$ and $(x_{0\parallel}, y_{0\parallel})$ are complicated and are not given here (they can, however, be derived in a straightforward manner). Then the principal radius of curvature R_1 is given by

$$R_1 = a_{\parallel}^2 b_{\parallel}^2 \left[\frac{x_{0\parallel}^2}{a_{\parallel}^4} + \frac{y_{0\parallel}^2}{b_{\parallel}^4}\right]^{3/2}. \tag{3.1.6}$$

To calculate R_2, consider the ellipse of intersection of the plane $(\mathbf{n_0}, \mathbf{b})$ with ellipsoid (3.1.3a), where $\mathbf{b} = \mathbf{n_0} \times \mathbf{t_0}$ and $\mathbf{t_0}$ is the tangent to the ellipsoid in the $(\mathbf{n_0}, \mathbf{z})$ plane at point (x_0, y_0, z_0) (See Figure 3.1.3, shaded ellipse). In a certain coordinate system $(x_{\perp}, y_{\perp}, z_{\perp})$ frame this ellipse can be describe by

$$\frac{x_{\perp}^2}{a_{\perp}^2} + \frac{y_{\perp}^2}{b_{\perp}^2} = 1, \tag{3.1.7}$$

where $a_{\perp}$ and $b_{\perp}$ are the semi-major (or semi-minor) and semi-minor (or semi-major) axes lengths of the ellipse. The point (x_0, y_0, z_0) is given by $(x_{0\perp}, y_{0\perp})$ on this ellipse.

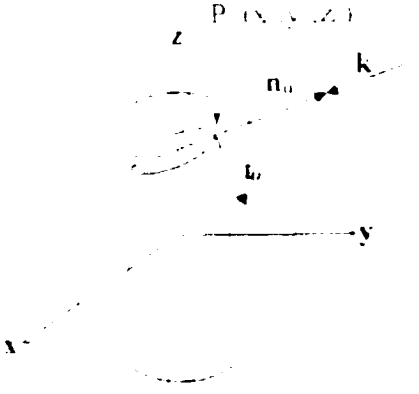

Figure 3.1.3 Schematic of ellipses used to calculate radii of curvature. When the incident wave **k** falls on the surface of an ellipsoid at point P_0 then two ellipses are used to calculate the radii of curvature. The first ellipse (lightly shaded region) is shown in the plane defined by the normal $\mathbf{n}_0$ and the z–axis. The second ellipse, shown by the darker shaded region, is in the plane defined by the normal $\mathbf{n}_0$ and the vector $\mathbf{t}_0 \times \mathbf{n}_0$, where $\mathbf{t}_0$ is the tangent vector in the plane of the first ellipse.

The expressions for $a_\perp$ and $b_\perp$ and $(x_{0\perp}, y_{0\perp})$ are also complicated and are not given here. Then the principal radius of curvature R_2 is given by

$$R_2 = a_\perp^2 b_\perp^2 \left[\frac{x_{0\perp}^2}{a_\perp^4} + \frac{y_{0\perp}^2}{b_\perp^4} \right]^{3/2}. \tag{3.1.8}$$

The radii of curvatures for both fish body (R_{f1}, R_{f2}) and the swimbladder (R_{s1}, R_{s2}) are calculated using the procedure described above along with the appropriate parameters for the fish body (b_f, h_f, l_f) and the swimbladder (b_s, h_s, l_s).

Then the back scattering coefficients and target strengths at 1 m for the swimbladder and the fish body are given by

$$\sigma_s = (\pi R_{Ps} R_{s1} R_{s2}). \tag{3.1.9a}$$

$$\mathrm{TS_s} = 10 \log(\mathrm{R_{Ps} R_{s1} R_{s2}}/4). \tag{3.1.9b}$$

$$\sigma_f = (\pi R_{Pf} R_{f1} R_{f2}). \tag{3.1.10a}$$

$$TS_f = 10\log(R_{Pf}R_{f1}R_{f2}/4). \qquad (3.1.10b)$$

The expressions for power reflection coefficients for the fish body (R_{Pf}) and for the swimbladder (R_{Ps}) are given below:

$$R_{Pf} = \left(\frac{\rho_f c_f - \rho_w c_w}{\rho_f c_f + \rho_w c_w}\right)^2. \qquad (3.1.11a)$$

$$R_{Ps} = \left(\frac{\rho_s c_s - \rho_f c_f}{\rho_s c_s + \rho_f c_f}\right)^2 \approx \left(\frac{\rho_s c_s - \rho_w c_w}{\rho_s c_s + \rho_w c_w}\right)^2 \qquad (3.1.11b)$$

where ρ_w, ρ_f, ρ_s are the densities of water, fish flesh, and an air filled swimbladder, respectively, and c_w, c_f, c_s are the speeds of sound in water, fish flesh, and the air filled swimbladder respectively. Typical values of these parameters are $\rho_w \sim 1030$ (sea water) kg/m^3, $\rho_f \sim 1070$ kg/m^3, $\rho_s \sim 1.29$ kg/m^3, $c_w \sim 1490$ m/s, $c_f \sim 1570$ m/s, and $c_s \sim 330$ m/s [Medwin and Clay, 1998; Mitson, 1983; Furusawa, 1988; Denny, 1993]. With these values, $R_{Pf} = 2.040 \times 10^{-3}$ and $R_{Ps} = 0.998$. The small value of R_{Pf} makes the target strength of the fish body much smaller than that of the swimbladder.

Target strengths TS_f and TS_s calculated using the procedure described above provide target strengths $TS_f(\theta_i, o_i, b_f, h_f, l_f, R_{Pf})$ and $TS_s(\theta_i, o_i, b_s, h_s, l_s, R_{Ps})$ of the fish body and the swimbladder, respectively, as functions of angles of incidence and fish and swimbladder parameters. The acoustic properties of the fish and the swimbladder are contained in the reflection coefficients. In this model, the target strengths of the swimbladder and the fish are independent of frequency. However, as discussed below, when combining the reflections from the fish flesh and the swimbladder, the frequency becomes important in the calculation of the relative phase of the echo from the fish body and the swimbladder.

For a first order approximation, the TS of a sockeye salmon can be calculated by considering the swimbladder alone. Foote [1980] showed that for fish with an air

filled swimbladder, usually about 95% of the reflected sound could be attributed to the reflection off the swimbladder alone. Second order effects arise considering that the wave has to first travel through the fish body before reaching the swimbladder. Figure 3.1.4 shows the geometry of the ray propagation used to calculate the effect of fish flesh on the target strength of the swimbladder with incident angle θ_0 and reflected angle θ_1. There are two effects to consider: (1) a slight bending of waves through the fish body and (2) the modification of the reflection coefficient.

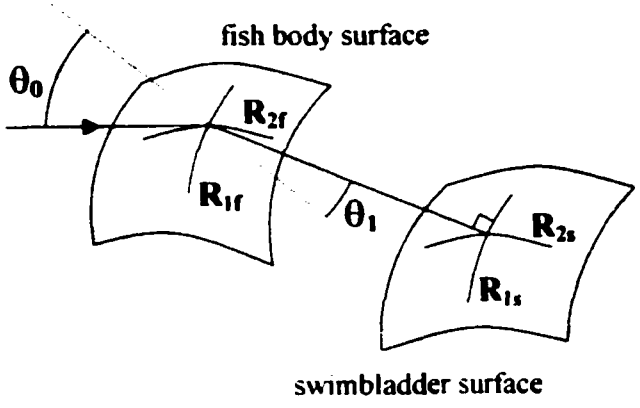

Figure 3.1.4 Geometry of ray propagation. Shown is the geometry of the ray propagation used to calculate the effect of fish flesh on the target strength of the swimbladder with incident angle θ_0 and transmitted angle θ_1. As the wave is transmitted through the fish body surface a slight bending of the direction is encountered before the wave falls incident on the swimbladder surface. At each point of incidence, whether on the fish body or the swimbladder surface, the principle radii of curvature (R_{1f}, R_{2f} for the fish body or R_{1s}, R_{2s} for the swimbladder) can be determined.

Consider a wave incident from the first medium (water) on the first convex surface (S_f), representing the fish body surface, at an angle θ_0. The wave refracts in the second medium (fish flesh), with an angle of refraction θ_1, and impinges normally on the second convex surface (S_s), representing the swimbladder. The inside of the swimbladder is the third medium, assumed air. It is assumed that the wave falling normally on the swimbladder retraces its path and returns to the source.

Because three medium and two convex surfaces are involved, both the reflection and refraction at each of the boundary and the geometric spreading of the waves as they fall on each of the convex surfaces must properly be taken into account. The back scattering cross section for this case is given by

$$\sigma_{sf} = (\pi R_{P_{sf}} R_{s1} R_{s2}) G_{\parallel} G_{\perp}. \tag{3.1.12}$$

where R_{s1} and R_{s2} are the two principle radii of curvature in the plane of incidence and in the plane perpendicular to the plane of incidence. The plane of incidence is defined as the plane containing the normal vectors $\mathbf{n_f}$ and $\mathbf{n_s}$ to the fish body at point P_f and the swimbladder at point P_s. $R_{P_{sf}}$ is the net reflection coefficient taking into account reflection and transmission at both the surfaces and is given by

$$R_{P_{sf}} = \frac{(4\rho_f c_f \rho_w c_w \cos\theta_0 \cos\theta_1)^2 (\rho_a c_a - \rho_f c_f)^2}{(\rho_f c_f \cos\theta_0 + \rho_w c_w \cos\theta_1)^2 (\rho_a c_a + \rho_f c_f)^2}. \tag{3.1.13}$$

The factors $G_{\parallel}$ and $G_{\perp}$ represent the geometric spreading of waves in the plane of incidence and in the plane perpendicular to this plane. The expressions for these two factors are given below.

$$G_{\parallel} = \frac{(1+\alpha_1)}{1+\alpha_1\left(\frac{R_{s1}}{R_{f1}}+\frac{2a}{R_{f1}}\right)+\alpha_1^2\left(\frac{aR_{s1}}{R_{f1}^2}+\frac{a^2}{R_{f1}^2}\right)} \tag{3.1.14a}$$

$$G_{\perp} = \frac{(1+\alpha_0)}{1+\alpha_2\left(\frac{R_{s2}}{R_{f2}}+\frac{2a}{R_{f2}}\right)+\alpha_2^2\left(\frac{aR_{s2}}{R_{f2}^2}+\frac{a^2}{R_{f2}^2}\right)} \tag{3.1.14b}$$

In Equations (3.1.14), a is the distance between the points P_s on the swimbladder and P_f on the fish body. The factors α_0, α_1, and α_2 are given below.

$$\alpha_0 = \frac{c_f}{c_w} - 1 \tag{3.1.15a}$$

$$\alpha_1 = \frac{c_f \cos\theta_0}{c_w \cos\theta_1} - 1 \tag{3.1.15b}$$

$$\alpha_2 = \alpha_1 \cos\theta_1 = \left(\frac{c_f \cos\theta_0}{c_w \cos\theta_1} - 1 \right) \cos\theta_1 \qquad (3.1.15c)$$

Note that the expression given for σ_{sf}, the combined reflection from two convex surfaces, is exact in the sense that it is valid for arbitrary values of medium parameters. For the special case of when the first surface is the fish body surface and the second surface is the swimbladder, particular values of the medium parameters are known. It is easy to show that for most values of θ close to 90°, the values of $R_{P_{sf}}$, and $G_{\parallel}$ and $G_{\perp}$ are close to unity and the $TS_{sf} \approx TS_s$, typically within a couple of dB. For incidence very close to the head or tail, the geometric factors become small (~ 0.1), mainly due to the $\frac{2a}{R_{f1}}$ and $\frac{2a}{R_{f2}}$ terms in the denominators. Consequently, the target strength of the swimbladder with the fish flesh taken into account is about 20 dB smaller than that without taking into account the fish flesh. A derivation of Equations (3.1.14) and (3.1.15) is given in Appendix A.

To the first order, the return signal can be considered as a superposition of reflections from the swimbladder and the fish body. Furthermore, since acoustic impedance of fish flesh is close to that of water, the bending and the spreading of the incident wave can be neglected at the water-fish body interface when calculating reflection from the swimbladder. (This will be referred to as the TS total ignoring the effect of fish flesh throughout this work.) The second order effect of fish flesh on the swimbladder TS is calculated below. (This will be referred to as the TS total including the effect of fish flesh throughout this work.) Thus several target strength quantities can be calculated: two different TS_s for the swimbladder, ignoring fish flesh and including it, and one TS_f for the fish body separately. To calculate the total target strength, then the results need to be combined properly (in or out of phase).

To calculate total target strength (TS_t) when the reflections from the fish body

and the swimbladder are added up, it is convenient to consider the back scattering cross section σ.

The time delay difference between the reflections from the swimbladder and the fish body is given by

$$\tau = 2\mathbf{k} \cdot \frac{(\mathbf{R_{0sf}} - \mathbf{R_{0s}})}{c_f} + 2\mathbf{k} \cdot \frac{(\mathbf{R_{0f}} - \mathbf{R_{0sf}})}{c_w}. \tag{3.1.16}$$

where, $\mathbf{k}$ is the unit vector in the direction of incident wave. $\mathbf{R_{0s}}$ and $\mathbf{R_{0f}}$ are the vectors from the origin to the points on the swimbladder and the fish body where the incident wave impinges normally. $\mathbf{R_{0sf}}$ is the vector from the origin to the point on the fish body where the wave vector normally incident on the swimbladder intersects the fish body. This path difference leads to a delay (τ) of a few μs to a few tens of μs between the echo from the swimbladder and that from the fish. Since typical pulse widths used in riverine sonar are in 100 - 1000 μs range, the two echoes overlap over a significant part of the received pulse width. Thus the measured target strength when the two echoes overlap is called the total target strength.

The corresponding phase difference in radians between the reflections from the swimbladder and the fish body is given by

$$\psi = 2\pi\tau f_c. \tag{3.1.17}$$

where f_c is the sonar carrier frequency. In this model, Equation (3.1.17) is the only equation where the frequency plays a role.

It is easy to show that the total back scattering cross-section (σ_t) that results from the contributions of both the fish body and the swimbladder is given by

$$\sigma_t = \sigma_s + \sigma_f + 2\sqrt{\sigma_s \sigma_f}\cos\psi. \tag{3.1.18}$$

Finally the net target strength (TS_t) taking into account both the fish body and

the swimbladder reflections is given by

$$\mathrm{TS_t} = 10 \log \left(\frac{\sigma_t}{4\pi} \right). \tag{3.1.19}$$

3.2 Limitations and Restrictions

The conditions for the validity of the model are given by Equation (3.1.2). These conditions essentially require that the radii of curvature be much larger than the wavelength. Using Equations (3.1.3) and (2.2.1) it is possible to write b_f and h_f in terms of l_f and then using the model of the swimbladder the three swimbladder parameters can be written in terms of l_f. Thus it is possible to calculate the radii of curvature in terms of l_f using typical parameters for α_b, α_h, p, q, r, and a swimbladder shape. Figure 3.2.1 illustrates $2\pi R_{s1}/\lambda$ and $2\pi R_{s2}/\lambda$ for various values of L_f/λ as a function of θ for side and dorsal aspects for the full ellipsoid model.

The figure shows that the values of both the ratios peak at normal incidences ($\theta = 90°$), remain roughly constant over $30° < \theta < 150°$ and then rapidly drop to smaller values as θ approaches the head or tail incidence. Similar results are obtained for the half ellipsoid model of the swimbladder and for the fish body. To determine more accurate values for $2\pi R_1/\lambda$ and $2\pi R_2/\lambda$ that satisfy the inequality described by Equation (3.1.2), a comparison of the model with the experimental data is used. As discussed later, the comparison of sockeye salmon, cod, and a few other types of fish TS data with this model suggests that $2\pi R_1/\lambda, 2\pi R_2/\lambda \geq 5$ gives a reasonably good (within a couple of dB) estimate of TS as calculated from this model. Using Figure 3.2.1 this model should be valid for ratios $L_f/\lambda > 25$ over most of the range of θ except near head ($\theta = 0°$) and tail ($\theta = 180°$). Figure 3.2.2 shows the minimum length of the fish as a function of frequency for which the model is

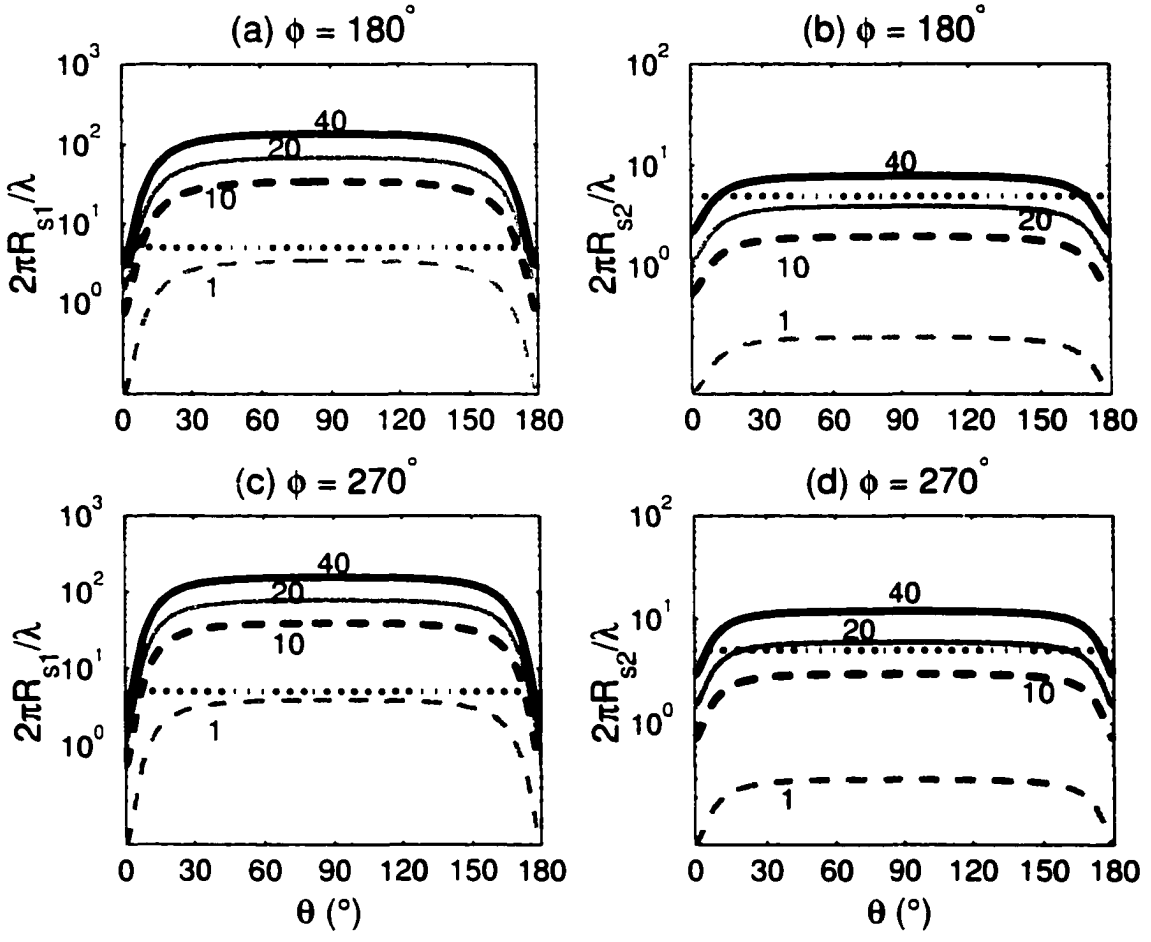

Figure 3.2.1 Validity range of the model. To show the range of validity for the TS model, the assumptions described by Equation 3.1.2 are analyzed pictorially assuming the fish is modeled by its swimbladder only. The terms $2\pi R_{s1}/\lambda$ and $2\pi R_{s2}/\lambda$ are plotted for a typical fish as a function of θ using the full-ellipsoid model. Various values of the ratio L_f/λ (the numbers shown by the curves) are shown using different curves with the dotted gray line for a ratio of 1, the dotted black line for 10, the solid gray line for 20 and the solid black line for 40. Results for side aspect are shown in panels (a) and (b) and dorsal aspect in panels (c) and (d). The following parameters were used: $\alpha_d = 0.13$, $\alpha_w = 0.20$, $p = 0.3$, $q = 0.075$, $r = 0.875$. The dotted line showing the minimum ratio value allowed is drawn at $2\pi R_{s1,2}/\lambda = 5$. The model is expected to be valid when the ratios are greater than 5 (see text for details).

valid and expected to give accurate estimates of target strengths plotted for a ratio of $L_f/\lambda = 25$ and 40.

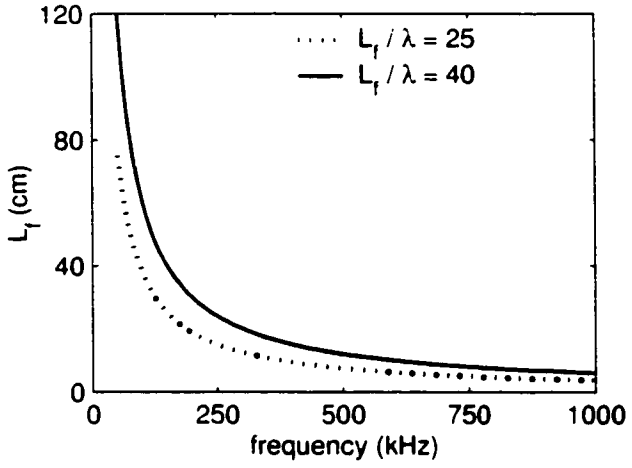

Figure 3.2.2 Minimum length vs. frequency from validity results. The minimum length (cm) of the fish is shown as a function of frequency (kHz) for which the model is valid. The model is expected to give accurate estimates of target strengths when the fish length is greater than the wavelength (λ). The validity condition is plotted for ratios of $L_f/\lambda = 25$ and 40.

3.3 Various TS Formulae and Special Cases

This model provides particularly simple formulae for the fish back scattering cross section and TS when the incident wave is normally incident at the side, dorsal, and head or tail aspect. It is easy to show that the radii of curvatures R_1 and R_2 for a general ellipsoid with parameters (b, h, l) for these angle of incidences are given as follows.

$$(R_1,\ R_2) = \begin{cases} \frac{l^2}{b},\ \frac{h^2}{b}, & \text{side aspect, normal incidence} \\ \frac{l^2}{h},\ \frac{b^2}{h}, & \text{dorsal aspect, normal incidence} \\ \frac{b^2}{l},\ \frac{h^2}{l}, & \text{head or tail aspect} \end{cases} \tag{3.3.1}$$

Substituting these values in Equations (3.1.9), (3.1.10), and (3.1.17) the back

scattering cross sections for the swimbladder and the fish as well as the phase ψ are obtained. Note that these formulae use the full ellipsoid model for swimbladder, although they can be easily modified for the half ellipsoid model keeping in mind that the swimbladder height becomes twice the breadth for that model.

$$\sigma_s = \begin{cases} \pi R_{Ps}^2 \frac{l_s^2 h_s^2}{b_s^2} = \pi R_{Ps}^2 p^2 r^2 l_f^2. & \text{side aspect} \\ \pi R_{Ps}^2 \frac{l_s^2 b_s^2}{h_s^2} = \pi R_{Ps}^2 \frac{p^2}{r^2} l_f^2. & \text{dorsal aspect} \\ \pi R_{Ps}^2 \frac{h_s^2 b_s^2}{l_s^2} = \pi R_{Ps}^2 \frac{q^2}{p^4} \frac{h_f^2 b_f^2}{l_f^2}. & \text{head or tail aspect} \end{cases} \tag{3.3.2}$$

$$\sigma_f = \begin{cases} \pi R_{Pf}^2 \frac{l_f^2 h_f^2}{b_f^2}. & \text{side aspect} \\ \pi R_{Pf}^2 \frac{l_f^2 b_f^2}{h_f^2}. & \text{dorsal aspect} \\ \pi R_{Pf}^2 \frac{h_f^2 b_f^2}{l_f^2}. & \text{head or tail aspect} \end{cases} \tag{3.3.3}$$

$$\nu = \begin{cases} \frac{4\pi f}{c_f}(b_f - b_s) = \frac{4\pi f}{c_f}\left(b_f - \sqrt{\frac{q h_f b_f}{pr}}\right). & \text{side aspect} \\ \frac{4\pi f}{c_f}(h_f - h_s) = \frac{4\pi f}{c_f}\left(h_f - \sqrt{\frac{qr h_f b_f}{p}}\right). & \text{dorsal aspect} \\ \frac{4\pi f}{c_f}(l_f - l_s) = \frac{4\pi f}{c_f}(1-p) l_f. & \text{head or tail aspect} \end{cases} \tag{3.3.4}$$

Equation (3.3.2) shows at normal incidence for both side and dorsal aspect the TS of the swimbladder is independent of the volume of the swimbladder, but depends on the length of the swimbladder and the ratio of the swimbladder height to swimbladder breadth, r. For head or tail aspect, the target strength depends on the length and volume of the swimbladder but not on the r factor. These equations provide a quick method to estimate TS at these special cases of practical importance.

The net back scattering cross section can now be calculated using Equation (3.1.18) and the total TS from Equation (3.1.19).

Together Equation (3.1.2) along with Equation (3.3.1) provide conditions for the validity of the geometric limit assumption for these special cases. These conditions are listed below. For the swimbladder, the following conditions exist.

Side aspect:

$$\begin{aligned}\frac{2\pi R_{s1}}{\lambda} &= \left(\frac{2\pi f_c}{c_w}\right)\left(\frac{p^3 r}{q}\right)^{1/2}\frac{l_f^2}{\sqrt{h_f b_f}} = \left(\frac{p^3 r}{q\alpha_b\alpha_h}\right)^{1/2}\left(\frac{l_f}{\lambda}\right) >> 1\\ \frac{2\pi R_{s2}}{\lambda} &= \left(\frac{2\pi f_c}{c_w}\right)\left(\frac{qr^3}{p}\right)^{1/2}\sqrt{h_f b_f} = \left(\frac{qr^3\alpha_b\alpha_h}{p}\right)^{1/2}\left(\frac{l_f}{\lambda}\right) >> 1\end{aligned} \tag{3.3.5a}$$

Dorsal aspect:

$$\begin{aligned}\frac{2\pi R_{s1}}{\lambda} &= \left(\frac{2\pi f_c}{c_w}\right)\left(\frac{p^3}{qr}\right)^{1/2}\frac{l_f^2}{\sqrt{h_f b_f}} = \left(\frac{p^3}{qr\alpha_b\alpha_h}\right)^{1/2}\left(\frac{l_f}{\lambda}\right) >> 1\\ \frac{2\pi R_{s2}}{\lambda} &= \left(\frac{2\pi f_c}{c_w}\right)\left(\frac{q}{pr^3}\right)^{1/2}\sqrt{h_f b_f} = \left(\frac{q\alpha_b\alpha_h}{pr^3}\right)^{1/2}\left(\frac{l_f}{\lambda}\right) >> 1\end{aligned} \tag{3.3.5b}$$

Head or tail aspect:

$$\begin{aligned}\frac{2\pi R_{s1}}{\lambda} &= \left(\frac{2\pi f_c}{c_w}\right)\left(\frac{q}{p^2 r}\right)\frac{h_f b_f}{l_f} = \left(\frac{q\alpha_b\alpha_h}{p^2 r}\right)\left(\frac{l_f}{\lambda}\right) >> 1\\ \frac{2\pi R_{s2}}{\lambda} &= \left(\frac{2\pi f_c}{c_w}\right)\left(\frac{qr}{p^2}\right)\frac{h_f b_f}{l_f} = \left(\frac{qr\alpha_b\alpha_h}{p^2}\right)\left(\frac{l_f}{\lambda}\right) >> 1\end{aligned} \tag{3.3.5c}$$

For the fish body, the following validity conditions exist.

Side aspect:

$$\begin{aligned}\frac{2\pi R_{f1}}{\lambda} &= \left(\frac{2\pi f_c}{c_w}\right)\frac{l_f^2}{b_f} = \frac{1}{\alpha_b}\left(\frac{l_f}{\lambda}\right) >> 1\\ \frac{2\pi R_{f2}}{\lambda} &= \left(\frac{2\pi f_c}{c_w}\right)\frac{h_f^2}{b_f} = \frac{\alpha_h^2}{\alpha_b}\left(\frac{l_f}{\lambda}\right) >> 1\end{aligned} \tag{3.3.6a}$$

Dorsal aspect:

$$\frac{2\pi R_{f1}}{\lambda} = \left(\frac{2\pi f_c}{c_w}\right)\frac{l_f^2}{h_f} = \frac{1}{\alpha_h}\left(\frac{l_f}{\lambda}\right) >> 1$$
$$\frac{2\pi R_{f2}}{\lambda} = \left(\frac{2\pi f_c}{c_w}\right)\frac{b_f^2}{h_f} = \frac{\alpha_b^2}{\alpha_h}\left(\frac{l_f}{\lambda}\right) >> 1 \qquad (3.3.6b)$$

Head or tail aspect:

$$\frac{2\pi R_{f1}}{\lambda} = \left(\frac{2\pi f_c}{c_w}\right)\frac{b_f^2}{l_f} = \alpha_b^2\left(\frac{l_f}{\lambda}\right) >> 1$$
$$\frac{2\pi R_{f2}}{\lambda} = \left(\frac{2\pi f_c}{c_w}\right)\frac{h_f^2}{l_f} = \alpha_h^2\left(\frac{l_f}{\lambda}\right) >> 1 \qquad (3.3.6c)$$

These formulae provide quick and easy methods of verifying TS calculations and restrictions for the special cases of incident angles most commonly used in both riverine and ocean experiments.

Using a numerical model to calculate the TS at an arbitrary angle of incidence is considered later in sections 3.5 and 3.6. Also, these equations given above can provide easy analysis of the relationship between certain parameters. For example, to check how the TS should change if the p ratio increased, consider Equation 3.3.2, the back scattering coefficient for the swimbladder alone. For the side aspect case, the TS should increase when p increases since TS is proportional to the square of p. For the head/tail aspect, the TS should decrease as p increases as TS is inversely proportional to the fourth power of p.

3.4 Comparison of Model to Kirchhoff's Integral

One method used to provide an analytical solution to the wave equation, the partial differential equation representing the sound pressure used in sonar, is called the

Kirchhoff Integral solution. Often, approximations are used in this process leading to the Kirchhoff approximation, also known as the geometrical optics approximation. These approximations assume that the reflection and transmission coefficients for scattering are equivalent to those calculated at an infinite plane surface [Medwin and Clay, 1998]. To test the validity of the geometric model presented in this work, a comparison is made to the results found through the Kirchhoff method.

The general wave equation is given by

$$-\rho\frac{\partial u_z}{\partial t} = \frac{\partial p}{\partial z}. \tag{3.4.1}$$

where ρ is the density of the medium, p is the pressure of the sound wave, t is time, and z the coordinate perpendicular to the surface. The term u_z is the velocity of the water measured along a line perpendicular to the surface. The wave equation must satisfy certain initial and boundary conditions. The initial condition of

$$\frac{\partial u_z}{\partial t} = 0 \tag{3.4.2}$$

leads to the boundary condition of

$$\frac{\partial p_1}{\partial z} + \frac{\partial p_2}{\partial z} = 0 \tag{3.4.3}$$

where p_1, is the resulting sound pressure when no target is present (and thus one solution to the wave equation) and p_2 is the correction to p_2 in the presence of a target to satisfy the boundary condition. Since the wave equation is a linear homogeneous differential equation, p_2 is also a solution to the wave equation. Here p_1 can also be thought of as the incident sound pressure and p_2 as the received sound pressure. Since the target strength (TS) of an object is always measured as the comparison of the received sound pressure to the incident sound pressure assuming the sound is both transmitted and received at the same location, then an analytical expression for p_2 must be derived under these conditions [Major, 1968].

The Fresnel zone method, generated by applying an additional approximation to the Kirchhoff integral, allows for an expression of p_2. The Fresnel zone approximation is valid under the considerations that the radius of curvature of the surface is large compared to the wavelength and there is near perfect reflection. (Note that both of these conditions hold true for the TS model presented in Chapter 3 as applied to the target of sockeye salmon with air-filled swimbladders.)

A general solution to the wave equation is given by

$$p = \frac{B}{r} e^{2\pi i(ft - r/\lambda)}, \tag{3.4.3}$$

where p is the pressure at a distance r from the transmitter, B is a constant representing the strength of the reflection from the target, t is time, f is the carrier frequency, and λ is the wavelength. This general solution leads to a specific solution of p_2 under the assumption that the value of B is determined by the incident sound pressure at a specific point on the target and given by the relationship

$$B = -\frac{1}{2pi} e^{-2\pi i f t} \frac{\partial p_2}{\partial z}. \tag{3.4.4}$$

Thus

$$p_2 = -\frac{iBe^{2\pi i f t}}{\lambda} \int \frac{cos\theta}{r^2} e^{-4\pi i r/\lambda} dS, \tag{3.4.5}$$

where the integral is evaluated over the surface S and both θ and r vary over the surface.

The Fresnel zone method assumes that a surface may be divided into areas in which the returned pulses are all relatively in phase causing negligible amounts of destructive interference. Each Fresnel zone is separated by a distance of $\lambda/4$, forcing consecutive zones to have an average phase difference of π. Thus the pressure received within one zone is mostly constructive interference and from consecutive zones is mostly destructive inference.

The pressure for the nth zone is given by

$$P_n = \int_{S_n} \frac{\cos\theta}{r^2} e^{-\pi i u_n} dS \tag{3.4.6}$$

where θ is the incident angle, r is the range to the point on the surface, S_n is the surface to integrate over, and u_n is given by

$$u_n = \frac{r - R - (n-1)\lambda/4}{\lambda/4} \tag{3.4.7}$$

where R is the distance on the surface closest to the receiver. Note that for each zone, the term u_n ranges from 0 to 1 as r ranges from $(n-1)\lambda/4$ to $n\lambda/4$.

The total received pressure given in Equation 3.4.5 can then be written as

$$p_2 = -\frac{iB}{\lambda} e^{2\pi i(ft - 2R/\lambda)}[P_1 - P_2 + P_3 \ldots + (-1)^{N-1} P_N]. \tag{3.4.8}$$

where N is the total number of zones.

When the radii of curvature at the incident point on the target is large compared to the wavelength, there will be a large number of zones and the values of P_n will not change very rapidly as n changes. Thus, on the average the total pressure received from the nth zone, P_n, is the average of the total pressure received from the preceding and following zones.

$$P_n = \frac{1}{2}(P_{n-1} + P_{n+1}). \tag{3.4.9}$$

Using this important assumption with Equation 3.4.8 and the practical case that P_N usually vanishes, leads to the further suggestion that the sum of the n zones can be approximated by half of the first Fresnel zone.

Substituting the total pressure, $P_1/2$, into Equation 3.4.5, using Equation 3.4.9 for P_1, and changing into log form provides the following definition for target strength.

$$TS = 20 \log \left| \frac{1}{2\lambda} \int_{S_1} \cos\theta e^{-\pi i u_1} \, dS \right| \tag{3.4.10}$$

where u_1 ranges from 0 to 1 as r runs from R to $R + \lambda/4$.

To find the range of limitations for the Fresnel zone approximation to the Kirchhoff integral solution, the TS was calculated using a sphere of radius A. Values of R/A and A/λ were used to show the range dependency and a frequency dependency. Figure 3.4.1 shows the TS dependence on range and frequency for Kirchhoff integral results using sphere. In panel (a) the TS value using the Kirchhoff integral is plotted as a function of the ratio of the range to the sphere radius (R/A) with fixed frequency of f_c = 1000 kHz. The dashed line shows the geometric limit to the Kirchhoff integral. At small ratio values ($R/A \sim 10$) the TS has an error of about 0.5 dB. At larger ratio values ($R/A \sim 1000$), the TS values are within 0.01 dB. In panel (b) the TS value using the Kirchhoff integral is calculated and plotted as a function of the ratio of the sphere radius to the wavelength (A/λ) with fixed range of R = 1000 m. The dashed line represents the TS value using the geometric calculation. At small ratio values ($A/\lambda \sim 30$) the TS values match within 0.05 dB. At larger ratio values ($A/\lambda \sim 300$) the TS values match within 0.005 dB.

To test the theory that as N gets large, the sum of the n Fresnel zones approaches half of the first Fresnel zone, the TS was calculated for various N values using a sphere of radius A and for three A/λ values. Figure 3.4.2 shows the TS vs. N for various A/λ values for sphere. The TS is calculated using the Fresnel zone approximation to the Kirchhoff integral for the first through the 45th zones for a sphere of radius A = 0.5 m. The number of Fresnel zones is shown along the $x-$axis. The dashed gray line is the geometric TS value for each of the 3 cases of A/λ = 100, 10, 1. The dashed black line represents the Fresnel zone approximation using only the reflections from the first and N^{th} zones for each case. The approximation for the higher ratio values matches well even within only 15 zones. However, for the

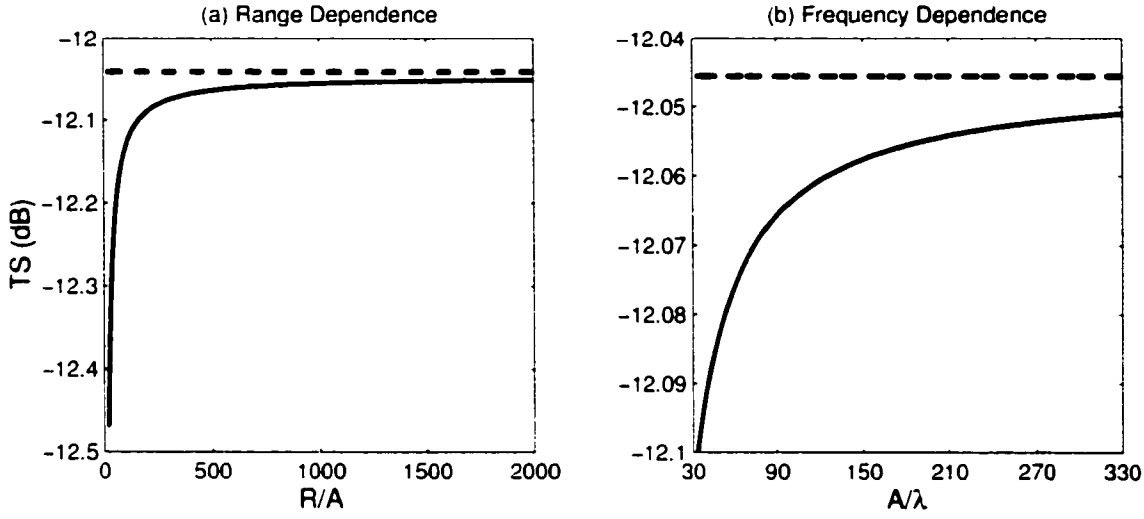

Figure 3.4.1 Range and frequency dependence on TS using Kirchhoff integral. (a) The TS value using the Kirchhoff integral is calculated and plotted as a function of the ratio of the range to the sphere radius (R/A) with fixed frequency of $f = 1000$ kHz. The dashed line shows the geometric limit to the Kirchhoff integral. At small ratio values ($R/A \sim 10$) the TS has an error of about 0.5 dB. At larger ratio values ($R/A \sim 1000$) the TS values are within 0.01 dB. (b) The TS value using the Kirchhoff integral is calculated and plotted as a function of the ratio of the sphere radius to the wavelength (A/λ) with fixed range of $R = 1000$ m. The dashed line represents the TS value using the geometric calculation. At small ratio values ($A/\lambda \sim 30$) the TS values match within 0.05 dB. At larger ratio values ($A/\lambda \sim 300$) the TS values match within 0.005 dB.

ratio of 1, the Fresnel zone approach is no longer valid as can be seen in panel (c).

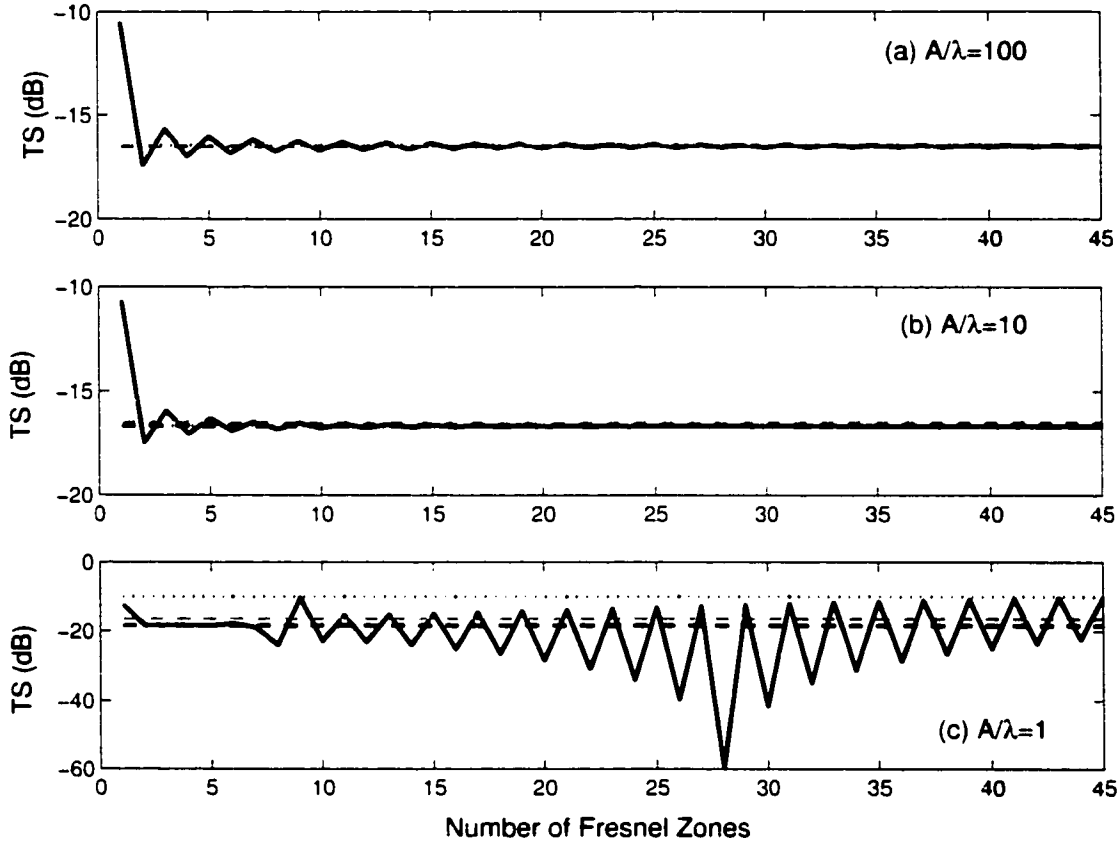

Figure 3.4.2 TS dependence on number of Fresnel zones. The TS is calculated using the Fresnel zone approximation to the Kirchhoff integral for the first through the 45th zones for a sphere of radius A = 0.5 m. The number of Fresnel zones is shown along the x–axis. The dashed gray line is the geometric TS value for each of the 3 cases of A/λ = 100, 10, 1. The dashed black line represents the Fresnel zone approximation using only the reflections from the first and N^{th} zones for each case. The approximation for the higher ratio values matches well even within only 15 zones. However, for the ratio of 1, the Fresnel zone approach is no longer valid.

Figure 3.4.3 shows a comparison of TS results from geometric and Kirchhoff integral approaches for special incident angles using an ellipsoid model. For an ellipsoid model with (L_f, H_f, B_f)=(565, 134.60 mm) the Kirchhoff approximation for the first through the 15th zones (black solid line) is shown for the four special cases of side aspect, normal and head/tail incidence, and dorsal aspect, normal and head/tail incidence. The Fresnel zone calculation using only the first zone is shown

with the dashed black line. The geometric results are shown with a gray dashed line. For normal incidence where the ratios of radii of curvature to wavelength are high, the Fresnel zone TS approximations are within hundredths of a dB. In particular, for side aspect, normal incidence as shown in (a) the TS values match within 0.05 dB. For dorsal aspect, normal incidence as shown in (c) the TS values match within 0.07 dB. Whereas for the head/tail incidences where the radii of curvature to wavelength ratios are smaller the TS matches are less accurate. For side aspect, head/tail incidence as shown in (b) the TS values match within 1.04 dB. For dorsal aspect, head/tail incidence as shown in (d) the TS values match within 1.86 dB.

Figure 3.4.4 shows a comparison of Kirchhoff results and ellipsoid model results as a function of incident angles. The TS results are shown versus θ for side and dorsal aspects. TS results using the Fresnel zone approximation to the Kirchhoff integral are shown with gray solid lines for side aspect (a) and dorsal aspect (b). The black dashed lines represent the geometric TS value. Both calculations use an ellipsoid model with (L_f, H_f, B_f)=(565, 134, 60 mm), frequency of 400 kHz, and a range of 1000 m.

Figure 3.4.5 shows an expanded view of the comparison of Kirchhoff results and ellipsoid model results from Figure 3.4.4. To better view the difference between the geometric calculation and the Kirchhoff results the absolute value of the TS difference is plotted for $\theta = 1-9°$ for side (a) and dorsal (c) and for $\theta = 10-90°$ for side (b) and dorsal (d). There is fluctuation in the differences due to the interference that still exists, but the limits of fluctuation match those shown in Figure 3.4.3.

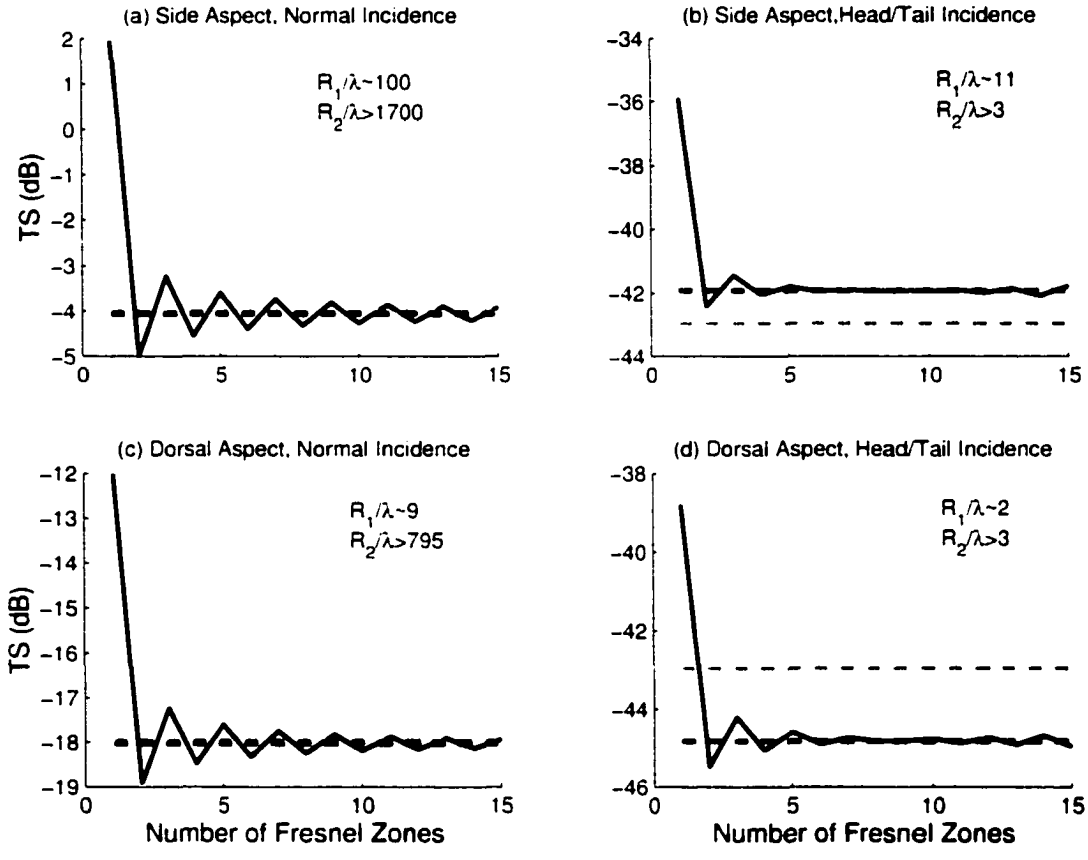

Figure 3.4.3 Comparison of TS from geometric and Kirchhoff integral approaches. For an ellipsoid model with (L_f, H_f, B_f)=(565, 134, 60 mm) the Kirchhoff approximation for the first through the 15th zones (black solid line) is shown for the four special cases of side aspect, normal and head/tail incidence, and dorsal aspect, normal and head/tail incidence. The Fresnel zone calculation using only the first zone is shown with the dashed black line. The geometric results are shown with a gray dashed line. For normal incidence where the ratios of radii of curvature to wavelength are high, the Fresnel zone TS approximations are within hundredths of a dB. In particular, for side aspect, normal incidence as shown in (a) the TS values match within 0.05dB. For dorsal aspect, normal incidence as shown in (c) the TS values match within 0.07 dB. Whereas for the head/tail incidences where the ratios are smaller the TS matches are only within dBs. For side aspect, head/tail incidence as shown in (b) the TS values match within 1.04 dB. For dorsal aspect, head/tail incidence as shown in (d) the TS values match within 1.86 dB.

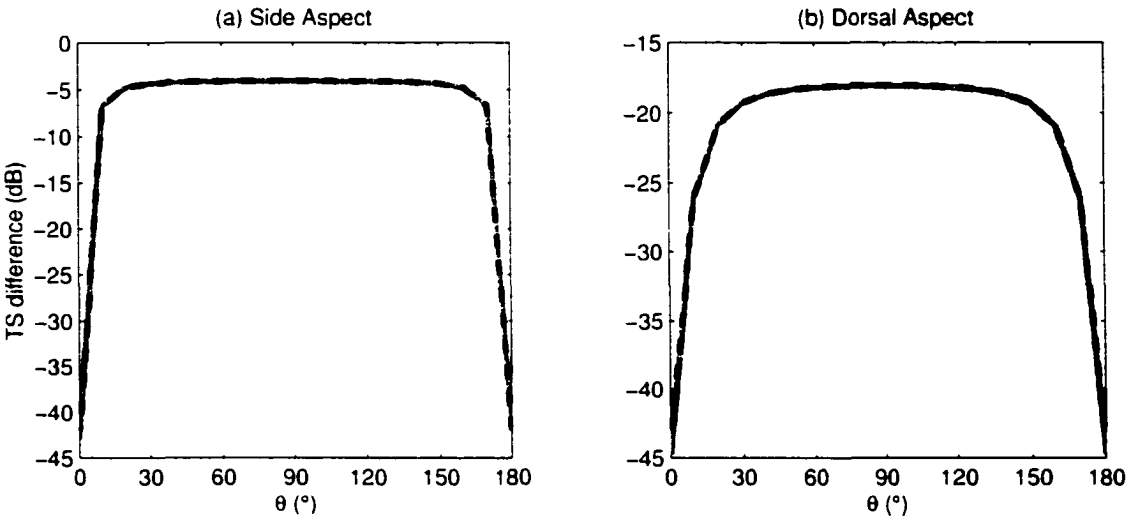

Figure 3.4.4 Comparison of Kirchhoff and ellipsoid TS model results. TS vs. θ for side and dorsal aspects. TS results using the Fresnel zone approximation to the Kirchhoff integral are shown with gray solid lines for side aspect (a) and dorsal aspect (b). The black dashed lines represent the geometric TS value. Both calculations use an ellipsoid model with (L_f, H_f, B_f)=(565, 134, 60 mm), frequency of 400 kHz, and a range of 1000 m.

3.5 Geometric TS Model Results

To show the results of the TS model and its various capabilities, examples focusing on the TS dependencies on various fish body and swimbladder parameters are given in this section specific to sockeye salmon. For consistency, fixed values of the following parameters are used unless otherwise stated. The model uses a standard fish size, $(L_f, H_f, B_f) = (565, 134, 60)$ in mm, with standard swimbladder parameter values of $p = 0.35$, $q = 0.08$ and $r = 0.875$ (full-ellipsoid model) or $r = 1.75$ (half-ellipsoid model). The ranges for these parameters are p: $25 - 40\%$, q: $7 - 10\%$ for fresh water, 5% for salt water, and r: $1.5 - 2.0$ for half ellipsoid model. TS is plotted with respect to varying $\theta_i = 0 - 180°$ for either side aspect ($\phi_i = 180°$) or dorsal aspect ($\phi_i = 270°$). Normal incidence occurs at $\theta_i = 90°$. For brevity sake, the 'i' will be dropped from the incident angles. Hereafter, all θ and ϕ are assumed to be incident

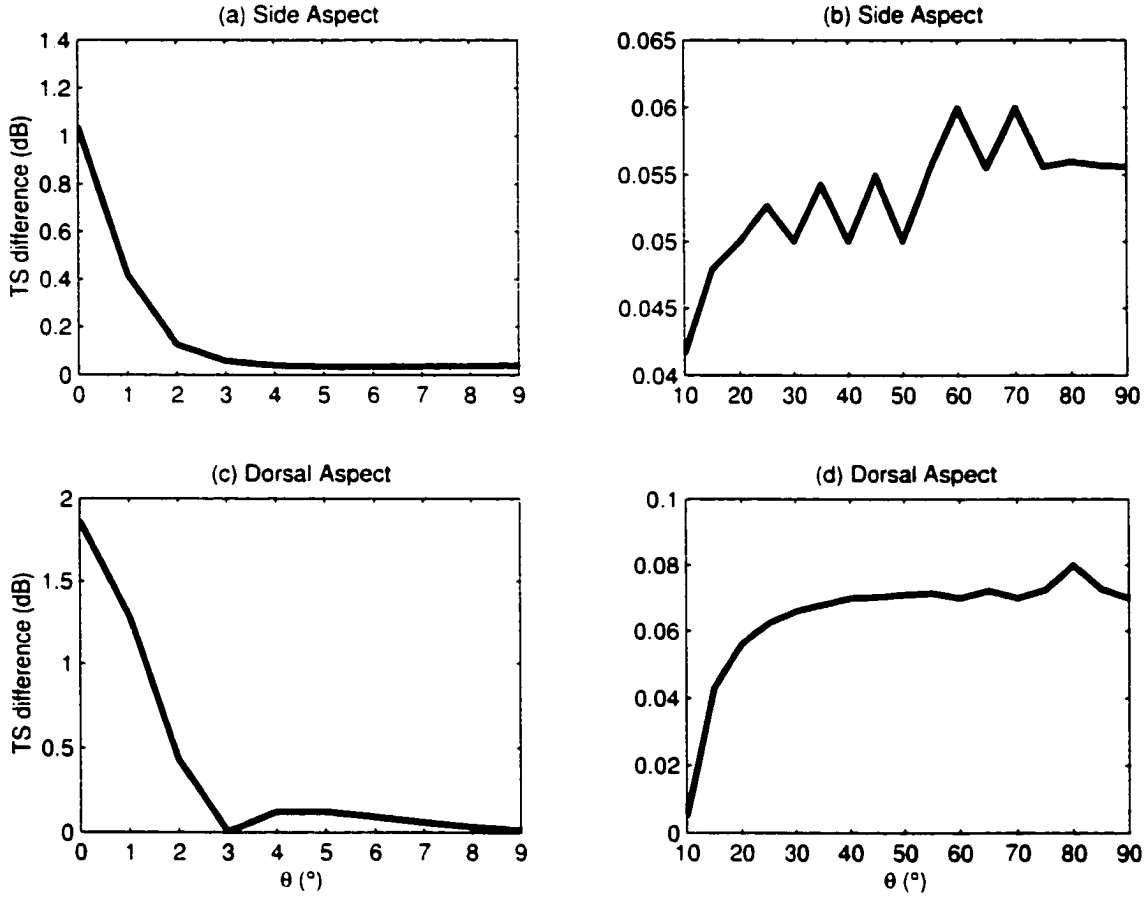

Figure 3.4.5 Comparison — zoomed in. The same calculations as shown in Figure 3.4.4 are shown for two different zoomed in views. To better view the difference between the geometric calculation and the Kirchhoff results the absolute value of the TS difference is plotted for $\theta = 1 - 9^{\circ}$ for side (a) and dorsal (c) and for $\theta = 10 - 90^{\circ}$ for side (b) and dorsal (d).

angles unless otherwise notes.

Figure 3.5.1 shows the various TS results for a standard sockeye salmon with a standard swimbladder. In panel (a) the TS using both full-ellipsoid and half-ellipsoid models are plotted for side aspect. The solid line represents the TS using only a swimbladder to model the fish for the half-ellipsoid model. The dashed line shows the same for the full-ellipsoid model. Notice that the half-ellipsoid model provides TS results $\sim$ 5 dB higher than the full ellipsoid. The dotted line shows the TS using only fish flesh to model the fish (no swimbladder). The results are lower than that from the swimbladder only as expected. The combination showing the effect of fish flesh on the TS of the swimbladder is shown for both swimbladder models in gray. Notice that around normal incidence, the TS from the swimbladder is predominant; however, at incident angles closer to the head or tail, the TS of the fish flesh significantly effects the total TS.

When considering that the wave has to first travel through the fish body before reaching the swimbladder, two effects arise: (1) a slight bending of the waves through the fish body and (2) the modification of the reflection coefficient. An analysis of these effects shows that both modify the reflection due to swimbladder by a few percent (less than a few dB) and can be neglected to first order for aspect angles within $\sim 60°$ of normal incidence for side aspect and within $\sim 40°$ of normal incidence for dorsal aspect. For aspect angles close to 0° or 180° (near head or tail aspect), the effect of fish flesh on swimbladder TS cannot be ignored.

The TS model has a weak dependence on frequency. The TS of the swimbladder and the fish flesh do not depend on the frequency; however, the net target strength of the fish does depend on frequency through the phase factor as given by Equation (3.1.17). The variation in back scattering cross section is thus within the range

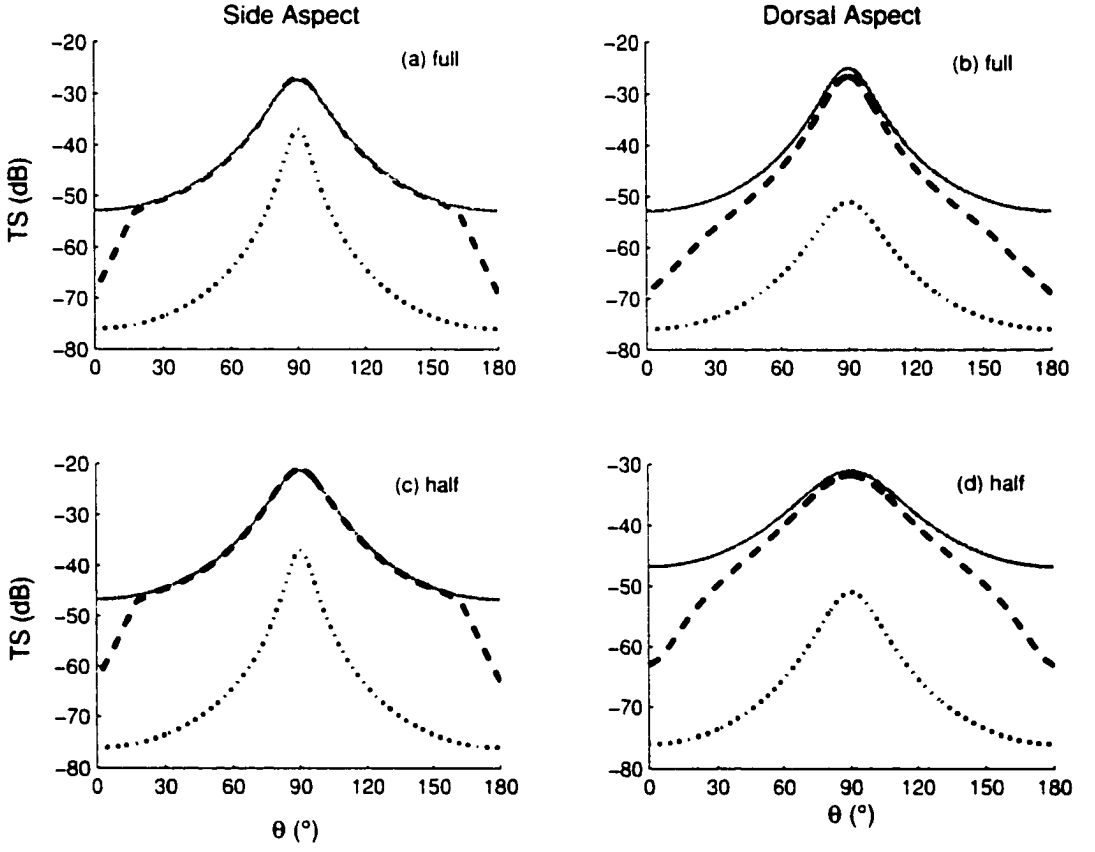

Figure 3.5.1 TS vs. incident angle for fixed aspect. Various TS results are shown for a standard sockeye salmon with a standard swimbladder. The TS calculated using just the swimbladder is plotted with a solid line. The TS for just the fish is shown with a dotted line. The TS using the swimbladder taking the fish flesh into account is shown with the dashed line. Panel (a) shows the TS results as a function of θ using the full ellipsoid swimbladder model at side aspect ($\phi = 180°$). Panel (b) shows the results using the full ellipsoid swimbladder model at dorsal aspect ($\phi = 270°$). Panel (c) shows the results using a half ellipsoid swimbladder model at side aspect. Panel (d) shows the results using a half ellipsoid swimbladder model at dorsal aspect.

$\sigma_t = \sigma_s \pm \sigma_f$. Panel (b) compares the total TS of the fish neglecting the effect of fish flesh (black dashed line) and accounting for it (gray dashed line). Although the corresponding variation in the TS for a typical salmon is about $\pm 2 - 3$ dB as seen for both models, when the fish flesh is taken into account, the variation is even more pronounced. Figure 3.5.2 shows the difference in second order target strength values of swimbladder taking fish flesh into account, and ignoring it. TS is plotted as a function of θ for both side and dorsal aspect.

Panel (c) shows similar TS calculations as in (a) using dorsal aspect. Comparing between side aspect and dorsal aspect, the pattern among the 5 TS calculations is consistent; however, the overall values are smaller near normal incidence and there is less variation from normal incidence to extreme incidences. Panel (d) shows similar TS calculations as in (b) using dorsal aspect.

Note that side aspect (normal incidence) gives the highest values of target strength whereas both head and tail aspect provide much lower results as would be expected. Both target strength for the swimbladder and the fish are plotted with the swimbladder providing the major contribution to target strength as expected. The contribution to target strength due to fish body is not negligible, particularly at angles close to normal incidence ($\theta \sim 90°$). Panels (b) and (d) show that the fish body contribution can lead to about $\pm 2 - 3$ dB variation in the net target strength of the fish as a whole.

Figure 3.5.3 shows the effects of varying only swimbladder parameters on TS of sockeye salmon for side aspect using the half ellipsoid model. Panel (a) shows the effects of varying p over the range $25 - 40\%$ on the TS values. Panel (b) shows the effects of varying q over the range $5 - 10\%$ on the TS values. Panel (c) shows the effects of varying r over the range $1.75 - 2.25$ on the TS values. Typical fish size

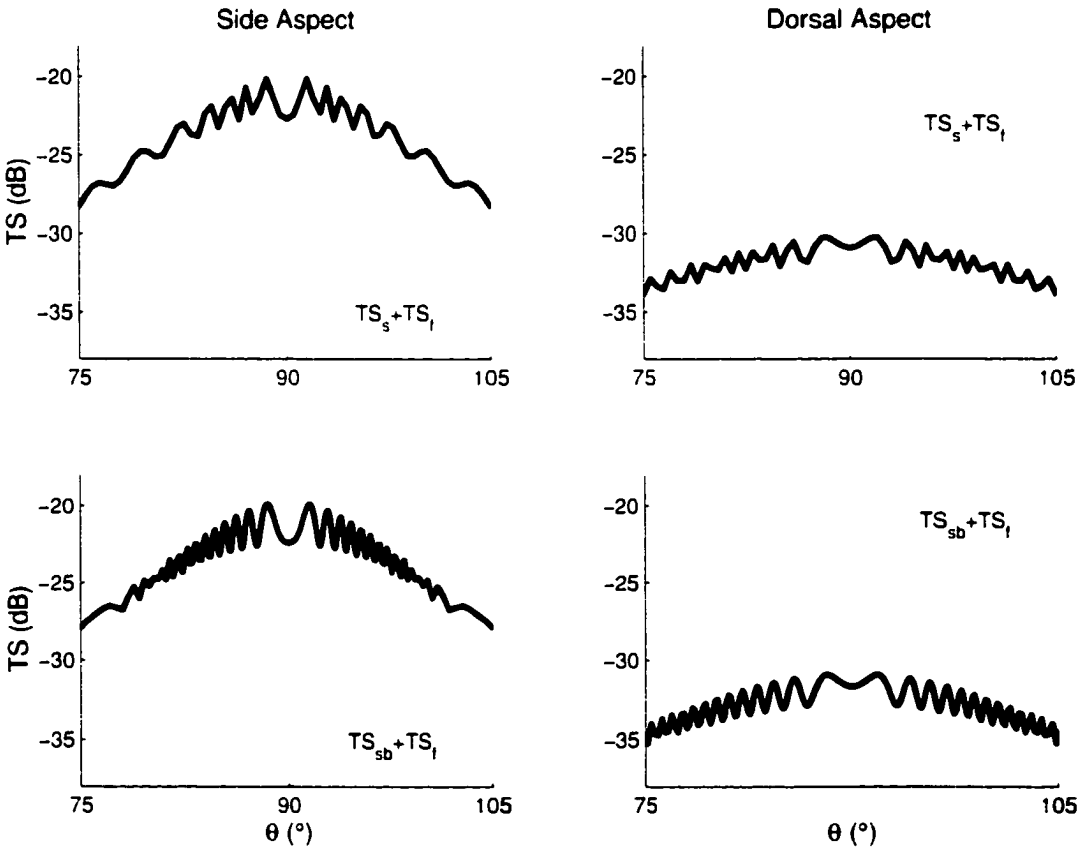

Figure 3.5.2 Effect of fish flesh on TS. Shown are the differences in second order target strength values of swimbladder taking fish flesh into account, and ignoring it. TS is plotted as a function of θ for (a) side aspect, ignoring fish flesh; (b) dorsal aspect, ignoring fish flesh; (c) side aspect, including fish flesh; (d) dorsal aspect, including fish flesh.

parameters were used and average swimbladder parameters values were used when holding that parameter fixed.

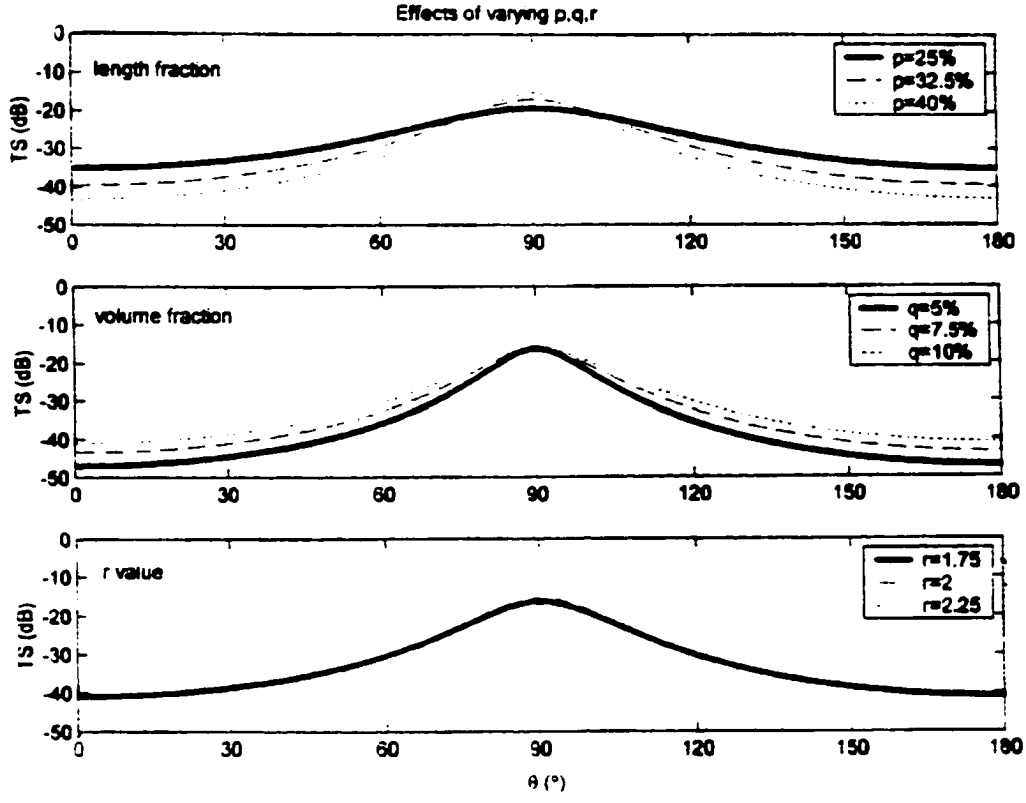

Figure 3.5.3 Effects of varying swimbladder parameters on TS. Effects of varying only swimbladder parameters on TS are shown for sockeye salmon at side aspect using the half ellipsoid model as a function of incident angle θ. Panel (a) shows the effects on TS of varying p over the range 25 – 40%. Panel (b) shows the effects on TS of varying q over the range 5 – 10%. Panel (c) shows the effects on TS of varying r over the range 1.75 – 2.25. Typical fish size parameters were used in each case. The average swimbladder parameter values were used when holding a parameter fixed.

Figure 3.5.4 shows the effects of varying size and swimbladder parameters on TS of sockeye salmon for side aspect. The minimum and maximum TS values were calculated by varying the described parameters and plotted using dotted and dashed lines respectively. The TS range depending on variable length is shown in panel (a)

using fixed height, breadth, and standard swimbladder parameters. The height and breadth were calculated using the regression lines provided in section 2.1.2 for each value of length. The TS range depending on variable height and breadth is shown in panel (b) for a sockeye salmon of fixed length with standard swimbladder parameters. The range of height and breadth for the fixed length were found using data within 2.5 standard deviations of the respective mean given in section 2.1.1. The TS range of a sockeye salmon of fixed length is shown in panel (c) with varying both size and swimbladder parameters. The swimbladder parameters were varied within appropriate values as discussed in chapter 2.

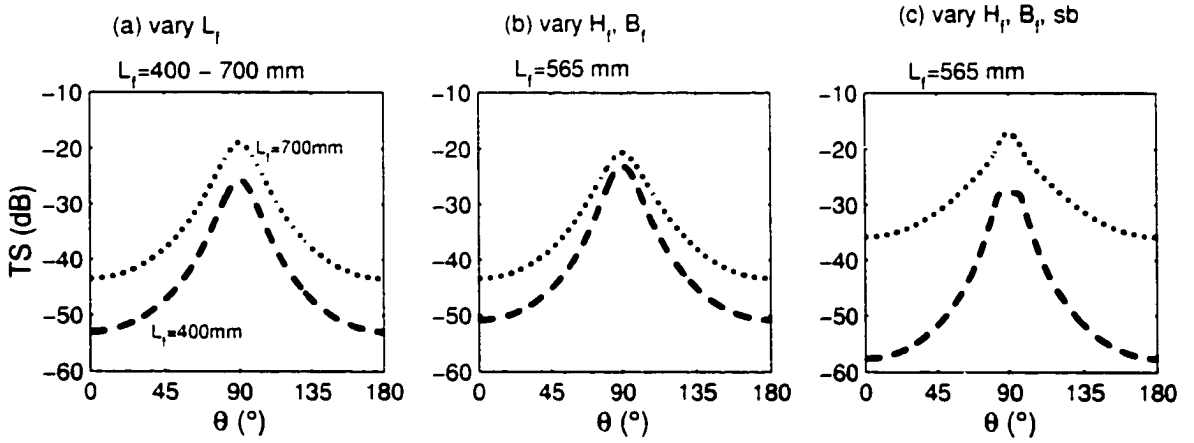

Figure 3.5.4 Effects of varying size and swimbladder parameters on TS. Shown are the effects of varying size and swimbladder parameters on TS of sockeye salmon for side aspect as a function of incident angle θ. The minimum and maximum TS values were calculated by varying the described parameters and plotted using dotted and dashed lines respectively. Panel (a) shows the results of TS vs. θ for varying fish length L_f = 400 – 700 mm. Panel (b) shows the results of TS vs. θ for varying height and breadth within the ranges given by the data for a fixed length of 565 mm. Panel (c) shows the results of TS vs. θ for varying both size (height and breadth) and swimbladder parameters for a fixed length of 565 mm.

Figure 3.5.5 shows the effect of swimbladder tilt on TS. The TS using tilt angles for the swimbladder of $\gamma = 0.10.20°$ for $L_f/\lambda = 40$ are shown for side aspect in (a) and dorsal aspect in (b). The total TS was calculated with no effect of fish flesh included for a standard sockeye salmon with standard swimbladder parameters.

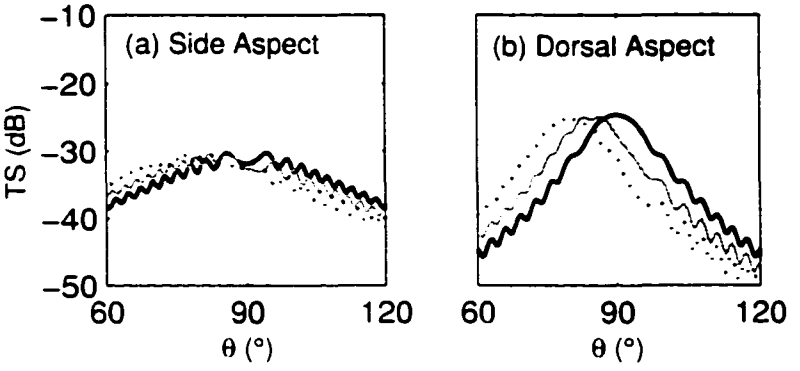

Figure 3.5.5 Effect of swimbladder tilt on TS. The effect of swimbladder tilt on TS is shown as a function of incident angle θ. The TS results using three tilt angles for the swimbladder for a fish with $L_f/\lambda = 40$ are shown for side aspect in (a) and dorsal aspect in (b). The solid black line represents the tilt of $\gamma = 0°$, the solid gray line shows $\gamma = 10°$ results, and the dashed black line is for $\gamma = 20°$. The total TS was calculated ignoring the effect of fish flesh for a standard sockeye salmon with standard swimbladder parameters.

Figure 3.5.6 shows the effect of the roll of the fish on TS. Roll is defined as a rotation about the $z-$axis of the fish from the vertical angle. The TS is calculated for a fixed o with varying θ for four roll angles $o_{roll} = 0, 15, 30, 45°$. For dorsal aspect $o = 90°$, shown in panel (a) the change is less than 2 dB from a roll angle of $0 - 45°$ at normal incidence and varies less at other incidences. For side aspect $o = 180°$, shown in panel (b) the change is more significant, up to 7 dB, from a roll angle of $0 - 45°$ at normal incidence. As the incidence angle strays from normal, the change becomes less significant and almost nonexistent past 30° from normal.

The TS model presented in this work is dependent on the fish size parameters, the swimbladder shape, size and orientation, the location and orientation of the fish in the beam, and the presence of the second order effects of fish flesh on the swimbladder TS. The results are quantifiable as a function of incidence angles and thus uncertainties can be measured and categorized. For example, as shown in Figure 3.5.3a the uncertainty in TS of 3 dB can be attributed to unknown swimbladder length near normal incidence, side aspect. Comparing the model results with exper-

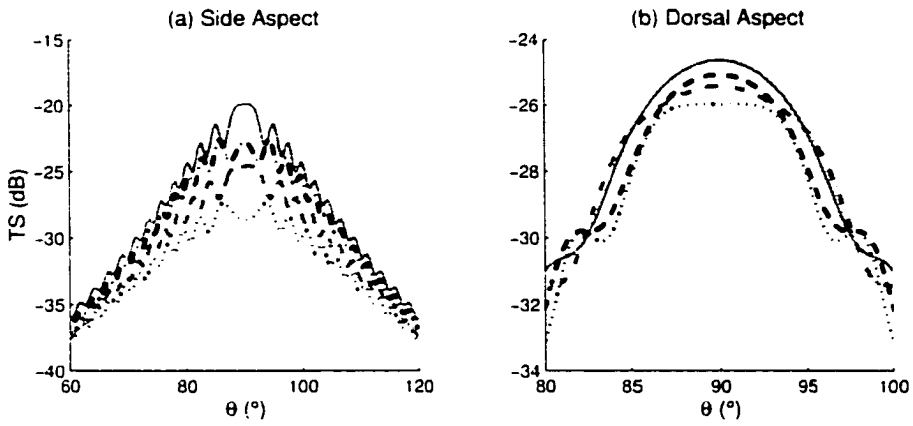

Figure 3.5.6 Effect of fish roll on TS. Roll is defined as a rotation about the z–axis of the fish from the vertical angle. The TS is calculated for a fixed ϕ with varying θ for four roll angles $\phi_{roll} = 0, 15, 30, 45°$. $\phi_{roll} = 0°$ is represented by the solid gray line, $\phi_{roll} = 15°$ by the dashed black line, $\phi_{roll} = 30°$ by the dash-dot gray line, and $\phi_{roll} = 45°$ by the dotted black line. The different axes scale are used to show that he effects on dorsal aspect in panel (b) are less evident than for those at side aspect as shown in panel (a).

imental results as in the following section provides justification for the model and also shows how to quantify and categorize uncertainties.

3.6 Comparison of Model to Experimental TS Results

Results using the TS model and the fish distribution models match experimental results very well in a variety of cases. The comparison begins by using information from anesthetized sockeye salmon, such as length, size, and swimbladder information, and then proceeds to generalize to information from groups of live, free swimming sockeye salmon in a river environment using multiple frequencies. In further generalizing steps, the data of other species in the river and ocean settings are used. In all cases the models provide reasonably accurate estimations of TS as well as explain where the uncertainties can be attributed.

Figure 3.6.1 shows a comparison of the TS model with experimental results

for 3 specific sockeye salmon. Dahl and Mathisen [1983] measured the TS of 3 tethered sockeye salmon at 10° intervals for side aspect only. The experimental results are shown as 'x' for the fish with L_f = 400 mm in (a). L_f = 520 mm in (b) and L_f = 610 mm in (c). A range of TS values were calculated from the model using the fish length provided, varying the height and breadth within 2.5 standard deviations of the respective mean as given in chapter 2, and varying the swimbladder parameters within an appropriate range as also discussed in chapter 2. The minimum and maximum TS values were chosen after varying the described parameters and plotted as solid and dashed lines. The average value of the TS with the effect of fish flesh was also calculated and plotted as a dotted line for each fish.

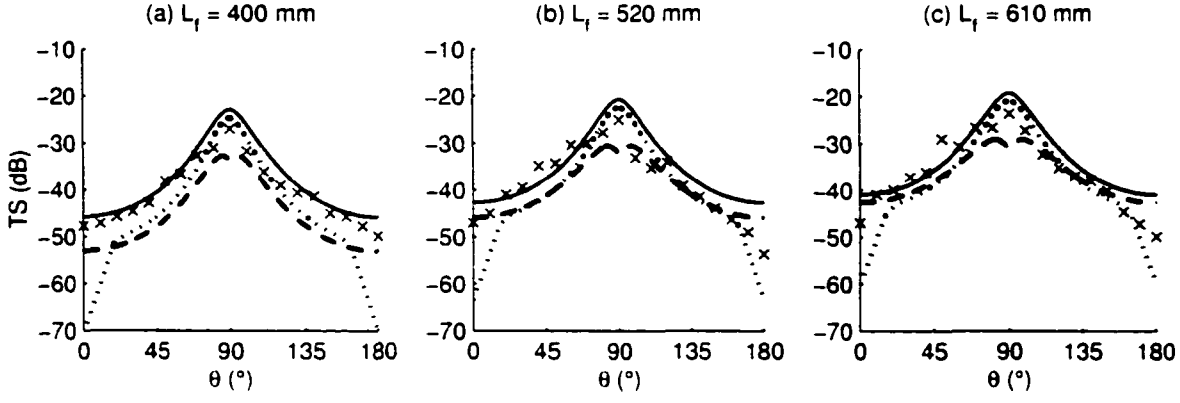

Figure 3.6.1 TS comparison with data from three specific sockeye salmon. Dahl and Mathisen [1983] measured the TS of 3 tethered sockeye salmon at 10° intervals for side aspect only. The experimental results are shown as 'x' for the fish with L_f = 400 mm in (a). L_f = 520 mm in (b) and L_f = 610 mm in (c). A range of TS values were calculated from the model using the fish length provided, varying the height and breadth within 2.5 standard deviations of the respective mean as given in chapter 2, and varying the swimbladder parameters within an appropriate range as also discussed in chapter 2. The minimum and maximum TS values were chosen after varying the described parameters and plotted as solid and dashed lines. The average value of the TS with the effect of fish flesh was also calculated and plotted as a dotted line for each fish.

The measured TS values for incidence close to head or tail lie between those given for TS_s and TS_{sf} indicating that the fish flesh contribution to the swimbladder

TS may become important for these angles of incidences. Note that the radii of curvature are well within the limitations discussed in section 3.2. Calculating R_{f1}, R_{f2}, R_{s1}, R_{s1} for the 400 mm salmon at $\theta = 20°$, the values obtained are 1600, 70, 98, 44 mm, respectively and the corresponding $2\pi R/\lambda$ ratios are 2826, 123, 172, 77, much larger than unity.

For the same data set, the range in TS calculated from the model based on varying parameters is plotted for each fish in Figure 3.6.2 assuming a half ellipsoid model of the swimbladder. Experimental results are plotted with 'x', mean TS with 'o', and the range from minimum to maximum TS as error bars. A similar plot is shown in Figure 3.6.3 assuming a full ellipsoid model of the swimbladder. Notice that the values using the full ellipsoid are lower than those for half ellipsoid and for the data.

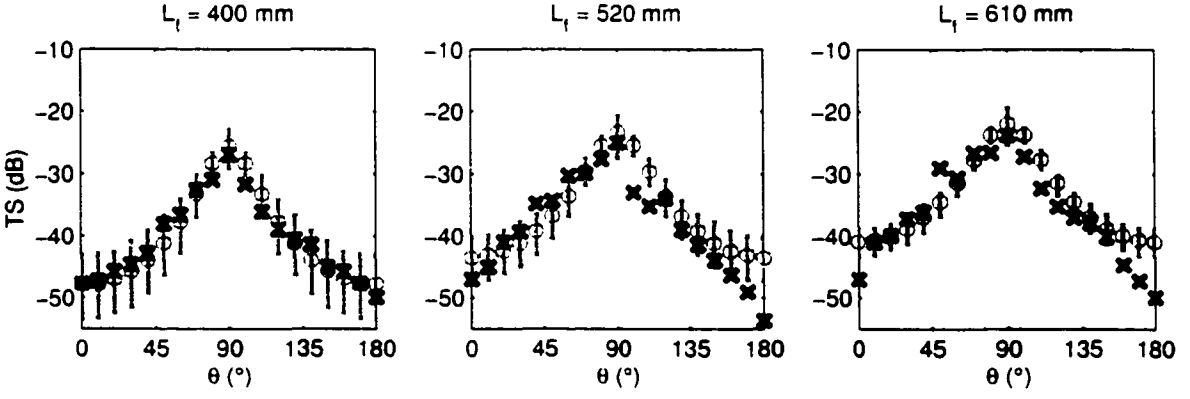

Figure 3.6.2 TS range over data using half ellipsoid swimbladder model. Dahl and Mathisen [1983] measured the TS of 3 tethered sockeye salmon at 10° intervals for side aspect only. The experimental results are shown as 'x' for the fish with $L_f = 400$ mm in (a). $L_f = 520$ mm in (b) and $L_f = 610$ mm in (c). The model results providing the mean TS are shown with 'o', and the range from minimum to maximum TS as error bars.

In Figure 3.6.4 the two cases from Dahl and Mathisen [1983] with asymmetrical TS data were used to calculate the TS with the proposed hybrid swimbladder model discussed in chapter 2. The TS was calculated using the length provided, the height

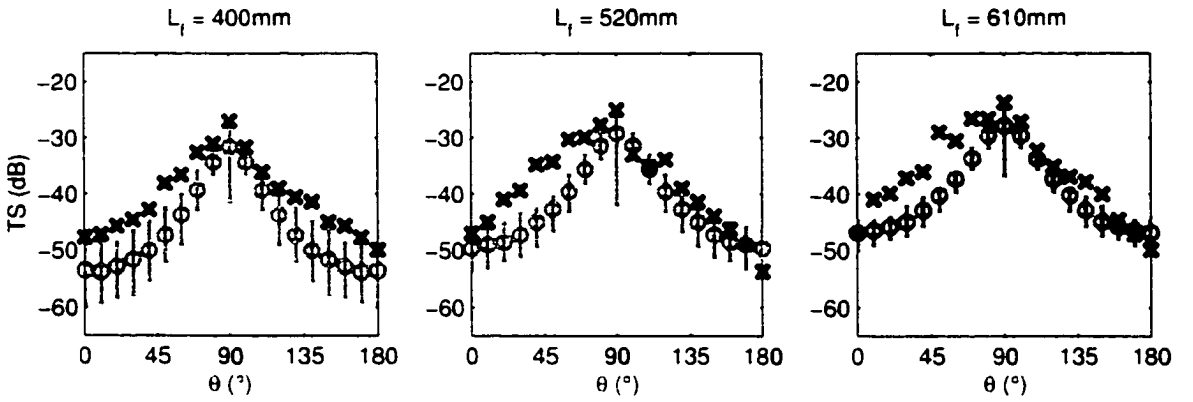

Figure 3.6.3 TS range over data using full ellipsoid swimbladder model. Dahl and Mathisen [1983] measured the TS of 3 tethered sockeye salmon at 10° intervals for side aspect only. The experimental results are shown as 'x' for the fish with $L_f = 400$ mm in (a), $L_f = 520$ mm in (b) and $L_f = 610$ mm in (c). The model results providing the mean TS are shown with 'o', and the range from minimum to maximum TS as error bars.

and breadth given by the regression lines in chapter 2, and standard swimbladder parameters. A value of $p = 0.25$ was used for the section of the swimbladder closer to the head ($\theta = 0-120°$) and $p = 0.40$ for the section closer to the tail ($\theta = 120-180°$). This provides the discontinuity at the point $\theta = 120°$.

In Figure 3.6.5, TS values from the model using a half ellipsoid swimbladder are plotted as a function of length for sockeye salmon. For each length found in the data given by Burwen and Fleischman [1998], the model was used to calculate the range of TS values for normal incidence, side aspect. The mean, minimum, and maximum target strength values were plotted for each length. Varying the height and breadth within 2.5 standard deviations of the appropriate mean provided the range of TS values plotted in (a). Experimental results are plotted with 'x', mean TS with 'o', and the range from minimum to maximum TS as error bars. The volume fraction is taken as $q = 0.1$ for fresh water. The TS is calculated for side aspect normal incidence ($\theta = 90°$, $\phi = 180°$). TS results found by varying the swimbladder parameters within an appropriate range along with the variations in

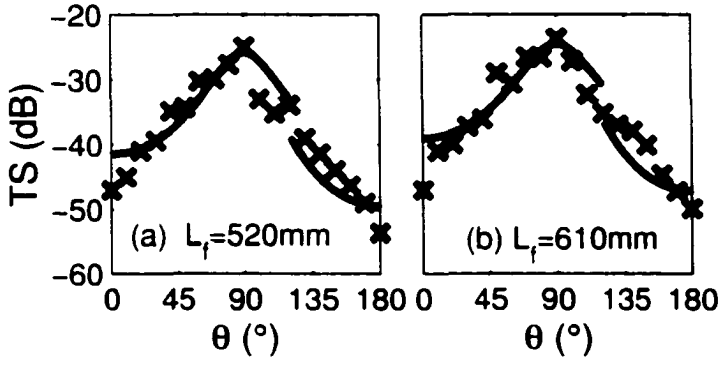

Figure 3.6.4 TS comparison using hybrid swimbladder model. A comparison of the hybrid swimbladder TS model is shown with experimental results for 2 specific sockeye salmon. The two cases from Dahl and Mathisen [1983] with asymmetrical TS data were used to calculate the TS with the proposed hybrid swimbladder model discussed in chapter 2. The TS was calculated using the length provided, the height and breadth given by the regression lines in chapter 2, and standard swimbladder parameters. A value of $p = 0.25$ was used for the section of the swimbladder closer to the head ($\theta = 0 - 120°$) and $p = 0.40$ for the section closer to the tail ($\theta = 120 - 180°$). This provides the discontinuity at the point $\theta = 120°$.

height and breadth are shown in (b) using the same symbols. Extreme ranges of p and r are chosen to cover the general range of these parameters.

Burwen and Fleischman [1998] tethered 93 live pacific salmon in front of a split-beam transducer operating at 200 kHz and measured their target strengths. About 37 of these were sockeye salmon with lengths ranging from 40 - 70 cm (average length 57 cm). Note that the model provides TS values that compare well with the experimentally measured TS. When taking into account $\pm 2 - 3$ dB fluctuations in TS arising from the variations in the heights and breadths, then a fixed $r = 1.75$ value provides a good match between the model and experiment. The variation in TS at a fixed length in general will be the result of both variations in the fish height and breadth as well as variations in the swimbladder parameters.

Figure 3.6.6 shows a comparison of the TS model with 3 frequency TS data. Burwen and Fleischman [1998] tethered 5 sockeye salmon and collected TS data using 120, 200, and 420 kHz at side aspect, normal incidence. The data show no

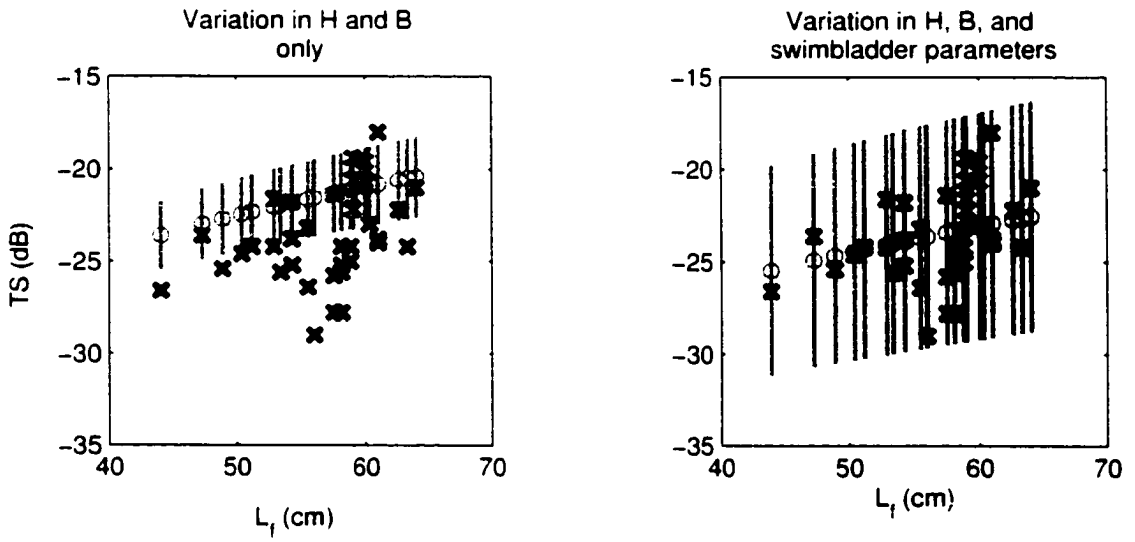

Figure 3.6.5 TS model covering the variation in TS data. TS values from the model using a half ellipsoid swimbladder are plotted as a function of length for sockeye salmon. Extreme ranges of p and r are chosen so as to cover the general range of these parameters. The volume fraction is taken as $q = 0.1$ for fresh water. The TS is calculated for side aspect normal incidence ($\theta = 90°$, $\phi = 180°$). Experimental results were extracted from Burwen and Fleischman [1998] and imposed on the model results as 'x'. Burwen and Fleischman tethered 93 live pacific salmon in front of a split-beam transducer operating at 200 kHz and measured their target strengths.

pattern between length and TS based on frequency. Using the known fish size data, an average TS value using appropriate swimbladder parameters was calculated for each fish and plotted as a gray dot. The minimum and maximum TS values were calculated independent of frequency and plotted as gray error bars. Note originally there are 2 sets of overlapping data: two fish with the same length ($L_f = 540$ mm), and one fish analyzed twice ($L_f = 645$ mm). These were each plotted with an offset to show the appropriate data.

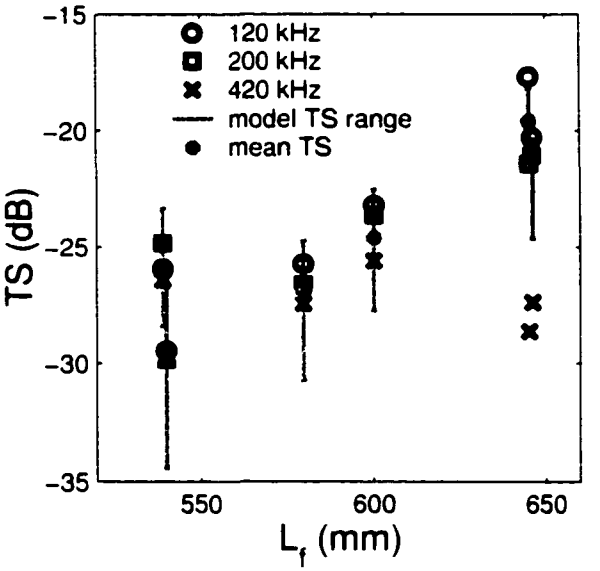

Figure 3.6.6 Comparison of TS vs. L for 3 frequency data. Burwen and Fleischman [1998] tethered 5 sockeye salmon and collected TS data using 120, 200, and 420 kHz at side aspect, normal incidence. The data show no pattern between length and TS based on frequency. Using the known fish size data, an average TS value using appropriate swimbladder parameters was calculated for each fish and plotted as a gray dot. The minimum and maximum TS values were calculated independent of frequency and plotted as gray error bars. Note originally there are 2 sets of overlapping data: two fish with the same length ($L_f = 540$ mm), and one fish analyzed twice ($L_f = 645$ mm). These were each plotted with an offset to show the appropriate data.

Figure 3.6.7 shows a comparison of the TS model results with data from other species in river setting. Kubecka [1994] collected TS data from tethered rudd (*Scardinius erythrophthalmus*) at normal incidence, side aspect rotating the fish in the

yaw plane several times. Kubecka fit a cosine cubed model to his data, as shown with the dash-dot line. For the fish with length, L_f = 190 mm, and swimbladder length, L_s = 50 mm, the TS model was used with varying height, breadth, and remaining swimbladder parameters to calculate a minimum and maximum TS. The height and breadth were varied as 30 to 38% of the length and 14 to 22% of the length respectively (values provided by Kubecka). The experimental data is plotted as dots and the minimum and maximum TS as solid and dashed lines respectively using the total TS neglecting the effect of fish flesh.

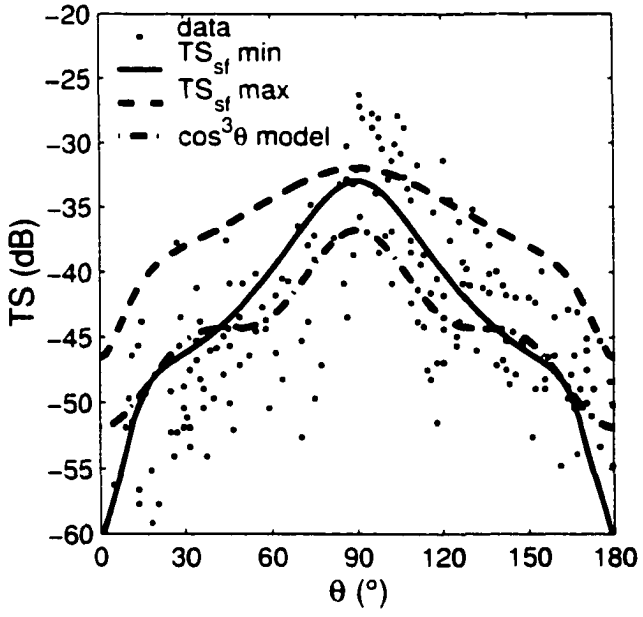

Figure 3.6.7 Comparison of TS between species within river setting. Kubecka [1994] collected TS data from tethered rudd at normal incidence, side aspect rotating the fish in the yaw plane several times. Kubecka fit a cosine-cubed model to his data, as shown with the dash-dot line. For the fish with length, L_f = 190 mm, and swimbladder length, L_s = 50 mm, the TS model was used with varying height, breadth, and remaining swimbladder parameters to calculate a minimum and maximum TS. The height and breadth were varied as 30 to 38% of the length and 14 to 22% of the length respectively (values provided by Kubecka). The experimental data is plotted as dots and the minimum and maximum TS as solid and dashed lines respectively using the total TS neglecting the effect of fish flesh.

Figure 3.6.8 shows the application of the TS model to species in an ocean setting. The TS is plotted as a function of length for 3 types of swimbladder fish at dorsal

aspect. The experimental results for TS of cod (*Gadus morhua*) shown using squares, saithe (*Pollachius virens*) shown using diamonds, and pollack (*Pollachius pollachius*) shown using circles were obtained by Foote [1980] for normal incidence at dorsal aspect using a frequency of 120 kHz. Note that Foote refers to these measurements as maximum TS, assumed here to occur at normal incidence. TS values for the swimbladder fish were calculated using a full-ellipsoid model with $q = 0.05$ (sea water) and with p and r taken at their nominal range of values. The minimum, average, and maximum TS results are plotted as dotted, dashed and solid lines respectively.

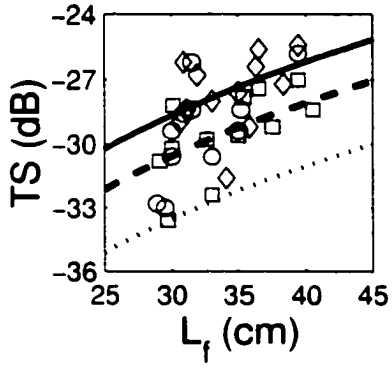

Figure 3.6.8 Application of TS model to species in ocean setting. The TS is plotted as a function of length for 3 types of swimbladder fish at dorsal aspect. The experimental results for TS of cod (square), saithe (diamond), and pollack (circle) were obtained by Foote [1980] for normal incidence at dorsal aspect using a frequency of 120 kHz. Note that Foote refers to these measurements as maximum TS, assumed here to occur at normal incidence. TS values for the swimbladder fish were calculated using a full-ellipsoid model with $q = 0.05$ (seawater) and with p and r taken at their nominal range of values. The minimum, average, and maximum TS results are plotted as dotted, dashed and solid lines respectively.

As noted previously the $\pm 2 - 3$ dB variation in the experimental values can be explained by typical variations in the fish height and breadth parameters or could result from variations in the swimbladder parameters as discussed in Chapter 2. These experimental data at lower frequency and smaller lengths allow for calculating the limit on the conditions of the model validity discussed in section 3.2. The

smallest fish in this data set is 28.9 cm long. Calculating R_{f1}, R_{f2}, R_{s1}, R_{s1} for this fish at $\theta = 90^{\circ}$ and $o = 90^{\circ}$ (dorsal, normal incidence), provides the values for these radii to be roughly 72, 1.22, 21, 1.16 cm respectively, and the corresponding $2\pi R/\lambda$ ratios to be 365, 6.2, 107, and 5.9. These numbers suggest that $2\pi R/\lambda \geq 5$ can be taken to be the limit of validity of the geometric model presented here.

The TS model presented in this chapter was developed using a geometric model approach. The approach has some limitations and restrictions, but is quite reasonable for the use of riverine sonar in Alaska to enumerate Pacific salmon and sockeye salmon in particular. The geometric approximation matches well with the Kirchhoff Integral approach which is much more difficult mathematically and more time consuming numerically. The model presented here allows for interpretation of TS data based on many independent parameters, such as fish morphological parameters, carrier frequency, and angle of incidence as opposed to some of the more typical dependencies seen in literature. For example, it is common to see TS as a function of ka where k is the wave number and a the radius of a cylinder or prolate spheroid or TS as a function of the fish length only. Next, the results of Chapter 2 and 3 will be used in the direct model of the fisheries acoustics problem to begin generating artificial sonar data (Chapter 4) in the steps to addressing the inverse problem (Chapter 5) of reconstructing the fish distribution given sonar data.

Chapter 4

DIRECT MODEL OF THE FISHERIES ACOUSTICS PROBLEM

The direct model is composed of a theoretical and a numerical model used to begin identifying uncertainties in the fisheries acoustics problem. A correct physical, theoretical formulation of the direct problem is essential for estimating various uncertainties inherent in the sonar technique, while a numerical model allows testing of the direct model under realistic conditions [Sonwalkar, 1999]. Up to now, this work has presented two of the critical elements in the direct model: the fish distribution model in Chapter 2 and the target strength or scattering model in Chapter 3. The remaining components of the direct model have been studied under work completed by other members of this research group: John Pham, M.S. [Pham, 1999]; Mark Ayers, M.S. [Ayers, 2001]; Biao Chen, M.S. [Chen, 2001]; and Zhiguo Lai, M.S. student [Lai, 2002]. This chapter compiles the work done on all the components of the direct model providing comparison of TS data with experimental data and generation of artificial sonar data to be used in the inverse model. Further, uncertainties are discussed at various levels within the model. First a discussion of the modular approach is given with details of each component. In the next section, motivation

for the direct model is discussed using background information that leads to a justification for the need to build the direct model using a modular approach so that uncertainties can be explained. Next, testing of the direct model is accomplished by comparing results to field data. Lastly, generating artificial data using the direct model concludes the chapter.

4.1 Modular Approach to the Direct Model

This work uses a modular approach to the direct model. Section 1.5 described the overall approach used in this work for the fisheries acoustics problem. Focusing on the direct problem only, Figure 4.1.1 schematically shows the various building blocks of the theoretical and numerical model for the direct model. The numerical model for each block is a separate entity and works independent of all the other blocks. In putting the direct model together, the overall numerical model utilizes the smaller modules whenever needed. Each block will be discussed separately below in reference to the sonar equation discussed in section 1.3.

4.1.1 Transmitter model

The transmitter model designed by Ayers [2001] and Chen [2001] simulates output from a single-beam elliptical or circular transducer. Here the transducer is modeled as a rectangular array of elements producing a known amount of pressure output at a selected frequency. The important features of the output signal include the time, frequency, amplitude, pulse length and ping rate. The amplitude is synonymous with the source level (SL) in the sonar equation. A model of the beam pattern factor is included here and based on work done by Ayers [2001]. This factor, $B(\theta, \varphi)$, compensates for weaker targets received off axis of the sonar beam depending on

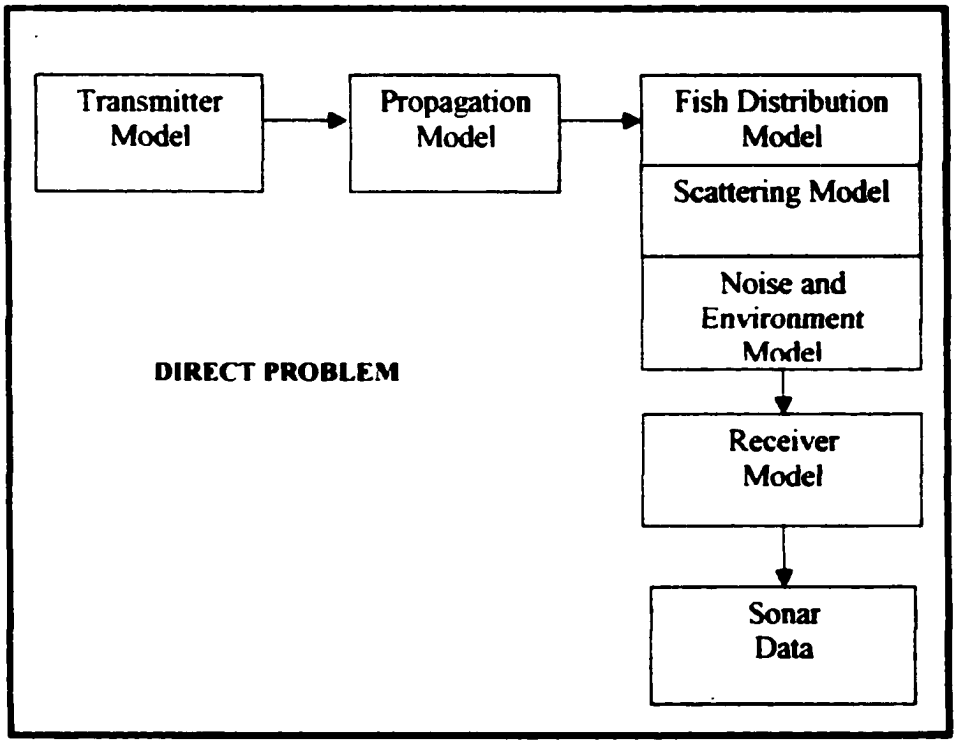

Figure 4.1.1 Block diagram of direct problem. A schematic is shown of the modular approach used in this work for the direct model. It is just a piece of the entire approach as shown in Figure 1.5.1.

their angular location.

In the simulation, a sonar pulse is modeled as a finite duration rectangular pulse with finite rising and falling times, modulated at the sonar carrier frequency [Lai, 2002]. Figure 4.1.1.1 shows a 120 kHz noise-free pulse with a pulse duration of 66.6 μs, rise and fall times of 41.6 μs and a sampling frequency of 1200 kHz. The pulse duration T_P is defined as the pulse period where the amplitude of the pulse is at 100% of it's peak value. T_R is the time taken for the pulse to pass from 0% to 100% of it's peak value or from 100% to 0% of it's peak value and T_D is the time from the initial transmission of the pulse to pulse reception [Ayers, 2001].

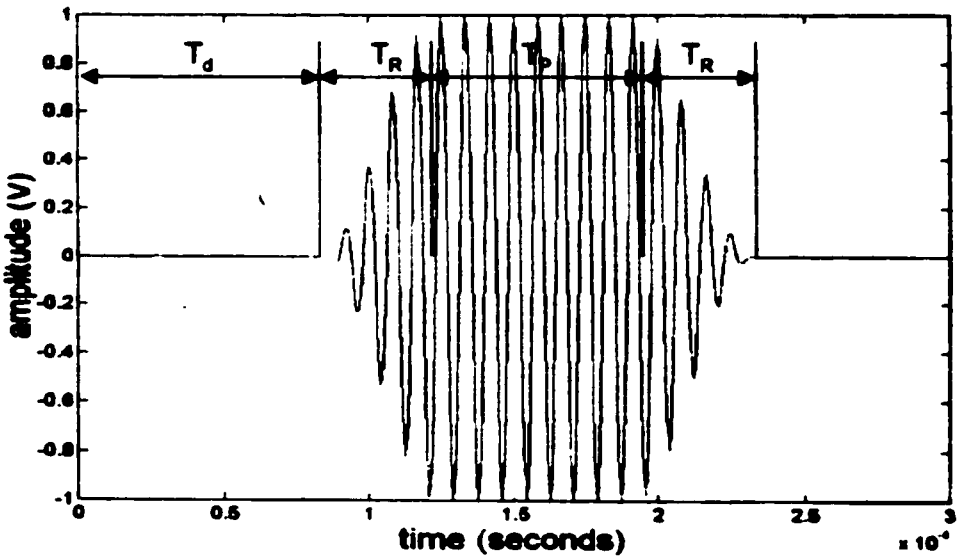

Figure 4.1.1.1 Example of a noise-free pulse. A 120 kHz noise-free pulse is shown with a pulse duration of 66.6 μs, rise and fall times of 41.6 μs and a sampling frequency of 1.2 MHz. The pulse duration T_P is defined as the pulse period where the amplitude of the pulse is at 100% of it's peak value. T_R is the time taken for the pulse to pass from 0% to 100% of it's peak value or from 100% to 0% of it's peak value and T_D is the time from the initial transmission of the pulse to pulse reception [Ayers, 2001].

The pulse carrier frequency used in most commercial riverine single beam sonar

systems ranges from about 100 kHz to about 420 kHz. The choice of carrier frequency affects the attenuation of the signal in the water and the target strength of the fish as discussed previously. The choice of carrier frequency is based on several factors including the size of the fish, the range and angular resolution required and the attenuation level allowed (based on the signal to noise ratio and the maximum expected range of the fish) [Ayers, 2001].

The duration of the sonar pulse affects the accuracy of the measured phase. Phase is calculated by the in-phase/quadrature method [Chen, 2001]. This method averages over the pulse duration. Therefore a longer pulse provides more averaging and thus more noise reduction. The trade-off is in the system resolution. The resolution of a sonar system is defined as

$$x_{min} = \frac{c\tau}{2}$$

where x_{min} is the minimum distance for two objects to be separated and still be resolved as discrete objects, τ is the pulse duration, and c is the speed of sound in water [MacLennan and Simmonds, 1992]. Typical pulse durations in commercial single beam sonar systems range from about 0.1 ms to 1 ms, corresponding to a resolution of 7.5 cm and 75 cm respectively [Ayers, 2001].

4.1.2 Propagation model

The propagation model takes into account the spreading and attenuation of spherical waves. These factors are represented by the time varied gain (TVG) and the absorption (ABS) in the sonar equation and depend on characteristics of the medium through which the sound is travelling. Often these are combined into one factor called the transmission loss (TL). Both factors were discussed in section 1.3.

4.1.3 Fish distribution model

The fish distribution model is based on the data collected on sockeye salmon dimensions, swimbladder characteristics, and the distribution of the salmon in the river as presented in Chapter 2. In the sonar equation of section 1.3, the essential elements of the fish distribution model are involved in the calculation of target strength (TS) and the angular location of a fish (θ, o). The range to the fish location also plays a role in the transmission loss (TL) as discussed in section 1.3 of the introduction.

4.1.4 Scattering model

The scattering model is the target strength model discussed in Chapter 3 used to calculate the target strength (TS) of sockeye salmon as a function of the morphological properties of the fish and the orientation of the fish in the sonar beam.

4.1.5 Noise model

The noise model for background noise, provided by Pham [1999], Ayers [2001] and Lai [2002], assumes a Gaussian distribution with zero mean and and finite variance (noise level). The noise level (NL) can be thought of relative to the source level through the signal to noise ratio given by $NL = SL - SNR$. According to Urick [1983], background noise is dominated by the thermal noise in the frequency band above 50 kHz. For ordinary temperatures, the noise level is given as $NL = -15 + 20\log_{10} f_c$ where NL is the noise level in dB//1 μPa and f is the frequency in kHz [Lai, 2002].

Figure 4.1.5.1 shows an unfiltered pulse with a signal to noise ratio of 5 dB using the same parameters as in the previous figure. This pulse is then demodulated and resampled to produce the sonar pulse in the receiver model.

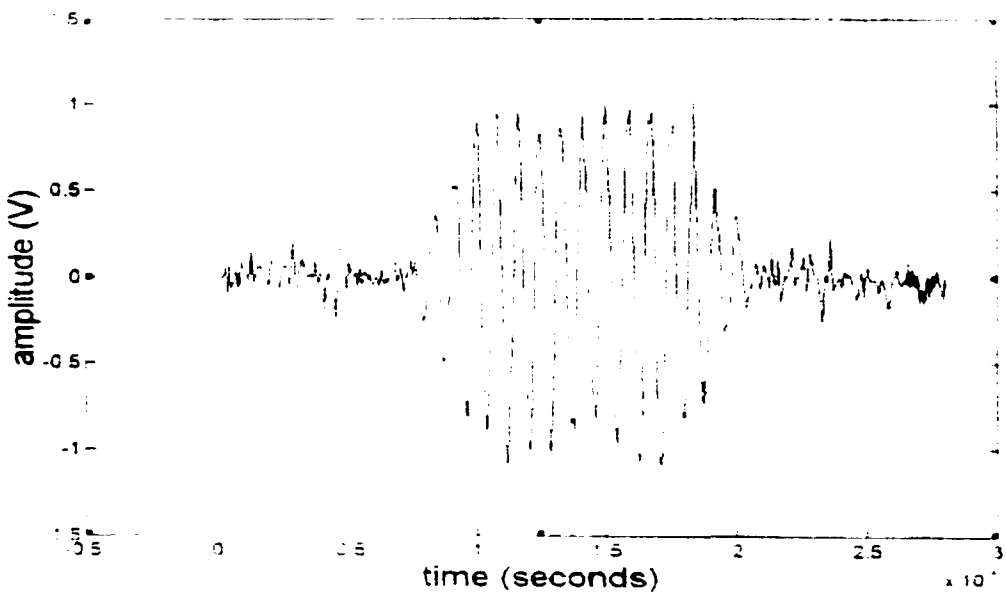

Figure 4.1.5.1 Example of pulse with 5dB SNR. Shown is an unfiltered pulse with a signal to noise ratio of 5 dB using the same parameters. This pulse is then demodulated and resampled to produce the sonar pulse in the receiver model. The pulse carrier frequency used in most commercial riverine single beam sonar systems ranges from about 100 kHz to about 420 kHz [Ayers, 2001].

Although ambient noise can usually be filtered if the SNR is not too low (although not perfectly), reverberation is more difficult to remove. If the unwanted targets produce a pattern unlike that of the desired targets, it may be possible to eliminate those echoes. For the purpose of this work, only ambient white noise is used and is added to the signal before demodulation. The sonar equation does not include a noise parameter, but the noise is inherent in the TS value, in the uncertainty of the angular location, and thus in the amplitude of the received echo, RL.

4.1.6 Receiver model

The receiver model is identical to the transmitter model. It uses the beam pattern of the sonar transducer to determine the amplitude of the received signal. Figure 4.1.6.1 shows an example of a ping or transmitted pulse, the reflection from a target, and the total returned echo in the absence of noise. The top panel shows the transmitted pulse with amplitude (pressure in Pascals) as a function of time in seconds. The middle panel shows the returned echo with the shape having a tapered effect as discussed. Note that the time axis is shifted to show the lapse time between the transmitted and received echo of ~ 0.0357 seconds. The bottom panel shows the demodulated pulse that is considered the total echo from that ping and is saved as a portion of sonar data.

Pham's [1999] work focused on the measurement of various parameters of the received echo in the presence of noise, such as signal amplitude, arrival time, pulse width, rise time, and phase. Measurement of the amplitude, pulse width and rise time of the received signal characterizes the fish with respect to body size and swimbladder size. The arrival time is indicative of the distance of the fish from the

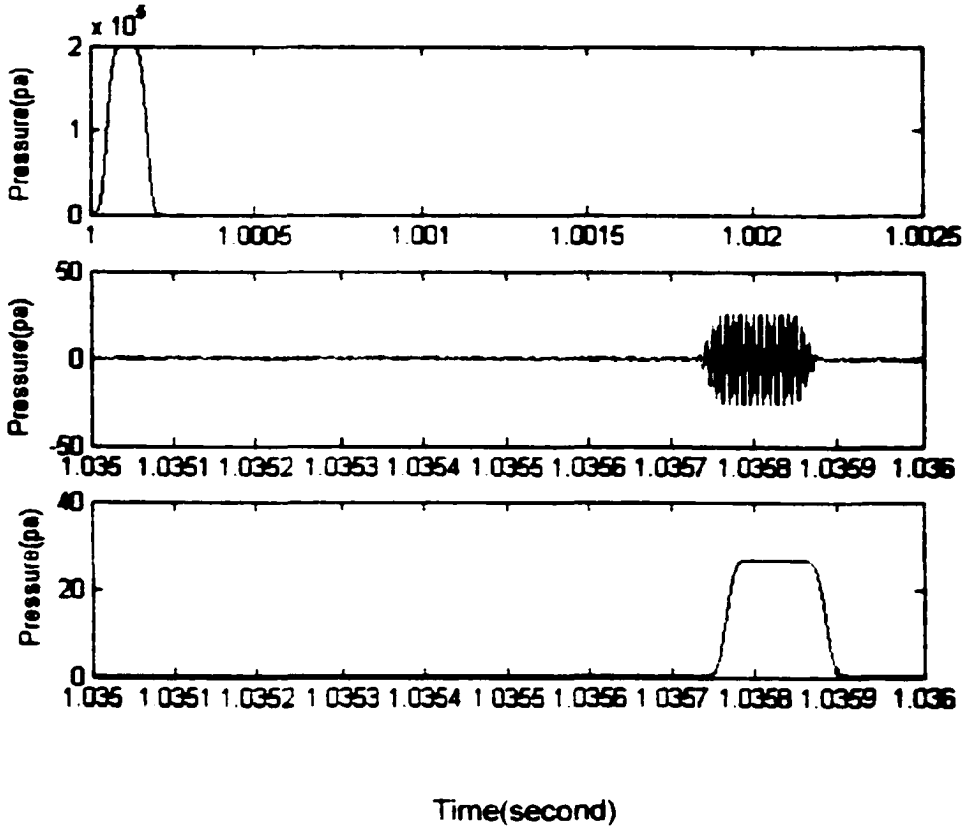

Figure 4.1.6.1 Transmitted and received pulse. An example is shown of a transmitted ping, the reflection from a target, and the total returned echo in the absence of noise. The top panel shows the transmitted pulse with amplitude (pressure in Pascals) as a function of time (sec). The middle panel shows the returned echo with the shape having a tapered effect as discussed. Note that the time axis is shifted to show the lapse time between the transmitted and received echo of ~ 0.0357 seconds. The bottom panel shows the demodulated pulse that is considered the total echo from that ping and is saved as a portion of sonar data [Chen, 2001].

sonar. And comparison of measured pulse phase in a split-beam sonar determines the direction of the fish. Additionally, all measurements of echo parameters (especially the phase measurement) may be useful in distinguishing two or more overlapped pulses. Monte Carlo simulations were used to study and quantify the effects of the noise filters found inside the sonar receiver on measurement accuracy and precision using an echo with fixed parameters and a fixed Butterworth low pass filter [Pham, 1999].

As seen in the field, the received pulse width is generally greater than the transmitted pulse width. This spreading-out effect is due to the fact that many parts of the fish body scatter the sonar energy back to the receiver. For a transmitted pulse width of 0.1 ms, the received pulse width may be up to 10 times greater.

The pulse-tapering effect may be caused by the drastic difference in reflectivity between fish flesh and air inside the swimbladder. As the sonar signal washes over the fish body, the early and late returns are due to the fish flesh and are relatively weak compared to the middle return from the air-filled swimbladder [Pham, 1999].

Using all of these models together, sonar data is constructed similar to that found in a riverine setting. Motivation for the need to construct and use the direct model in given in section 4.2. Results for a variety of fish rates are shown in section 4.4 for both a statistical approach (100 sets of data) and several case studies (1 set of data only). At each stage of the direct model, the goal is to pinpoint the origin of uncertainty and to quantify this amount. This allows for better interpretation of the *in situ* data as well as better understanding of each component for future work.

4.2 Motivation for the Direct Model

Collection of sonar data using single beam systems was relatively simple needing only a small capacity of memory, but much information was lost or never even collected. Today, with the wide spread use of split-beam systems in Alaska, the amount of data is tremendous and post-processing is used yearly to better understand the data collected. However, some real-time processing is performed on the sonar data during operation while receiving the echoes. Although it is not usually performed at the transducer itself, once the data is sent to the computers for storage, only the post-processed data is stored. This processing may include setting a collection threshold in which data with TS values lower than a preset value are automatically excluded. The data are often compressed for ease of storage. Also, filters may be applied to the number of echoes returned, the target strength values of echoes within a track, and the number of missing echoes in a track, just to name a few examples. Later, after the data collection is completed and most often after management decisions have been made, the data is then sent through a more rigorous post-processing system in hopes the research will provide understanding of the details of the fisheries for that year and insight into making the sonar a more accurate system. The above mentioned filters are sometimes applied during collection of sonar data and other times used during post-processing of the data. Note that those working in this field of research usually refer to the initial data as raw data, although some processing has been performed. Post-processed data usually refers to data that has been manipulated well after the data collection is final.

An analysis of echoes due to the effects of filter characteristics was performed using data obtained from a BioSonics' split-beam sonar. It was discovered that the

data possessed certain fundamental discrepancies. At the most basic level, there is the question of how to estimate echo parameters: the amplitude, arrival time, pulse duration and the phase of an echo in the presence of noise. Figure 4.2.1 shows an example of TS values of an echo as determined from the individual samples of the echo. The figure shows the variability in TS within one echo and thus underscores the importance of the need to accurately measure the pulse parameters. The question remains what TS to assign to this echo? Furthermore, how do the TS values change if the front end low pass filter (used to reduce noise) characteristics are varied? Results based on the model by Pham [1999] provided two major conclusions. (1) The measurement of echo parameters depends on the front end low pass filter characteristics. (2) The optimal filter that will provide best measurements on one echo parameter (e.g., amplitude) will not necessarily provide the best measurement of some other parameter (e.g., phase). Note that the uncertainty in the measurement of pulse parameters also leads to an uncertainty in the measurement of fish angular position using split-beam sonar. The presence of noise leads to uncertain measurement of phases of the returned echo as measured by four quadrants of split-beam sonar, which in turn leads to uncertainty in the measurement of fish location.

Almost always, the true solutions (fish count, fish distribution) are not known. There have been a few experiments performed to validate sonar counts using tower counts, but these can only be carried out in limited cases.

Tower counts are performed visually by a person located on a tower about 15 - 20 feet above the river surface counting the fish as they pass by a fixed location. There are difficulties counting fish using tower counts although often these counts are considered accurate. This counting method can only be conducted in rivers with very clear water and even under ideal conditions observation is limited by distance.

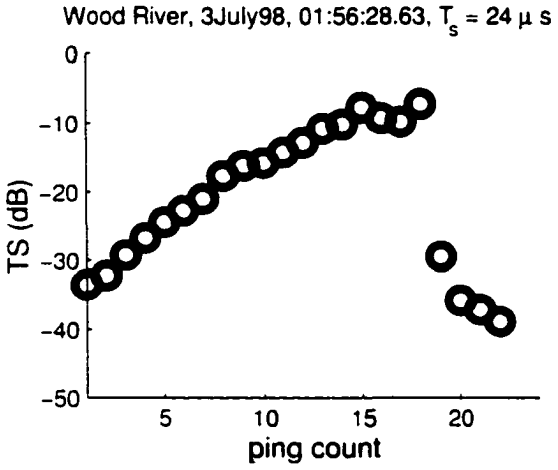

Figure 4.2.1 TS of the individual samples from an echo. An example of TS of an echo determined from the individual TS of samples of the echo. The figure shows the variability in TS within one echo and thus underscores the importance of the need to accurately measure the pulse parameters.

Also, the counters can only observe for a limited amount of time. Lastly, when the amount of fish in the water becomes dense, observers count by grouping in 5s or 10s, thus leading to human error.

Figure 4.2.2 shows the results from an experiment conducted at the Wood River on 3 July 1998 [Sonwalkar and Adams, 1999] where tower counts versus sonar counts for 24 10-minute intervals were collected. The dashed line, with unity slope, represents the case when these two counts match. The solid line represents the least squared regression line fit to the data. This figure shows that sonar and tower counts match closely when the fish passage rates are below $\sim$ 600 fish/10 minute (or 1 fish/sec). However, when fish passage rates begin to exceed 600 fish/10 minute, the sonar counts begin to fall below the tower counts, typically half of the latter. More importantly, without the tower counts to aid in defining the best choice of filters to set, it is possible that for even low fish passage rates the counts could be drastically different than reality. By using various filters through post-processing of this same data, it was possible to generate outcomes of anywhere from one-tenth to

10 times the actual fish count.

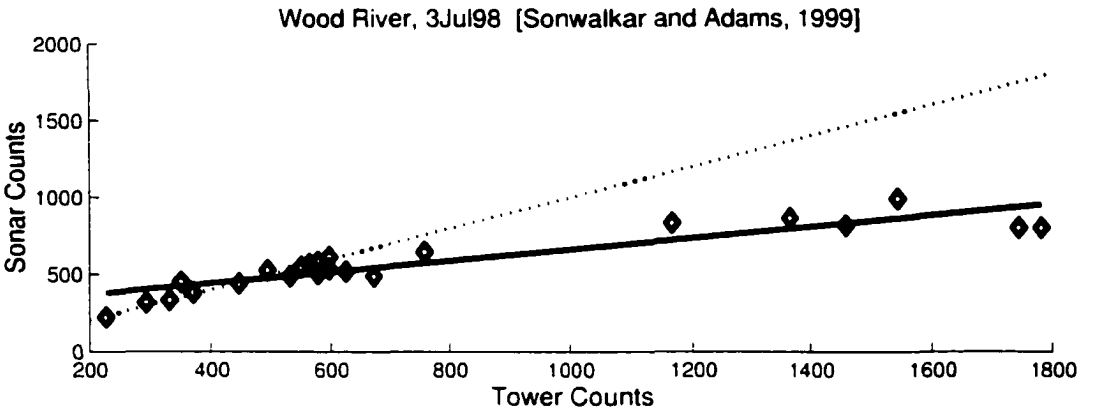

Figure 4.2.2 Comparison of tower and sonar fish counts. The results are shown from an experiment conducted at the Wood River on 3 July 1998 [Sonwalkar and Adams, 1999] where tower counts versus sonar counts for 24 10-minute intervals were collected. The dashed line, with unity slope, represents the case when these two counts match. The solid line represents the least mean square regression line fit to the data.

Table 4.1 shows an example of the effects of filter parameters on sonar data. The data was post-processed using various filter parameters to obtain a fish count. The actual fish count of 228 fish was obtained by a tower count over a 10 minute period of time. The sonar system was located very near the tower and also collected data during the same time period, producing a real time sonar count of 209 fish. Filter parameters were set for the real time collection by observation of the situation previous to collecting data.

The filter types include net distance, fish length, milling factor, ping concentration, target strength, and aspect ratio. If chosen, each of these options requires a minimum and maximum value. The user may choose no filters, all filters, or any combination of filters desired. For a judicious selection of filter-parameter values, the user must have some knowledge of the characteristics of the target species and their behavior at the site where data was collected.

When selecting the net distance filter, a track is classified as a fish if the distance

traveled in the beam is within the range specified in meters. This distance is merely calculated from the beginning of the track to the end of the track. The fish length filter forces tracks to have returned echoes inside the range of number of pings designated before the track can be labeled as a fish. This filter deals not only with how long the fish is in the beam but also with how fast the fish is moving. Milling factor is a filter that allows longer tracks to be designated as a single fish, taking into account the milling behavior. If fish at a site are not traveling in a mostly straight path then appropriate values for this filter could be helpful in allowing the correct number of fish to be determined. Ping concentration filter requires a certain percentage of returned echoes to be necessary before allowing a track to be counted as a fish. This filter could compensate for fish leaving the edge of the beam and then returning or for fish changing aspect with respect to the beam and thus producing weak echoes within its track. If the target strength filter is selected, the track designates fish only when the average value of echo target strengths falls within the decibel range defined. Finally, aspect ratio is a measure of direction traveled through the beam, forcing tracks to be counted as fish if the value for a track falls within the range chosen. The aspect ratio is defined as the change in y-value over the change in x-value using the locations at the start and end of the track only.

Although the real time sonar count and the tower count are relatively close, changing the filter parameters can produce very different results as seen in the table. If the observation analysis previous to data collection is incorrect, the sonar counts can be highly inaccurate. Also, if the fish density situation changes during data collection, then the filters need to change as well to fit the situation. Currently, there is no process in place to handle this automatically [Sonwalkar, 1999].

Thus the direct model is constructed to first reproduce data collected during

Table 4.1 Effects of Filter Parameters on Sonar Data. Wood River: 3 July 1998 1:50:18.17 am - 1:59:53.37 am [Sonwalkar and Adams, 1999].

Filter Name	Filter Values	Fish Count
No Filter		1193
Net Distance	0.5 to 4 meters	23
	0 to 100 meters	1193
Aspect Ratio	-0.5 to 0.5	237
	0 to 0.5	237
Fish Length	2 to 8 pings	512
	4 to 20 pings	162
Milling Factor	1 to 10%	53
	15 to 100%	191
Ping Concentration	40 to 100%	1170
	75 to 100%	950
Average TS	-30 to -20 dB	381
	-40 to -10 dB	1074

real time experiments and field work. The sonar data generated through the direct model is not thresholded at first providing the actual raw data. Once a threshold is applied to the artificially generated data, it takes on the same format as the raw data used by the various agencies. Since uncertainties are observed at various levels of processing, as shown in the range of TS values of samples within an echo and in the range of fish counts based on the use of various filters, a method to separate these uncertainties is needed. The modular approach to the direct model allows for the pinpointing of where and when the uncertainty arises. It also allows for a quantification of these extracted errors as discussed in the following section, testing the direct model.

4.3 Testing the Direct Model

The direct model can be tested by comparing the generated sonar data with that of experimental data. This comparison shows the accuracy and reasonableness of the direct model and methods of calculating uncertainty inherent in the experimental data.

The analysis was performed on data obtained from the US Fish and Wildlife Service (USFWS) sonar project on the Chandalar river in 1995 [Daum and Osborne, 1996]. The data was collected with a 200 kHz split beam sonar system operating at 10 pings per second. The elliptical beams had nominal beam widths (measured at -3 dB point down the acoustic axis) of 4.6° by 10.8°. For the sonar transducer on the left bank sonar, there was a 5° angle of tilt into the river, a pulse width of 0.2 ms, and low background noise levels ranging from -49 to -42 dB. During this experiment, USFWS staff captured 41 migrating adult chum salmon (*Oncorhynchus keta*) and attached a numbered balloon to the dorsal fin of the fish using monofilament line. Before releasing, length measurements were taken on each fish and referenced with the balloon number. The fish were then released back into the river. Farther upstream, when the fish were spotted and identified by the balloon number before entering the section of the river where the sonar was stationed, the split-beam sonar was turned on to track only that fish as it moved through the beam. It was assumed that the balloon did not affect the movement of the fish.

Note that the fish distribution model presented in Chapter 2 was based on data obtained from sockeye salmon. However, as shown with the example of the rainbow trout, other Pacific salmon species tend to follow a similar distribution as that found for the sockeye salmon. Thus, the distribution from Chapter 2 was applied to the

chum salmon with reasonable expectations.

One fish track, number L215-5, was analyzed using the direct model. In Figure 4.3.1 the motion of a chum salmon in three dimensions obtained from the experimental data is plotted. The location of the fish was estimated from the sonar data using both angles off-axis and the range reported for each ping. The figure shows the 3D position as a circle with the ping number marked close by. The location of the fish at the starting ping, or beginning of the track, and the ending ping are labeled along with a time stamp showing this fish was in the beam for 4.5 seconds. The small arrows attached to each circle provide the direction of fish travel at that time, thus pointing to the next location. Note that this same fish track was shown in Figure 1.4.6 as a projection in the $x - y$ plane excluding range.

Assuming that the fish length is oriented along the current fish velocity and that the height of the fish is in the vertical plane, it is possible to predict the TS at each ping using the TS model described in Chapter 3. Since for each fish, the length was known, the parameters left to vary include the fish height and breadth, the swimbladder parameters, and the incident angles. The incident angles were calculated from the location determined by the experimental data; however, this assumes no fish roll.

Figure 4.3.2 shows a comparison between the calculated TS and the measured TS based on the location of this chum salmon in three dimensions. The filled circles in the figure indicate echoes for which the calculated and measured TS are within a 6 dB cut-off limit of each other while the open circles indicate when they are not. Again, the numbers close to the circles represent the ping number for that echo. For this example, 19 of the 29 echoes have TS values within 6 dB of the model TS results. The TS was calculated using the exact length measurement, an average

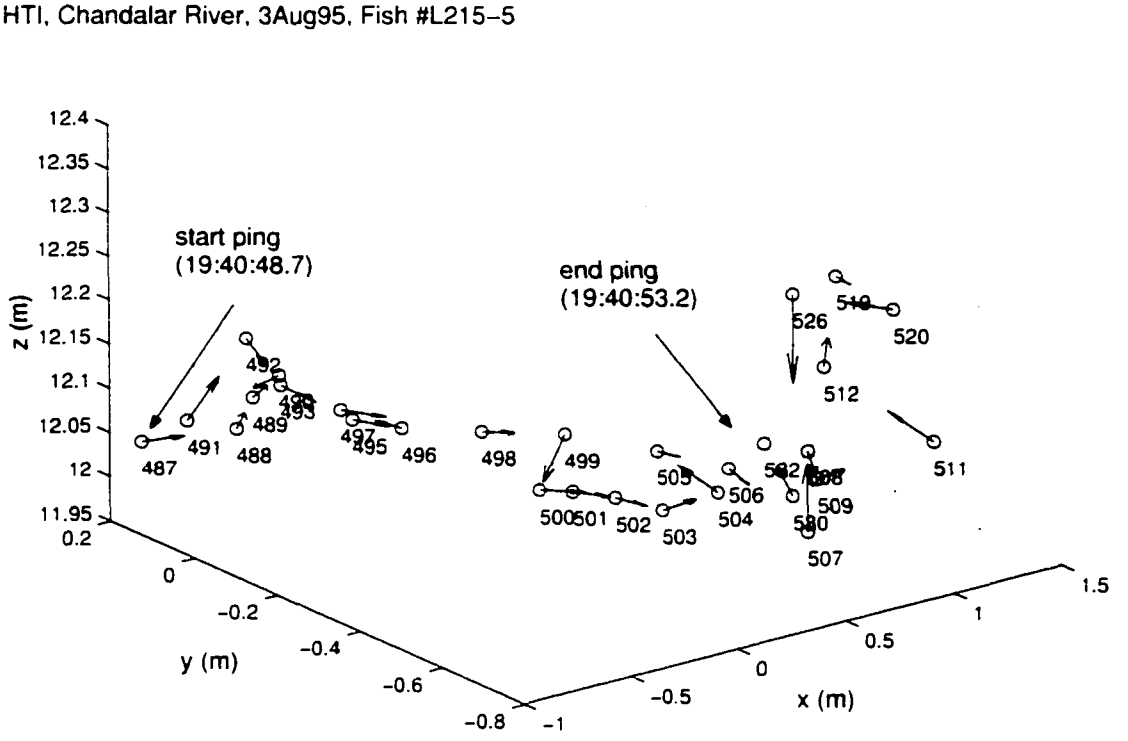

Figure 4.3.1 Fish location from sonar data. The location of a chum salmon (*Oncorhynchus keta*) is shown in three dimensions as a function of time (ping number). The experimental sonar data was used to extract the angular location of the fish while moving through the sonar beam at each ping. The angular location was transformed into x, y, z coordinates and the position was plotted as a circle. The numbers close to the circles represent the ping number for that echo. The start and end pings are marked with a time stamp showing this fish was in the beam for 4.5 seconds. The small arrows attached to each circle provide the direction of fish travel at that time, thus pointing to the next location.

height and breadth value based on the fish distribution model, average swimbladder parameters discussed in Chapter 2 ($p = 0.30$, $q = 0.10$, $r = 1.75$ with half ellipsoid model for the swimbladder), and the incident angles provided by the experimental data.

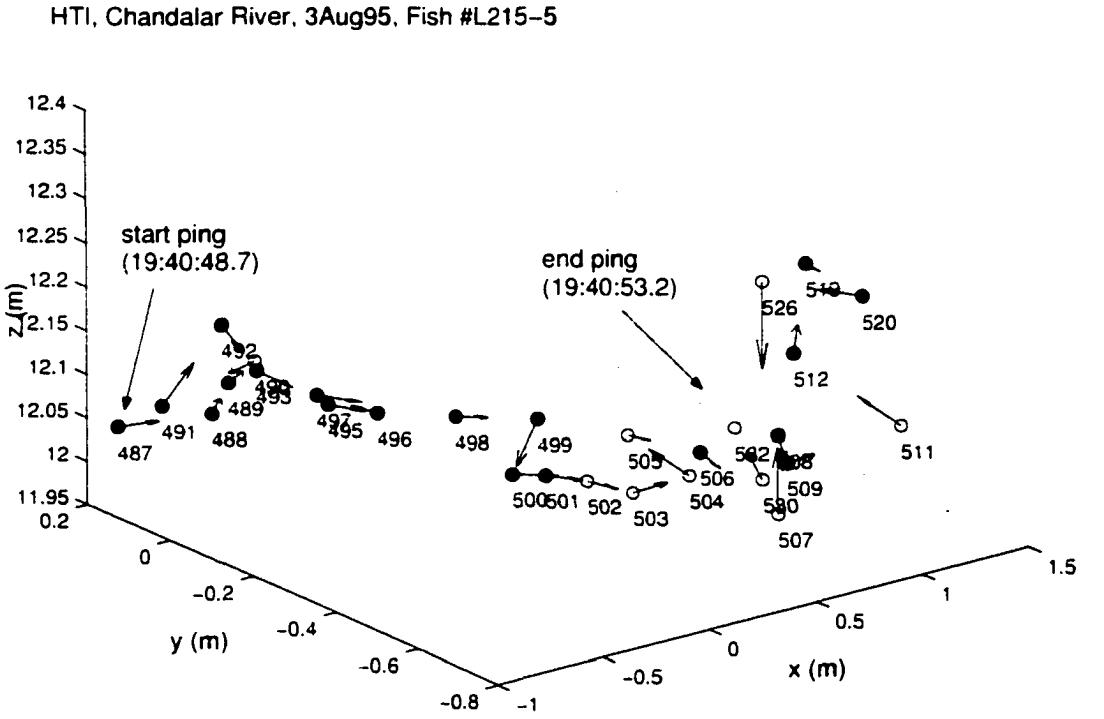

Figure 4.3.2 TS comparison based on fish motion. A comparison between the calculated TS and the measured TS based on the location of a chum salmon is shown in three dimensions. The filled circles in the figure indicate echoes for which the calculated and measured TS are within a 6 dB cut-off limit of each other while the open circles indicate when they are not. For this example, 19 of the 29 echoes have TS values within 6 dB of the model TS results. The TS was calculated using the exact length measurement, an average height and breadth value based on the fish distribution model, average swimbladder parameters discussed in Chapter 2 ($p = 0.30$, $q = 0.10$, $r = 1.75$) with half ellipsoid swimbladder), and the incident angles provided by the experimental data.

A cut-off value of 6 dB was chosen as uncertainty in TS values allowing for this amount of discrepancy in the data. It was seen in section 3.5 that as the fish height and breadth vary for a fixed length; the TS values vary within 3 dB. In addition,

as the second order effects of fish flesh on TS are taken into account, the TS values vary again within 3 dB. Thus to have the calculated and measured TS values within 6 dB shows that at most these two variations provide uncertainty at that point.

From viewing video tapes of chum salmon swimming, an additional swimming behavior trait was modeled by including a fish roll factor. In the fish movement model discussed in section 2.3, the y-axis of the fish was assumed to be in the vertical plane (see Figure 2.1.1). However, in reality the fish tend to roll about the z-axis as they swim. Although it was difficult with the resources at hand to provide a measurement, angles of $\pm 45°$ seem reasonable based on inspection of the video (video provided by David Daum, U.S. Fish and Wildlife Service, Fairbanks, Alaska).

By adding a fish roll factor, o_{roll} ranging from 0 to $\pm 45°$, 4 more TS values can be brought within limits of the model results. Figure 4.3.3 shows the addition of echoes with matching TS values within 6 dB if a roll angle of $\pm 45°$ is included in calculating the model TS values. At this second stage 23 of the 29 echoes have model TS results within 6 dB of the actual TS values. This shows that the roll may be an important factor often missing from analysis of riverine sonar data. The implication is that if the incident angles calculated always are assumed to give side aspect angles with the fish height in the vertical plane, then the TS values may be inaccurate and lead to an underestimation of fish, especially when using the echo integration process.

Figure 4.3.4 shows the addition of echoes with matching TS values within 6 dB if the incident angles are allowed to vary $\pm 30°$ from normal incidence, side aspect in addition to the inclusion of the roll angle. Here 28 of the 29 echoes have model TS results within 6 dB of the actual TS values. The implication is that uncertainties exist in estimating the incident angles based on experimental data, since the better

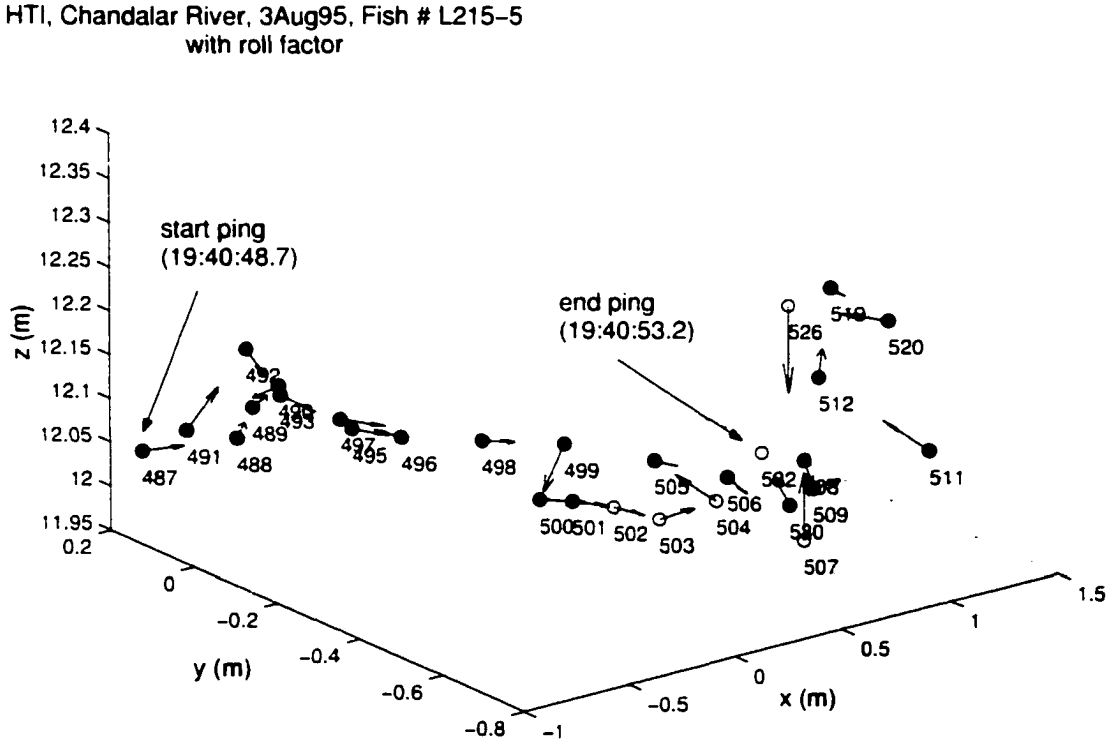

Figure 4.3.3 TS comparison based on fish motion including fish roll. The additional echoes are shown with matching TS values within 6 dB if a roll angle of $\pm 45°$ is included in calculating the model TS values. At this second stage 23 of the 29 echoes have model TS results within 6 dB of the actual TS values.

fit came from modifying the incident angles found from the data.

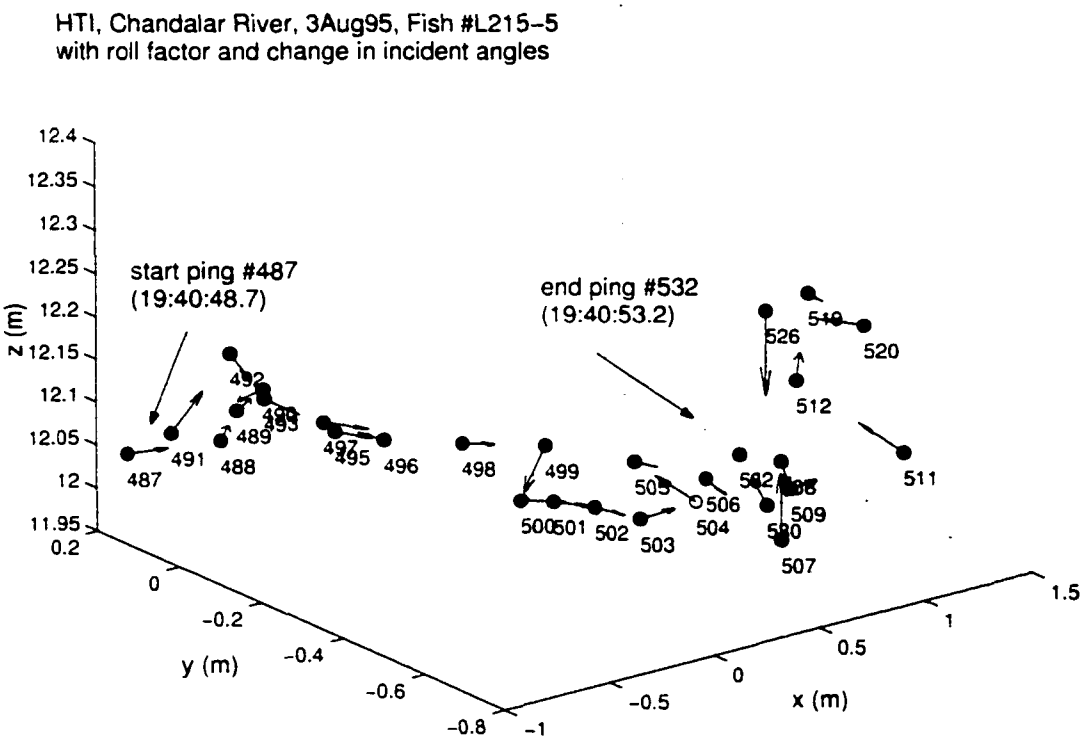

Figure 4.3.4 Uncertainty in TS calculations based on incident angles. The additional echoes are shown with matching TS values within 6 dB if the incident angles are allowed to vary ±30° from normal incidence, side aspect in addition to the inclusion of the roll angle. Here 28 of the 29 echoes have model TS results within 6 dB of the actual TS values.

For this example, 28 of the 29 echoes were able to be matched automatically or by changing the incident angles by including a roll factor or allowing the aspect to change. Other examples may provide better or worse results. For the one data point when the model is not able to predict the TS accurately it is likely that there were stronger uncertainties inherent in the location based on the experimental data (the aspect angles were off by more than the 30° used) or the noise was not accounted for in the model (higher noise level than expected).

4.4 Generating Artificial Data from the Direct Model

Using all the modules for the direct model as discussed in section 4.2 above, artificial sonar data can be generated. In doing so, parameters are needed for the river cross-section and sonar data generation. The values chosen here are typical values used in many experimental situations such as those published in reports concerning the Chandalar River by Daum and Osborne [1996], Osborne and Daum [1997]; the Kenai River by Burwen, Bosch, and Fleischman [1995], Burwen and Bosch [1996], and BioSonics, Inc. [1998]; the Yukon River by Huttunen and Skvorc [1994], Huttunen and Skvorc [1996], and Konte *et al.* [1996]; the Lower Yukon River by Fleischman, *et al.* [1995] and Maxwell *et al.* [1997]; the Noatak River by LaFlamme [1995]; the Aniak River by Vania and Huttunen [1996]; the Kuskokwim River by Vaught and Molyneaux [1995]; and the Wood River by BioSonics, Inc. [1998].

More specifically, to generate the data the transmitter model is used with a fixed carrier frequency $f_c = 105$ kHz and a source level of 166 dB//1 μPa. A variety of ping rate and pulse width values are used and discussed when needed. The propagation model uses a fresh water assumption to calculate the absorption term. The fish size distribution developed in Chapter 2 is used in the scattering model that takes advantage of the TS model described in detail in Chapter 3. Various noise levels are used assuming only background noise. The receiver is assumed to be the same as the transmitter and thus uses the same beam factor. Further details on the spatial fish distribution and the processing of the data follow.

Fish track data is produced using the model described in section 2.3.2. The river cross-section is defined by three segments providing a river 70 m wide with a maximum depth of 4 m at 25 m from the left bank and a depth of 3.8 m at 35 m

from the right bank, consistent with several of the smaller rivers in Alaska [Daum and Osborne, 1996; LaFlamme, 1994]. Next the fish is assumed to be a point target with the center of the fish assumed to be at the location generated by the fish track data. To generate the fish track data, a range of fish rate parameters are used as defined by an average rate (fish per second) entering the beam with a standard deviation (fish per second), referred to hereafter as $[\mu_{fr}, \sigma_{fr}]$ where the subscript of 'fr' refers to fish rate.

Examples are provided in this section displaying typical sonar data generated using the direct model for one value of low fish rate and one value of high fish rate. To generate low fish rates the parameters are assumed to be $[\mu_{fr}, \sigma_{fr}] = [0.3, 0.3]$. This fish rate is comparable to those found in the Wood River experiment seen in Figure 4.2.2 corresponding to a fish passage rate of approximately 180 fish per 10 minutes, falling into the region where the sonar fish counts match the tower fish counts reasonably well. For high fish rate, $[\mu_{fr}, \sigma_{fr}] = [3.0, 0.3]$ is used. This rate is equivalent to 1800 fish per 10 minutes or when fish counts from sonar data are much lower than the tower fish count estimates as seen in Figure 4.2.2.

As the fish track data is generated, it is processed using the following range of receiver and noise parameters: ping rate of 5 - 15 pings per second (in intervals of 5), a pulse width of 0.3 - 1.5 ms (in intervals of 0.4), and a noise level of 0 - 60 dB//1 μPa (in intervals of 20). Varying one parameter at a time allows for analysis of that parameter; the non varying parameters are held constant at 5 pings per second, 0.7 ms pulse width, and 0 dB//1 μPa NL. These ranges provide extreme and typical values consistent with those used in the field and shown in literature [Burwen and Bosch, 1995; Daum and Osborne, 1996; Ransom *et al.*, 1995].

Using the receiver and low fish rate parameters defined above, an ensemble of fish

tracks were generated such that all began within a 5 second time period. Choosing a 5 second time period with various fish rates allows for a varying amount of fish to be present in the beam at the same time simulating higher and lower fish passage rates in the field. Each track is forced to begin 7 m downstream and end 7 m upstream (migrating salmon are traveling upstream, against the water flow) from the acoustical axis of the sonar beam, although the range from the transducer varies. Also, the time in the beam varies for each fish depending on each location in the track and fish velocity. The sonar data is collected when the sound, defined by the transmitter model, intercepts a fish track and echoes are produced. In the remainder of this chapter, a variety of fish rates for a the river cross-section described above, transmitter parameters, and noise levels are used to analyze the artificial sonar data. The various methods used to display and interpret the artificial sonar data include (a) data over a total time period, (b) data for a 1 second time period, and (c) data for 1 ping.

The total sonar data using a noise level of 0 dB//1 μPa for an example of low fish track data is shown in Figure 4.4.1. The figure shows the echoes as a function of time with amplitude in Pascals. Each vertical bar represents an echo returned by one fish. The figure simulates the sonar data collected in the field as viewed on an oscilloscope running in real time. Two fish entered the beam within the 5 second starting period, and took a total time of about 16 seconds (or about 90 pings) until both left the beam. Figure 4.4.2 shows a 3D plot of the two fish tracks, with the first fish entering the beam around 12 m and the second fish at about 45 m. Each echo from the track is plotted as a square with a line connecting the echoes in time. Although the depth of the fish in the water column is important in determining the incident angle and location in the beam, each fish track is also plotted for viewing

in two dimensions. in the plane showing the distance off the acoustical axis in the x direction and the range. in Figure 4.4.3. Here each echo is plotted as a cross and the line again connects consecutive echoes in time.

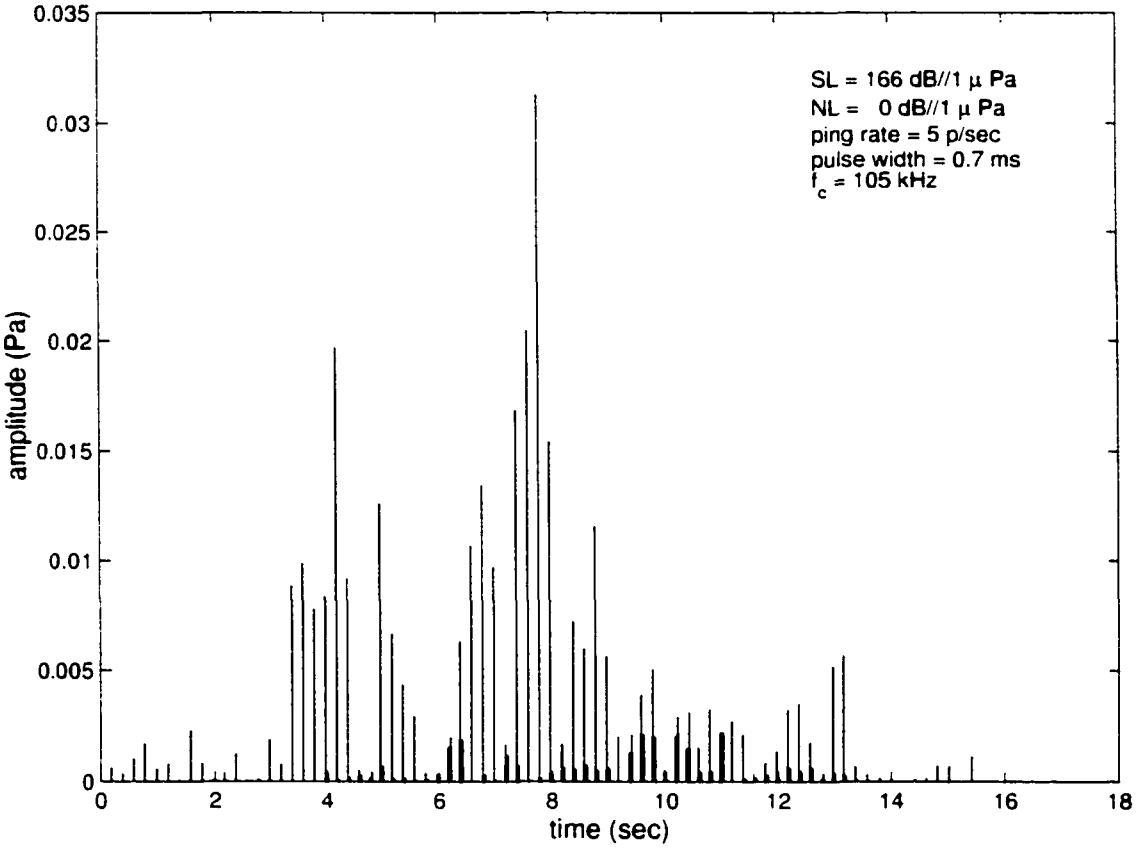

Figure 4.4.1 Example of low fish rate sonar data. An example of low fish rate sonar data is calculated and shown using the parameters defined in section 4.4. This example shows the sonar system collected data for ~ 16 seconds until the only two fish in the fish track data passed through the beam. The figure shows the echoes as a function of time with amplitude in Pascals. Each vertical bar represents an echo returned by one fish. The figure shows simulated sonar data collected in the field as viewed on an oscilloscope running in real time.

To better understand this example of sonar data in the framework of the known fish track data. a 1 second section from the total data is illustrated in Figure 4.4.4, from time 2 - 3 seconds. From the fish track information (fish #1 entered at time 0 and fish # 2 entered at time 3.37 sec). only one fish is in the beam at this time, fish

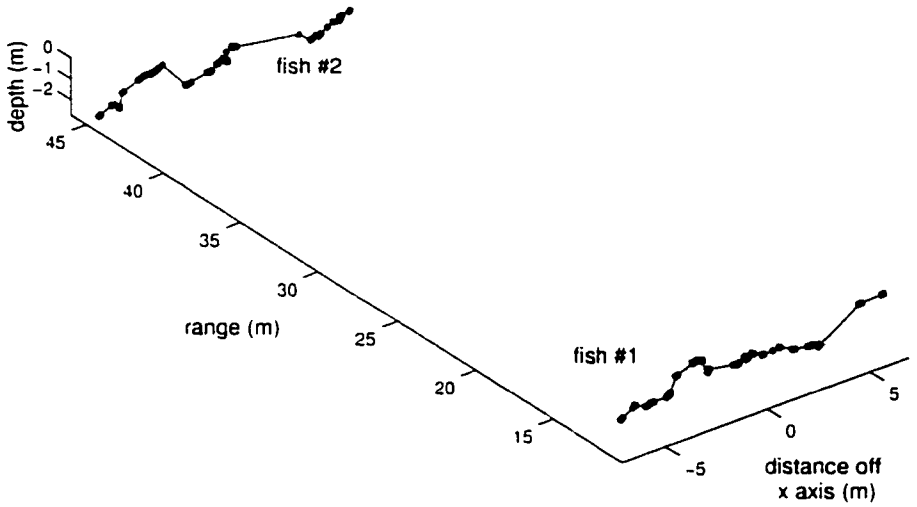

Figure 4.4.2 Two fish tracks in 3D. A 3D plot is shown of the two fish tracks used in generating the sonar data in the previous figure. The first fish entered the beam around 12 m and the second fish at about 45 m. Each echo from the track is plotted as a square with a line connecting the echoes in time.

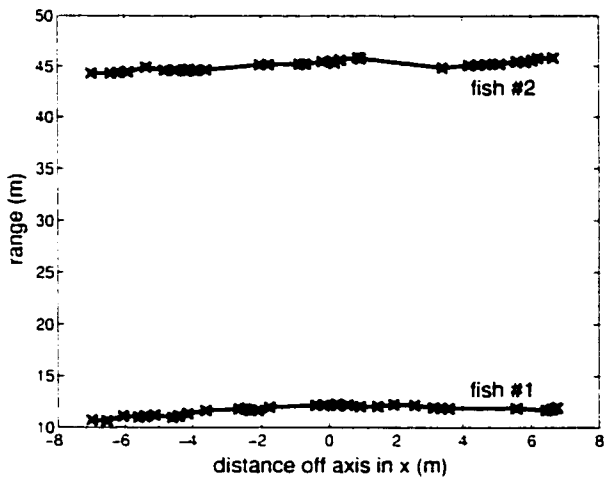

Figure 4.4.3 Two fish tracks from model in 2D. Each fish track shown in the previous figure is also plotted for viewing in two dimensions. in the plane showing the distance off the acoustical axis in the x direction and the range both in meters. Here each echo is plotted as a cross and the line again connects consecutive echoes in time.

#1. Here it is possible to see the returned echo from each of the 5 pings transmitted at that time from that one fish. Figure 4.4.5 shows another 1 second example from the same sonar data, time period 9 - 10 seconds, a time when both fish are in the beam. This figure shows the echo from each of the two fish easily distinguishable due to the large difference in range and thus the large time delay in echoes.

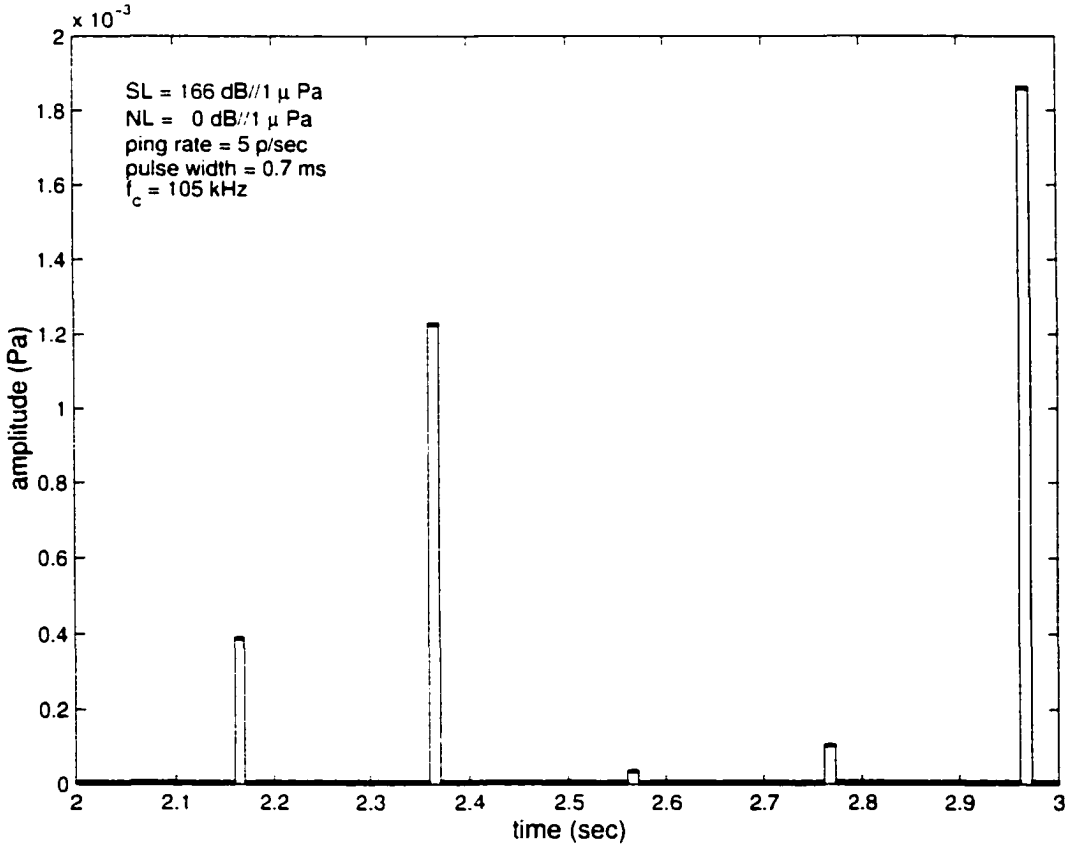

Figure 4.4.4 One second of low fish rate sonar data. A one-second section from the total data, from time 2 - 3 seconds, is shown. From the fish track information (fish #1 entered at time 0 and fish # 2 entered at time 3.37 sec), only one fish is in the beam at this time, fish #1. Here it is possible to see the returned echo from each of the 5 pings transmitted at that time from that one fish.

An example of artificial sonar data generated from the high fish rate is shown in Figure 4.4.6. In this case, 16 fish entered the beam within a 5 second time period and took $\sim$ 21 seconds to swim through the beam. In this view, the data is difficult

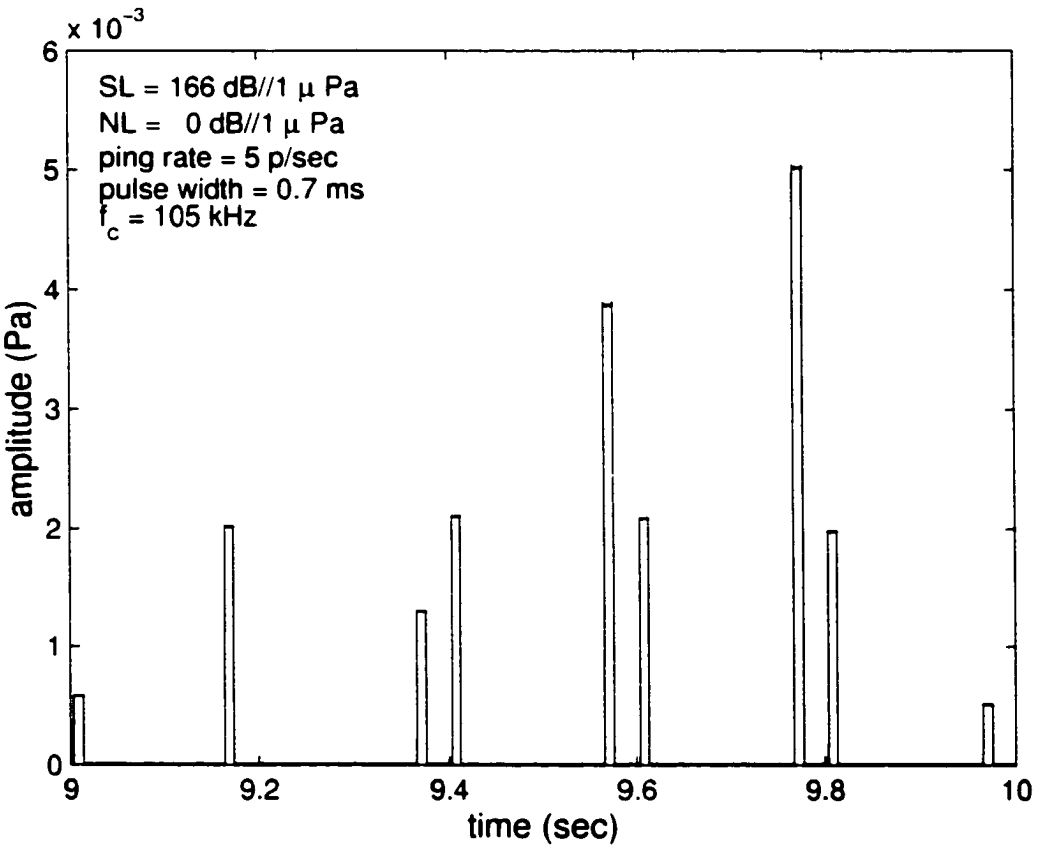

Figure 4.4.5 Another second of low fish rate sonar data. Another one-second example from the same sonar data. time period 9 - 10 seconds. is shown. This is a time when both fish are in the beam. This figure shows the echo from each of the two fish easily distinguishable due to the large difference in range and thus the large time delay in echoes.

to see as the amplitude of one echo is so large compared to the others. Figure 4.4.7 shows the same data with a maximum amplitude of 0.035 Pa. similar to the previous example of sonar data. Although several of the echoes have amplitude larger than this value, this view allows a comparison between the three densities. Fish tracks for this example are shown in Figure 4.4.8 in 3D and Figure 4.4.9 in 2D with each group of fish labeled in order of when they entered the beam.

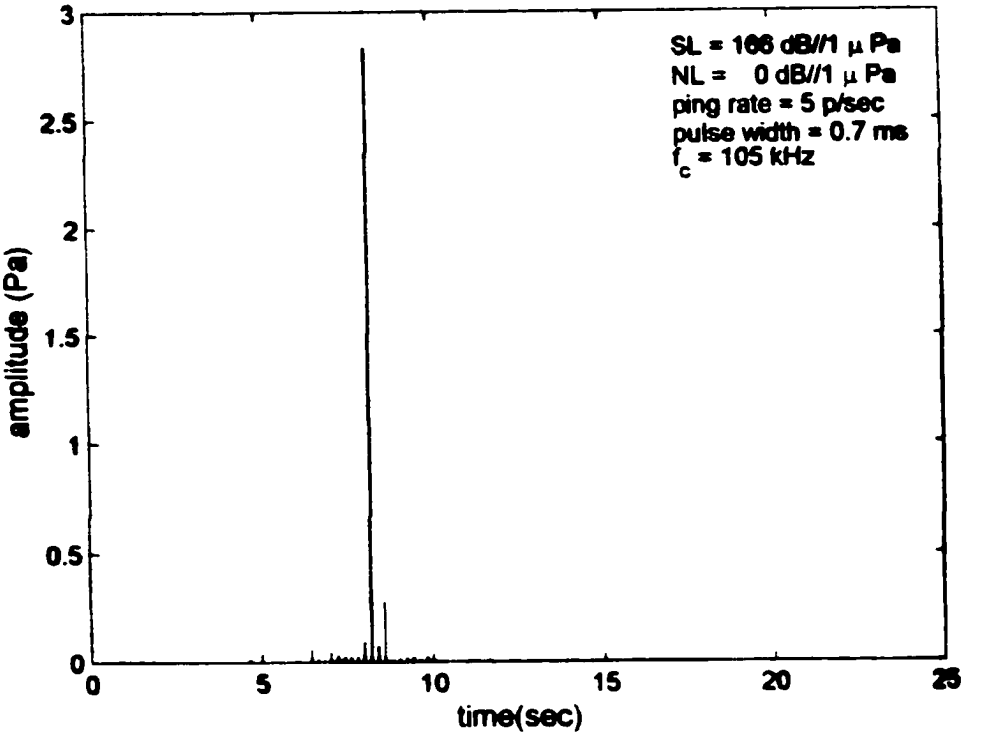

Figure 4.4.6 Example of high fish rate sonar data. An example of artificial sonar data generated from a high fish rate is shown. In this case, 16 fish entered the beam within a 5 second time period and took ~ 21 seconds to swim through the beam. In this view, the data is difficult to see as the amplitude of one echo is so large compared to the others.

Figure 4.4.10 shows a one second time period (7 - 8 sec) from the high fish rate sonar data. The maximum amplitude shown was chosen to aid in viewing the shape of the smaller echoes. In this case, most of the echoes are combined returns from two or more fish. If the echoes from each of the 16 fish in the beam at this time were

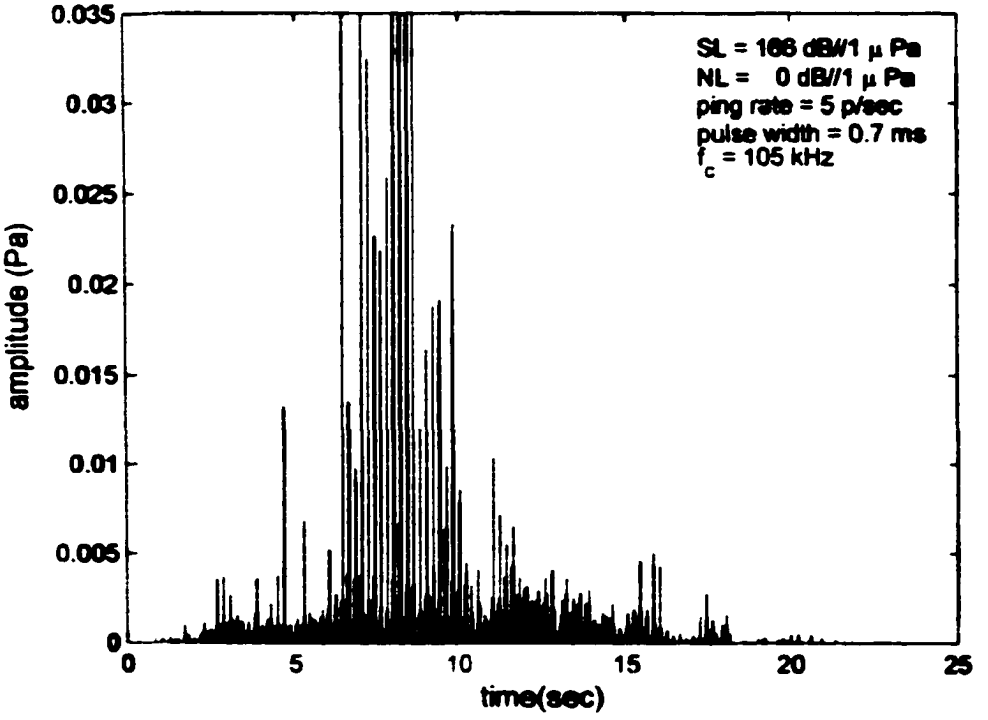

Figure 4.4.7 Detailed view of high fish rate sonar data. The same data with a maximum amplitude of 0.035 Pa. is shown similar to the previous example of sonar data.

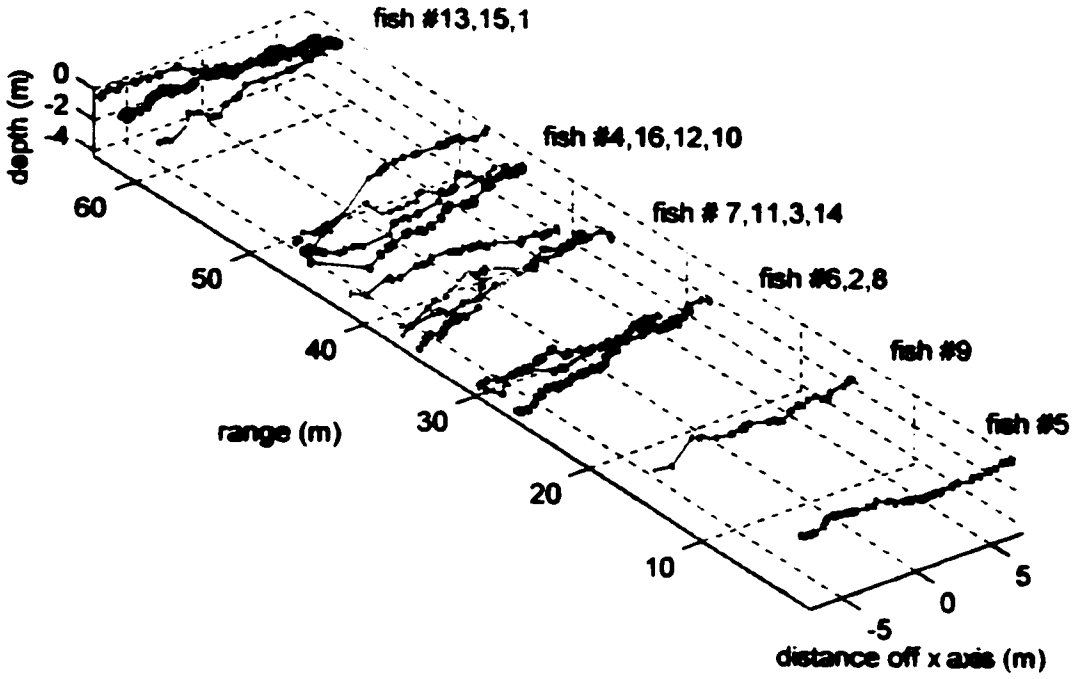

Figure 4.4.8 Sixteen fish tracks in 3D. A 3D plot of the 16 fish tracks used in generating the high fish rate sonar data is shown. The average range for the fish tracks fall between ~ 1.5 - 62 m. Each echo from the track is plotted as a square with a line connecting the echoes in time.

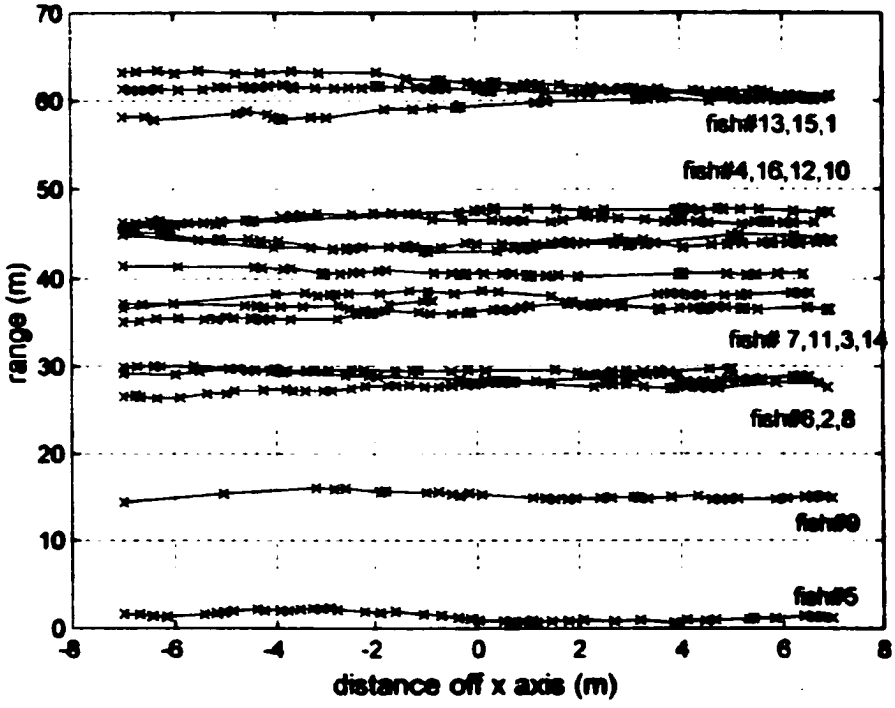

Figure 4.4.9 Sixteen fish tracks in 2D. Each fish track from the previous figure is also plotted for viewing in two dimensions, in the plane showing the distance off the acoustical axis in the x direction and the range both in meters. Here each echo is plotted as a cross and the line again connects consecutive echoes in time.

plotted individually, it would be possible to locate exactly which fish contributed to which echo, in the same manner discussed for Figure 4.4.10.

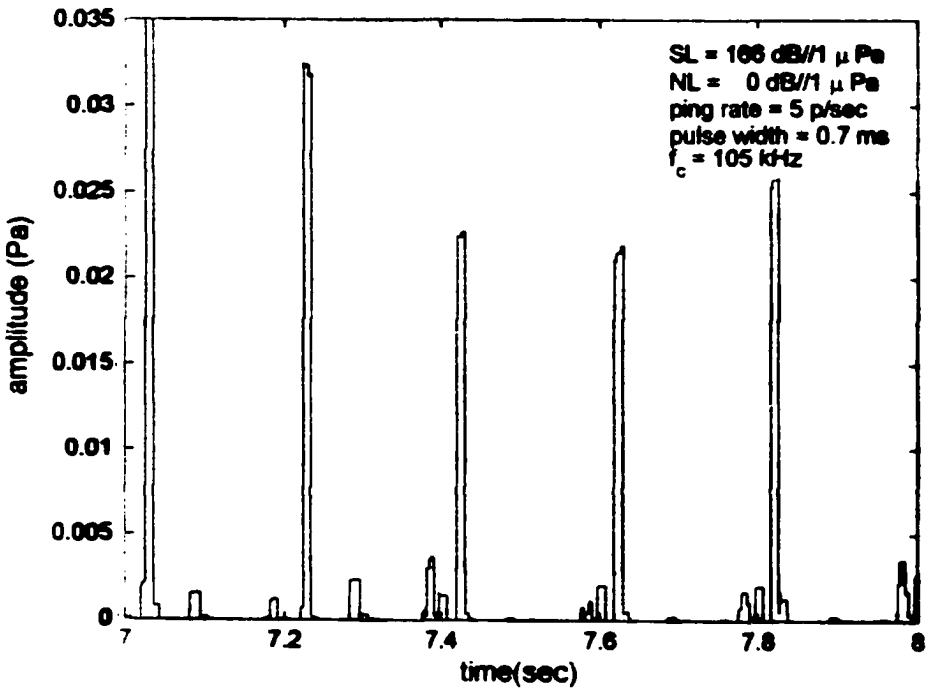

Figure 4.4.10 One second of high fish rate sonar data. A one second time period (7 - 8 sec) from the high fish rate sonar data is shown. The maximum amplitude shown was chosen to aid in viewing the shape of the smaller echoes. In this case, most of the echoes are combined returns from two or more fish. If the echoes from each of the 16 fish in the beam at this time were plotted individually, it would be possible to locate exactly which fish contributed to which echo.

To better view the contributions from individual fish to the entire sonar data, a more manageable example is provided in Figure 4.4.11. The total sonar data using a noise level of 0 dB//1 μPa for an example of fish rate of $[\mu_{fr}, \sigma_{fr}] = [1.0, 0.3]$ providing 600 fish in 10 minutes is shown. The figure shows the echoes as a function of time with amplitude in Pascals. Here there are six total fish entering the beam within the 5 second starting period, and taking a total time of about 17 seconds until all swim outside the beam. Table 4.2 shows data relating to these fish tracks,

including the fish number and the time each fish entered and left the beam. The fish size and swimbladder size information is also listed in mm. This information is useful in interpreting and understanding the sonar data.

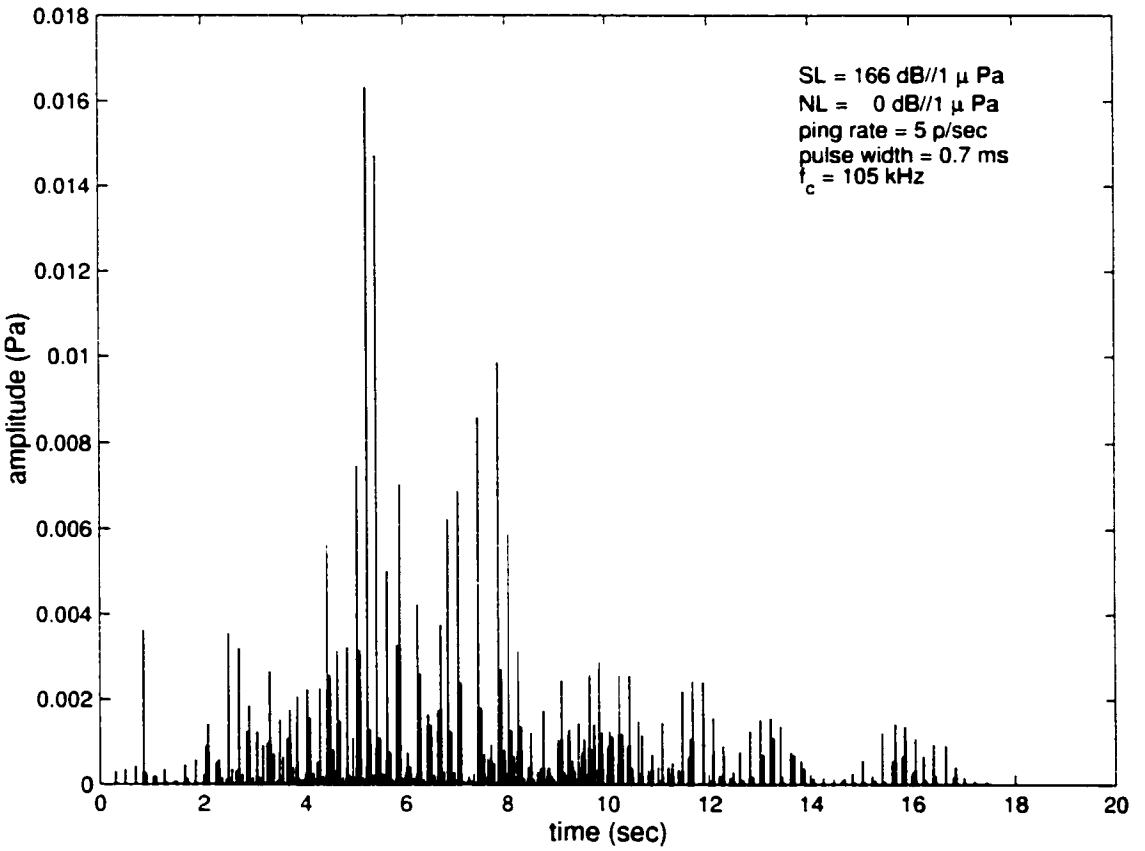

Figure 4.4.11 Sonar data example for 1 fish per second. The figure shows the echoes as a function of time with amplitude in Pascals. Here there are six total fish entering the beam within the 5 second starting period, and taking a total time of about 17 seconds until all left the beam.

To better understand this example of sonar data in the framework of the known fish track data, a 1 second section from the total data is illustrated in Figure 4.4.12, from time 9 - 10 seconds, a time period when all six fish are in the sonar beam. It is possible to see the returned echo from each fish for each of the 5 pings transmitted at that time. For a ping rate of 5 pings per second, a ping is sent out every 0.2 seconds. Thus in between 9.0 and 9.2 seconds there are six echoes corresponding

Table 4.2 Time and Range Data for 6 Fish Generated Tracks.

fish #	start time (sec)	end time (sec)	average range (m)	L_f (mm)	H_f (mm)	B_f (mm)	L_s (mm)	H_s (mm)	B_s (mm)
1	0	12.2	20.4	614.1	141.0	63.5	194.3	62.2	36.4
2	0.6	10.6	16.9	591.2	153.4	60.7	234.6	58.2	32.3
3	1.4	9.1	55.4	550.2	129.8	56.4	153.8	61.2	34.2
4	2.4	13.5	35.2	628.0	141.7	63.1	248.1	57.7	31.4
5	3.2	16.9	45.7	542.7	135.0	62.4	137.3	67.4	39.6
6	4.7	16.9	63.3	535.8	131.5	51.4	183.3	50.8	31.1

to each of the six fish. Notice that from the first ping in this time period, the six echoes are easily distinguishable; however, by the third ping (time period between 9.4 and 9.6 sec) the echoes begin to overlap as seen by the stair step shape of the fourth and fifth echoes combined. By the last ping (time period between 9.8 and 10.0 sec) even more echoes are overlapping creating only 3 echoes from the six fish combined.

To further see exactly which of the returned echoes can be attributed to which fish, Figure 4.4.13 shows the returned echoes from each fish individually during the time period from 9 - 10 seconds in panels (a) - (f). The bottom panel (g) shows the combined data for that time period (same figure as Figure 4.4.12). Selecting any echo from the bottom panel it is possible to find its match in any of the above panels attributing that echo to that fish. Thus, for the first example of an overlapping echo received just previous to time 9.5 the returns are from two fish, #1 and #4. Consulting Table 4.2 shows that these two fish have an average range within 15 m of each other. For the appropriate location of the fish in the beam, this overlap is possible. Next, during time period 9.6 - 9.8 fish #2 and #6 provide overlapping echoes as well as fish #1 and #4 still.

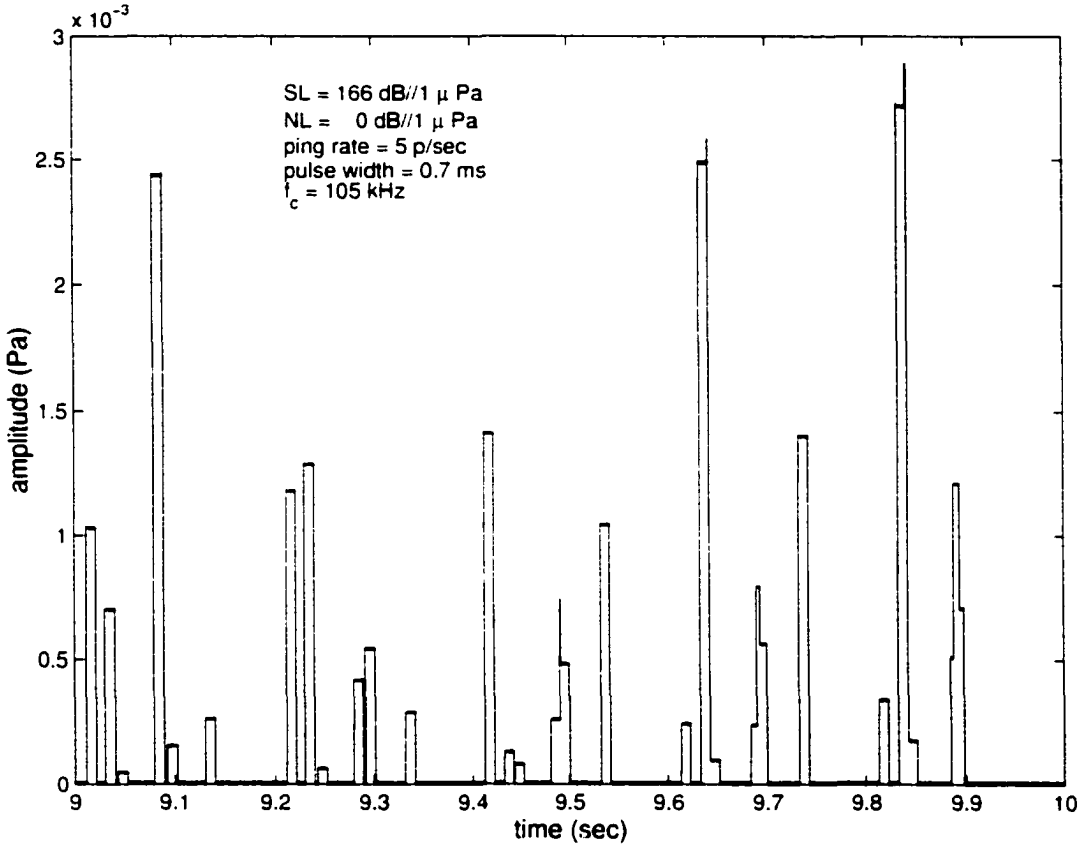

Figure 4.4.12 One second of sonar data using 1 fish per second. The figure shows a one second section, from time 9 - 10 seconds, a time period when all six fish are in the sonar beam. It is possible to see the returned echo from each fish for each of the 5 pings transmitted at that time. For a ping rate of 5 pings per second, a ping is sent out every 0.2 seconds. Thus in between 9.0 and 9.2 seconds there are six echoes corresponding to each of the six fish.

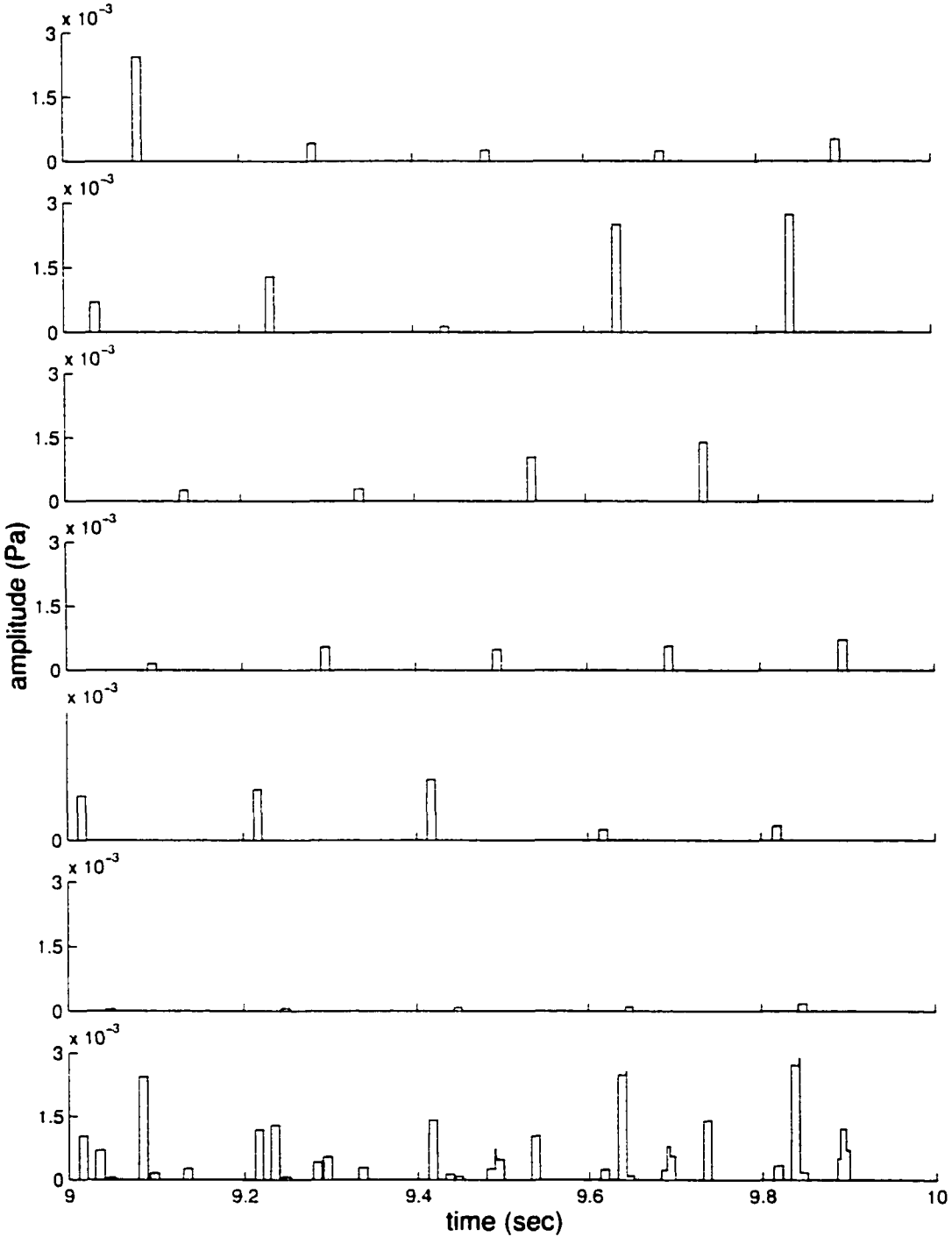

Figure 4.4.13 Echoes from individual fish for one second time period. The figure shows the returned echoes from each fish individually during the time period from 9 - 10 seconds in panels (a) - (f). The bottom panel (g) shows the combined data for that time period (same figure as Figure 4.4.9). Selecting any echo from the bottom panel it is possible to find its match in any of the above panels attributing that echo to that fish. Thus, for the first example of an overlapping echo received just previous to time 9.5 the returns are from two fish, #1 and #4.

At this stage, the direct model produces reasonable and understandable sonar data for the low and high fish rate cases under the conditions of 0 dB//1 μPa noise level. It is possible to identify the target with the echo it produced at each ping, even when overlapping echoes are returned. Next, the effects of increased noise level, changes in ping rate and changes in pulse width are analyzed. In each case, an appropriate fish rate is used that best shows the point at hand.

Figure 4.4.14 shows the same low fish rate data shown in Figure 4.4.1 but with 20 dB//1 μPa noise level included. This level of noise adds little effect to the sonar data. Figure 4.4.15 shows the same low fish rate data shown in Figure 4.4.1 but with 40 dB//1 μPa noise level included. The general pattern remains the same, but many of the smaller echoes are becoming muddled in the noise. Figure 4.4.16 shows the same data with 60 dB//1 μPa noise level included. At this stage, most of the smaller echoes are consumed by the noise and only the most dominant echoes, those with the highest amplitudes, remain recognizable.

The effects of varying the ping rate work as expected. Figure 4.4.17 shows the same 1 second of data as shown in Figure 4.4.4, but with 10 pings per second. Here it is possible to see the returned echoes from each of the 10 pings transmitted at the time from 2 to 3 seconds. In each case, the echo from the one fish can still be seen in the beam during this time period. Notice that all the echoes produced with a ping rate of 5 pings per second are also shown in the data produced with at 10 pings per second. Thus, the higher ping rate only provides more information. Figure 4.4.18 shows the same 1 second of data with a ping rate of 15 pings per second. Again, the same data as shown with 5 or 10 pings per second is present along with additional data.

Lastly, the effects of varying the pulse width work as expected. Figure 4.4.19

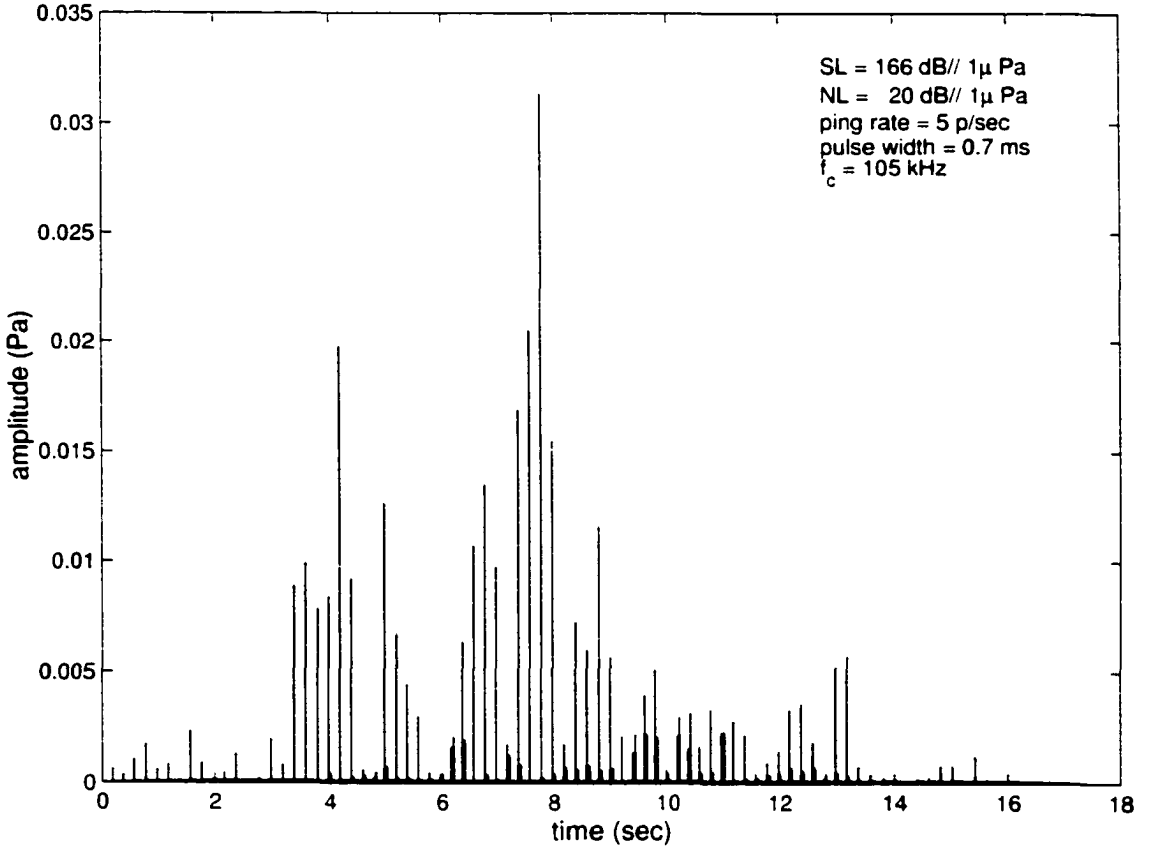

Figure 4.4.14 Low fish rate sonar data with NL = 20 dB//1 μPa. Shown is the same low fish rate data shown in Figure 4.4.1 but with 20 dB//1 μPa noise level included. This level of noise adds little effect to the sonar data.

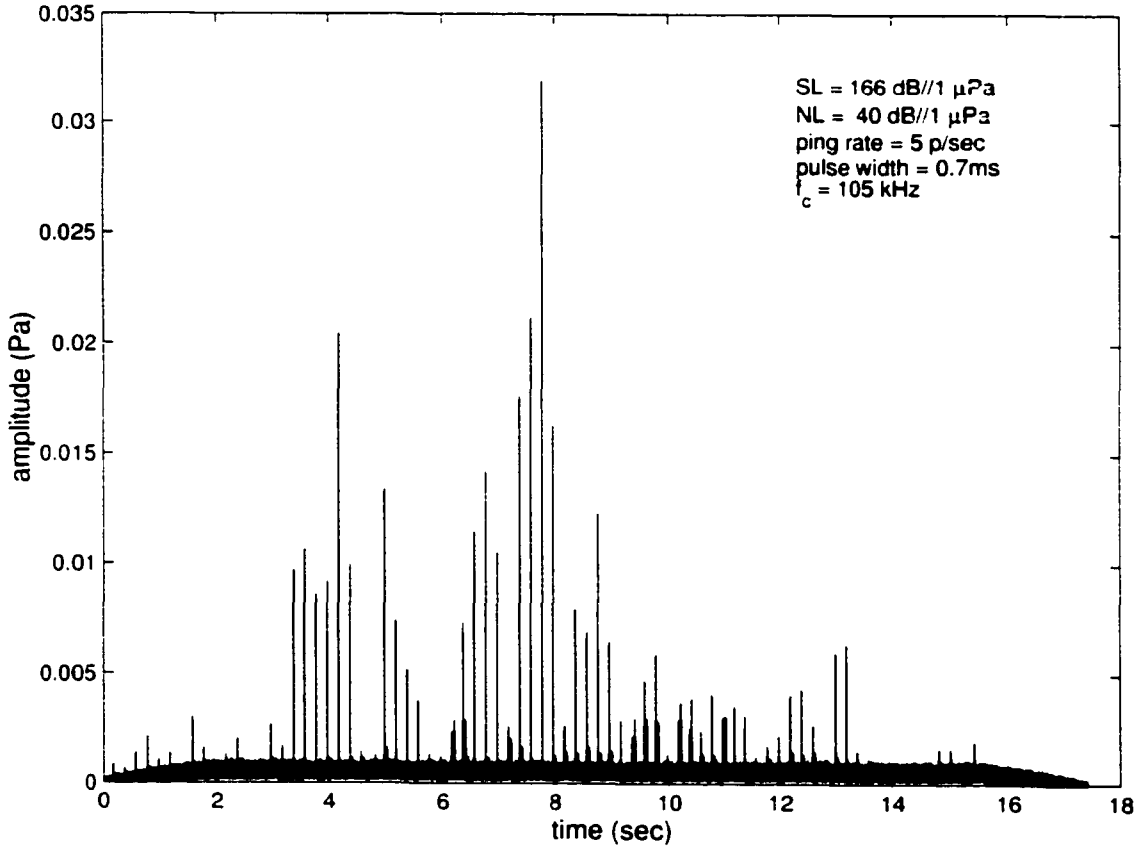

Figure 4.4.15 Low fish rate sonar data with NL = 40 dB//1 μPa. Shown is the same low fish rate data shown in Figure 4.4.1 but with 40 dB//1 μPa noise level included. The general pattern remains the same, but many of the smaller echoes are becoming muddled in the noise.

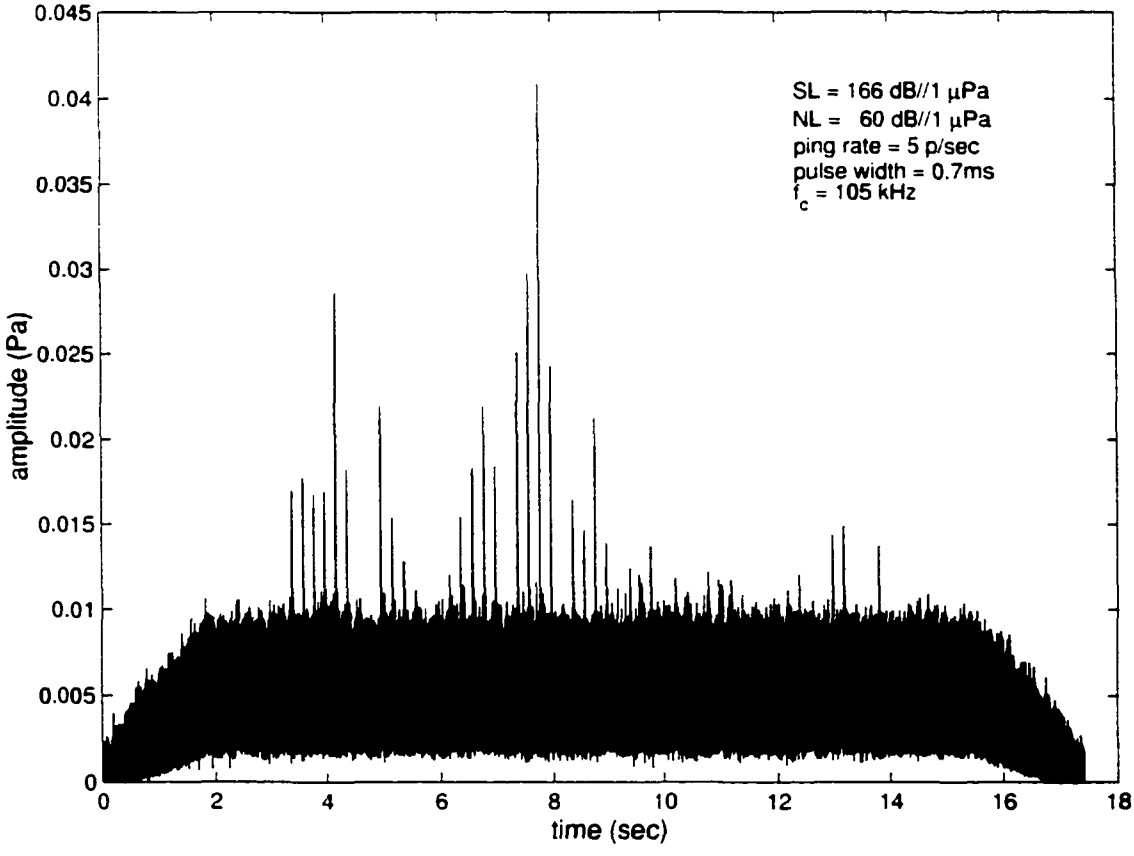

Figure 4.4.16 Low fish rate sonar data with NL = 60 dB//1 μPa. Shown is the same low fish rate data shown in Figure 4.4.1 but with 60 dB//1 μPa noise level included. At this stage, most of the smaller echoes are consumed by the noise and only the most dominant echoes, those with the highest amplitudes, remain recognizable.

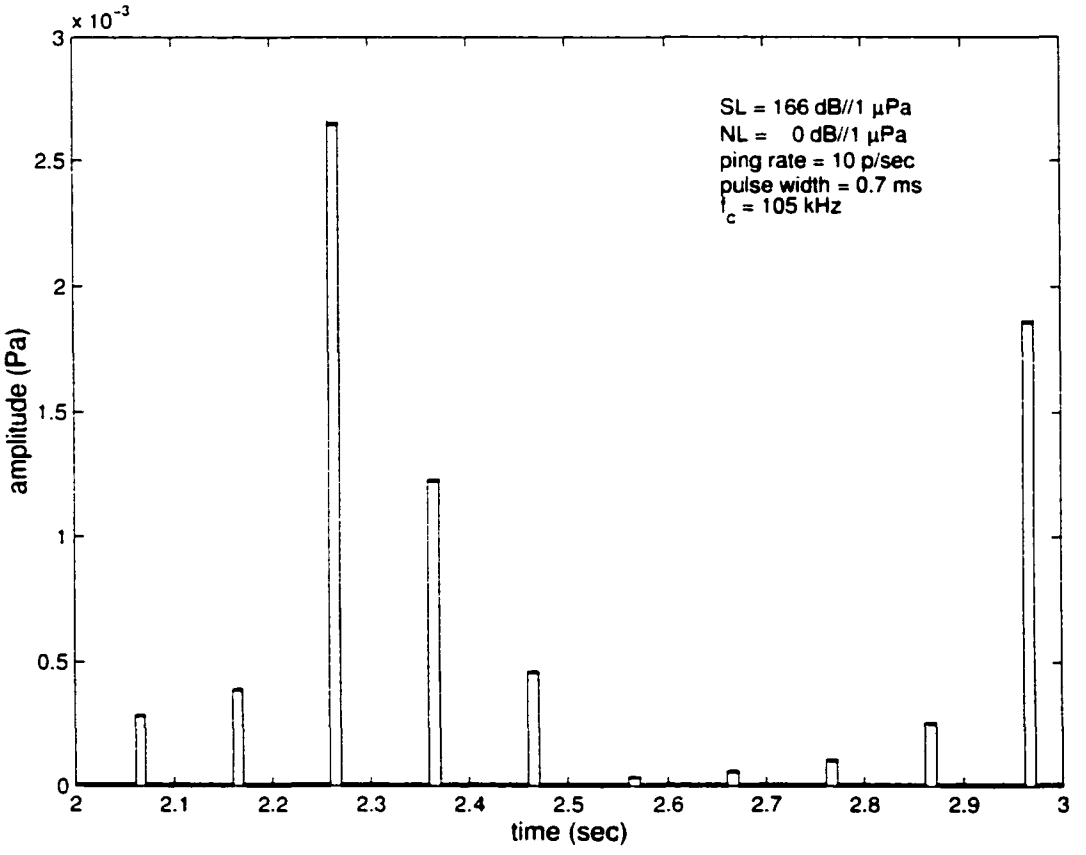

Figure 4.4.17 Low fish rate sonar data with 10 pings per second. Shown is the same 1 second of data as shown in Figure 4.4.4, but with 10 pings per second. Here it is possible to see the returned echoes from each of the 10 pings transmitted at the time from 2 to 3 seconds. In each case, the echo from the one fish can still be seen in the beam during this time period. Notice that all the echoes produced with a ping rate of 5 pings per second are also shown in the data produced with at 10 pings per second. Thus, the higher ping rate only provides more information.

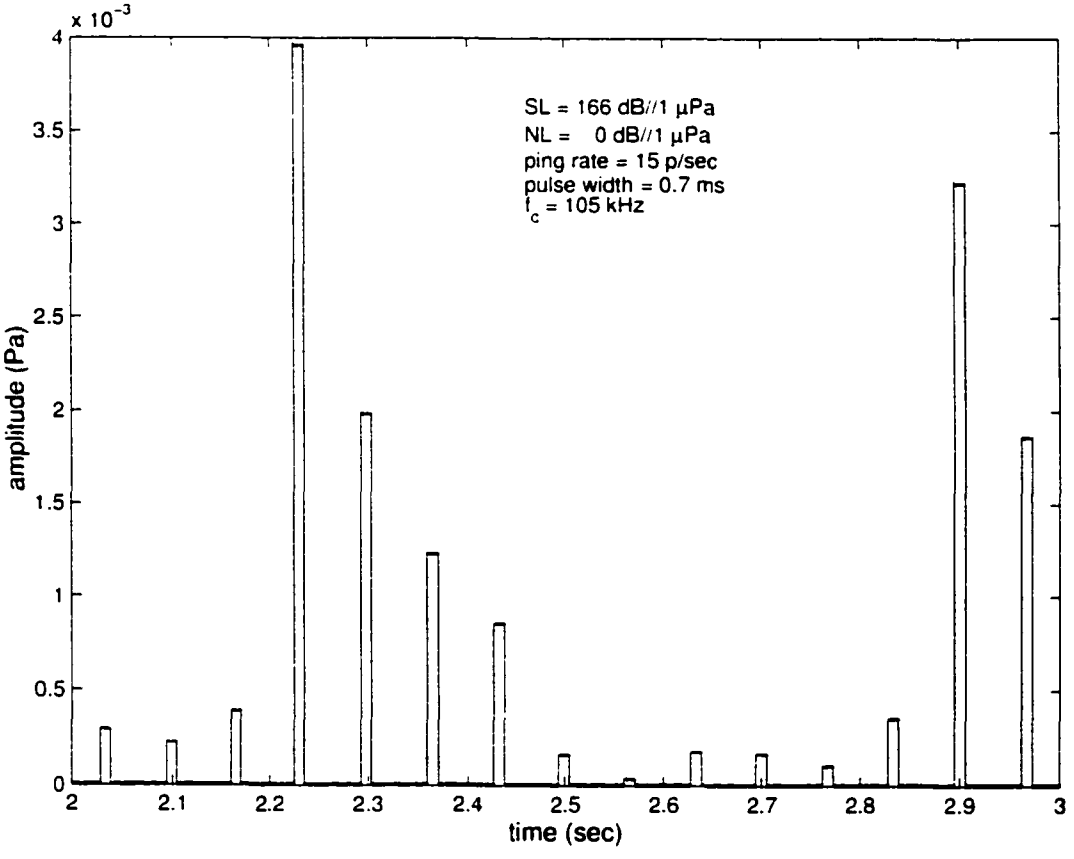

Figure 4.4.18 Low fish rate sonar data with 15 pings per second. Shown is the same 1 second of data as shown in Figure 4.4.4 and Figure 4.4.17 with a ping rate of 15 pings per second. Again, the same data as shown with 5 or 10 pings per second is present along with additional data.

shows the same data as in Figure 4.4.12. but generated with a pulse width of 0.3 ms. Using a smaller pulse width for the transmitted ping generates returned echoes with smaller pulse widths. Thus some echoes that were previously overlapped are now separated into individual echoes. In particular. comparing to Figure 4.4.12 which had 5 echoes combining returns from two or more fish. the data generated with the smaller pulse width provides only 1 of those 5 echoes from combined returns.

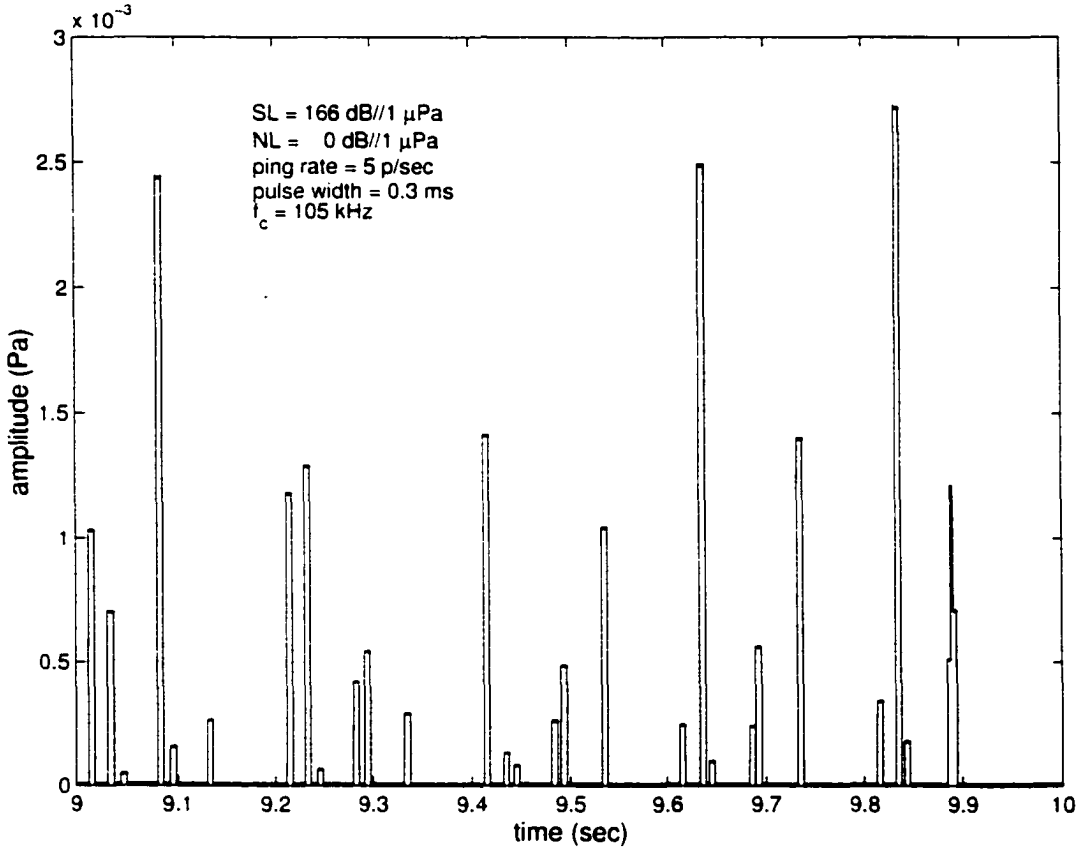

Figure 4.4.19 Effects of shorter pulse width on sonar data. Shown is the same data as in Figure 4.4.12. but generated with a pulse width of 0.3 ms. Using a smaller pulse width for the transmitted ping generates returned echoes with smaller pulse widths. Thus some echoes that were previously overlapped are now separated into individual echoes. In particular. comparing to Figure 4.4.12 which had 5 echoes combining returns from two or more fish. the data generated with the smaller pulse width provides only 1 of those 5 echoes from combined returns.

In Figure 4.4.20 the same data as in Figure 4.4.12 is shown but with a pulse width

of 1.1 ms. The echoes have a wider pulse width as expected, since the transmitted pulse had a wider pulse width. Comparing with Figure 4.4.12, several more echoes are received from combined returns of two or more fish than previously. With an even longer pulse width, these echoes will begin to show even more combined patterns.

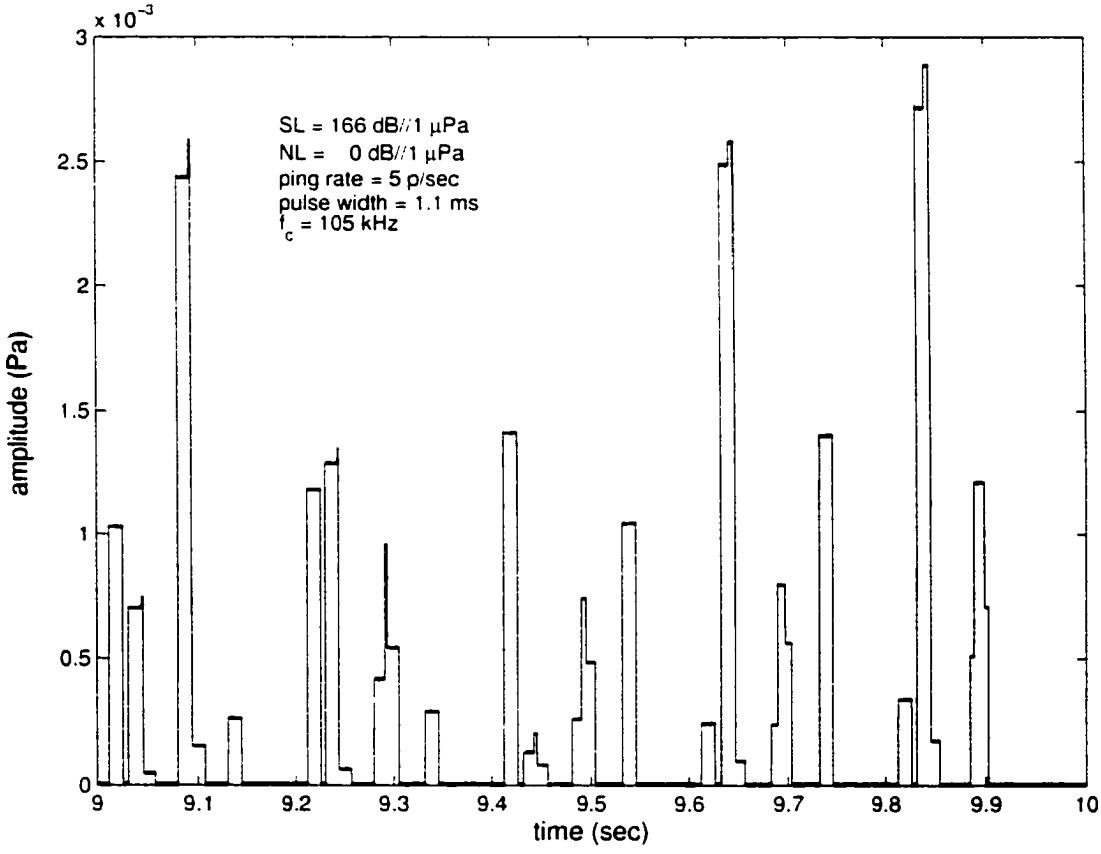

Figure 4.4.20 Effects of longer pulse width on sonar data. Shown is the same data as in Figure 4.4.12 but with a pulse width of 1.1 ms. The echoes have a wider pulse width as expected, since the transmitted pulse had a wider pulse width. Comparing with Figure 4.4.12, several more echoes are received from combined returns of two or more fish than previously. With an even longer pulse width, these echoes will begin to show even more combined patterns.

Lastly, the ping rate and pulse width must be considered in relationship to each other and to an average range. When selecting a ping rate and pulse width, the time it takes for a ping to travel to a target at an average range, reflect, and return back to the receiver as an echo must be considered. For a target at 30 m, an echo will

take approximately 0.04 seconds to return. If the ping rate is 20 pings per second. then a new ping is sent every 0.05 seconds. With a pulse width of 0.002 seconds. it is conceivable that an echo may interfere with the following ping. thus creating a higher level of overlap in the sonar data. Figure 4.4.21 shows an example of sonar using the fish rate of 1 fish per second with an extreme ping rate of 20 pings per second and a long pulse width of 2 ms for a 1 second time period. The ideal situation of 0 dB//1 μPa noise level is used.

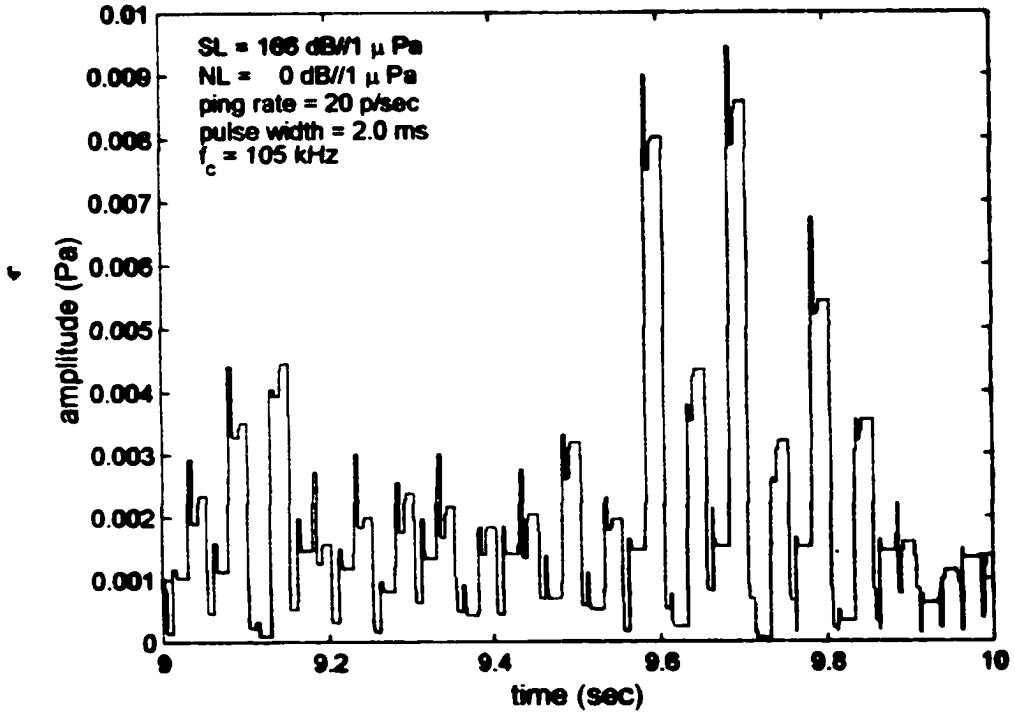

Figure 4.4.21 Relationship of ping rate and pulse width. Shown is an example of a data generated with a fish rate of 1 fish/sec with high ping rate (20 pings per second) and a long pulse width of 2 ms for a 1 second time period. The ideal situation of 0 dB//1 μPa noise level is used. Here a higher level of overlap is found in the sonar data due to echoes interfering with following pings.

In summary. the direct model uses a modular approach to create artificial sonar data. The data is reasonable and understandable. What remains is to numerically estimate the fish count using the artificial data. Three methods were discussed

in Chapter 1 including echo integration, echo counting, and target tracking. The following chapter will discuss the method of echo integration, apply it to the data generated in this chapter, and describe the effects of the different parameter values on the estimated fish counts. An echo counting algorithm is considered in the thesis by Lai [2002]. Application to target tracking requires combining results presented here with the split beam sonar model considered by Ayers [2001] and is left for future work.

Chapter 5

INVERSE MODEL OF THE FISHERIES ACOUSTICS PROBLEM

The inverse model of the fisheries acoustics problem is shown in Figure 1.5.1. The model begins with the sonar data, either collected in the field or generated artificially, and applies an analysis tool using the sonar equipment model along with all the assumptions used throughout the direct model. These assumptions include assuming fish size and biological parameters follow the distributions developed in Chapter 2, fish movement follows the distribution developed in section 2.3, the fish body and swimbladder are roughly convex surfaces, the wavelength of the transmitted sound is small compared to the radii of curvature of the fish body and swimbladder surfaces, the fish is a point source target, and the sonar signal levels are high enough compared to noise levels. The results of the inverse problem provide an abundance estimate and perhaps even a count broken down by species (species apportionment). One analysis tool for calculating fish counts from sonar data obtained using a single beam sonar is echo integration described briefly in section 1.4.

In this chapter, echo integration is applied to sets of artificial data generated using the methods described in Chapter 4 for various fish rates ranging from 0.1

fish per second up to 5 fish per second for a specific river cross-section. Specific examples of sonar data generated for a fixed fish rate while varying other parameters such as noise level, ping rate, and pulse width are also considered. A discussion of how varying parameters effects the fish count follows. Lastly, the technique will be applied to experimental data in an effort to test its effectiveness.

5.1 Echo Integration Results from Artificial Sonar Data

Echo integration is a simple technique where all of the energy in the returned echoes is summed. This integrated energy is then divided by an average energy expected for one fish, providing a quantitative measure of the number of fish present. A brief description of this process is given in section 1.4; however, a more detailed explanation of Figure 1.4.5 follows.

In general, the transmitter sends out pings of a given length over a given time period. The amplitude of these pings can be thought of in volts (proportional to Pascals) as a function of time, $V(t)$, and are specified for a certain range provided by the time limits. For a range section between R_1 and R_2 the time limits would be $t_1 = 2R_1/c$ and $t_2 = 2R_2/c$, where c is the speed of sound in water. As the echoes are received in time and processed through the time varied gain function, the amplitude of the echoes, $v(t)$, are collected and the intensity, $|v(t)|^2$, is summed over the time frame. For the i^{th} time period the summed energy, E_i, is given by

$$E_i = \int_{t_{1,i}}^{t_{2,i}} |v(t)|^2 \, dt \qquad 5.1.1$$

The summed energy for each time period must then be scaled by an average value of energy relating to an average backscattering coefficient value expected for

one fish. Thus, the fish count, C_f, is given by

$$C_f = \sqrt{\sum_{i=1}^{N} \frac{E_i}{\overline{RL_i}}} \qquad 5.1.2a$$

where N is the total number of range sections based on the maximum range of the sonar system and $\overline{RL_i}$ is an average receive level (in volts) corresponding to an average backscattering coefficient for the fish in that range. The process used most commonly today scales the output signal by factors other than just the average backscattering coefficient, mostly relating to transducer parameters. Thus the fish count is found by

$$C_f = A\sqrt{\sum_{i=1}^{N} E_i} \qquad 5.1.2b$$

where

$$A = \frac{1}{c\tau\pi p^2 g^2 \bar{b}^2 \bar{\sigma}} \qquad 5.1.3$$

and where c is the speed of sound in water, τ is the ping delay or the inverse of the ping rate, p^2 is the pressure calculated from the source level (SL) of the sonar, g^2 is the gain calculated from the receiver sensitivity, $\bar{b}$ is the average beam pattern factor, and $\bar{\sigma}$ is the average backscattering cross-section. Note that the average backscattering cross-section relates to the average receive level in Equation 5.1.2a.

This scaling factor is just one of the two given in literature [Ransom *et al.*, 1995] to be useful. The second factor corrects for the time varied gain. In most systems today, this factor is corrected for in the collection of the sonar data. Thus the second factor is no longer needed to scale the output of echo integration.

Often during data collection, before applying an echo integration algorithm, the returned signals are compared to a threshold level. The term thresholding means that only signals higher than a fixed threshold level are stored in the data

collection process. The other signals that are too small are replaced with a value of 0. Thresholding the data allows for small echoes to be eliminated in order to reduce noise. On the positive side, since echo integration uses all the returned echoes, high levels of noise can provide extreme effects on the fish count outcomes and thus thresholding is helpful. On the other hand, often smaller echoes are returned from fish swimming near the edge of the beam or at a high aspect ratio with respect to the beam. Thus fish counts can be dramatically under represented by implementing the echo integration technique depending on the threshold level. Although some work has been done on alternatives to thresholding [Nunnallee, 1990] this method is still common in practice. Nunnallee [1990] suggested using a noise cancellation process by measuring intensities when the transducer is not running and use these values for compensation. In general though, thresholding is performed not only to lower noise, but also to reduce the amount of data collected [Daum and Osborne, 1996].

To test the inverse problem using artificial data from the direct model, an echo integration algorithm was applied to each set of data for a fixed fish rate calculating a fish abundance estimate. Since the actual number of fish is known from the direct model, the comparison between inverse model results and the actual count provides an indication of the accuracy of the echo integration model. For the artificial sonar data generated and described in section 4.4 the total return signal, $V(t)$, is the received signal plotted as amplitude in Pascals as a function of time in seconds. The echo integration algorithm is able to estimate the fish count with or without implementing a threshold level. Following the process outlined in Equations 5.1.1 through 5.1.3, the sum of the squared amplitudes for the total amount of data in each case is divided by an estimated average amplitude expected for one fish. This

expected amplitude value is based on average fish size parameters on-axis at an average range in each of the range sections. Further, the value was then divided by an adjustment term using the time period and the number of pings per second to estimate the actual number of fish passing through the beam in that time interval.

As described in the work on the fish track data [Chen, 2001] and sonar data [Lai, 2002] statistical models are employed at various stages. To analyze fish counts of the artificial sonar data a large number of examples must be used for each case. Thus, 100 fish tracks are generated and used in the direct model to generate the sonar data under three fish rates of $\mu_{fr} = 0.1$, 0.5, and 1 fish per second. Due to time and processing constraints, only an additional 25 fish tracks are generated for the situation of 5 fish per second. Here, the sonar parameters include a fixed carrier frequency $f_c = 200$ kHz, a source level of 220 dB//1 μPa, ping rate of 5 pings per second, a pulse width of 0.5 ms, and a noise level of 0 dB//1 μPa. The river cross-section is now defined by two segments providing a river 100 m wide with a maximum depth of 4 m at 25 m from the left bank. Also, each ensemble of fish tracks were generated such that all began within a 30 second time period. Choosing a 30 second time period with various fish rates allows for a varying amount of fish to be present in the beam at the same time. Note that in this chapter, different sonar and river parameters are used with the set of 100 data than when considering a single example of sonar data (as those discussed and used in Chapter 4). The results are consistent without regard to the parameters; however, the more useful examples are shown and discussed in each case to make the point at hand.

Figure 5.1.1 shows the distribution of fish counts using the echo integration algorithm for each set of 100 sonar data using the four fish rates. The frequency of estimated fish counts is shown as a percentage in each case. With an average fish

rate of 0.1 fish per second, the expected fish count is 3 fish for 30 seconds although each case may have had an actual fish count of more or less than 3.

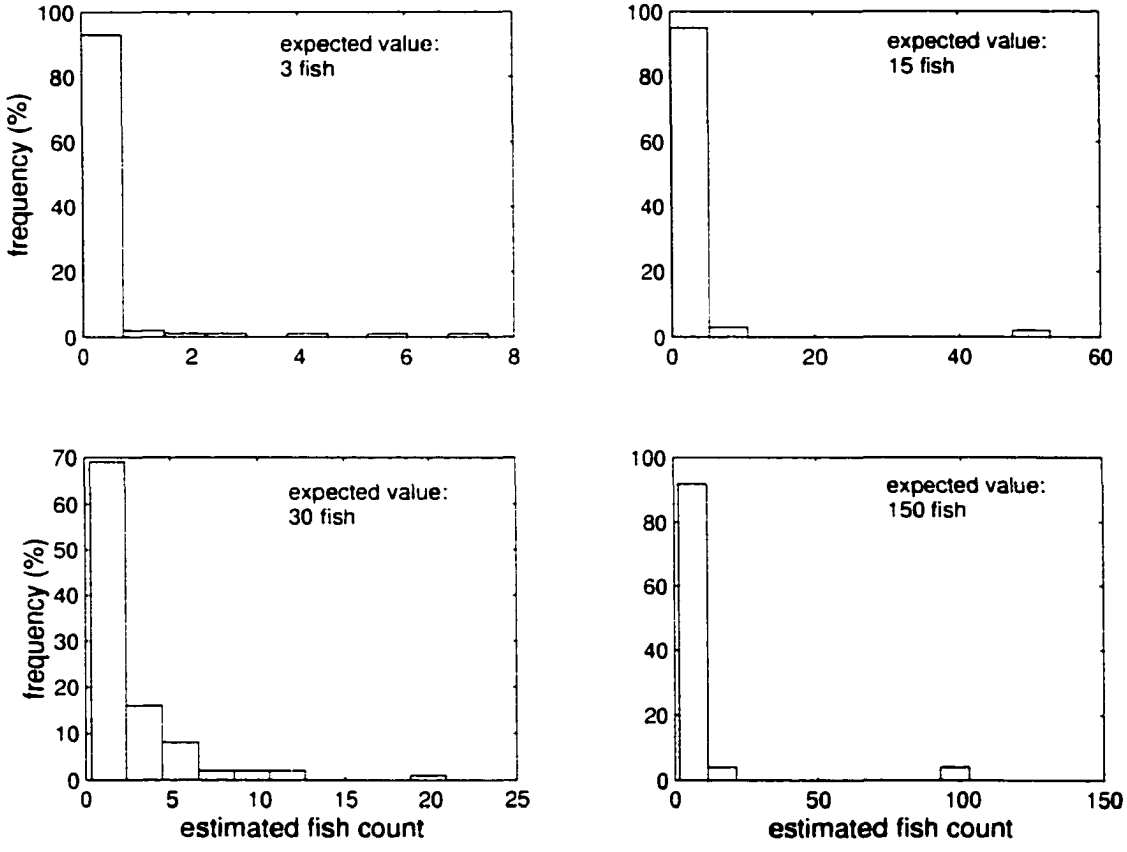

Figure 5.1.1 Histograms of fish counts for 4 fish rates. The distribution of fish counts using the echo integration algorithm is shown for each set of 100 sonar data using the four fish rates. The frequency of estimated fish counts is shown as a percentage in each case. With an average fish rate of 0.1 fish per second, the expected fish count is 3 fish for 30 seconds although each case may have had an actual fish count of more or less than 3.

Figure 5.1.2 shows a plot of the estimated fish count for each example with respect to the actual fish count for that example. A logarithmic scale is used on the y-axis to allow for better viewing of the data. The line shows the one to one correspondence for the fish rate, thus showing the ideal situation.

From both Figures 5.1.1 and 5.1.2 many conclusions can be discussed. Notice that although the echo integration algorithm provides the correct count, it only does

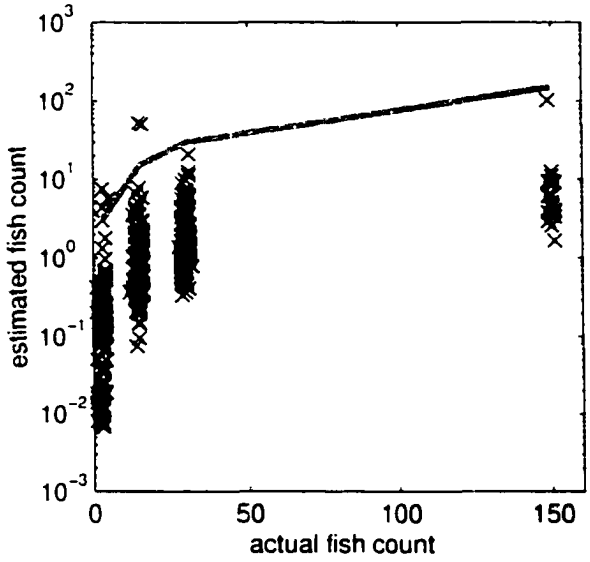

Figure 5.1.2 Estimated vs. actual fish count. The estimated fish count for each example with respect to the actual fish count for that example is shown with an 'x'. A logarithmic scale is used on the y-axis to allow for better viewing of the data. The line shows the one to one correspondence for the fish rate, thus showing the ideal situation.

so a small fraction of the time. Most of the estimated fish counts are much lower than expected although there are cases when the algorithm does over count as well. This seems to occur across fish rate levels. For the case of 5 fish per second, over counting is not seen, but only 25 fish tracks are used. It's reasonable to assume that if more tracks were generated, an over count would be possible.

As the fish rate increases, the data becomes tighter around an average as seen in Figure 5.1.2. The average in each case is lower than the actual result. The number of tracks was determined by looking at the distribution of actual fish counts and collecting enough fish track data (number of fish tracks in each set of data) to fit a Gaussian distribution.

When considering the range of values obtained for each fish count, high errors are involved. Table 5.1 contains the results of the echo integration in numerical form for the four cases. Notice that the averages obtained from the data counts

Table 5.1 Results of Echo Integration for Various Fish Counts.

fish count	mean true count	minimum count	maximum count	mean data count
3	2.93	0.01	7.53	0.41
15	14.84	0.08	52.80	2.25
30	30.04	0.34	20.88	2.62
150	149.96	1.67	102.30	9.73

are always lower than the averages obtained from the true counts. This shows that under counting is predominant. Also, in the case of 150 fish the true count was never achieved. Note that this is just one example of a statistical simulation providing such large variation in fish counts. This implies that when this echo integration algorithm is used in the field with a situation of unknown actual fish counts, it is possible to obtain any of these fish count results without knowing if the sonar is over counting, under counting, or correctly estimating the fish count.

Figure 5.1.3 shows an example fish counts calculated using echo integration as a function of noise level. Here one case uses a fish rate of 0.3 fish per second and the other uses 1 fish per second. The sonar and river parameters are those defined in Chapter 4. The left panel uses the same fish rate data shown in Figure 4.4.1 with the sonar data generated assuming a ping rate of 5 pings per second, a pulse width of 0.7 ms, and varying noise levels (NL) from 0 to 60 dB//1 μPa. The right panel uses the same fish rate data as shown in Figure 4.4.11 with the same remaining parameters mentioned. The actual fish count is marked with the dashed line. The estimated total fish count for that time period using no thresholding is marked with the filled circle for each NL case. The estimated total fish count for that time period using a target strength threshold level of -39.9 dB is marked with an 'x'. In both cases,

the fish count estimates are reasonably close to the actual count for NL cases of 40 dB//1 μPa and below. For the case of NL = 60 dB//1 μPa, the counts calculated without applying a threshold are extremely high ($\sim$ 10 for an actual count of 3 in the first case and $\sim$ 24 for an actual count of 6 in the second case). As to be expected, the counts after thresholding are slightly lower. In the case of NL = 60 dB//1 μPa, the counts after thresholding are much lower (from $\sim$10 down to $\sim$4 in the left panel and from $\sim$24 down to $\sim$5 in the right panel) showing how thresholding makes a significant difference for higher noise levels.

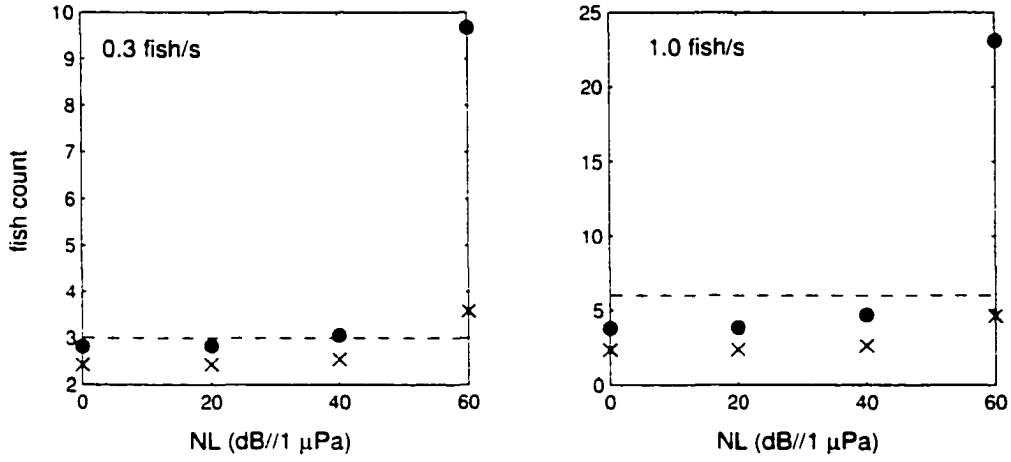

Figure 5.1.3 Fish count estimates as a function of noise level. The plots show fish counts calculated using echo integration for two fish rate cases as a function of noise level. Using the same data shown in Figure 4.4.1 and in Figure 4.4.11 with varying noise levels, fish counts are calculated and compared to the known value. The actual fish count is marked with the dashed line. The estimated total fish count for that time period using no thresholding is marked with the filled circle for each NL case. The estimated total fish count for that time period using a target strength threshold level of -39.9 dB is marked with the 'x'.

To further understand the implications of thresholding, the same 2 data sets were processed again using echo integration under target strength threshold values of -29.9 and -49.9 dB. Figure 5.1.4 shows the results for both examples previously used at 3 different NL cases (0, 20, and 40 dB//1 μPa) using 3 threshold levels. The case of NL = 60 dB//1 μPa was eliminated as it already proved to give poor results.

In Figure 5.1.4 the actual fish count is shown with a dashed line. The estimated fish count using the lowest threshold (-49.9 dB) and thus keeping the most data is shown with a star. The circle represents the estimated fish count using the highest threshold (-29.9 dB) and thus keeping the least amount of data. The 'x' is the same fish count estimate plotted in Figure 5.1.3 calculated with a threshold level of -39.9 dB. As to be expected, the higher threshold provides estimates that under count the data (all values of ~ 0). The lower threshold provides the highest fish counts. With NL below 40 dB//1 μPa, these estimates are close to the actual counts with $\sim$3 for the actual fish count of 3 and $\sim$4 for the case with actual fish count of 6.

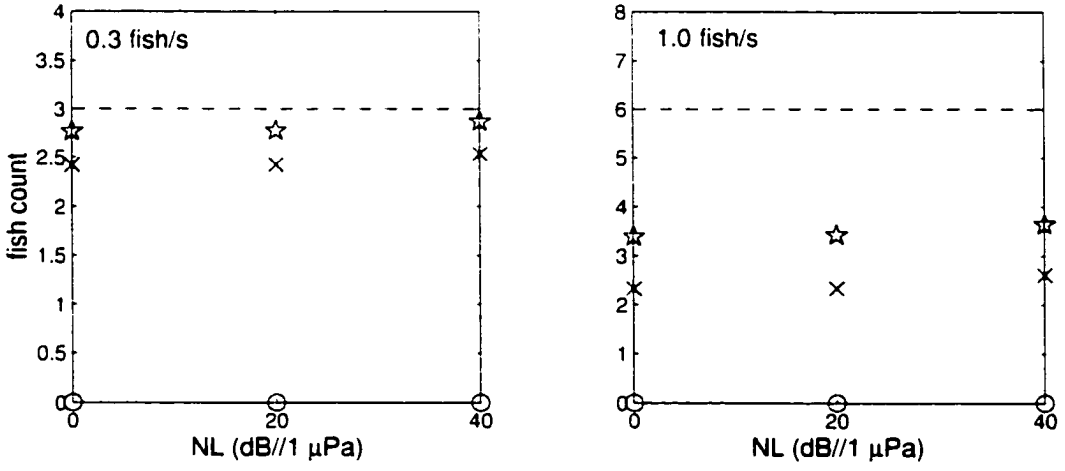

Figure 5.1.4 Effects of thresholding on fish counts. The fish count results for both data sets used in Figure 5.1.3 are calculated at 3 different NL cases (0, 20, and 40 dB//1 μPa) using 3 threshold values each. The actual fish count is shown with a dashed line. The estimated fish count using the lowest threshold (-49.9 dB) and thus keeping the most amount of data is shown with a star. The circle represents the estimated fish count using the highest threshold (-29.9 dB) and thus keeping the least amount of data. The 'x' is the same fish count estimate plotted in Figure 5.1.3 calculated with a threshold level of -39.9 dB.

Figure 5.1.5 shows the sonar output for an example of 0.3 fish per second fish rate data used in the echo integration algorithm with a NL = 60 dB//1 μPa. The dotted line is placed at the amplitude value corresponding to a target strength threshold level of -29.9 dB. For this example, only a very small amount of data is used to

estimate the fish count for this time period, thus providing the value of 0 shown in the left panel of Figure 5.1.4. The dashed line is placed at the amplitude value corresponding to a target strength threshold level of -39.9 dB. Here a reasonable amount of data is kept, and a significant portion of the noise is eliminated during the thresholding. The solid line is placed at the amplitude value corresponding to a threshold level of -49.9 dB. At this stage, most of the noise data is stored along with the signal. Although using this data in the echo integration algorithm may provide estimates closer to the actual count, it is obvious that the algorithm is not actually counting fish at this stage. An analysis of this type should be done before selecting a threshold value to provide some assurance that useful data is being collected.

Next, the effects on fish count results of changing other parameters in the echo integration process are considered. Figure 5.1.6 provides fish count estimates as a function of pulse width. The pulse width ranged from 0.3 to 1.5 ms and the echo integration algorithm was applied using NL = 0 dB//1 μPa, ping rate of 5 pings per second, and a threshold value of -39.9 dB. Results are shown for one example of both 0.3 and 1.0 fish per second fish rate with and without thresholding. Again, the actual fish count is plotted as a dashed line. The filled circle represents fish count estimates without thresholding and the 'x' shows the results after thresholding. In both cases, as the pulse width increases, the fish count increases as well. Since a wider pulse is sent out, less resolution in the fish location is allowed before overlap of the echoes occurs. When the echoes overlap, amplitudes tend to increase, thus providing higher fish count estimates.

Lastly, the effects of ping rate are shown in Figure 5.1.7. Here the echo algorithm is used with NL = 0 dB//1 μPa, pulse width of 0.7 ms, and a threshold value of -39.9 dB. The ping rate ranges from 5 to 15 pings per second. Again, the actual fish

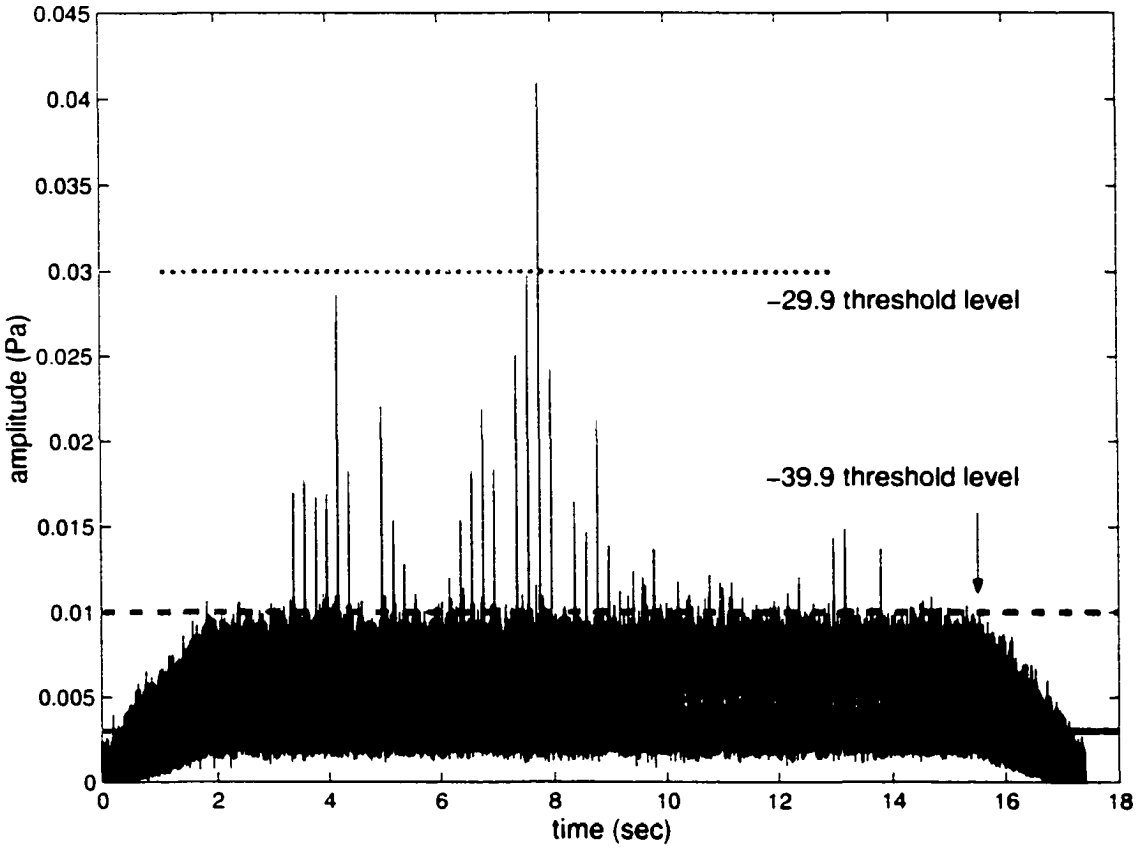

Figure 5.1.5 Threshold values and sonar data. The same sonar output from Figure 4.4.16 is shown with 3 target strength threshold values. The dotted line is placed at the amplitude value corresponding to a threshold level of -29.9 dB. For this example, only a very small amount of data is used to estimate the fish count for this time period, thus providing the value of 0 shown in the left panel of Figure 5.1.4. The dashed line is placed at the amplitude value corresponding to a threshold level of -39.9 dB. Here a reasonable amount of data is kept, and a significant portion of the noise is eliminated during the thresholding. The solid line is placed at the amplitude value corresponding to a threshold level of -49.9 dB. At this stage, most of the noise data is stored along with the signal. Although using this data in the echo integration algorithm may provide estimates closer to the actual count, it is obvious that the algorithm is not actually counting fish at this stage.

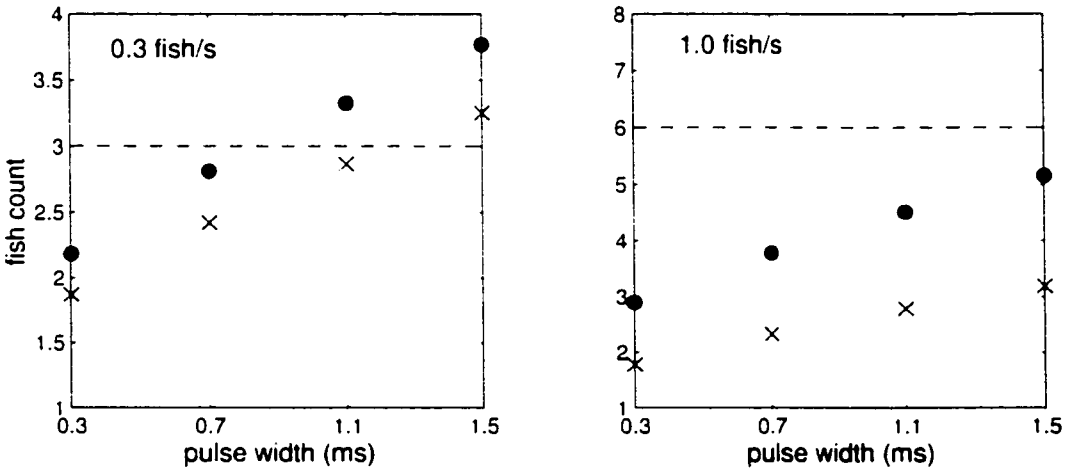

Figure 5.1.6 Effects of pulse width on fish counts. The fish count estimates as a function of pulse width for the same two examples as in Figure 5.1.3 are shown. The pulse width ranged from 0.3 to 1.5 ms and the echo integration algorithm was applied using a threshold value of -39.9 dB. Results are shown for both cases of 0.3 and 1.0 fish per second fish rate data with and without thresholding. Again, the actual fish count is plotted as a dashed line. The filled circle represents fish count estimates without thresholding and the 'x' shows the results after thresholding.

count is plotted as a dashed line. The filled circle represents fish count estimates without thresholding and the 'x' shows the estimates after thresholding. In both cases, as the ping rate increases, the fish count estimates decrease.

Histograms were also plotted for the varying ping rate and pulse width cases. The results are shown in Figure 5.1.8 and values are provided for analysis in Table 5.2 along with the first line of results from Table 5.1.

In comparing the mean data count for the different ping rates, as the ping rate increases, the mean count decreases. Again, this shows that a smaller ping rate may provide more accurate fish counts. On the other hand, when comparing the maximum count for the different ping rates, notice that the smaller maximum (and closer to the true count) is provided by the larger ping rate. This may in fact show that choosing an in between value is most useful. In comparing the mean data count for the different pulse widths, as the pulse width increases, the mean count increases

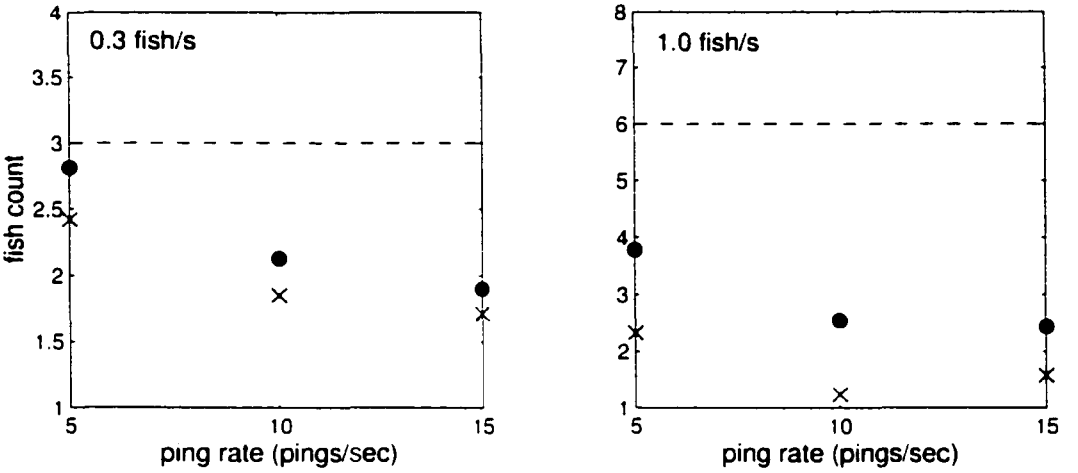

Figure 5.1.7 Effects of ping rate on fish counts. The fish count estimates are shown as a function of ping rate for the same two examples used throughout this section. Again, the actual fish count is plotted as a dashed line. The filled circle represents fish count estimates without thresholding and the 'x' shows the estimates after thresholding. In both cases, as the ping rate increases, the fish count estimates decrease.

Table 5.2 Results of Echo Integration with Varying Parameters.

Expected count of 3 fish. Average True Count of 2.93			
parameter value	minimum count	maximum count	mean data count
ping rate = 1 ping/s	0.01	18.43	0.67
ping rate = 5 ping/s	0.01	7.53	0.41
ping rate = 10 ping/s	0	4.22	0.27
pulse width = 0.1 ms	0	4.12	0.22
pulse width = 0.5 ms	0.01	7.53	0.41
pulse width = 1.0 ms	0.01	10.30	0.55

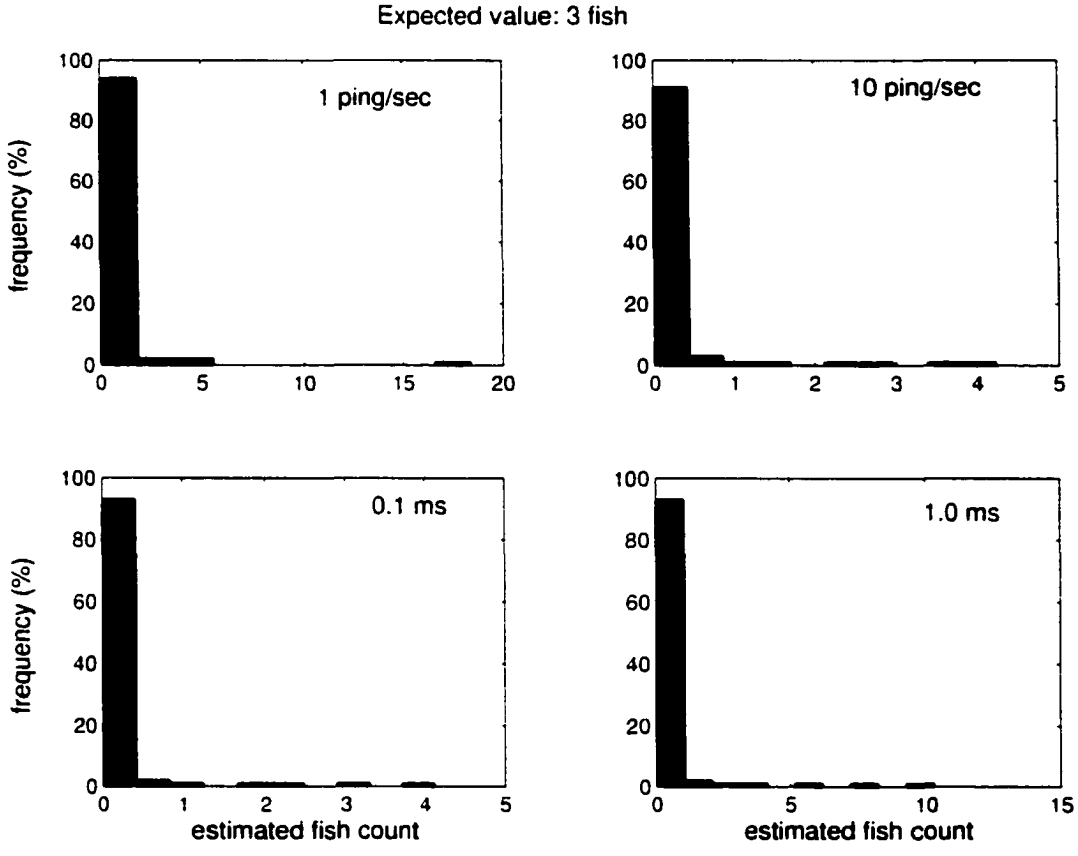

Figure 5.1.8 Histograms of fish counts for varying ping rate and pulse width. The distribution of fish counts using the echo integration algorithm is shown for each set of 100 sonar data with varied pulse width (0.1 ms and 1.0 ms) and ping rate (1 pings/sec and 10 pings/sec). The frequency of estimated fish counts is shown as a percentage in each case. With an average fish rate of 0.1 fish per second, the expected fish count is 3 fish for 30 seconds although each case may have had an actual fish count of more or less than 3. These results are in comparison to the fish count results using average ping rate and pulse width as seen in Figure 5.1.1.

closer towards the true count. Notice that the maximum counts also get larger as the pulse width increases, but are moving away from the true count. The same dilemma exists with pulse width and thus a medium value may be most appropriate.

Although the echo integration results shown here seem to be more accurate for lower fish rate data, in practice the algorithm is used under conditions of high fish rate data. Under counting occurs using all fish rates but seems less obvious when the actual fish count is low. Thresholding also plays a role in both under and over counting. The conclusions from this analysis indicate that a balance of higher pulse width and lower ping rate with in reason should provide more accurate echo integration results for the lower noise level situations. Next, the echo integration algorithm is applied to experimental sonar data from the Chandalar River, Alaska.

5.2 Echo Integration Results from Experimental Sonar Data

The data described in section 4.3 is used again to compare the artificial sonar data to an example of sonar data collected in the field. The Chandalar River data [Daum and Osborne, 1996] provide a useful comparison since the size of the fish and the range are known for an individual fish in the beam for a given time period. In that experiment, an elliptical beam with nominal beam widths of 4.6° by 10.8° was employed with the transducer operating at a frequency of 200 kHz with a pulse width of 0.2 ms and a ping rate of 10 pings/sec.

The sonar data was obtained on 3 August 1995. The raw data files (consisting of a time and amplitude) have already been sent through a threshold, thus eliminating much of the noise. Also saved in the raw data is information on the range and angles off axis representing the location of each echo as calculated from the sonar data, the TS for each echo, and a measure of pulse width for each echo. The Chandalar River

data for fish L215-5 is shown in Figure 5.2.1.

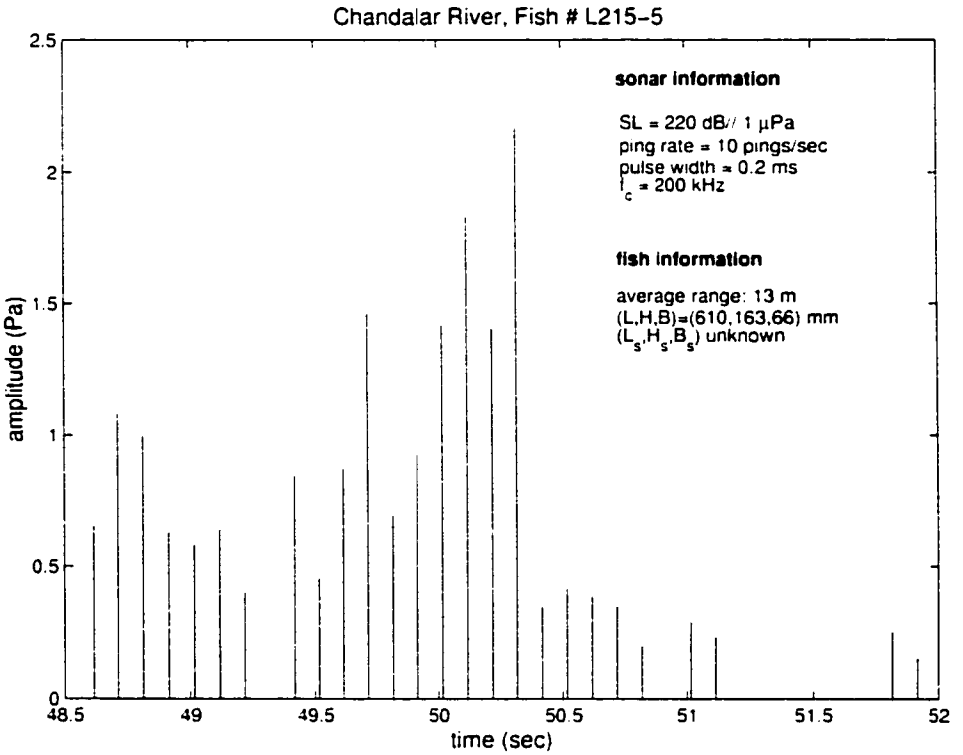

Figure 5.2.1 Example of experimental sonar data. The received echoes with amplitude in Pascal as a function of time in seconds is shown for the one fish, L215-5, from the Chandalar River experiment. The sonar data were obtained using f_c = 200 kHz, pulse width of 0.2 ms, and ping rate of 10 p/sec. The fish measured 610 mm in length and passed through the beam at an average range of about 13 m.

Since the data was collected and stored using certain parameters, these can not be varied freely as in the case of the artificial data. The only comparisons that can be done are with respect to the cases used in collecting the experimental data. Using the same known parameters for the same data set from section 4.3 (L215-5), a random fish track was created and then artificial sonar data generated. The artificial sonar data is shown in Figure 5.2.2.

In comparison, the artificial data matches the experimental data well. The lower amplitude for the artificial data is attributed to the longer average range of the artificial fish track compared to that of fish L215-5. Note that the fish size data are

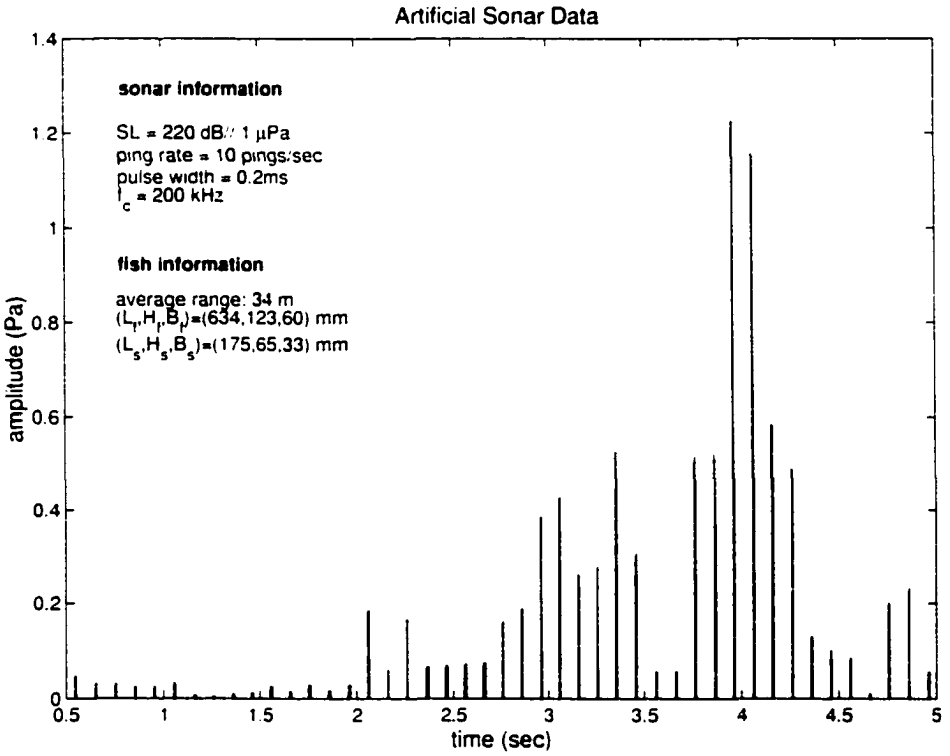

Figure 5.2.2 Example of artificial sonar data using parameters from experimental data. The received echoes with amplitude in Pascal as a function of time in seconds is shown for the modeled fish track using the parameters obtained from the Chandalar River data for fish L215-5. The sonar data were generated using $f_c = 200$ kHz, pulse width of 0.2 ms, and ping rate of 10 p/sec. The fish measured 634 mm in length and passed through the beam at an average range of about 34 m.

reasonably close, but that the swimbladder data for fish L215-5 is unknown.

Using the experimental data with the echo integration algorithm provides insight into the effectiveness of the algorithm. In applying the echo integration algorithm a count of 0.52 is obtained from the experimental data, rather close to the actual count of 1 fish. In calculating the fish count, the known target strength values are used. When applying the algorithm to the artificial sonar data, a count of 1.5 fish is obtained. The higher fish count may seem at odds with the lower sonar amplitude for the artificial data as compared to the experimental data. This is a function of the compensation factor for the range in the echo integration algorithm. Thus the algorithm works in the same manner with the experimental data as it does with the artificial data, providing a sense of assurance that the artificially generated data is comparable to that collected in the field. This also provides justification for using the direct and inverse models on data collected in the field.

The echo integration algorithm is just the first step in understanding the inverse problem. In the future, the algorithm should go through modifications representative of progress made in this research area. Presently, work has been conducted with the direct and inverse model approach using an echo counting technique as found in Lai [2002]. Future work is planned to apply target tracking techniques in the inverse model. This requires combining results presented here with the split beam sonar model considered by Ayers [2001]. In each case, the appropriate assumptions must be considered and implemented. The closer the assumptions come to being realistic, the closer the inverse model becomes useful in the field. One main goal is to implement these processes in field experiments to calculate real time sonar fish counts. Prior to implementation, filter parameters and thresholds must be decided theoretically so as to not be changed during collection to match expected tower

counts or other expectations. In post processing the various uncertainties can be recognized and quantified thus leading to a higher accuracy of reporting the fish count data.

Chapter 6

CONCLUSIONS AND DISCUSSION

In conclusion, a comparison to past work is presented, followed by a summary of the results presented in this work. Lastly recommendations for future work are listed.

6.1 Comparison to Past Work

The field of fisheries acoustics combines many professionals from different areas of expertise: biologists, oceanographers, physicists, electrical engineers, mathematicians, statisticians, and others. The variety in literature shows this representation.

Most literature focuses on only one part of the fisheries acoustics problem. For example, target strength of individual species has drawn much attention providing insight into the acoustical properties of the fish biology and movement. There is extensive literature on the measurements [Love, 1978; Dahl and Mathison, 1983; Kubecka, 1994; Sawada, et al., 1997; Foote, 1978; Haslett, 1962a, 1965; Drew, 1980] and theoretical estimates [Shibata, 1970; Foote, 1985; Ye and Farmer, 1994; Ye and Furusawa, 1995; Ye, 1996a, b] of TS of fish. The earlier work on TS involved experimental work using physical spheroidal models to determine scattering [Haslett, 1962b; Lauchle, 1975] and empirical fits to observed scattering from marine fish

[Love, 1977; Foote, 1985]. Most of the theoretical work is done for marine animals (e.g., zooplankton) at low frequencies (< 100 kHz) such that typical length (L) to wavelength (λ) ratio is smaller than $\sim$ 25 [Stanton, 1988a, b, 1989a, b], sometimes even less than one. As a result increasingly complicated anatomical models such as those constructed from x-rays of swimbladders are used with Kirchhoff's integral scattering approach to calculate TS of marine fish [Clay 1991, 1992; Clay and Horne, 1994; Horne and Clay, 1998]. These numerical models involve complex calculations based on a detailed physical shape of the swimbladder at either dorsal or side aspect. These models are important because they verify that the Kirchhoff theory provides good results matching with experiments for fish with $L/\lambda < 25$ and that at low frequencies the details of fish and swimbladder shape are important. This approach is not useful in practice because the detailed shapes of swimbladders of an unknown fish distribution are not available and the calculations are too complex to be useful to interpret sonar data from a large number of fish.

Other directions in the literature show an emphasis on the biological organism or species of interest, whether it be a specific fish species or type of zooplankton. Detailed analysis of the morphology of fish and their swimbladders have been presented since the begin of the research and are still considered today [Haslett, 1962c; Shibata, 1970; Hawkins, 1981; Horne and Clay, 1998; Ye and McClatchie, 1998]. Environmental parameters such as the study of noise, reverberation, and attenuation are often considered separately [Dahl and Mathisen, 1984; Dahl, 1999; Furusawa *et al.*, 1982].

Other efforts have been directed to hardware design leading to the development of improved technology such as the split-beam or wide band sonar [Ehrenberg and Torkelson, 1996; Ransom *et al.*, 1996; Simmonds *et al.*, 1996; Sawada and Furusawa,

1993: Thompson and Love, 1996: Chu and Stanton, 1998: Demer *et al.*, 1999: Ma *et al.*, 1995] and even video analysis [Hughes and Kelly, 1996]. Yet other efforts focus on improving the data processing for the various hardware designs [Burwen *et al.*, 1995: Mulligan and Kieser, 1996: Ehrenberg *et al.*, 1981: Ehrenberg, 1972: Foote, 1996: Furusawa and Miyanohana, 1988: Mesiar *et al.*, 1990: Soule *et al.*, 1996]. The consideration of forward scattering as opposed to backscattering [Dahl, 1996: Ding, 1997: Ding and Ye, 1997: Ding *et al.*, 1998: Ye, 1995: Ye and Farmer, 1996] is a more recent idea in the area of data processing.

There has been relatively little work done on modeling Pacific salmon [Dahl and Mathison, 1983] and little emphasis placed on gathering acoustical information in the riverine environment. With the exception of Dahl and Mathisen [1983] most of the work dealing with Pacific salmon in the riverine environment has been performed as field surveys in Alaska [Burwen and Bosch, 1996: Daum and Osborne, 1996: Fleischman, *et al.*, 1995: Huttunen and Skvorc, 1994, 1996: Konte *et al.*, 1996: LaFlamme, 1995: Maxwell *et al.*, 1997: Osborne and Daum, 1997: Vania and Huttunen, 1996: Vaught and Molyneaux, 1995] and Canada [Enzenhofer *et al.*, 1998: Mulligan *et al.*, 1997: Xie *et al.*, 1997] as described in section 1.2 of the introduction.

Riverine fisheries acoustics used in Alaska involve relatively high frequencies ($\sim 200 - 400$ kHz) and large fish ($L > 50$ cm) giving a rather large $L/\lambda \geq 150$. The Pacific salmon and its swimbladder have roughly convex shape that can be approximated by convex shapes such as ellipsoids. Recognition of these two factors allowed development of a geometrical approach to TS calculation for salmon as a function of size, shape, and aspect.

It was shown in Chapter 3 that this TS model compares well with results obtained using the Kirchhoff method, and with data obtained in the field under a

variety of conditions. Furthermore, the TS model provides quantification of the uncertainties in the field data and was able to attribute those errors to specific parameters, whether it be angle of incidence, swimbladder parameters, or variation in the fish size parameters based on fish length for example. Although no literature exists on the fish size distribution for sockeye salmon or Pacific salmon in general, the ability of this distribution to aid in calculating uncertainties in the field data provide its justification.

6.2 Summary of Results Presented

This work models the entire fisheries acoustic problem using a modular approach to the direct and inverse problems. The modular approach is the key to analyzing effects of numerous parameters independent of others. Using the direct and inverse problems allow for construction and generation of data under various conditions ranging from ideal (no noise, low fish rates for a given river cross-section, fish movement in linear tracks) to the worst case scenario found in the field (high noise level, high fish rates). Comparison between a known fish distribution producing artificial sonar data and the estimated fish distribution using sonar data allows for improvement in the model and quantification of uncertainties.

Overall, the geometric scattering model for TS gives good results for salmon and can be used for riverine fisheries acoustics in Alaska and Canada. In particular, using the fish size distribution and TS distribution provide powerful new insight into a key aspect in the fisheries acoustics problem. The TS model provides dependence of TS on several parameters not recognized in earlier work on sound scattering by fish.

1. The TS model allows for quantification of the variations in TS dependent on the fish parameters and the swimbladder size and shape. In fact, effects of each parameter on TS can be analyzed independently (unlike the ka terms typical in other models where k is the wave number and a is the radius of the sphere or cylinder). The method is limited to high frequencies. These calculations provide uncertainties in using TS to estimate biomass or to perform species discrimination.

2. By taking into account both the scattering from swimbladder (major contribution to TS) and fish body (minor contribution), the model shows the fish flesh plays an important role in the TS of swimbladder at large aspects and can reduce the same by as much as 10 dB or more. It also shows that most of the contribution to the TS comes from the swimbladder as presented by Foote [1985].

3. The height and breadth variation of the fish plays as important a role as the length in determining TS. Previous studies have in general modeled fish by one (length) or two (length and average diameter) parameters [Love, 1977; Furusawa, 1988]. However, the ellipsoid model for the fish size provides a more realistic shape for a fusiform fish such as salmon as well as their swimbladders and requires three parameters (L, H, B). Note that both fish and swimbladder need only be convex surfaces with $L/\lambda > 25$ for the model to be valid. This TS model can be used as long as the radii of curvature can be obtained for any point on the surface of the target.

4. The TS model allows for placement and orientation of the swimbladder at arbitrary location within the fish body allowing for a general approach.

5. The TS model can easily be adapted to other species given appropriate morphological parameters as long as both fish body and swimbladder are convex surfaces. It can also be applied to fish with no swimbladder.

6. The TS model predicts a weak dependence on frequency that results from the varying phase of return from the fish body and swimbladder. This dependence on frequency results in a 2-3 dB variation in TS with frequency.

In its base essentials the model only requires that both fish body and swimbladder be represented as convex surfaces, and the model presented here can be generalized to the case when both the fish body and swimbladder are represented by a convex surface of arbitrary shape. Furthermore, in the model, for any given angle of incidence, the TS value is determined only by the local radii of curvatures and therefore the fish can, in principal, be represented by a convex surface more complicated than the ellipsoids considered here. This also implies that for the same fish we can consider that the swimbladder is represented by one model for side incidence, such as the half ellipsoid model with flat bottom, and by another dorsal incidence, such as the full ellipsoid.

The model accurately predicts TS of fish of varying lengths and at arbitrary angle of incidence. The comparison between the model prediction of TS and the experimental values of TS show an excellent agreement. The comparison of the model prediction with experimental data gives the conditions for the validity of our model. The TS model presented here is valid for $L_f/\lambda > 20$ for all angles of incidence within $50 - 60^\circ$ of normal incidence at dorsal or side aspect. Thus the TS model is valid for many common fish such as cod, saithe, pollack, salmon at almost all angles of incidence for frequencies higher than 100 kHz, assuming the fish size is $> 25 - 30$ cm. For larger fish, such as Chinook salmon, which are typically larger

than 50 cm. the model is valid at $\sim$ 50 kHz. Thus the model presented here should be useful in a wide range of applications in riverine and ocean fisheries acoustics.

In many applications such as acoustic surveys conducted to determine the estimates of fish counts in a river, it is important to consider the acoustic returns from an ensemble of fish. Using the TS and fish distributions presented in this work, generalizing to an ensemble of fish is computationally very efficient since the TS at a given angle of incidence depends only on the local radii of curvatures. Thus it can be used in calculating acoustic wave returns from many fish moving in a complicated manner. The results of this analysis using the direct model are described in Chapter 4 providing artificial sonar data from an ensemble of fish and then compared to experimental data in Chapter 5. The artificial data works as expected in terms of fish rate, noise levels, ping rate, and pulse widths and compares well with one example of data collected in the field. Lastly, estimates of fish counts for several examples of artificially generated data at various fish rates are given using the inverse problem approach. One method, echo integration, of estimating fish counts from sonar data is applied to each case under varying ranges of sonar and noise parameters.

The echo integration results provide fish counts from 0 to 7 for a known fish distribution of 3 fish generated using a fish rate of 0.1 fish per second. When the ping rate is changed from 1 to 10 pings per second, then the fish count range narrows from 0.01 to 18.43 fish to 0.01 to 4.22 fish. When pulse width varies from 0.1 to 1.0 ms, the echo integration algorithm provides a fish count range of 0 to 4.12 fish to 0.01 to 10.30 fish. In all cases, under counting is more likely than over counting, although both are evident. For a similar example of fish rate data at the 0.3 fish per second rate, noise levels under 40 dB//1 μPa do not effect the fish counts; however, once the noise level reaches 60 dB//1 μPa, the echoes from the noise dominate the

signal and fish counts can be as much as ~10 fish for an expected value of 3 fish.

The echo integration results provide a wider range of fish counts as the number of fish entering the beam in a fixed period of time increases. For example, for a known distribution of 15 fish, the algorithm provides a range of fish counts from 0 to ~30 fish. For a true count of 30, the algorithm provides a count ranging from 0 to ~50 fish. For a higher fish rate, such as 5 fish per second, considering 30 second simulations, the echo integration algorithm was never able to obtain the accurate count of 150 fish, but estimated fish counts from 0 to 100 fish.

In conclusion, the echo integration results are more accurate for lower fish rates, for lower noise levels, and for lower ping rates. Using accurate threshold values, which depend on the noise level, aid in correct estimating of fish counts. However, in the field, with the number of fish unknown, it is difficult to know which parameters are best to use.

6.3 Recommendation for Future Work

Future work is foreseen at each stage of the fisheries acoustics problem.

Modeling of the transmitter as a split-beam system needs to be integrated into the direct problem. In this work, a model of single beam sonar is used. Although it is still the most common transducer used in the field, split-beam systems are gaining popularity due to the amount of extra information gained by its design. Once a split-beam model is incorporated, then the interpretation of the sonar data can include not only echo integration methods but also target tracking methods.

The sonar data used throughout this work was collected under good environmental conditions, for example, in rivers with little to no suspended particles. Often, sonar systems in Alaska are implemented in rivers with high reverberation from

suspended particles, such as the Yukon River. A propagation model allowing for scattering by these particles would aid interpretation of that data.

More size, shape and spatial data for the fish distribution model could allow improvements for the sockeye salmon model and generalizations to other species. The fish distribution model is built on an average amount of data, but could only be improved with the collection of more size data on sockeye salmon for both the fish body and the swimbladder. For better modeling of the direct problem using other fish species, an appropriate fish size distribution would lend itself to better estimates of uncertainty. However, the fish size model is constructed general enough to accommodate any species of fish with mostly convex surface. A few hybrid models for the swimbladder shape and size are presented. Depending on the species of consideration, further hybrid models could be constructed to better represent them, thus providing a more accurate TS model for that species. Also, most of the data used in this work was collected in rivers with one dominant species; however, on both the Yukon River and the Kenai River more than one dominant species migrates during the same time period. Differences in fish behavior between species may aid in species apportionment. Developing a spatial distribution more consistent with known properties of fish behavior will aid in generating artificial data using the direct problem that closely resembles data collected under these situations in the field.

For the inverse problem, the echo integration techniques used in this work need improvement. In the field, echo integration is generally applied under higher fish rates; however, in this work the technique is more accurate for the lower fish rates.

Lastly, all of this data collection and interpretation is done in real-time in the field. Various methods are applied to allow for real-time management of the data,

such as thresholding before storing the raw data. These methods are not used in this work during the generation of the artificial data since information is lost in this process. However, programming techniques should be applied to minimize the time used in generating the artificial data. At the present stage, this modeling of the fisheries acoustics problem can be used in post processing of real-time sonar data collected in the field to better understand the fish distribution generating the data and thus providing fish counts. Future work should allow for this method to be used in real-time.

Appendix A

DERIVATIONS

Presented in this appendix is the derivation of the target strength of the swimbladder taking the effect of fish flesh into account.

Consider an incident wave $\mathbf{k_i}$ with an arbitrary angle of θ_0 to the surface of the fish at a point with principle radii of curvature $R_{f\|}$ (R_{f1} in text) and $R_{f\perp}$ (R_{f2} in text). Since the acoustic impedance of the fish flesh is different than that of water, refraction inside the fish flesh will occur at an angle of θ_1, given by Snell's Law. As the refracted wave travels through the fish flesh it will fall normally at some point upon the swimbladder surface with principle radii of curvature $R_{s\|}$ and $R_{s\perp}$ (see Figure 3.1.4 in text).

A.1 Spreading of Rays in the Plane of Incidence

Let $\mathbf{k_i}$ lie in the plane containing both the normal to the fish surface $\hat{n}_f$ and the normal to the swimbladder $\hat{n}_{sb}$. Figure A.1 illustrates the reflection and refraction occurring between the two surfaces. Note that $R_{f\|}$ is the distance $PP_{0\|}$, and $R_{s\|}$ is the distance $QQ_{0\|}$. Let the distance travelled between the surfaces (PQ) be called a. The arc covered by the incident plane wave at the fish surface forms an angle of

$2d\theta_{0\|}$. The refracted wave appears to originate at a distance from the fish surface (at point $P'_{\|}$) forming the angle $2d\theta_{1\|}$ given by

$$d\theta_{1\|} = \alpha_1 d\theta_{0\|}. \tag{A.1}$$

where

$$\alpha_1 = \frac{c_f cos\theta_0}{c_w cos\theta_1} - 1. \tag{A.2}$$

The parameters c_f and c_w are the speeds of sound in fish flesh and water respectively.

When the wave falls normally on the swimbladder surface it will reflect within the fish flesh due to the difference in acoustic impedance between fish flesh and the air in the swimbladder (Figure A.1). The arc covered by the scattered wave at the swimbladder surface forms an angle of $2d\theta_{2\|}$ such that

$$d\theta_{2\|} = \delta_{\|} d\theta_{0\|}. \tag{A.3}$$

where

$$\delta_{\|} = \frac{(a + \gamma_{\|} R_{s\|})(2\beta_{\|} + \alpha_1)}{R_{f\|}} \tag{A.4}$$

and

$$\gamma_{\|} = \frac{\beta_{\|}}{2\beta_{\|} + \alpha_1} \tag{A.5}$$

and

$$\beta_{\|} = \frac{R_{f\|} + \alpha_1 a}{R_{s\|}}. \tag{A.6}$$

This scattered wave appears to have come from the point $Q'_{\|}$ within the swimbladder forming an angle $2d\theta_{3\|}$ given by

$$d\theta_{3\|} = (2\beta_{\|} + \alpha_1) d\theta_{0\|}. \tag{A.7}$$

Finally, the reflected wave from the swimbladder surface will travel through the fish flesh and be refracted into the water (Figure A.2). This wave appears to derive

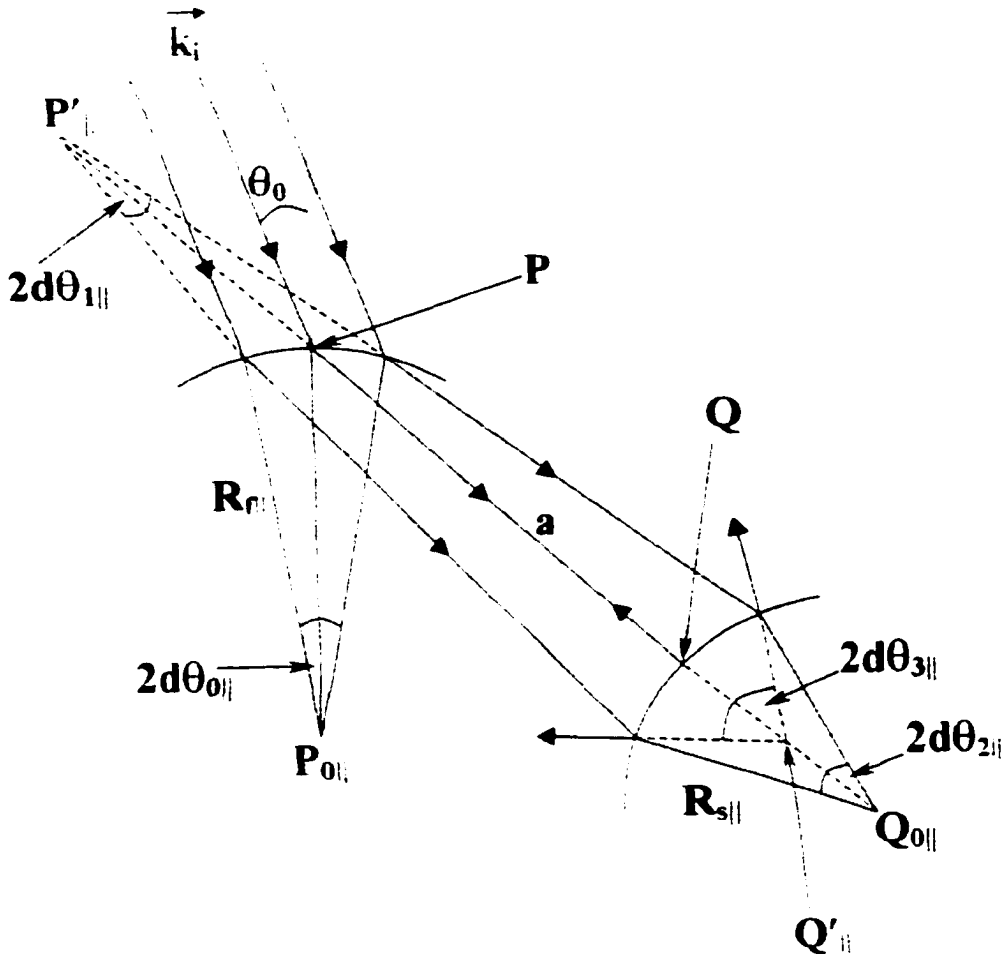

Figure A.1 Spreading of rays inside fish flesh. The incident wave, $\mathbf{k}_i$, is shown hitting the fish surface at the point P, transmitting through the fish flesh, and reflecting from the swimbladder boundary at the point Q. The angle of the rays transmitting through the fish flesh incident on the fish surface appear to have originated at point $P_{\|}'$. The reflected waves at point Q appear to have originated from point $Q_{\|}'$.

from the point $P''_{\|}$ creating the angle

$$d\theta_{4\|} = (\delta_{\|} + \epsilon_{\|})d\theta_{0\|}. \tag{A.8}$$

where

$$\epsilon_{\|} = \frac{2\beta_{\|} + \alpha_1 - \delta_{\|}}{1 + \alpha_1}. \tag{A.9}$$

This angle can be rewritten in terms of $d\theta_{0\|}$, the angle formed by the original incident wave, as

$$d\theta_{4\|} = \frac{2R_{f\|}}{R_{s\|}(1+\alpha_1)}\left[1 + \alpha_1\left(\frac{2a}{R_{f\|}} + \frac{R_{s\|}}{R_{f\|}}\right) + \alpha_1^2\left(\frac{a^2}{R_{f\|}^2} + \frac{aR_{s\|}}{R_{f\|}^2}\right)\right]d\theta_{0\|}. \tag{A.10}$$

A.2 Spreading of Rays in the Plane Perpendicular to the Plane of Incidence

Next consider an incident wave $\mathbf{k_i}$ that lies in the plane perpendicular to the plane of incidence. The derivation is similar to the above parallel case and the same figures can be referenced replacing all $\|$ symbols with $\perp$. Again allow a plane wave to fall on the fish surface now with radius of curvature $R_{f\perp}$ at an incident angle of θ_0 producing a refracted wave $\mathbf{k_r}$ with angle θ_1. The refracted wave (Figure A.1) appears to originate from the point $P'_{\perp}$ forming the angle $2d\theta_{1\perp}$ given by

$$d\theta_{1\perp} = \alpha_2 d\theta_{0\perp}. \tag{A.11}$$

where

$$\alpha_2 = \alpha_1 cos\theta_1. \tag{A.12}$$

The refracted wave travels through the fish flesh and falls normally on the surface of the swimbladder with radius of curvature $R_{s\perp}$. The arc covered by the scattered

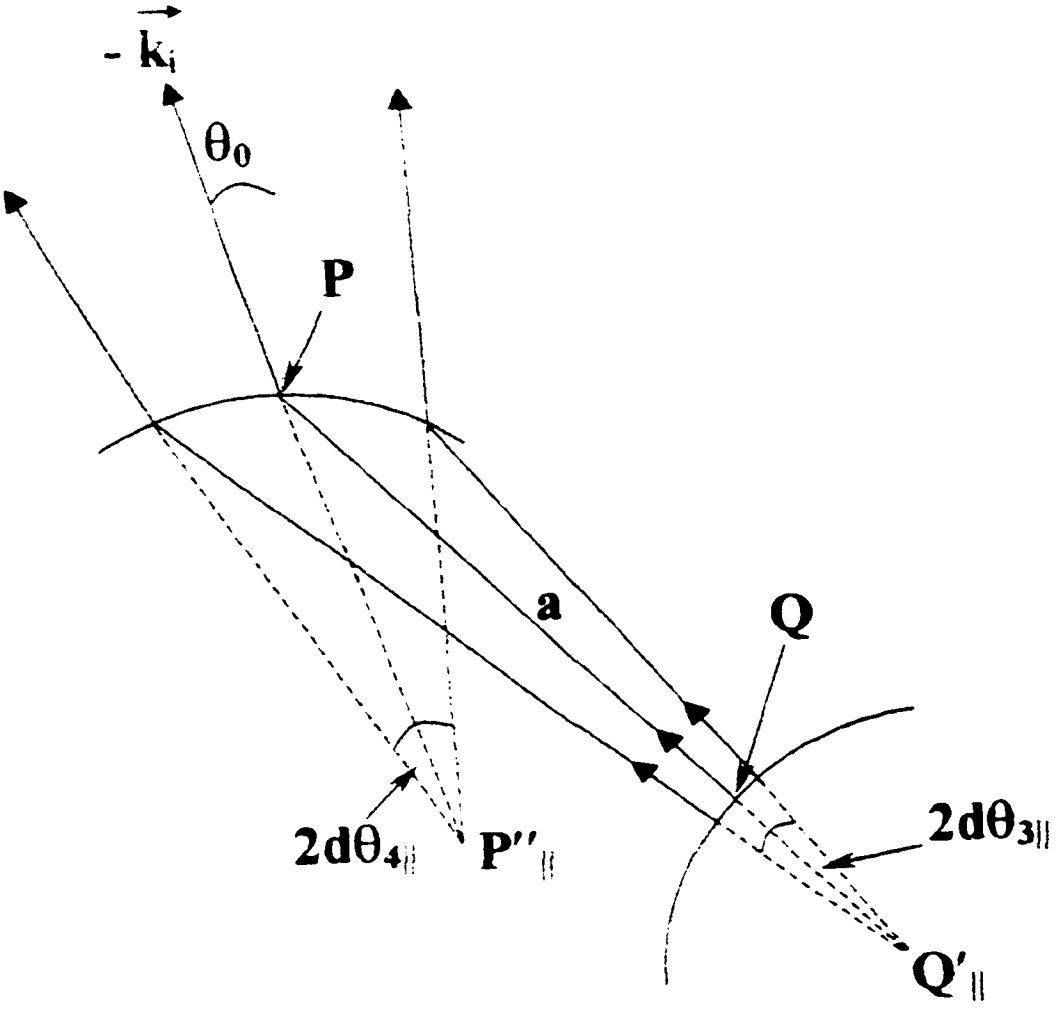

Figure A.2 Geometry of total reflected wave. The wave reflected from the swim-bladder boundary shown in Figure A.1 continues to propagate through the fish flesh and transmits back into the water. The total reflected wave, $-\mathbf{k}_i$, forms the same angle of incidence, θ_0, as the original incident wave, $\mathbf{k}_i$.

wave at the swimbladder surface forms the angle $2d\theta_{2\perp}$ such that

$$d\theta_{2\perp} = \delta_\perp d\theta_{0\perp}. \tag{A.13}$$

where

$$\delta_\perp = \frac{(a + \gamma_\perp R_{s\perp})(2\beta_\perp + \alpha_2)}{R_{f\perp}} \tag{A.14}$$

and

$$\gamma_\perp = \frac{\beta_\perp}{2\beta_\perp + \alpha_2} \tag{A.15}$$

and

$$\beta_\perp = \frac{R_{f\perp} + \alpha_2 a}{R_{s\perp}}. \tag{A.16}$$

This wave reflects back into the fish flesh from an apparent angle of $2d\theta_{3\perp}$ given by

$$d\theta_{3\perp} = (2\beta_\perp + \alpha_2) d\theta_{0\perp}. \tag{A.17}$$

Finally, the reflected wave travels through the fish flesh and refracts out into the water (Figure A.2) apparently from the point $P''_\perp$ forming the angle

$$d\theta_{4\perp} = \frac{2R_{f\perp}}{R_{s\perp}(1+\alpha_0)} \left[1 + \alpha_2 \left(\frac{2a}{R_{f\perp}} + \frac{R_{s\perp}}{R_{f\perp}} \right) + \alpha_2^2 \left(\frac{a^2}{R_{f\perp}^2} + \frac{aR_{s\perp}}{R_{f\perp}^2} \right) \right] d\theta_{0\perp}. \tag{A.18}$$

where

$$\alpha_0 = \frac{c_f}{c_w} - 1. \tag{A.19}$$

A.3 Backscattering Coefficient of Swimbladder with the Fish Flesh Taken into Account

To calculate the back scattering coefficient of the swimbladder with the fish flesh taken into account we proceed as follows.

The incident power is given by

$$P_i = 4 I_i R_{f\parallel} R_{f\perp} d\theta_{0\parallel} d\theta_{0\perp} cos\theta_0. \tag{A.20}$$

The back scattered power at a distance r from the fish is given by

$$P_b = 4I_b r^2 d\theta_{4\parallel} d\theta_{4\perp} cos\theta_0 R_{Psf}. \tag{A.21}$$

but

$$I_b \triangleq \frac{\sigma_{sf} I_i}{4\pi r^2}. \tag{A.22}$$

The three previous equations above (Eqs. (A.20 - A.22)) give Eq. (26) stated in section I.F. The total power reflection coefficient, R_{Psf}, (Eq. (27)) is simply the product of the square of the transmission coefficient at the water - flesh interface and the reflection coefficient at the flesh - swimbladder interface.

References

[1] Anderson. Victor C. Sound scattering from a fluid sphere. *J. Acoust. Soc. Am.*. 22 (4). July. 1950. p. 426.

[2] Andreeva. I.B. Scattering of sound by air bladders of fish in deep sound-scattering ocean layers. *Soviet Physics -Acoustics*. 10 (1). July - Sept. 1964. p. 17.

[3] Andreeva. I.B. and V.G. Samovol'kin. Sound scattering by elastic cylinders of finite length. *Soviet Physics -Acoustics*. 22 (5). Sept.-Oct. 1976. p. 361.

[4] Athanassoulis. Gerassimos A. and Aristides M. Prospathopoulos. Three-dimensional acoustic scattering of a source-generated field from a cylindrical island. *J. Acoust. Soc. Am.*. 100 (1). July. 1996. p. 206.

[5] Ayers. Mark L. Uncertainty in Fish Location Using a Split Beam Sonar, MS thesis. University of Alaska Fairbanks. Fairbanks. AK. 2001.

[6] Beylkin. G. and R. Burridge. Linearized inverse scattering problems in acoustics and elasticity. *Wave Motion*. 12. 1990. North-Holland. p. 15.

[7] BioSonics. Inc. Alaska Statewide Sonar Project Results of 1998 Field Demonstrations. Technical Report to Alaska Department of Fish and Game. December 1998.

[8] Boag, Amir, Alona Boag, and Eric Michielssen. Complex multipole beam approach to acoustic scattering problems. *J. Acoust. Soc. Am.*, 102 (3), September 1997, p. 1319.

[9] Bond, Carl E. Biolgoy of Fishes, 2nd ed. Saunders College Publishing, Fort Worth, TX, 1996.

[10] Burov, V. A. and S. N. Sergeev. Inverse scattering problems in the acoustics of moving media. *Acoustical Physics*, 42, 1996, p. 668.

[11] Burwen, Debby and Daniel Bosch. Estimates of Chinook Salmon abundance in the Kenai River using split-beam sonar, 1995. Fishery Data Series No. 96-9, April 1996.

[12] Burwen, Debby, Daniel Bosch and Steven J. Fleischman. Evaluation of hydroacoustic assessment techniques for Chinook Salmon on the Kenai River using split-beam sonar. Fishery Data Series No. 95-45, December 1995.

[13] Burwen, Deborah L. and Steven J. Fleischman. Evaluation of side-aspect target strength and pulse width as potential hydroacoustic discriminators of fish species in rivers. *Canadian Journal of Fisheries and Aquatic Sciences*, 55 (11), 1998, p. 2492.

[14] Chen, Biao. Modeling Fish Behavior in Sonar Beam, MS Thesis. University of Alaska Fairbanks, Fairbanks, AK, 2001.

[15] Chu, Dezhang, Kenneth G. Foote and Timothy K. Stanton. Further analysis of target strength measurements of Antarctic krill at 38 and 120 kHz: Comparison with deformed cylinder model and inference of orientation distribution. *J. Acoust. Soc. Am.*, 93 (5), May, 1993, p. 2985.

[16] Chu, Dezhang and Timothy K. Stanton. Application of pulse compression techniques to broadband acoustic scattering by live individual zooplankton. *J. Acoust. Soc. Am.*, 104 (1), January, 1999. p. 39-55.

[17] Clay, C.S. and B. G. Heist. Acoustic scattering by fish - Acoustic models and a two-parameter fit. *J. Acoust. Soc. Am.*, 75 (4), April, 1984, p. 1077.

[18] Clay, Clarence S. and John K. Horne. Acoustic models of fish: The Atlantic cod (/it Gadus morhua). *J. Acoust. Soc. Am.*, 96 (3), September, 1994, p. 1661.

[19] Clay, C.S. Low-resolution acoustic scattering models: Fluid-filled cylinders and fish with swim bladders. *J. Acoust. Soc. Am.*, 89 (5), May 1991, p. 2168.

[20] Clay, Clarence S. Composite ray-mode approximations for backscattered sound from gas-filled cylinders and swimbladders. *J. Acoust. Soc. Am.*, 92 (4) Pt. 1, October 1992, p. 2173.

[21] Clay, C.S. and Medwin.H. Acoustical Oceanography: Principles and Applications. Wiley, New York, 1977.

[22] Cooper, G. and J.A.G. Temple, Calculations of acoustic scattering from ellipsoidal voids: bends, krill and fish. *Ultrasonics*, July 1983, p. 171.

[23] Cushing, D.H., F.R. Harden Jones, R.B. Mitson, G. H. Ellis, and G. Pearce. Measurements of the target strength of fish. *Journal Brit. I.R.E.*, April 1963, p. 299.

[24] Dahl, P.H. and O.A. Mathisen. Some experiments and considerations for development of doppler-based riverine sonars. *IEEE J. Oceanic Eng.*, Vol. OE-9, No.3, July 1984, p. 214.

[25] Dahl. P.H. and O.A. Mathisen. Measurement of fish target strength and associated directivity at high frequencies. *J. Acoust. Soc. Am.*, 73 (4). April 1983. p. 1205.

[26] Dahl. Peter H. On the spatial coherence and angular spreading of sound forward scattered from the sea surface: Measurements and interpretive model *J. Acoust. Soc. Am.*. 100 (2). August 1996. p. 748.

[27] Dahl. Peter Hans. Analysis of salmonid target strength and doppler structure for riverine sonar applications. MS thesis. University of Washington, Seattle. WA. 1982.

[28] Dahl. Peter H. On bistatic sea surface scattering: Field measurements and modeling. *J. Acoust. Soc. Am.*. 105 (4). April 1999. p. 2155.

[29] Dahl. Peter H., Harold J. Geiger. Deborah A. Hart. James J. Dawson, Sam V. Johnston. and Donald J. Degan. The Environmental Acoustics of Two Alaskan Rivers and its Relation to Salmon Counting Sonars. APL-UW TR 2001 Technical Report. August 2000.

[30] Daum. David W. and Bruce M. Osborne. Use of fixed-location. split-beam sonar to describe temporal and spatial patterns of adult Fall Chum Salmon migration in the Chandalar River. Alaska. *North American Journal of Fisheries Management*. 18. 1998. p. 477.

[31] Daum. David W. and Bruce M. Osborne. Enumeration of Chandalar River Fall Chum Salmon using split-beam sonar. 1995. Alaska Fisheries Progress Report Number 96-2. June. 1996.

[32] Dawson, J.J. and W.A. Karp. In situ measures of target-strength variability of individual fish. *Rapp. P.-v.Reun. Cons. Int. Explor. Mer.* 189. 1990. p. 264.

[33] Dawson, Jim and Sam Johnston. The 1997 Alaska Riverine Sonar Shortcourse. March 3-4. 1997.

[34] Demer, David A., Michael A. Soule, and Roger P. Hewitt. A multiple-frequency method for potentially improving the accuracy and precision of *in situ* target strength measurements. *J. Acoust. Soc. Am.*, 105 (4), April 1999, p. 2359.

[35] Denny, Mark W. Air and Water: the Biology and Physics of Life's Media. Princeton University Press, New Jersey, 1993.

[36] Ding, Li. Direct laboratory measurement of forward scattering by individual fish. *J. Acoust. Soc. Am.*, 101 (6), June 1997, p. 3398.

[37] Ding, Li and Zhen Ye. A method for acoustic scattering by slender bodies. II. Comparison with laboratory measurements. *J. Acoust. Soc. Am.*, 102 (4), October 1997, p. 1977.

[38] Ding, Li and Y. Takao, K. Sawada, T. Okumura, Y. Miyanohana, M. Furusawa, and D. M. Farmer. Laboratory measuremnts of forward and bistatic scattering of fish at multiple frequencies. *J. Acoust. Soc. Am.*, 103 (6), June, 1998, p. 3241.

[39] Do, Manh A. and Aspi M. Surti. Estimation of dorsal aspect target strength of deep-water fish using a simple model of swimbladder backscattering. *J. Acoust. Soc. Am.*, 87 (4), April 1990, p. 1588.

[40] Drew. Albert W. Initial results from a portable dual-beam sounder for in situ measurements of target strength of fish. *IEEE*. 1980. p. 376.

[41] Ehrenberg. John. FM Slide/Chirp signals. HTI Report. 1995.

[42] Ehrenberg. John E. A method for extracting the fish target strength distribution from acoustic echoes. *Ocean '72*. 1972. p. 61.

[43] Ehrenberg. John E. In situ measurement of the acoustic target strength of marine organisms. Paper presented at the Tenth International Congress on Acoustics. Sydney. 1980. p. 176.

[44] Ehrenberg. John E. Analysis of split beam backscattering cross section estimation and single echo isolation techniques. Applied Physics Laboratory. Report 8108. Univ. Wa.. May 1981.

[45] Ehrenberg. John E. A review of in situ target strength estimation techniques. Selected papers of the ICES/FAO Symposium on Fisheries Acoustics. Bergen. Norway. 21-24 June 1982. FAO fisheries report. 1983a. p. 85-90.

[46] Ehrenberg. John E. New methods for indirectly measuring the mean acoustic backscattering cross section of fish. Selected papers of the ICES/FAO Symposium on Fisheries Acoustics. Bergen. Norway. 21-24 June 1982. FAO fisheries report. 1983b. p. 91.

[47] Ehrenberg. John E. A review of target strength estimation techniques. Proceeding of July 1988 NATO Advanced Study Institute. *Underwater Acoustic Data Processing*. 1989. p. 161.

[48] Ehrenberg, John E. An evaluation of the acoustic enumeration of upstream salmon in Upper Cook Inlet Rivers in 1989. Report prepared for The Trans-Alaska Pipeline Liability Fund. 1989.

[49] Ehrenberg, John E., T.J. Carlson, J.J. Traynor and N.J. Williamson. Indirect measurement of the mean acoustic backscattering cross section of fish. *J. Acoust. Soc. Am.*, 69 (4), April 1981, p. 955.

[50] Ehrenberg, John E. and Samuel V. Johnston. Evaluation of the use of hydroacoustic pulse width data to separate fish by size group. HTI report, June, 1996.

[51] Ehrenberg, John E. and T.C. Torkelson. Application of dual-beam and split-beam target tracking in fisheries acoustics. *ICES J. Mar. Sci.*, 53, 1996, p. 329.

[52] Ehrenberg, John E., J.J. Traynor, and Vlad M. Kaczynski. The application of multibeam acoustic techniques to marine resource assessment. Proceedings of the Pacific Congress on Marine Technology, Honolulu, Hawaii, April 24-27, 1984, MRMI p. 8-14.

[53] Elmore, William C. and Mark A. Heald. Physics of Waves. Dover Publications, Inc., New York, 1969.

[54] Enzenhofer, Hermann J. and Norm Olsen and Timothy J. Mulligan. Fixed-location riverine hydroacoustics as a method of enumerating migrating adult Pacific salmon: comparison of split-beam acoustics vs. visual counting. *Aquat. Living Resour.*, 11 (2), 1998, p. 61.

[55] Feuillade. C. Scattering from collective modes of air bubbles in water and the physical mechanism of superresonances. *J. Acoust. Soc. Am.*, 98 (2). Pt. 1. August 1995. p. 1178.

[56] Feuillade. Christopher. Richard H. Love. Michael F. Werby. Characteristic resonance signatures for acoustical scattering from fish. Proceedings of SPIE - The International Society for Optical Engineering. 2234. 1994. p. 120.

[57] Feuillade. Christopher and R.W. Nero. A viscous-elastic swimbladder model for describing enhanced-frequency resonance scattering from fish. *J. Acoust. Soc. Am.*, 103(6). June 1998. p. 3245.

[58] Fleischer. Guy W. and Ray L. Arglye and Gary L. Curtis. In situ relations of target strength to fish size for Great Lakes pelagic planktivores. *Transactions of the American Fisheries Society*. 126. 1997. p. 786.

[59] Fleischman. Steve J., David C. Mesiar and Paul A. Skvorc. II. Lower Yukon River sonar project report. 1993. Regional Information Report No. 3A95-33. December. 1995.

[60] Foote. K. G. Importance of the swimbladder in acoustic scattering by fish: a comparison of gadoid and mackerel target strengths. *J. Acoust. Soc. Am.*, 67. 1980. p. 2084.

[61] Foote. K.G. Rather-high-frequency sound scattering by swimbladdered fish. *J. Acoust. Soc. Am.*, 78 (2). August. 1985. p. 688.

[62] Foote. K.G. Coincidence echo statistics. *J. Acoust. Soc. Am.*, 99 (1), January, 1996. p. 266.

[63] Foote. Kenneth G. Analysis of empirical observation on the scattering of sound by encaged aggregation of fish. *Fisk. Dir. Skr. Ser. HavUnders.*. 16. 1978. p. 422.

[64] Foote. Kenneth G. and Egil Ona. Swimbladder cross sections and acoustic target strengths of 13 pollack and 2 saithe. *Fisk. Dir. Skr. Ser. HavUnders.*. 18. 1985. p. 1.

[65] Frisk. George V. Ocean and Seabed Acoustics: a theory of wave propagation. Prentice-Hall. New Jersey. 1994.

[66] Frolik. Jeffrey L. and Andrew E. Yagle. Forward and inverse scattering for discrete layered lossy and absorbing media. *IEEE Transactions on Circuits and Systems II: Analog and Digital Signal Processing*. 44 (9). September 1997. p. 710.

[67] Furusawa. Masahiko. Prolate spheroidal models for predicting general trends of fish target strength. *J. Acoust. Soc. Jpn.*. (E) 9. 1. 1988. p. 13.

[68] Furusawa. Masahiko and Ken Ishii and Youichi Miyanohana. Attenuation of sound by schooling fish. *J. Acoust. Soc. Am.*. 92 (2). August 1982. p. 987.

[69] Furusawa. Masahiko and Ken Ishii. Youichi Miyanohana. Yoshinobu Maniwa. Experimental investigation of an acoustic method to estimate fish abundance using culture nets. Proceedings of 4th Symposium on Ultrasonic Electronics. Tokyo. 1983. Japanese Journal of Applied Physics. 23 (1). 1984. p. 101.

[70] Furusawa. Masahiko and Yoichi Miyanohana. Application of echo-trace analysis to estimation of behaviour and target strength of fish. *J. Acoust. Soc. Jpn.*, (E) 9. 4. 1988. p. 169.

[71] Furusawa, Masahiko and Kouich Sawada. Effects of transducer motion on quantifying single fish echoes. Nippon Suisan Gakkaishi 57(5), 1991, p. 857.

[72] Furusawa, Masahiko, Youichi Miyanohana, Minoru Ariji, and Yoshifumi Sawada. Prediction of krill target strength by liquid prolate spheroid model. *Fisheries Science*, 60 (3), 1994, p. 261.

[73] Gaunaurd, Guillermo C. Sonar cross sections of bodies partially insonified by finite sound beams. IEEE J. Oc. Eng., OE-10 (3), July 1985, p. 213.

[74] Gaunaurd, Guillermo C. Acoustic scattering by an air-bubble near the sea surface. *IEEE J. Oc. Eng.*, 20 (4), Oct. 1995, p. 285.

[75] Geng, P. and J.T. Oden, and L. Demkowicz. Numerical solution and a posteriori error estimation of exterior acoustics problems by a boundary element method at high wave numbers. *J. Acoust. Soc. Am.*, 100 (1), July 1996, p. 335.

[76] Goodman, Ralph R. and Raya Stern. Reflection and transmission of sound by elastic spherical shells. *J. Acoust. Soc. Am.*, 34 (3), March 1962, p. 338.

[77] Griffiths, David F. and Desmond J. Higham. Learning LATEX. Society for Industrial and Applied Mathematics, Philadelphia, PA, 1997.

[78] Hanselman, Duane and Bruce Littlefield. Mastering MATLAB 5. Prentice Hall, New Jersey, 1998.

[79] Harris, John W. and Horst Stocker. Handbook of Mathematics and Computational Science. Springer-Verlag, New York, NY, 1998.

[80] Haslett, R.W.G. The quantitative evaluation of echo-sounder signals from fish. *Brit. I.R.E.*, July 1961, p. 33.

[81] Haslett, R.W.G. The back-scattering of acoustic waves in water by an obstacle. II. Determination of the reflectivities of solids using small specimens. *Proc. Phys. Soc.*, 79, 1962a, p. 559.

[82] Haslett, R.W.G. Measurement of the dimensions of fish to facilitate calculations of echo-strength in acoustic fish detection. *Journal du conseil*, 27 (3), 1962b, p. 261.

[83] Haslett, R.W.G. Determination of the acoustic back-scattering patterns and cross section of fish. *Brit. J. Appl. Phys.*, 13, 1962c, p. 349.

[84] Haslett, R.W.G. Determination of the acoustic scatter patterns and cross sections of fish models and ellipsoids. *Brit. J. Appl. Phys.*, 13, 1962d, p. 611.

[85] Haslett, R.W.G. The acoustic back-scattering cross sections of short cylinders. *Brit. J. Appl. Phys.*, 15, 1964a, p. 1085.

[86] Haslett, R.W.G. Physics applied to echo sounding for fish. *Ultrasonics*, Jan. - March 1964b, p. 11.

[87] Haslett, R.W.G. Acoustic backscattering cross sections of fish at three frequencies and their representation on a universal graph. *J. Appl. Phys.*, 16, 1965, p. 1143.

[88] Hawkins, A.D., Some biological sources of error in the acoustical assessment of fish abundance. 1981, p. 183.

[89] Horne, John K. and Clarence S. Clay. Sonar systems and aquatic organisms: matching equipment and model parameters. *Can. J. Fish. Aquat. Sci.*, 55, 1998, p. 1296.

[90] Huang, Kung and Clarence S. Clay. Backscattering cross sections of live fish: PDF and aspect. *J. Acoust. Soc. Am.*, 67 (3), March 1980, p. 795.

[91] Hughes, Nicholas F. and Lon H. Kelly. New techniques for 3-D video tracking of fish swimming movements in still or flowing water. *Can. J. Fish. Aquat. Sci.*, 53, 1996, p. 2473.

[92] Huttunen, Daniel C. and Paul A. Skvorc, II. 1992 Yukon River border sonar progress report. Regional Information Report No. 3A94-16, April, 1994.

[93] Huttunen, Daniel C. and Paul A. Skvorc, II. 1993 Yukon River border sonar progress report. Regional Information Report No. 3A94-06, January, 1996.

[94] Iverson, Tom K. Feasibility of using split-beam hydroacoustics to monitor adult Chinook Salmon escapement in Deep Creek, Alaska. Hydroacoustic Technology, Inc. report prepared for Alaska Department of Fish and Game, Division of Sport Fish, November, 1995.

[95] Jech, Josef M., and D.M. Schael and C.S. Clay. Application of three sound scattering models to threadfin shad (/it Dorosoma petenense). *J. Acoust. Soc. Am.*, 98 (4), October 1995, p. 2262.

[96] Johnson, Richard K. Sound scattering from a fluid sphere revisited. *J. Acoust. Soc. Am.*, 61 (2), February 1977, p. 375.

[97] Kieser, R. and J. E. Ehrenberg. An unbiased, stochastic echo-counting model. *Rapp. P.-v. Reun. Cons. int. Explor. Mer.* 189, 1990, p. 65.

[98] Konte, Michael D., Daniel C. Huttunen, and Paul A. Skvorc,II. 1994 Yukon River border sonar progress report. Regional Information Report No. 3A96-26. May. 1996.

[99] Kraeutner, Paul H. and John S. Bird. A PC-based coherent sonar for experimental underwater acoustics. *IEEE Transactions on instrumentation and measurement*. Vol. 45, no. 3, June 1996, p. 693.

[100] Kubecka, Jan. Simple model on the relationship between fish acoustical target strength and aspect for high-frequency sonar in shallow water. *J. Appl. Ichthyology*. 10 (2-3), October, 1994, p. 75.

[101] LaFlamme, Todd R. Noatak River sonar escapement estimate, 1994. Regional Information Report No. 3A95-16, April, 1995.

[102] Lai, Zhiguo. Uncertainty in fish counting using and echo-counting technique as applied to data from a single-beam sonar. MS Thesis. University of Alaska Fairbanks. Fairbanks, AK. To be published, 2002.

[103] Lambert, Marc and Rodrigo de Oliveira Bohbot and Dominique Lesselier. Born-type schemes for the acoustic probing of 1-D fluid media from time-harmonic planar reflection coefficients at two incidences. *J. Acoust. Soc. Am.*, 99 (1), January 1996, p. 243.

[104] Lauchle, Gerald C . Short-wavelength acoustic diffraction by prolate spheroids. *J. Acoust. Soc. Am.*, 58 (3), September 1975, p. 568.

[105] Lauchle, Gerald C., Short-wavelength acoustic backscattering by prolate spheroid. *J. Acoust. Soc. Am.*, 58 (3), September 1975, p. 576.

[106] Leighton, Timothy G., Andy D. Phelps, and David G. Ramble. Acoustic bubble sizing: from the laboratory to surf zone trials. *Acoustics Bulletin*, May/June 1996. p. 5.

[107] Li, Saimu and C.S. Clay. Acoustic reverberation from a laboratory model of a shelf break. *J. Acoust. Soc. Am.*, 102 (5). November 1997. p. 2663.

[108] Lindgren, Bernard W. Statistical Theory 3rd ed. Macmillan Publishing Co., Inc., New York, NY. 1976.

[109] Love, Richard H., Dorsal-aspect target strength of an individual fish. *J. Acoust. Soc. Am.*, 49 (3) pt.2.1971. p. 816.

[110] Love, Richard H. Target strength of an individual fish at any aspect. *J. Acoust. Soc. Am.*, 62 (6). December 1977. p. 1397.

[111] Love, Richard H. Resonant acoustic scattering by swimbladder-bearing fish. *J. Acoust. Soc. Am.*, 64 (2). August 1978. p. 571.

[112] Ma, Xing and Didier Vray, Philippe Delachartre, and Gerard Gimenez. Sea-bottom backscattering modeling with a wideband constant beamwidth sonar at normal incidence. *1995 IEEE Ultrasonics Symposium*, 1995. p. 1077.

[113] MacLennan, D.N. and A. Menz. Interpretation of in situ target-strength data. *ICES J. of Mar. Sci.*, 53, 1996. p. 233.

[114] MacLennan, David N. and D.V. Holliday, Fisheries and plankton acoustics: past, present and future: Part VIII: Conclusion. *ICES J. of Mar. Sci.*, 53, 1996, p. 513.

[115] MacLennan, David N. and E. John Simmonds. Fisheries Acoustics. Chapman and Hall, London, England, 1992.

[116] Major, J.K., ed. Physics of Sound in The Sea Part III: Reflection of Sound from Submarines and Surface Vessels. Gordon and Breach Science Publishers, 1968.

[117] Marshall, William J. Descriptors of impulsive signal levels commonly used in underwater acoustics. *IEEE J. Oc. Eng.*, Vol. 21, No. 1, January 1996, p. 108.

[118] Maxwell, Suzanne L., Daniel C. Huttunen and Paul A. Skvorc, II. Lower Yukon River sonar project report, 1995. Regional Information Report No. 3A97-24, May, 1997.

[119] McCartney, B.S. and A.R. Stubbs. Measurements of the acoustic target strengths of fish in dorsal aspect, including swimbladder resonance. *J. Sound Vib.*, 15 (3), 1971, p. 397.

[120] McClatchie, Sam, Gavin Macaulay, Roger F. Coombs, Paul Grimes and Alan Hart. Target Strength of an oily deep water fish, orange roughy (*Hoplostethus atlanticus*) I. Experiments. *J. Acoust. Soc. Am.* 106 (1), 1999, p. 131.

[121] Medwin, Herman and Clarence S. Clay. Fundamentals of Acoustical Oceanography, Academic Press, San Deigo, CA, 1998.

[122] Menin, Al. The Bendix Salmon Counter. Presentation given at The 1997 Alaska Riverine Sonar Workshop, Anchorage, AK, March 5-7, 1997.

[123] Mesiar, David C., Douglas M. Eggers, and David M. Gaudet, Development of techniques for the application of hydroacoustics to counting migratory fish in large rivers. *Rapp. R.-v. Reun. Cons. Int. Explot. Mer*, 189, 1990, p. 223.

[124] Michalopoulou, Zoi-Heleni and Dimitri Alexandrou. Bayesian modeling of acoustic signals for seafloor identification. *J. Acoust. Soc. Am.*, 99 (1), January 1996, p. 223.

[125] Mitson, R. B. Fisheries Sonar. Fishing News Books, Ltd. Surrey, England. 1983.

[126] Mulligan, Timothy J. and Robert Kieser. A split-beam echo-counting model for riverine use. *ICES J. Mar. Sci.*, 53, 1996, p. 403.

[127] Mulligan, T.J., D.G. Chen and Patrice Aubry. A stochastic migration model for the Fraser River salmon management. Reprinted from the 1997 Proceedings of the Section on Government Statistics and Section on Social Statistics of the American Statistical Association. 1997, p. 216.

[128] Mulligan, T.J. and D.G. Chen. A split-beam echo counting model: development of statistical procedures. *ICES. J. Mar. Sci.*, 55, 1998, p. 905.

[129] Nakken, O. and K. Olsen. Target strength measurements of fish. ***Rapp. R.-v. Reun. Cons. Int. Explot. Mer***, 170, Feb. 1977, p.52.

[130] Nero, Redwood W. and Michael E. Huster. Low-frequency acoustic imaging of Pacific salmon on the high seas. *Can. J. Fish. Aquat. Sci.*, 53, 1996, p. 2513.

[131] Nunallee, Edmund P. Scaling of an echo integrator using echo counts, and a comparison of acoustic and weir count estimates of a juvenile sockeye salmon

population. Symposium on Fisheries Acoustics. Bergen. Norway. 21-24 June 1982. p. 261.

[132] Nunallee. E.P. An alternative to thresholding during echo-integration data collection. *Rapp. P.-v. Reun. Cons. Int. Explor. Mer.* 189. 1990. p. 92.

[133] Osborne. Bruce M. and David W. Daum. Enumeration of Chandalar River Fall Chum Salmon using split-beam sonar. 1996. Alaska Fisheries Technical Report Number 42. July. 1997.

[134] Partridge. Chris and Edgar R. Smith. Acoustic scattering from bodies: Range of validity of the deformed cylinder method. *J. Acoust. Soc. Am.*. 97 (2). February 1995. p. 784.

[135] Pauly. Timothy and John D. Penrose. Laboratory target strength measurement of free swimming Antarctic krill (*Euphausia superba*). *J. Acoust. Soc. Am.*. 103 (6). June. 1998. p. 3268-80.

[136] Pedersen. Jens. Discrimination of fish layers using the three-dimensional information obtained by a split-beam echo-sounder. *ICES J. of Mar. Sci.*. 53. 1996. p. 371.

[137] Pham. Hoang X. Applications of Digital Spectral Analysis and Monte Carlo Simulation to the Measurement of Signal Characteristics. M.S. Thesis. University of Alaska Fairbanks. Fairbanks. AK. 1999.

[138] Ransom. Bruce H.. Samuel V. Johnston. Thomas C. Torkelson. Tracey W. Steig. Improved split-beam hydroacoustic techniques. Paper presented at the International Workshop on Shallow Water Fisheries Sonar. England. 16-18 September 1996.

[139] Ransom, Bruce H., Tracey W. Steig, and Patrick A. Nealson. Comparison of hydroacoustic and net catch estimates of Pacific salmon smolt (it Oncorhynchus spp.) passage at hydropower dams in the Columbia River Basin, USA. *ICES J. Mar. Sci.*, 53, 1996, p. 477.

[140] Ransom, B. H., T. W. Steig, S. V. Johnston, J. E. Ehrenberg, and T. C. Torkelson. Using hydroacoustics for fisheries assessment. Companion Manual to the Short Course presented by HTI, 1995.

[141] Reinen, Tor Arne, and John Dalen. Correction for an unknown extinction cross section in acoustic fish abundance estimation. *Proc. I.O.A.*, 13 (9), 1991, p. 293.

[142] Rottingen, Ingolf. On the relation between echo intensity and fish density. *FiskDir. Skr. Ser. HavUnders.*, 16, 1976, p. 301.

[143] Rouseff, Daniel and Terry E. Ewart. Effect of random sea surface and bottom roughness on propagaion in shallow water. *J. Acoust. Soc. Am.*, 98 (6), December 1995, p. 3397.

[144] Safaeinili, Ali and Ronald A. Roberts. Support minimized inversion of incomplete acoustic scattering data. *J. Acoust. Soc. Am.*, 97 (1), January 1993, p. 414.

[145] Sawada, Kouichi and Masahiko Furusawa. Precision calibration of echo sounder by integration of standard sphere echoes. *J. Acoust. Soc. Jpn.*, (E) 14 (4), 1993, p. 243.

[146] Sawada. Kouichi. Masahiko Furusawa and Neal J. Williamson. Conditions for the precise measurement of fish target strength *in situ*. *Ocean Acoustic Magazine*. 20 (2). 1993. p. 15.

[147] Sawada. Kouichi. Yoichi Miyanohana. and Ken Ishii. Precise target strength pattern measurement in an indoor tank. *J. Acoust. Soc. Jpn.*, (E) 18, 1997, p. 231.

[148] Schwinghamer. P.. J.Y.Guigne. and W.C. Siu. Quantifying the impact of trawling on benthic habitat structure using high resolution acoustics and chaos theory. *Can. J. Fish. Aquat. Sci.*. 53. 1996. p. 288.

[149] Senior. T.B.A. The scattering from acoustically hard and soft prolate spheroids for axial incidence. *Canadian Journal of Physics*. 44. 1966. p. 655.

[150] Shibata. Keishi. Study on details of ultrasonic reflection from individual fish. PhD. Thesis. Hokkaido University. Japan. 1970.

[151] Silbiger. Alexander. Scattering of sound by an elastic prolate spheroid. *J. Acoust. Soc. Am.*. 35 (4). 1963. p. 564.

[152] Simmonds. E. John. Fisheries and plankton acoustics: Introduction. *ICES J. of Mar. Sci.*. 53. 1996. p. 129.

[153] Simmonds. E. John. F. Armstrong. Philip J. Copland. Species identification using wideband backscatter with neural network and discriminant analysis. *ICES J. of Mar. Sci.*. 53. 1996. p. 189.

[154] Skalski. John R. and Annette Hoffmann. Bruce H. Ransom. and Tracey W. Steig. Fixed-location hydroacoustic monitoring designs for estimating fish pas-

sage using stratified random and systematic sampling. *Can. J. Fish. Aquat. Sci.*. 50. 1993. p. 1208.

[155] Sonwalkar. Vikas S. Annual Progress Report (20May 1998 - 30 April 1999): Modeling Riverine Fisheries Acoustics: New Methods to Estimate Fish Abuncance. Composition. and Uncertainties in Data Analysis. May 1999.

[156] Sonwalkar. Vikas S. Annual Progress Report (1May 1999 - 30 April 2000): Modeling Riverine Fisheries Acoustics: New Methods to Estimate Fish Abuncance. Composition. and Uncertainties in Data Analysis. May 2000.

[157] Sonwalkar. Vikas S. and Barbara L. Adams. An analysis of Sonar Data Obtained at Wood River (July 1998) Using BioSonics' 418 kHz Split-beam Sonar System: (a) Analysis of Raw Data and (b) Analysis of VTrack Algorithm. Report to Alaska Department of Fish and Game. May 1999.

[158] Sonwalkar. Vikas S.. Barbara L. Adams. and John J. Kelley. Target strength of fish at arbitrary angle of incidence at high frequencies. *Submitted to J. of Acoust. Soc. Am.*. August. 1999a.

[159] Sonwalkar. Vikas S.. Barbara L. Adams. and John J. Kelley. Acoustic wave echoes from an ensemble of fish: (a) fish size distribution function (FSDF). (b) target strength for an ensembe of fish. (c) uncertainties in fish size determination from the target strength data. *Submitted to J. of Acoust. Soc. Am.*. August. 1999b.

[160] Sonwalkar. Vikas S.. Barbara L. Adams. Mark L. Ayers, Biao Chen, Zhiguo Lai. and Hoang X. Pham. Numerical simulations in fisheries acoustics. Inter-

nal Report, Institute of Northern Engineering, University of Alaska Fairbanks, INER03.02, 2002.

[161] Soule, Michael, Ian Hampton, and Manuel Barange. Potential improvements to current methods of recognizing single targets with a split-beam echo-sounder. *ICES J. of Mar. Sci.*, 53, 1996, p. 237.

[162] Stanton, T. K. Sound scattering by cylinders of finite length. I. Fluid cylinders. *J. Acoust. Soc. Am.*, 83 (1), January, 1988a, p. 55.

[163] Stanton, T. K. Sound scattering by cylinders of finite length. II. Elastic cylinders. *J. Acoust. Soc. Am.*, 83 (1), January, 1988b, p. 64.

[164] Stanton, T. K. Sound scattering by cylinders of finite length. III. Deformed cylinders. *J. Acoust. Soc. Am.*, 86 (2), August, 1989a, p. 691.

[165] Stanton, Timothy K. Simple approximate formulas for backscattering of sound by spherical and elongated objects. *J. Acoust. Soc. Am.*, 86 (4), October 1989b, p. 1499.

[166] Stanton, Timothy K., Clarence S. Clay and Dezhang Chu. Ray representation of sound scattering by weakly scattering deformed fluid cylinders: Simple physics and application to zooplankton. *J. Acoust. Soc. Am.*, 94 (6), December 1993, p. 3454.

[167] Stanton, Timothy K., Dezhang Chu, Peter H. Wiebe, Linda V. Martin, and Robert L. Eastwood. Sound scattering by several zooplankton groups. I. Experimental determinaion of dominanat scattering mechanisms. *J. Acoust. Soc. Am.*, 103 (1), January, 1998a, p. 225.

[168] Stanton, Timothy K., Dezhang Chu, and Peter H. Wiebe. Sound scattering by several zooplankton groups. II. Scattering models. *J. Acoust. Soc. Am.*, 103 (1), January, 1998b, p. 236-53.

[169] Stanton, Peter H. Wiebe, and Dezhang Chu. Differences between sound scattering by wealky scatering spheres and finit-length cylinders with applications to sound scattering by zooplankton. *J. Acoust. Soc. Am.*, 103 (1), January, 1998c, p. 254-64.

[170] Steig, Tracey W. and Tom K. Iverson. Feasibility of using split-beam hydroacoustics to count adult Atlantic salmon and sea trout in the River Torridge. Hydroacoustic Technology, Inc. Report, March, 1996.

[171] Steig, Tracey W. and Samuel V. Johnston. Monitoring fish movement patterns in a reservoir using horizontally scanning split-beam techniques. *ICES J.of Mar. Sci.*, 53, 1996, p. 435.

[172] Takao, Yoshimi and Masahiko Furusawa. Dual-beam echo integration method for precise acoustic surveys. *ICES J. Mar. Sci.*, 53, 1996, p. 351.

[173] Tappert, F.D. Comment on "Ray chaos in underwater acoustics in view of local instability" [J. Acoust. Soc. Am., 94, 2739-2745 (1993)]. *J. Acoust. Soc. Am.*, 99 (4) Pt. 1, April 1996, p. 2433.

[174] Thiel, H.U., Plankton and krill studies, Subject group M. *Rapp. R.-v. Reun. Cons. Int. Explot. Mer.* 184, 1984, p. 134.

[175] Thompson, Charles H. and Richard H. Love. Determination of fish size distributions and areal densities using broadband low-frequency measurements. *ICES J. Mar. Sci.*, 53, 1996, p. 197.

[176] Tran Van Nhieu, Michel and Frederique Ywanne. Sound scattering by slender bodies of arbitrary shape. *J. Acoust. Soc. Am.*, 95 (4), April 1994, p. 1726.

[177] Traynor, Jimmie J. and John E. Ehrenberg. Fish and standard-sphere target-strength measurements obtained with a dual-beam and split-beam echo-sounding system. *Rapp. P.-v. Reun. Cons. Int. Explor. Mer.* 189, 1990, p. 325.

[178] Urick, Robert J. Principles of Underwater Sound for Engineers, 3rd ed. McGraw-Hill, New York, 1983.

[179] Vania, Thomas D. and Daniel C. Huttunen. Aniak River sonar progress report, 1996. Regional Information Report No. 3A97-20.

[180] Vaught, Kyle D. and Douglas B. Molyneaux. Kuskokwim River sonar project abundance estimates of salmon species, 1994. Regional Information Report No. 3A95-18, May, 1995.

[181] Westwood, Evan K., C. T. Tindle, and N.R. Chapman. A normal mode model for acousto-elastic ocean environments. *J. Acoust. Soc. Am.*, 100 (6), December 1996, p. 3631.

[182] Wiebe, Peter H., Timothy K. Stanton, Mark C. Benfield, David G. Mountain, Charles H. Greene. High-frequency acoustic volume backscattering in the Georges Bank Coastal Region and its interpretation using scattering models. *IEEE J. of Oceanic Eng.*, 22 (3), July 1997, p. 445.

[183] Xie, Yumbo and George Cronkite and Timothy Mulligan. A split beam echosounder perspective on migratory salmon in the Fraser River: A progress report on the split-beam experiment at Mission, B.C., in 1995. Pacific Salmon Commission Technical Report No. 8, December 1997.

[184] Ye. Zhen. A novel approach to sound scattering by cylinders of finite length. *J. Acoust. Soc. Am.*. 102 (2) pt.1. August 1997. p. 877.

[185] Ye. Zhen. Theoretical description of possible detection of swimbladdered fish in forward scatter. *J. Acoust. Soc. Am.*. 98 (5). Pt. 1. November 1995. p. 2717.

[186] Ye. Zhen. Acoustic scattering from fish swimbladders. *J. Acoust. Soc. Am.*. 99 (2). February 1996a. p. 785.

[187] Ye. Zhen. On acoustic attenuation by swimbladder fish. *J. Acoust. Soc. Am.*. 100 (1). July 1996b. p. 669.

[188] Ye. Zhen. Low-frequency acoustic scattering by gas-filled prolate spheroids in liquids. *J. Acoust. Soc. Am.*. 101 (4). April 1997. p. 1945.

[189] Ye. Zhen. and David M. Farmer. Acoustic scattering from swim-bladder fish at low frequencies. *J. Acoust. Soc. Am.*. 96 (2) Pt. 1. August 1994. p. 951.

[190] Ye. Zhen. and David M. Farmer. Acoustic scattering by fish in the forward direction. *ICES J. of Mar. Sci.*. 53. 1996. p. 249.

[191] Ye. Zhen and Christopher Feuillade. Sound scattering by an air bubble near a plane sea surface. *J. Acoust. Soc. Am.*. 102 (1). August 1997. p. 798.

[192] Ye. Zhen and Masahiko Furusawa. Modeling of target strength of swimbladder fish at high frequencies. *J. Acoust. Soc. Jpn.*, (E) 16. 6. 1995, p. 371.

[193] Ye. Zhen and Emile Hoskinson. Richard K. Dewey. Li Ding. David M. Farmer. A method for acoustic scattering by slender bodies. I. Theory and verification. *J. Acoust. Soc. Am.*. 102 (4). Oct 1997. p. 1964.

[194] Ye. Zhen and Emile Hoskinson. Low-frequency acoustic scattering by gas-filled prolate spheroids in liquids. II. Comparison with the exact solution. *J. Acoust. Soc. Am.*, 103 (2). February, 1998. p. 822-6.

[195] Ye. Zhen and Sam McClatchie. On inferring speed of sound in aquatic organisms. *J. Acoust. Soc. Am.*, 103 (3). March 1998. p. 1667.

[196] Zuikova, N.V., T.V. Kondrat'eva, and V.D. Svet. Application of speckle interferometry to problems of ocean acoustics. *Acoustical Physics*, 42 (2), 1996. p. 196.